Towards Cancer Treatment: Synthesis and Characterization of Photoactive Theranostic Nanoclinics

by
Patrizio Salice
M. S. in Materials Science, University of Milano-Bicocca, 2006

A Thesis Submitted to the
Faculty of Mathematical, Physical and Natural Sciences
in Partial Fulfillment of the
Requirements for the degree of

Doctor of Philosophy
in Materials Science

Approved by the
Examining Committee:

_____

Thesis Adviser : Giorgio A. Pagani,
Full Professor at the Department of Materials Science, University of Milano-Bicocca

_____

Referee: Peter R. Ogilby,
Full Professor at the Department of Chemistry, University of Aarhus

_____

Referee: Tomás Torres
Full Professor at the Department of Organic Chemistry, Universidad Autonoma de Madrid

University of Milano-Bicocca
Milano, Italy

December, 2009

Declaration

This thesis was submitted in part fulfilment of the requirements for the degree of Doctor of Philosophy at the University of Milano-Bicocca. Unless otherwise stated the work described in this thesis is original and has not been submitted previously in whole or in part for any degree or other qualifications at this, or any other university. To the best of my knowledge and belief, this thesis contains no material previously published or written by another person, except where due reference has been made.

Acknowledgements

This dissertation would not have been possible without the expert guidance of my esteemed advisors, Professor Giorgio A. Pagani and Luca Beverina. I deeply appreciate both the scientific and emotional encouragement I have received from them over the past years.

My thanks go out to Professor Peter R. Ogilby, Jacob Arnbjerg, Brian Wett Pedersen, Rasmus Toftegaard, Anita Gollmer and all the people at the Center for Oxygen Microscopy and Imaging in Aarhus for welcoming me so warmly to Denmark, and to teach me some excellent photophysics. This work would miss a huge piece without their terrific contribution.

I have to thank Stefano Snaier for his lucky contribution in the bioimaging probes syntheses, and Elisabetta Ronchi for contradicting my opinion always: I have learned a lot from her. Besides the people in the lab, I would like to thank the NMR technician at the University of Milano-Bicocca, Giorgio "Cioccio" Patriarca, for spending many hours looking for the few ^{13}C atoms in my compounds and the group of Professor Claudio Maria Mari and Riccardo Ruffo for electrically shocking some of my squaraines.

The different biological aspects of this project has been investigated in collaboration with the groups of Silvia Bradamante at the Institute of Molecular Science and Technologies (ISTM), CNR Research Centre (Italy) (bioimaging), of Professor Giulio Jori at the Department of Biology, University of Padua (Italy) (in vivo testing), and of Professor Luigi Xodo and Valentina Rapozzi at the Department of Biomedical Technology and Science, University of Udine (Italy) (cellular essays).

I would like to thank the members of my reading committee, Professor Peter R. Ogilby at the Department of Chemistry, University of Aarhus, and Professor Tomás Torres at the Department of Organic Chemistry, Universidad Autonoma de Madrid, for reading and approving my PhD thesis.

A special thought to the few friends that worth a mention: Ferro, Nik, Bario, Ciro and Lu, Glauco, Brodo, Dino, Paolino, Roby, Tommy, Elena, Glo.

My sincere gratitude goes to my parents, Lorenza and Meo, my sister Greta, my grandparents, my cousin Marco, my uncles Sergio and Teresa, my brother-in-law Cassi, my parents-in-law Luisa and Silvano, my sister-in-law Susi, and all the relatives that

grant me their love, support, and patience over the last years.

My most truthful gratitude goes to Elisabetta. I am greatly indebted to her for being the origin and backbone of my happiness. I owe my every achievement to her.

Finally, I would like to thank myself for being so stubborn to believe in this project and see the end of it.

Patrizio Salice

Milano, December 2009

Abstract

This thesis describes the synthesis, the photophysical, photochemical and biological characterization of some organic aromatic heterocycle derivatives and their theranostical applications to cancer treatment. Although the topic thus falls within the general area of photomedicine, the approach adopted here takes advantage of the strong interdisciplinary character of a materials science PhD course to explore an original perspective in the molecular design of novel photosensitizers and fluorescent probes in the fight against cancer.

In the initial part of this work, we explore the synthetic accessibility of squaraine dyes candidates as second generation sensitizers for Photodynamic Therapy (PDT). This well-established treatment involves the insurgence of citotoxic species in the cellular environment after irradiation of a dye with visible light. Typically, the sensitizer excited triplet state generated after irradiation can induce the formation of singlet oxygen, $O_2(^1\Delta_g)$, the lowest excited state of molecular oxygen, and/or reactive oxygen species (ROS). It is generally accepted that production of sufficient quantities of $O_2(^1\Delta_g)$ and/or ROS, can perturb cellular processes and ultimately cause cell death. Among the large number of known photosensitizers, squaraine dyes (1,3-dicondensation products of squaric acid and electron rich molecules) possess an intense one-photon absorption in the transparency window of biological tissues. Furthermore, squaraines possess an exceedingly strong two photon absorption enabling for their use at the wavelengths relevant for clinical applications (644 nm and 806 nm, respectively). We herein report multiple strategies aimed at the improvement of the reaction yield, of byproducts removal and of time sparing.

Because of the many demanding requirements of modern PDT sensitizers, I felt important to investigate with greater effort the photophysical behavior of heterocycle-based π-extended polymethine dyes to get further insight into the possible oxygen-mediated mechanism leading to cellular phototoxicity. To this aim, we have measured singlet oxygen yields (Φ_Δ), fluorescence quantum yield (Φ_f), triplet yield (Φ_T) and singlet oxygen rates (k_q) in toluene and acetonitrile and cyclic voltammetry in dichloromethane. All of the data collected point out that these electronrich polymethine compounds have a strong affinity with molecular oxygen leading to the formation of a charge transfer encounter complex. This results in low singlet oxygen yields and high singlet oxygen rates for these dyes.

To elucidate the photodamaging mechanism I designed simple photochemical experiments: firstly, I analyzed the photobleaching behavior of a benzothiazole-based squaraine by GC-MS and I observed the formation of two carbonyl compounds in accordance with a photooxygenation of the enaminic bond; secondly, I studied the product distribution of the reaction between light, squaraines and biologically relevant targets (i.e., limonene, cholesterol, and methyl linoleate) pointing out the presence of a radical chain of oxidative events. Consistently with the photophysical characterization, I established that the encounter complex between squaraine and molecular oxygen could evolve either by photooxygenation of the enaminic bond in the squaraine backbone or by ROS production leading to lipid peroxidation that culminate in cell death by a Type I mechanism.

Indeed, the in-depth biological evaluation of two benzothiazole-based squaraine dyes showed that these dyes internalized in lipid vesicles in the cytoplasm and, although they are non-significantly cytotoxic in the dark, they promote a strong dose-dependent phototoxic effect in four different cancer cells after irradiation. In HeLa and MCF-7 cells **3.1c** and **3.30,** through their hydrocarbon chain substitutions, associate to the membranes and induce lipid peroxidation, as expected from the photophysical and photochemical study, causing cell death primarily by necrosis

A challenge that occurs when dealing with photosensitizers is the way they are solubilized and specifically delivered to the biological target. In order to overcome thisp roblem, I have shown how the wide flexibility of the squaraine structure provides a powerful tool aimed at the improvement of bioavailability. In particular, we designed and synthesized a library of squaraine dyes functionalized with ionic groups (sulfonate), alkyl groups and biologically relevant groups (e.g. cholesterol), apt to be delivered in the free form, into liposomes or into low-density lipoproteins (LDL). Through photophysical and photochemical characterization, estimate of singlet oxygen generation efficiencies, subcellular localization and phototoxicity studies in cancer cell lines, we obtained encouraging results about the theranostical capabilities of some of these squaraine dyes, opening the way for their use in cancer-related PDT applications.

To further validate the previous observations, I designed an experiment aim to activate the production of ROS in a family of cyanine dyes. I chose to engineer the progenitor Cy5 at the molecular level and increase its photooxidation capabilities by exploiting the effect plays by heteroaryl meso-substituents on the cyanine oxidation potential. By

monitoring the degradation of 1,3-diphenylisobenzofuran (DPBF) after irradiation of a sensitizer in the presence of oxygen in solution I showed that it is possible to control the redox behavior, hence the ROS production, by modulating the extent of electron density pulled by the chromophoric side-group in the meso position and boost the photooxidative capability in the series of cyanine derivatives investigated.

Moreover, I report on the synthesis, characterization and spectroscopic study both in solution and ex vivo of seven quadrupolar eteroaryl compounds which have been designed to be promising candidates as tumor-specific fluorescent molecular probes. Basic photophysical characteristics of these dyes, their subcellular localization in human umbilical vein endothelial cells (HUVEC), and their hydrophilicity based on logP values have provided in-depth insight into the processes that lead to accumulation in either mitochondria or lysosomes. I have also succeeded in recording its fluorescence spectrum ex vivo, obtaining further information about the interaction between this heteroaromatic dicationic dye and the biological environment.

Contents

List of Abbreviations

For Greek letters symbolizing variables, see end of list.

ALA	δ-aminolaevulinic acid
AlPcS	aluminum phthalocyanin sulfonates
BPDMA	benzoporphyrin derivative mono acid, ring A
DCC	*N,N'*-dicyclohexylcarbodiimide
DDQ	2,3-dichloro-5,6-dicyano-*p*-quinone
FDA	Food and Drug Administration
GPC	gel permeation chromatography
HpD	haematoporphyrin derivative
HPLC	high pressure liquid chromatography
HPPH	2-[1-hexyloxyethyl]-2-devinyl pyropheophorbide-*a*
ICG	indocyanine green
*m*THPC	tetra(*m*-hydroxyphenyl)chlorin
PBS	phosphate buffer solution
PDT	photodynamic therapy
PpIX	protoporphyrin IX
p-THPP	*meso*-tetra(*p*-hydroxyphenyl)porphyrin
ROS	reactive oxygen species
SDS	sodium dodecyl sulphate
THF	tetrahydrofuran
THPP	*meso*-tetra(hydroxyphenyl)porphyrin
TMPyP	α,β,γ,δ-tetrakis(1-methylpyrid-4-yl)porphyrin *p*-toluensulfonate
TPP	5,10,15,20-tetraphenylporphyrin
TPPS	tetraphenyl porphine sulfonate
ε_{max}	maximum molar extinction coefficient

Φ_Δ	quantum yield of $O_2(^1\Delta_g)$ formation

List of Figures

List of Tables

1. Introduction

With neoplasm we referred to a physiological state in which a group of cells proliferate beyond the normal limits of the organism which they are part of. In particular, malignant neoplasm, commonly referred as cancer, differs from benign neoplasm because of their ability to intruse or destruct adjactent tissues (invasion) and spread to other location of the organism via lymph or blood (metastasis). If the spread is not controlled, it can result in the death of the organism. One in eight deaths worldwide, corresponding to seven million people, is due to cancer according to the American Cancer Society.[1] By 2050, the global burden is expected to increase to 27 million new cancer cases and 17.5 million cancer deaths simply due to the growth and aging of the population.

A balanced approach to cancer control includes prevention, early detection, and effective treatment.[5] Successful national cancer control policies and programs raise awareness of cancer, reduce exposure to cancer risk factors, provide information and support for the adoption of healthy lifestyles, and increase the proportion of cancers detected early. It is estimated that more than half of all new cancers and cancer deaths worldwide are potentially preventable (Figure 2), depending on the greater availability of early detection screening techniques and on the effectiveness of the treatments. This consideration is supported by the large survival* differences between developing and economically developed countries, for which better diagnostic and therapeutic methodology are available. For example, five-year survival rates for breast cancer in the United States are approximately 81%, compared to 32% in Sub-Saharan Africa.[3] The World Health Organization (WHO) emphasizes that four broad approaches should be considered when developing strategies for controlling cancer:[2]

Cancer diagnosis, including careful clinical and pathological assessments, is the first step to cancer management. The development of most cancers requires multiple steps that occur over many years. Other potential malignancies can be detected before cells become cancerous or at an early stage, when the disease is most treatable. Early detection is therefore a valuable tool that could lead to timely diagnostic follow up and effective treatment. Cancers that have proven early detection methods include cervix, colon and rectum, and breast. However, wide implementation of screening for these

* Survival from a specific cancer is usually measured as the proportion of people diagnosed with cancer who are still alive five years after diagnosis.

cancers has not been fully achieved. Once-in-a-lifetime screening between the ages of 35 and 40 can reduce lifetime cervical cancer risk by 25%-35%.[9] New low-tech methods of screening for cancer with direct visualization and oftentimes immediate treatment are needed.

Once a diagnosis is confirmed, it is necessary to determine cancer stage, where the main goals are to aid in the choice of therapy, to determine prognosis, and to standardize the design of research treatment protocols. The primary modalities of cancer treatment are surgery, chemotherapy, and radiotherapy. Photodynamic therapy these may be used alone or in combination.

These considerations justify the increasing emphasis worldwide on the design and the development of novel photosensitizers and fluorescent probes in the fight against cancer.

1.1. Background to the research

Photodynamic therapy (PDT) is a well-established treatment that involves the insurgence of citotoxic species in the cellular environment after irradiation of a dye with visible light. The presence of molecular oxygen is usually required to induce the generation of highly citotoxic agents like reactive oxygen species (ROS) and/or singlet oxygen ($O_2(^1\Delta_g)$). The ability of clinician to administrate locally and systematically light and/or sensitizers into the human tissues permit to cause cellular damage in a very selective and specific way. Therefore PDT is considered a minimally invasive therapeutic modality and nowadays it has application in cancer treatment, dermatology, age-related macular degeneration treatment, …

Since the first modern clinical trial of PDT by Dougherty et al. was reported in 1978, PDT has been used in people with cancer to help them live longer and improve their quality of life. Although PDT works and causes no long-term problems, it is not widely used to treat cancer today. Still, it is offered in some treatment centers, and is being studied in many clinical trials, becoming more widely recognized as a valuable treatment option for localized cancers (cancers that have not spread far from where they started). The three drugs currently approved by the United States Food and Drug Administration (FDA) for cancer treatment are: porfimer sodium (Photofrin®), aminolevulinic acid (ALA or Levulan®) and the methyl ester of ALA (Metvixia® Cream). They are used in the therapy of solid tumors localized into the esophagus, of a

type of non-small cell lung cancer, of certain skin cancers, such as basal cell carcinoma and squamous cell carcinoma, of Bowen disease and nevoid basal cell carcinoma syndrome and of some tumors of the vagina, vulva, and cervix that can be reached by the activating light. Nevertheless, in order to enhance the efficacy of PDT and extend its applications, a variety of second and third generation photosensitizers are now being assessed for their efficacy in cancer therapy. An example of one of these new drugs, Photochlor®, is now being used in clinical trials. Photochlor or HPPH (2-[1-hexyloxyethyl]-2-devinyl pyropheophorbide-a) is a second-generation photosensitizer. It is being studied in the treatment of tumors that block the esophagus, early stage esophageal cancer, lung cancer, skin cancer, mouth and throat cancer, and locally recurring breast cancer on the chest wall after mastectomy. So far, studies have shown that photosensitivity lasts a much shorter time, and the drug is removed from the body much faster than Photofrin.

1.2. Research problem and hypothesis

1.2.1 Photosensitivity reactions

The photodynamic treatment practised today has some limitations mainly related with the drugs employed. Among these, haematoporphyrin derivative (HpD) and various commercial preparations derived from it (eg Photofrin®) have been used in clinical experimentation for many years. (ref) It is useful to take into consideration the course of action during the treatment with these sensitizers. As soon as HpD is put into the bloodstream, it begins to collect in the cells of the body. Due to the great stability of porphyrins derivatives, some of it will retained in the cells for several weeks. The skin and eyes become very sensitive to light during this time. If exposed to sunlight or other forms of bright light, the skin can quickly become swollen, sunburned, and blistered. Patients must be careful for at least 30 days after injection to avoid bright lights and direct sunlight. Some patients may remain photosensitive for up to 90 days. The same effects afflict patients treated with ALA and its derivatites. These drugs assure porphyrin sensitization after being converted endogenously into protoporphyrin IX by making use of the body's enzymatic pathway. This strategy is widely used in the PDT of superficial tumors, particularly basal cell carcinoma, squamous cell carcinoma, Bowen's disease and actinic keratoses Reactions caused by light can show up on the skin where the drug is applied. They usually involve redness and a tingling or burning sensation. For about 2 days after the drug is used, patients must take care to stay out of

strong, direct light, stay indoors as much as possible, wear protective clothing and wide-brimmed hats to avoid sunlight when outdoors, avoid beaches, snow, light colored concrete, or other surfaces where strong light may be reflected, keeping in mind that sunscreens will not protect the skin from photosensitivity reactions. The skin being treated will likely turn red and may swell after treatment. This usually peaks about a day after treatment, gets better within a week, and should be gone by 4 weeks after treatment. The skin may also be itchy or change color after treatment. More active sensitizers, for which lower dose are required, with a faster kinetics of body clearance could overcome this limitation.

1.2.2 Activation modality

The photodynamic treatment required light to be administered at the tissues where the sensitizer is localized. While optical fibers technology and surgery guarantee the access to many endogenous organs (bladder, esophagus, brain, lungs, intestine), the treatment is limited by the action spectra of the sensitizers. For example, HpD has an etio type spectrum[2] in which the band at highest energy has the strongest absorption in correspondence with the intense absorption of tissues, around 400 nm. This feature limits the depth of penetration of irradiation in this spectroscopic region activating the sensitizer only in the first few millimeters of the target tissue. Some clinicians take advantage of the weakest absorption band of HpD in the tissue transparency window[3] at 630 nm to enhance the depth at which tissue are treated. Nonetheless higher photosensitzer doses or high light doses (or a combination of these) are required to generate an adequate level of cytotoxic species due to the sensitizer low molar extinction coefficient (ε) at this wavelength. Despite synthetic efforts have been useful in the synthesis of unsymmetrical porphyrin derivatives with a retro type spectrum, like 15-carboxyrhodoporphyrin anhydride methyl ester (ε_{max} = 14050 @ 652 nm) and mesoverdin methylester (ε_{max} = 10500 @ 704 nm), deep tumor treatment requires the development of novel active sensitizer with a huge molar extinction coefficient in the near IR, in correspondence to the biological transparency window.

1.2.3 Mechanism of action

Despite the huge number of sensitizers that have found application in PDT, the mechanism that lead to cellular death in the tissues exposed to the photodynamic stress is often object of controversies due to the multifactorial nature of cytotoxicity after PDT

in vivo. Indeed, the cellular response depends on the localization of the photosensitizing molecules at the time of irradiation, the total administered dose, the total light exposure dose, light fluence rate, the time between administration of the photosensitizer and irradiation, the type of tumor and its level of oxygenation. The nature of the primary photochemistry involved in the generation of the cytotoxic species and their activity against the biological targets will then determine the sensitizer role in stopping the cellular proliferation. A large percentage of the porphyrin sensitization work published has centered in the mechanism of action of porphyrin derivatives, like HpD and α,β,γ,δ-tetrakis(1-methylpyrid-4-yl)porphyrin *p*-toluensulfonate (TMPyP) (ref), but also furocoumarins, flavins, xanthenes, thiazines and others. These studies has pointed out the presence of two main pathways in the primary photochemistry. After the sensitizer is excited in his first singlet excited state by light of proper wavelength, radiationless relaxation processes populate lower lying triplet states via intersystem crossing and ultimately yield the first excited state in a spin-allowed process. The interaction of the excited sensitizer with ground state molecular oxygen ($O_2\left(\,^3\Sigma_g^-\right)$) may result in the transfer of energy (Type II) or an electron (Type I) to oxygen. In the first case, the energy transfer populates the first singlet excited state of oxygen ($O_2\left(\,^1\Delta_g\right)$), we refer to as singlet oxygen. In the second case, the electron is accepted by the ground state O_2 molecule in one of the π^* antibonding orbitals forming the superoxide radical ($O_2^{\bullet-}$). These species, singlet oxygen and superoxide radical, are dramatically different in many aspects, among which the reactivity against oxidable substrates. As discussed in section (ref), the product distribution of unsaturated lipid oxidation, like cholesterol, is different for $O_2\left(\,^1\Delta_g\right)$ and $O_2^{\bullet-}$. It is therefore fundamental assess the nature of the sensitizer primary photochemistry and determine which factors influence the relative importance of one pathway over the other. Unfortunately, both singlet oxygen and reactive oxygen species, like superoxide radical and its derivatives, are short-lived reactive species that require proper instrumentations and expertise to be quantified accurately. In this thesis work we discuss how it is possible to determine directly singlet oxygen quantum yields by phosphorescence measurements and we apply this knowledge to squaraine dyes. We then argue an indirect method based on the oxidation of D-limonene and cholesterol to highlight the concurrence of a Type I mechanism in the sensitization process. It is important to keep in mind that Type I and II mechanism for a given sensitizer do not exclude each other. Their relative contribution depends on the polarity, on the

lipophilicity and on the molecular oxygen concentration at the chromophore localization site.

1.2.4 Cellular and subcellular localization

For PDT to be of use clinically, effective strategies for the photosensitizer to be solubilized and delivered to the site of action are necessary. Factors such as physicochemical properties of the sensitizer, sensitizer dose to be delivered, barrier properties of the target site and patient acceptability all impact upon the method of drug delivery. Among the disadvantages of HpD is the lack of selectivity against tumor tissues and cells. This involves that higher doses of sensitizer are required to grant an adequate concentration of sensitizer at the target area. Because of the poor selectivity, the drug accumulates also in the skin and eyes and the sensitization of normal tissue remains for several weeks. The strategies employed to improve the sensitizer selectivity could be roughly divided into active and passive targeting. Passive targeting uses a drug carrier with physicochemical properties (dimensionality, hydrophilic properties, etc.) suitable to control accumulation at specific tissues. Due to disordered metabolism and blood flow peculiar to neoplastic tissue, photosensitizing concentrations of drug accumulate in the target lesions relatively quickly. Active targeting tightly control the accumulation ability by using carriers functionalized with ligands specifically recognized by the target cells. In general, an active tumor-targeting photosensitizer delivery system consists of a tumor recognition moiety connected directly or through a suitable linker to the photoactive molecular fragment to form a conjugate. A rapidly growing tumor requires various nutrients and vitamins. Therefore, tumor cells overexpress many tumor-specific receptors, which can be used as targets to deliver PDT sensitizer into tumors. For example, monoclonal antibodies, polyunsaturated fatty acids, folic acid, aptamers, oligopeptides, and hyaluronic acid have been applied as tumor-specific moieties (ref ojima drugs). A desirable sensitizer should be conveniently adapted to either strategies, by compatibilization with passive targeting carriers or by functionalization with an active biomolecule. In this work, we explore some examples pertinent to either strategies.

1.2.5 Synthesis and purification

The main disadvantage of the HpD is that it is a mixture of many different compounds poorly characterized from the chemical point of view. Indeed, in the early

1960s Lipson and his colleagues treated haematoporphyrin dihydrochloride with sulphuric acid in acetic acid at room temperature for 15 minutes, precipitated it out with aqueous sodium acetate, then treated it with alkali before neutralizing to pH 7.4. The resulting black powder was called Haematoporphyrin Derivative (HpD), but nowadays it is referred as HpD Stage I. Examination of this black precipitate by HPLC reveals a mixture of about 10 components.[4] Preparative separation and characterization of these components shows that esterification and elimination reactions have occurred, the main product being the diacetate derivative of haematoporphyrin, the next abundant components being the monoacetate fraction. The second stage of the preparation of HpD involves treatment of this mixture with alkali at room temperature leading to the formation of hydrolysis and elimination products. Haematoporphyrin, mono(1-hydroxyethyl)monovinyldeuteroporphyrins, protoporphyrin and higher molecular weight material are all detected. The last fraction is a complex mixture of oligomers mainly in the range dimer to examer and it is responsible for the biological activity of HpD, although attemps to isolate the very high active component have failed. The commercial preparation (e.g., Photofrin®) are based on this higher molecular weight fraction, which is separated out by either HPLC or by GPC giving a higher molecular weight enriched fraction with a ratio monomer:dimer:oligomer 14:19:67 for Photofrin® compared to 22:23:55 for HpD Stage II.[5] Indeed, capillary electrophoresis has revealed 60 components in Photofrin®.[6] These complexity could be attributed to one structural feature, namely that haematoporphyrin is a bis-benzyl alcohol from which a highly reactive benzylic carbocation is readily formed. In order to evaluate the photodynamic activity of a given sensitizer it is vital to know the drug chemical identity and this is not possible for HpD and its derivatives. A photosensitizer should be of constant composition, and preferably a single substance which does not have stereogenic centers (e.g., haematoporphyrin has two stereogenic centers). If the presence of one or more stereogenic centers is allowed, then the stereoisomers may be expected to locate differently in cells, and the photodynamic effects will be different and the regulatory authorities will ask for test results on each stereoisomer. The need for a single substance is an overriding requirement because there are far more variables in PDT than in conventional pharmacology (e.g., drug-light interval duration, wavelength, total energy, fluence rate of the light administrated). Each component may respond differently to each variable, and logical analysis of biological results from a sensitizer which is a complex mixture becomes very difficult indeed. The synthesis should be as

straightforward and as high-yielding as possible as well. All the compounds object of this work are fully characterized and this advantage has helped during the investigation of the molecular structure-photodynamic activity relationship.

1.3. Justification for the research

Newer photosensitizing drugs should have advantages over the ones now being used. An accurately designed photosensitizer should possess an intense absorption band in the tissue transparency window (600 – 800 nm) guarantying the treatment of tumors that are deeper under the skin or in body tissues, should be more selective for cancer cells as opposed to normal cells and tissues, should be removed from the body more quickly, reducing the time patients need to worry about photosensitivity reactions, should have low intrinsic dark cytotoxicity. We are also looking more closely at how PDT works and how the cancer cells respond to its effects. Understanding how cells respond to PDT may allow doctors to enhance those effects that promote cancer cell death and suppress or counteract those that protect the cancer cells.

Bibliography

1. Garcia, M.; Jemal, A.; Ward, E.; Center, M.; Hao, Y.; Siegel, R.; Thun, M., Global cancer facts & figures 2007. *Atlanta, GA: American Cancer Society* **2007,** *18*.

2. Fischer, H.; Orth, H., *Die Chemie des pyrrols*. Akademische Verlagsgesellschaft MBH: 1940.

3. Anderson, R. R.; Parrish, J. A., The Optics of Human Skin. *J Investig Dermatol* **1981,** *77* (1), 13-19.

4. Bonnett, R.; Ridge, R.; Scourides, P.; Berenbaum, M., On the nature of 'haematoporphyrin derivative'. *Journal of the Chemical Society, Perkin Transactions 1* **1981,** *1981*, 3135-3140.

5. Nyman, E. S.; Hynninen, P. H., Research advances in the use of tetrapyrrolic photosensitizers for photodynamic therapy. *Journal of Photochemistry and Photobiology B: Biology* **2004,** *73* (1-2), 1-28.

6. Bowser, M.; Sternberg, E.; Chen, D., Development and application of a nonaqueous capillary electrophoresis system for the analysis of porphyrins and their oligomers (PHOTOFRIN). *Analytical Biochemistry* **1996,** *241* (2), 143-150.

2. Literature review

2.1 Photodynamic Therapy

Photodynamic therapy, PDT, has now reached the level of being an accepted treatment for a number of diseases, among which are several forms of cancer. Many countries have approved its use. The number of articles on PDT published in a year, both clinical and basic, seems to be steadily increasing, however, we should be aware of the early work done in this field.

2.1.1 Historical background

With "photodynamic therapy" we refer to the treatment of certain pathologies by the concerted action of visible or near infrared light, a chromophore and, usually, molecular oxygen. This effect was modernly exploited by Oscar Raab at the Ludwig-Maximillian University in Munich in 1898 who observed that paramecia treated with acridine were killed in the presence of daylight, but that they survived in the darkness.[1] This result stimulated much further activity leading to various dermatological applications for photosensitizers such as eosin fluorescein, sodium dichloroanthracene disulfonate and 'Grubler's Magdalene red' by Jodlbauer and Raab's mentor, Hermann von Tappeiner, who introduced the term "photodynamic action" (*photodynamische Wirkung*[*]) in 1904.[2, 3] We have to wait till the period 1908-1913 for the first phorphyrin sensitizer to appear on the photodynamic scene. Hematoporphyrin (HpD) was used in a number of photobiological experiments which demonstrate how it sensitized paramecia, erythrocytes, mice,[4] guinea pigs[5] and humans[6] to light. The last case was reported by Friedrich Meyer-Betz, who became extremely photosensitive for more than two months after injecting 200 mg of hematoporphyrin into himself. The first observation of porphyrin fluorescence from tumors was published by Policard in 1924 who attributed the red fluorescence from endogenously produced porphyrins in experimental rat sarcomas to bacteria infecting the tumors mistakenly.[7] Hans Fischer, who was awarded the Nobel Prize for his work on porphyrins, reported that uroporphyrin was almost as phototoxic as hematoporphyrin in 1925.[8] Körbler reported preferential accumulation of

[*] The term "photodynamic action" should be used only for photosensitized reactions requiring oxygen, according to the original work of von Tappeiner. Nevertheless, in some special case among the Type I reactions, a long lived excited state of the sensitizer may interact with an neighboring molecule by exchange of an electron or an hydrogen atom. If the interacting molecule is not molecular oxygen, the usage of the more general term "photodynamic therapy" is recommended with respect to "photodynamic action".

porphyrins and porphyrin precursors in neoplastic tissue.[9] Despite the favorable results reported, there was no long-term followup, and PDT was soon forgotten, probably because of the advent of ionizing radiation in cancer therapy.

A renew interest in PDT arose during the '60s when Lipson at the Mayo Clinic was inspired by the work of Samuel Schwartz, who studied in porphyrins from the point of view of radiosensitization.[10] Schwartz realized that commercial samples of hematoporphyrin were impure and tried to purify them. Surprisingly, he found that pure hematoporphyrin was a poor tumor-localizer. Treatment with acetic-sulfuric acid mixture gave some components which had better properties with respect to tumor-localization. These components came to be known as 'hematoporphyrin derivative', HPD. Lipson and co-workers used this knowledge both for diagnostic and therapeutic in a large number of clinical investigations.[11]

HPD contains several porphyrin monomers as well as dimers and oligomers. Among others, Moan and co-worker studied HPD by means of HPLC and fluorescence methods and found three different groups of components, monomers (hematoporphyrin stereoisomers, hematoporphyrin vinyl deuteroporphyrin isomers and protoporphyrin) with a high fluorescence quantum yield but with a poor tumor uptake, dimers with a lower fluorescence quantum yield but with a higher tumor uptake and non-fluorescent aggregates with the best tumor-localizing properties. The cellular uptake of these components, and of other related porphyrin compounds, increased with increasing lipophilicity, and so did the quantum yield of cell inactivation.[12-14] The modern era of PDT was founded in the 1970s with the pioneering work of Dougherty and co-workers at the Roswell Park Memorial Cancer Institute in Buffalo who partly purified HPD by removing the monomers. The resulting product was called Photofrin (**2.1**) and is still one the most widely used sensitizer for clinical PDT.[15] As soon as it was realized that hematoporphyrin was difficult to purify and that HPD was a mixture of a number of porphyrins with widely different properties, the search for pure substances started. Winkelman introduced tetraphenyl porphine sulfonate (TPPS, **2.2**) and claimed that it had a better tumor-localizing ability than HPD.[16] The phthalocyanines were introduced by Ben-Hur and co-workers.[17] TPPS and aluminum phthalocyanin sulfonates (AlPcS, **2.3**) produced with different numbers of sulfonate groups, hence different water solubilities, have been very useful for experiments carried out to elucidate structure-function relationships with respect to a number of parameters: specificity and absolute

tumor uptake, intratumoral and intracellular localization, and quantum yield of photoinactivation of cells and tumors.[18-21] The phthalocyanines are also relevant for clinical use, mainly due to their strong absorption in the far-red spectral band (λ_{max} ~ 670 nm) where the tissues are more transparent. The meso-substituted chlorine, tetra(*m*-hydroxyphenyl)chlorin (*m*THPC, **2.4**) was introduced by Berenbaum and co-workers[22] and is being used in clinical trials. Recently, some other new photosensitizers have also been introduced for clinical trials[23]. A novel concept of clinical PDT and photodetection is the use of endogenous protoporphyrin IX (PpIX, **2.5**) induced by exogenous δ-aminolaevulinic acid (ALA, **2.6**).[24] This was experimentally introduced by Malik et al. in 1987 in the treatment of erythroleukemic cells in vitro.[25] A few years later, Kennedy and Pottier successfully treated human skin tumors with topically ALA-based PDT.[26]

2.2.2 State of the art in PDT sensitizer development

In the past year, new sensitizers has emerged and claimed to improve the first generations of sensitizers. Pagani, Morone et al.[27] demonstrated that the introduction of a push-pull conjugated fragment in the β position of the TPP (**2.18**) skeleton leads to an efficient electronic coupling between the two units assuring a significant enhancement in TPA performances. The new porphyrin derivatives **2.7** and **2.8** represent good model compounds as efficient one- and two-photon promoted sensitizers in PDT.

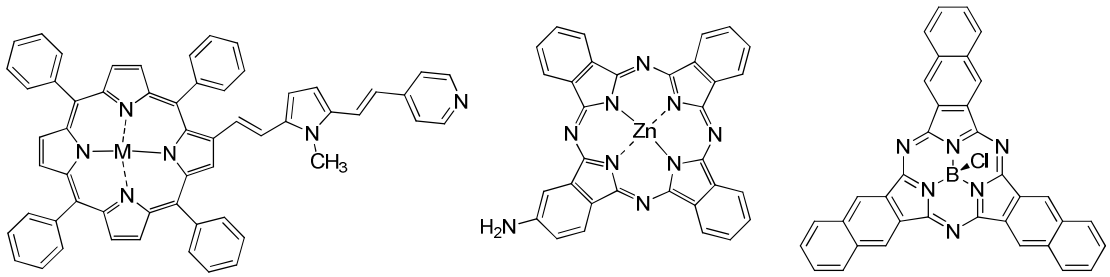

2.7 M = 2H
2.8 M = Cu(II)

2.9

2.10

Scheme 2.1

On the other end, Torres, Hanack and Sastre[28] proposed an interesting approach to the synthesis of a non symmetrical post-bioconjugable monoaminated phthalocyanine (**2.9**). Along the year, Torres have presented other innovative PDT sensitizer based on his experience on the synthesis and characterization of phthalocyanine derivatives, among the other the subnaphthalocyanine **2.10**.[29-32]

2.2 Chemical aspects of PDT sensitizers

HpD and its commercial variants comprise the first generation of photosensitizers. Second generation photosensitizers are those subsequently developed and are generally single substances, not necessarily porphyrin derivatives, with improved activity and selectivity, but which are rapidly cleared from the body after phototherapy so that general photosensitization is minimized. It has emerged that amphiphilic sensitizers meet the last requirement. Great effort has been dedicated to the functionalization of hydrophobic macrocyclic nuclei (e.g., porphyrins, phthalocyanines, naphthalocyanines) with hydroxy, sulphonic acid, pyridinium and quaternary ammonium groups in order to explore the effect on the variation of hydrophilicity.

2.2.1 Porphyrin photosensitizers

The porphyrins have a special position amongst the PDT sensitizers because of the priority of haematoporphyrin (**2.11**). Among them, hydroporphyrins and chlorins have emerged as promising second generation photosensitizers. Also porphyrins with extended chromophoric systems (e.g., *meso*-alkynyl porphyrins) and endogenously produced protoporphyrin deserve special attention. There are three main sources of porphyrins which are important in the present context: porphyrins derived from haemoglobin, porphyrins prepared by total synthesis in the laboratory and porphyrins generated by manipulation of the endogenous biosynthetic pathway to protohaem.

Blood from the slaughghterhouse is the starting material in the first case: after treatment with heparin to prevent coagulation, haemolysis and removal of the erythrocyte ghosts by centrifugation, haemoglobin can be isolated and crystallized. Alternatively chloroiron(III) protoporphyrin (aka protohaemin or haemin, **2.12**) can be crystallized by suitable treatment with acetic acid and sodium chloride. Demetallation with acid in the presence of iron(II) sulphate as reductant gives protoporphyrin. Otherwise, if haemin is treated with HBr/HOAc demetallation of the complex with concomitant Markovnikov addition of hydrogen bromide to the two vinyl groups is observed. Hydrolysis of the benzylic bromide functions gives a generally impure sample of haematoporphyrin. Finally, treatment of haemin with molten resorcinol causes protiodevinylation to produce deuterohaemin, which on demetallation gives deuteroporphyrin (**2.13**).[33]

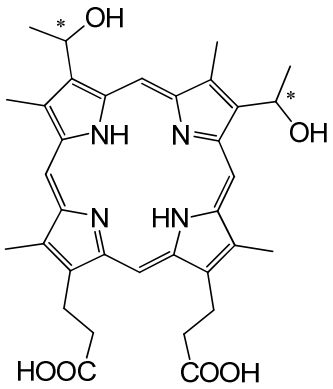

2.11 haematoporphyrin

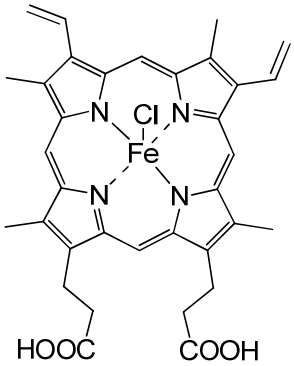

2.12 protohaemin

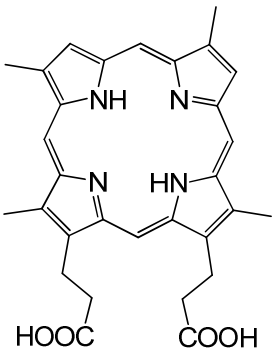

2.13 deuteroporphyrin

Scheme 2.2

Deuteroporphyrin, protoporphyrin and haematoporphyrin have been the most common starting materials for the synthesis of PDT sensitizers originating from haemoglobin. Commonly their dimethyl esters have been used in chemical synthesis since their improved solubility in organic solvents. For example, protoporphyrin dimethyl ester is the starting material for the so-called benzoporphyrin derivative mono acid, ring A (BPDMA, **2.14**). Haematoporphyrin and protoporphyrin have been functionalized at the C-3/C-8 substituents and at the propionic acid groups. A bis-pentyl ether derivative (**2.15**) is the most active accordingly to biological assays. Thioether and amino derivatives have also been evaluated, as well as compounds with various carboxyamide functions at C-17 and C-18. None of them appears to have been taken further attention because they are diastereoisomeric mixtures and they retain the inherently unstable bis-benzylic chemical reactivity.

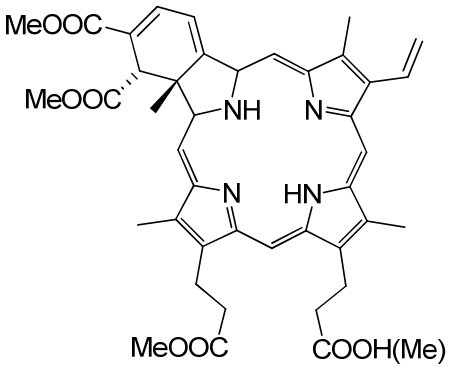

2.14 BPDMA

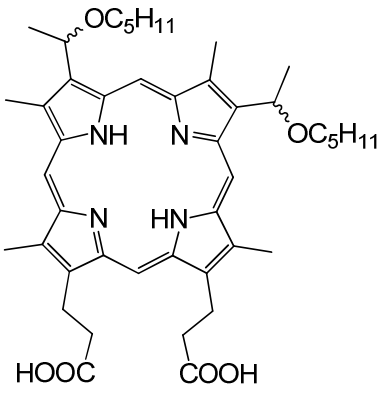

2.15

Scheme 2.3

Synthetic porphyrins offer the advantage of being a well-developed subject. The majority of synthetic approaches could be divided according to the way in which the

four ring are assembled.[34] For systems with a substitution pattern with low symmetry a stepwise synthesis is necessary (Classes A or B). Among these, we remind the Johnson's synhthesis of copper(II) coproporphyrin II tetraethyl ester (**2.16**) (Scheme 2.4),[35] the Woodward's chlorophyll synthesis (Scheme 2.5) [36] and MacDonald synthesis of uroporphyrin III octamethyl ester (**2.17**) (Scheme 2.6)[37]. For compounds with a D_{4h} symmetry, the class C reactions (4x1) are appropriate.

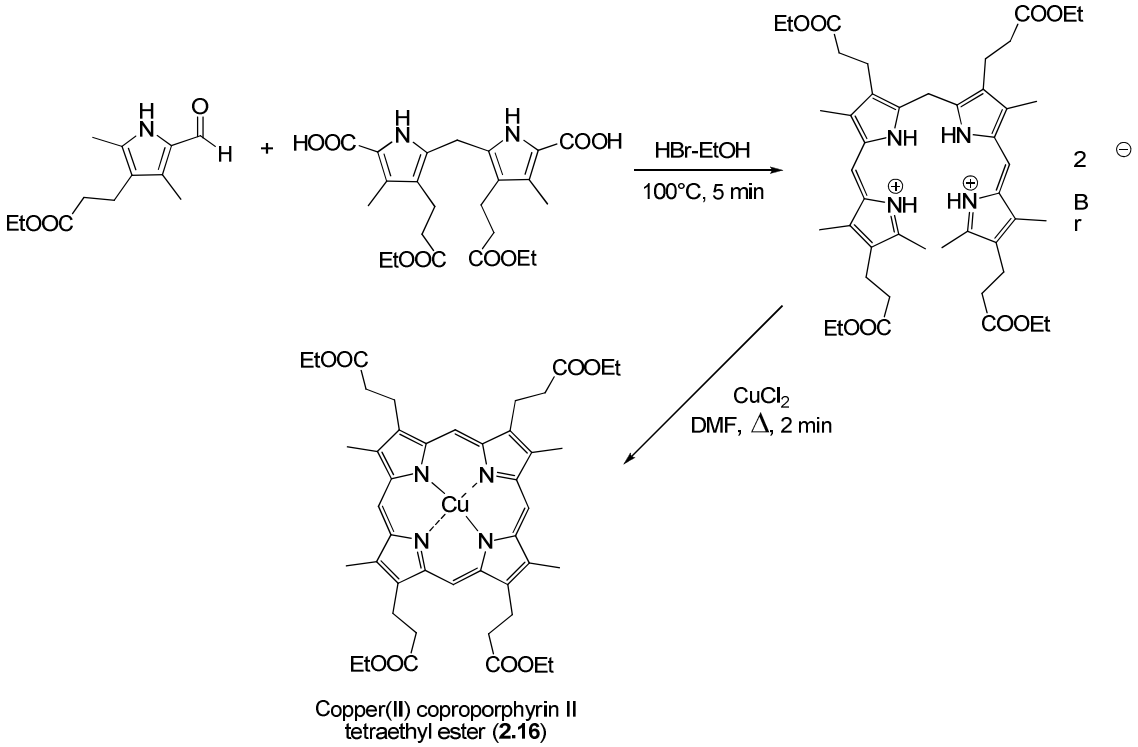

Scheme 2.4: Johnson's biladiene-ac synthesis

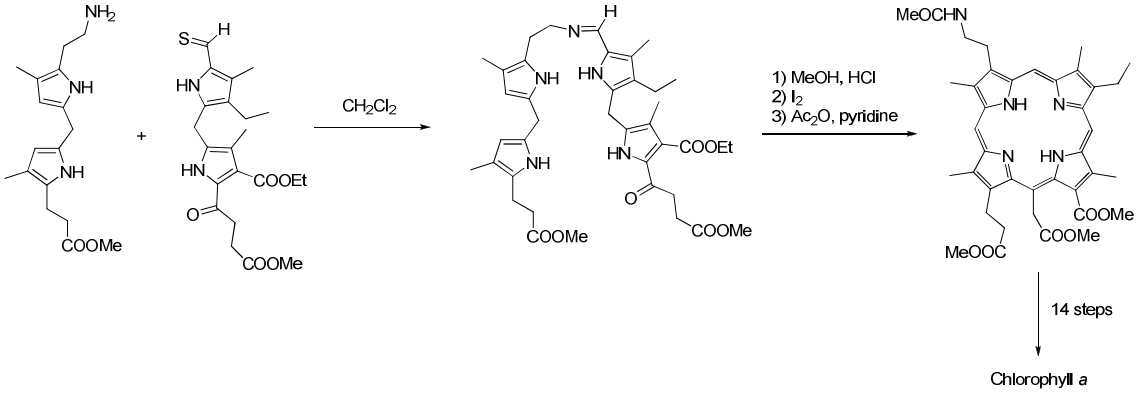

Scheme 2.5: Woodward's Chlorophyll synthesis

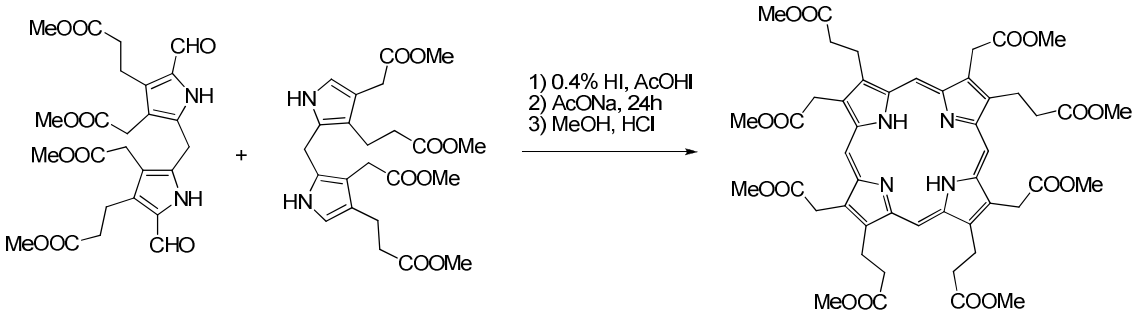

Scheme 2.6: MacDonald Synthesis

This strategy is advantageous on economic grounds because the cyclization step requires a one-pot reaction from which the product crystallizes directly in many cases. Some classic examples are the Rothemund-Adler reaction of the synthesis of *meso*-substitued porphyrins[38, 39] (e.g., 5,10,15,20-tetraphenylporphyrin, TPP, **2.18**) and the synthesis of β-substituted porphyrins[40]. Two modifications of these synthesis have led to interesesting porphyrin sensitizers. The Lindsey's mild method for the synthesis of substituted *meso*-tetraphenylporphyrins[41] and Bonar-Law's micellar assembly method for the synthesis of *meso*-tetra(*p*-hydroxyphenyl)porphyrin (*p*-THPP, **2.19**)[42]. In the first case, the intermediate porphyrinogen is formed in dilute solution (~10^{-2} M) at room temperature or below, and then dehydrogenated with a high potential quinine, such as 2,3-dichloro-5,6-dicyano-*p*-quinone (DDQ). The yield could be increased when triethyl orthoacetate is included as dehydrating agent. This method is generally better than the Rothemund-Adler reaction for compound with reactive substituents and for meso-tetraalkylporphyrins. With benzaldehyde itself, tetraphenylporphyrin is isolated in 45% yield. Bonar-Law used sodium dodecyl sulphate (SDS) in aqueous medium with the intention of assembling the reactants (pyrroles and benzaldehydes) in the lipophilic interior of micelles for reaction to give the porphyrinogen. Dehydrogenation is carried out with *p*-chloranil. This procedure appears to be particularly useful for porphyrins with sensitive polar functions, where the Lindsey's method suffers of solubility problem.

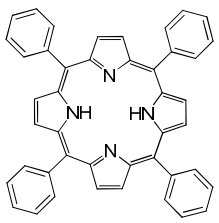

2.18 5,10,15,20-tetraphenylporphyrin (TPP)

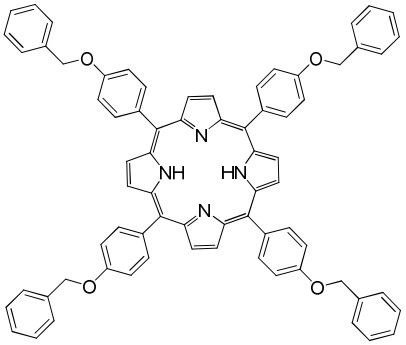

2.19 *meso*-tetra(*p*-hydroxyphenyl)porphyrin (*p*-THPP)

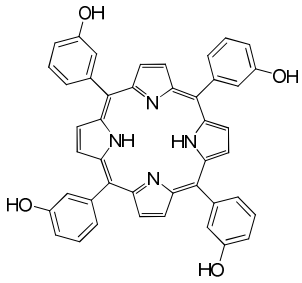

2.20 meso-tetra(hydroxyphenyl)porphyrin (*m*THPP)

Scheme 2.7

Other specific examples of porphyrin sensitizer syntheses are the synthesis of tetraphenylporphyrin sulphonic acids derivatives,[43] which are obtained by treatment of TPP with fuming sulphuric acid causing sulphonation at the *p*-positions of the phenyl rings, and the synthesis of the three regioisomer of *meso*-tetra(hydroxyphenyl)porphyrin (*m*THPP, **2.20**).[44] They are conveniently prepare by the Rothemund-Adler route starting from the protected phenolic functions. The hydroxyl functions make the system more amphiphilic and cause small hyperchromic and bathochromic effects on the Q-bands. In experiment measuring the depth of photonecrosis in tumor implants in mice, these compounds are all potent sensitizer, being up to about 25 times as effective as HpD. Indeed, *m*-THPP has been commercialized with the proprietary name Foscan® and In October 2001, it was approved in the European Union, Norway and Iceland as a local therapy for the palliative treatment of patients with advanced head and neck cancer who have failed prior therapies and are unsuitable for radiotherapy, surgery or systemic chemotherapy.[45]

Porphyrins bearing a six-memberd anhydride, imide, or isoimide ring fused across a *meso*-position and a neighboring β-position are characterized by a retro-etio spectrum, in which Band I is the most intense Q-band. Indeed, mesoverdin (**2.21**) might be worth consideration as a PDT sensitizer since it is available from mesoporphyrin dimethyl ester, but the Friedel-Crafts reaction gives regioisomers (13,15 and 15,17), which have to be separated by fractional crystallization and chromatography. However, such anhydrides and related fused ring compounds are more commonly prepared from chlorophyll *a* or bacteriochlorophyll. Thus the chlorophyll-derived purpurin 18 methyl ester on dehydrogenation with DDQ in chloroform gives the corresponding porphyrin **2.22**, now being examined as PDT sensitizer.[46]

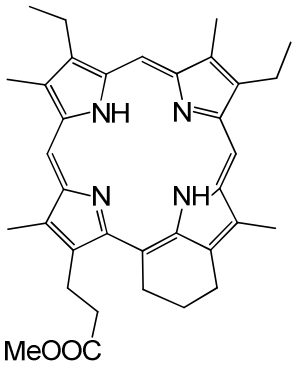

2.21 Mesoverdin

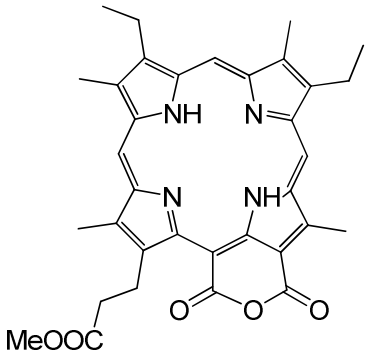

2.22

Scheme 2.8

As we have seen so far, the synthesis of a pure porphyrin could be difficult, frustrating and expensive. A smart strategy currently employed is feeding cells with an appropriate easily synthesized porphyrin precursor and making use of the body's enzymatic pathway to generate the corresponding protoporphyrin endogenously. This is possible taking advantage of the biosynthetic pathway to protohaem from δ-aminolaevulinic acid (ALA, **2.23**). The pathway is normally controlled by the concentration of protohaem which acts by a negative feed-back mechanism on the activity of the enzyme ALA synthase, thus controlling the levels of ALA. If this control is bypassed by adding ALA to the organism, the biosynthetic production line inevitable takes over. The intermediate porphyrinogens are formed in excess and these may oxidize adventitiously to porphyrins; and excess of protoporphyrin IX (PpIX, **2.24**), which is on the direct biosynthetic line, is produced. It appears that protoporphyrin is the key photosensitizer in this form of therapy. Interestingly, exogenous protoporphyrin that does reach the tumor site localizes in the plasma membrane and shows little activity, but when generated by the cellular biosynthetic pathway from the pro-drug ALA, protoporphyrin accumulates in the tumor cell mitochondria and proves to be very photoactive indeed. Protoporphyrin has potential not only as phototherapeutic agent, but also as photodiagnostic agent because of this sensitizer red fluorescence. ALA is commercially available as its hydrochloride at a reasonable price. This report led to intense activity on the use of this method in the PDT of superficial tumors, particularly basal cell carcinoma, squamous cell carcinoma, Bowen's disease and actinic kerotases.[47-50]

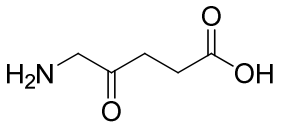

2.23 δ-aminolaevulinic acid (ALA)

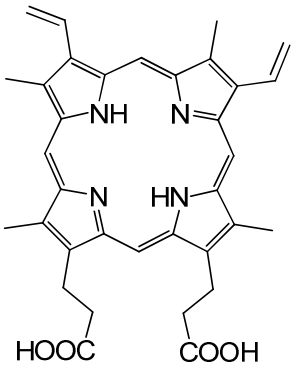

2.24 protoporphyrin IX (PpIX)

Scheme 2.9

2.2.2. Chlorins and bacteriochlorins

Chlorins and bacteriochlorins are β-dihydroporphyrins and β-tetrahydroporphyrins respectively. Actually, there are two types of β-tetrahydroporphyrins: isobacteriochlorin, in which the saturated bonds lay in two adjacent pyrrole moieties, and bacteriochlorin, in which the saturated bonds lay in two opposite pyrrole moieties. These compounds retain the porphyrin spectroscopic features since they still have a 18-π electron system. Oppositely, the hydroporphyrins obtained by reduction in the *meso* positions (e.g., porphyrinogens) have the conjugation interrupted and are so characterized by a visible absorption diminished in intensity or absent. Hence, they lack the first requirement for PDT sensitization and are not discusses furthermore.

These compounds may be isolated by natural natural sources or could be synthesized by total synthesis. The commonest example of a natural chlorine is the chromophore of chlorophyll *a* and chlorophyll *b*; bacteriochlorin, as the name suggests, is the chromophore of the bacterial photosynthethic pigment, bacteriochlorophyll *a*; while the isobacteriochlorin occurs at an intermediate stage in the biosynthesis of vitamin B_{12} and is the prosthetic group in the sulphite and nitrite reductases which occur in plants and bacteria. Nonetheless, chlorophylls and bacteriochlorophylls are waxy substances which are not themselves suitable for administration. Chemical modification generates products which are more easily purified and formulated for injection. The natural sources for chlorophylls are not higher plants, since their photosynthesic processes are based in a mixture of chlorophyll *a* and its 7-formyl-7-demethyl derivative, chlorophyll *b* in a ratio about 3:1, difficult to be separated. Fortunately, the alga *Spirulina maxima* provides such a source, and it is readily available. Two steps may be taken to simplify

the handing of these compounds. Firstly, the vinyl group at C-3 may be catalytically reduced to ethyl, giving compound of the so-called meso series. SSecondly, the β-ketoester function in ring E can be thermally demetoxycarbonylated leading to the pyro series in which ring E is a fused cyclopentanone. The same synthetic procedures apply also to bacteriochlorins but they are not so conveniently available and must be isolated from photosynthetic bacteria (e.g., *Rhodobacter spheroids* or *Rhodobacter capsulatus)* in yield about 4 mg per gram of bacterial culture. Since natural chlorins and bacteriochlorins are available in this way, it is not surprising that PDT studies with them have been very active. The range of the investigations could be illustrated by the following examples:

(i) *Chlorin e_6* (as triacid, **2.25**) has been studied by Gurinovich's group in Minsk.[51]

(ii) Hexyl ether of *pyropheophorbide a* (**2.26**) has been developed to the clinical level by Dougherty in Buffalo.[52]

(iii) *Chlorins ols*. Vallés has shown that lithium aluminium hydride reduction of methyl mesopyropheophorbide *a* gives a mixture of the hydrogenolysis product and the diol (**2.27** and **2.28**), while reduction of methyl mesopheophorbide *a* gives the triol (**2.29**). In vitro assay showed that cell inactivation increases in the series mono-ol < diol < triol.[53]

(iv) *Chlorin p_6 derivatives* (**2.30**). Bioassay of a series of chlorine p_6 derivatives indicated that the 3-formyl-3-devinyl derivative (λ_{max} = 698 nm) was the most active. [54] Smith and Kessel have also reported various conjugates of chlorin p6, for example the C13 lysyl derivative, prepared by opening the cyclic anhydride of purpurin 18 ester with a large excess of lysine in pyridine. In vivo assay showed that this compound was fast acting and more selective, in such a way that severe cutaneous photosensitivity was avoided.[55]

(v) *Bacteriopurpurin derivatives*. Both Smith[56, 57] and Mironov[58, 59] have studied analogues of purpurin 18, but in the bacteriochlorophyll series. They have prepared imide (e.g., **2.31**) and isoimide analogues with absorption maxima above 800 nm.

(vi) *Carbene insertion into 13^2-oxopyropheophorbide a*. Kozyrev *et al.* have shown that carefully controlled autoxidation of methyl pyropheophorbide *a* in

LiOH/THF gives the 13^2-oxo derivative (λ_{max} = 678 nm).[60] Treatment with large excess of CH_2N_2 causes carbine insertion to give three products, the main one being xxx. This structure recalls that one of mesoverdin and like that substance it shows a considerable bathochromic shift at Band I (λ_{max} = 777 nm).

The chlorophyll-derived PDT sensitizer with the longest track record is monoaspartyl chlorin e6 (MACE).[61] MACE is been developed in Japan, under the acronym NPe6. [62]This is prepared from chlorin e_6 (tricarboxylic acid) by DCC coupling with di-*t*-butyl aspartate. Cleavage of the *t*-butyl esters with trifluoroacetic acid gives xxx. It has a λ_{max} at 777 nm (ε = 40000) in PBS and Φ_Δ ~ 0.8. It has the advantage of a short drug-light interval (3-4 h) and any generalized photosensitization is short-lived. PDT using it has been recorded to be effective against recurrent breast adenocarcinoma, as well as basal cell carcinoma and squamous cell carcinoma.

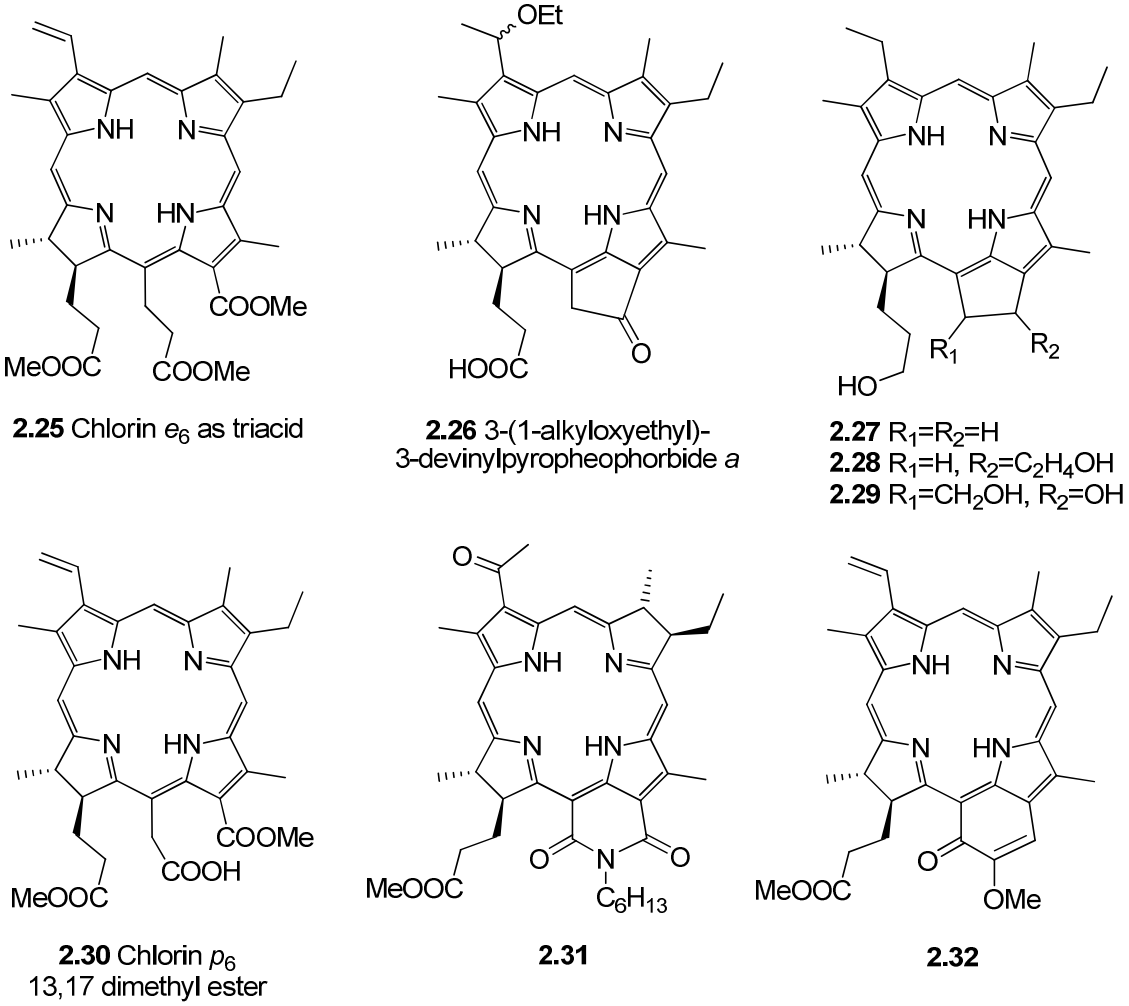

2.25 Chlorin e_6 as triacid

2.26 3-(1-alkyloxyethyl)-3-devinylpyropheophorbide *a*

2.27 R_1=R_2=H
2.28 R_1=H, R_2=C_2H_4OH
2.29 R_1=CH_2OH, R_2=OH

2.30 Chlorin p_6 13,17 dimethyl ester

2.31

2.32

Scheme 2.10

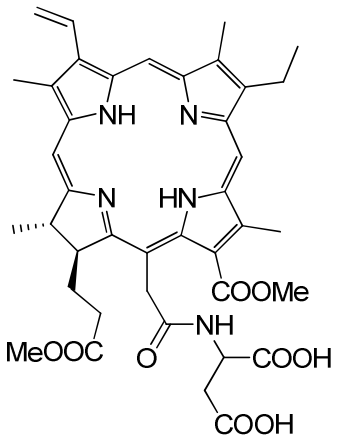

2.33 MACE

Scheme 2.11

2.2.3 Phthalocyanines and naphthalocyanines

Substitution of nitrogen for a *meso* carbon bridge in a porphyirin gives an azaporphyrin, while replacement of all four *meso* carbon bridges by nitrogens gives a porphyrazine. The benzocondensate analogue of porphyrazine with four benzene rings in the β,β'-positions is called phthalocyanine. The electronic spectrum changes dramatically so that the Q band in the region 670-700 nm now becomes the most intense band in the spectrum (ε ~ 100000-400000 l cm^{-1} mol^{-1}). The metal-free phthalocyanines have two strong bands in this region (Q_x and Q_y) whereas the metallated phthalocyanines usually have one. Various elaboration of the phthalocyanine backbone are known, for example the benzenoid annellation effect (i.e., naphthalocyanine) in order to move the Q bands further in the red. Unfortunately, these modifications lead to a decrease in the oxidation potential and solubility, therefore these dyes are not seriously in contention as PDT sensitizers.

Indeed, the chromophores considered for PDT applications are 5-azaporphyrins, benzoporphyrins and phthalocyanines. A rather uncommon azaporphyrin could be synthesized starting from bilirubin[63] by dehydrogenation with ferric chloride, esterification, and cyclization in the presence of zinc ions as template to give the oxonium salt which is converted into 5-azaprotoporphyrin dimethyl ester **2.34** with ammonia. The analogue azachlorin isomers **2.35** could be prepared by vinylporphyrin photooxygenation. The protoporphyrin ester has Band I at 624 nm (ε = 22700 l cm^{-1} mol^{-1}) in chloroform, while the chlorin isomers have λ_{max} at 674 nm (ε = 66000) and Φ_Δ

~ 0.6. Both these compounds are good example of the hyperchromic effect of the meso-aza function on Band I (for protoporphyrin dimethyl ester, Band I at 631 nm, ε = 5600 l cm^{-1} mol^{-1}). The parent porphyrazine **2.36** has been prepared by reductive cyclotetramerization of maleodinitrile and of succinimidine.

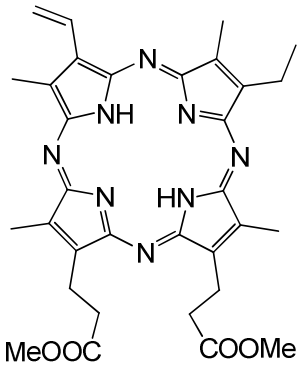

2.34

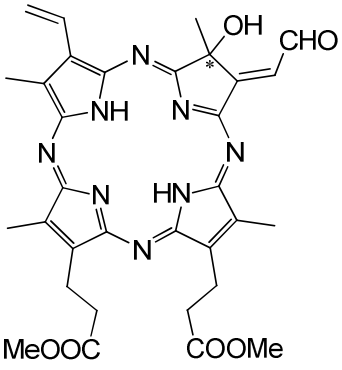

2.35

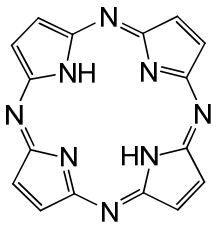

2.36

Scheme 2.12

Benzoporphyrinìs are much less common substances than either porphyrins or phthalocyanines and they could be synthesized by 4x1 synthesis starting from 3-carboxymethylphthalimidine and zinc acetate,[64] or from 1,3,4,7-tetramethylisoindole and magnesium at 350 °C.[65] Benzoporphyrins could also be synthesized by self-condensation of benzopyrromethenes,[34] by Dieckmann cyclization of porphyrin diesters,[66] by Diels-Alder annellation of a porphyrin,[67] and from tetrahydroisoindole precursors.[68] In vitro and in vivo experiments have shown that the *opp*-benzoporphyrins (**2.37**) and the tetrabenzoporphyrin are biologically active where administered in liposomes.[69] Actually, no benzoporphyrin derivative is on clinical trial.

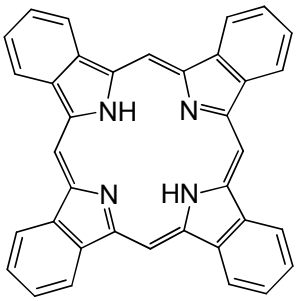

2.37 Tetrabenzoporphyrin

Scheme 2.13

Phthalocyanines are the only chromophores so far investigated which are produced commercially in tonnage amounts because of their applications as blue and green pigments and dyes. Copper(II) phthalocyanines (Monastral Blue) (**2.38**) is a common

blue pigment produced in amounts of 50000 tons/year. Nearly all the synthesis of phthalocyanines are of the 4x1 type. This puts a severe symmetry restriction on the products which can be obtained, despite various ingenious strategies have been proposed for circumventing this inflexibility. Iron phthalocyanine was discovered in 1928 by accident in an iron reactor where phthalimide was being prepared.[70] It was found that during certain preparations traces of a dark blue substance were formed in the molten phthalimide. This material was stable, crystalline, and contained iron which was not eliminated by treatment with concentrated sulphuric acid. Chemical study by Linstead who laid the foundation to the chemistry of these compounds, resulted in the correct structure formulation in 1934[71, 72] and the confirmation by X-ray analysis by Robertson the next year.[73] The syntheses which emerged from these and derived studies are summarized in Scheme 2.14.

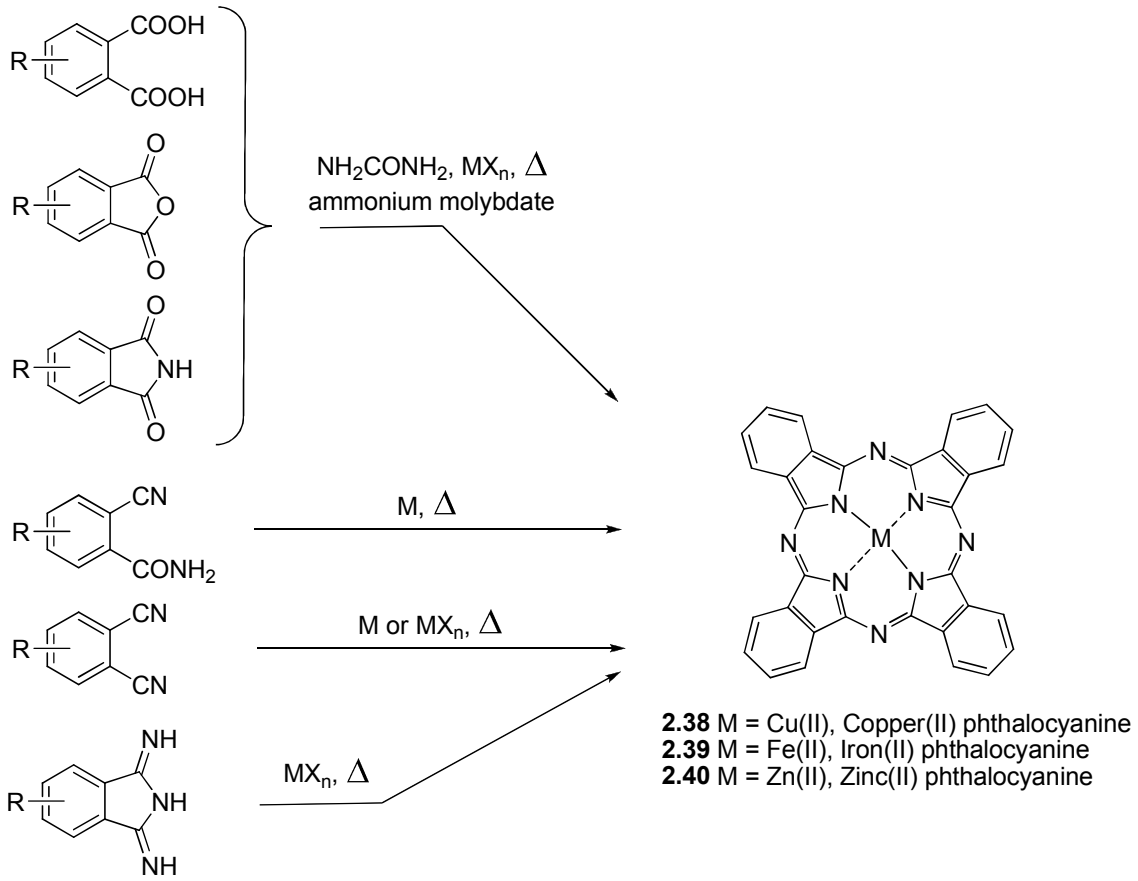

Scheme 2.14: synthethic routes to metallophthalocyanines.

Industrially it is preferable on cost grounds to start with phthalic acid or anhydride, but in the laboratory, or where purer materials are required, the phthalonitrile or diiminoisonindoline routes are preferable. The diiminoisoindolines are prepared from the *o*-dinitriles by nucleophilic cyclization (i.e., potassamide in liquid ammonia); while

the *o*-dinitriles may be obtained by dehydration of the corresponding diamides, by nucleophilic substitution or by Diels-Alder reaction. Alternative routes to the metal-free compound are to treat the phthalonitrile with ammonia gas in 2(*N*,*N*-dimethylamino)ethanol or to reflux thediiminoisoindole in this solvent. The following general points apply to this type of synthesis:

(i) The reactions are generally carried put in a melt or a highly boiling point solvent, despite Leznoff has describe what appears to be a general room temperature procedure.[74]

(ii) Alkyl substitution renders the products soluble in organic solvents, and amenable to chromatographic purification. In the absence of substituents, the phthalocyanines and their metal complexes are usually very sparingly soluble and have to be purified by washing out the impurities, but since the system is quite rugged, the impurities charring.

(iii) The reaction is a reductive cyclotetramerization. The dianion of the product requires four of these monomeric units plus two electrons, the electron source being the metal, the metal ion, the solvent or the catalyst (e.g., ammonium molybdate).

(iv) Yields are very variable and the reaction could be extended to aromatic and heteroaromatic 1,2-dinitriles in general.

(v) If the monomer is unsymmetrically substituted than four isomers will be formed in statistical distribution, provided that steric interactions do not intervene.

There have been several studies on phthalocyanines as PDT sensitizers, because they are available off the shelf, though they are usually poorly soluble. Among these chromophores, zinc(II) phthalocyanine (**2.40**) administred in a liposomal preparation on induced or transplanted rhabdomyosarcoma in harmsters has been studied by Shopova and Jori.[75, 76] Phthalocyanine octalkyl derivatives could be readily prepared from 3,6-dialkylphthalonitriles and they are fairly soluble substrate for chemical and PDT studies. Zinc(II) octapentyl phthalocyanine (**2.41**), administered as an emulsion, is more effective and more selective than zinc(II) phthalocyanine in in vivo bioassay.[77]

Another strategy widely employed for the delivery of PDT sensitizers is to prepare water-soluble derivatives by sulphotation. Direct sulphonation of aluminium or gallium

phthalocyanines leads to a mixture of regioisomers, the distribution of which depending on the substrate. If sulphonation at just the *exo* positions is required, this can be achieved by ring synthesis starting from 4-sulphophthalic acid to give the tetra *exo* sulphonic acid derivative.[78] In biological assay, the activity of these compounds appears to be $S_{2a}>S_{2o}$ and $S_2>S_1>S_3>S_4$ while aggregation effects increase in the sequence $S_4<S_1$. Indeed, a mixture of di- and tri- sulphonic acids chloroaluminium phthalocyanines (Photosens, **2.42**) have been used in extensive clinical trials against skin, breast and oropharyngeal human cancers since 1992.[79, 80]

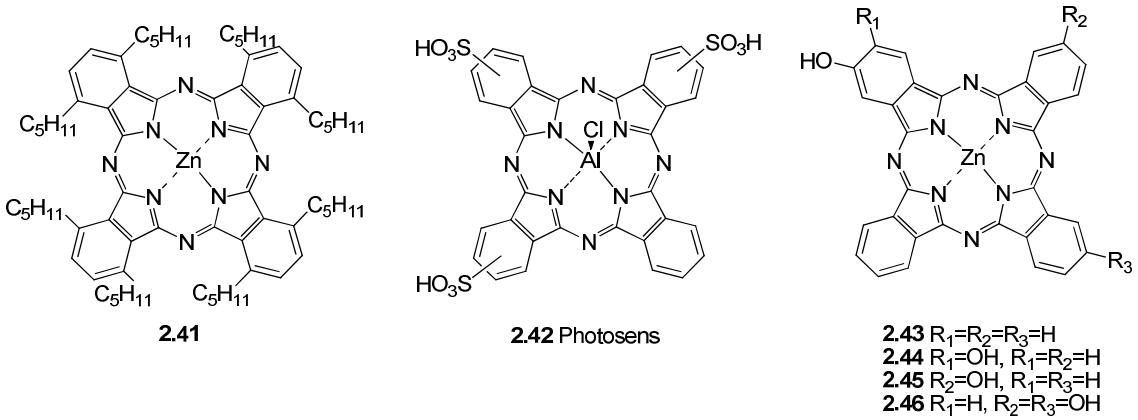

Scheme 2.15

Various other polar derivatives of phthalocyanine have been prepared for PDT applications. These include anionic (carboxylic acid, phosphonic acid), cationic (e.g., pyridinium quaternary salts) and neutral (e.g., polyethylene glycol derivatives).

Since in the tetraphenylporphyrin series the functionalization by hydroxyl groups has led to increased effectiveness in PDT, it was clearly of interest to determine if a similar effect occurred in the phthalocyanine series. Tetrahydroxylated phthalocyanines are made in the usual way using ether protection (e.g., benzyloxy); mono-, di- and trihydroxy compounds are available by alternative routes. For biological assay the compounds were emulsified with Chremophor. Evaluation in vitro against the EMT-6 mammary tumor cell lone showed that the monohydroxy compound was the most active, activity falling off in the sequence 2-mono > 2,3-di > 2,9-di > 2,9,16-tri (**2.43**-**2.46**).[81] However, in vivo the zinc(II) 2,9-dihydroxyphthalocyanine proved to be the most effective in causing complete tumor regression, being more potent than Photofrin, but less potent than zinc(II) phthalocyanine.[82]

There is some evidence that the hydrophobicity of the phthalocyanines can be

adjusted by varying the axial ligands to improve biological interactions. Thus the silicon phthalocyanine with a quaternary salt side chain is poorly taken up by V79 cells in culture, whereas the corresponding tertiary amine shows high uptake and photoinactivation.[83]

The naphthalocyanines come in two varieties, derived from naphthalene-1,2-dinitrile or naphthalene-2,3-dinitrile, and it is the latter that have been extensively studied in the PDT area. As with phthalocyanine, naphthalocyanine is a very sparingly soluble compound, but solubility in organic solvents can be enhanced by bulky substituents. The synthetic strategy is also the same as that in the phthalocyanine series, i.e. a 4x1 approach starting with the 2,3-dinitrile. Initial results of PDT studies with naphthalocyanines were not encouraging. For example, silicon(IV) naphthalocyanine with hydrophilic axial ligands (polyethylene glycol) were water soluble, and accumulate in fibrosarcoma in mice, but showed little photodynamic activity. Studies with mixture of sulphonated naphthalocyanines made by direct sulphonation showed them to be less potent PDT sensitizers than the corresponding phtalocyanines, and to be susceptible to photodegradation. More recently these compounds have begun to look more promising in the treatment of melanoma, because the screening absorption of melanin, strong throughout the visible, begin to decrease significantly in the near infrared (770-800 nm) where the naphthalocyanines have an intense absorption maximum. Indeed, Shopova and Wöhrle have demonstrated that zinc(II) naphthalocyanine localizes in and photoinactivates pigmented melanoma cells,[84] while Jori, Kenney and Rodgers have studied the effect of two silicon(IV) naphthalocyanines (**2.47**) substituted with trialkylsiloxy ligands on melanotic cells.[85]

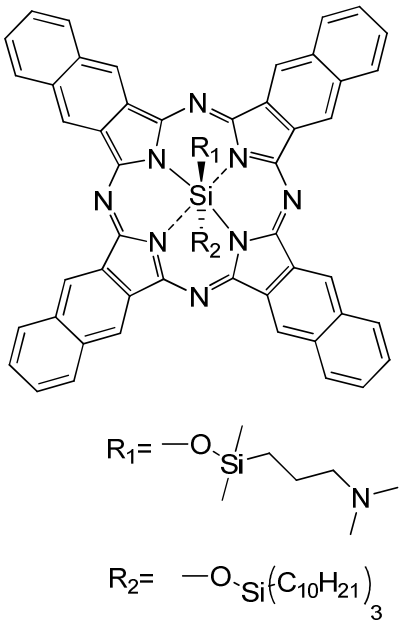

2.47

2.2.4 Other photosensitizers

In the previous sections, major emphasis was placed on PDT sensitizer related to porphyrins, because they have the advantage of priority. However, the reasons that led the first PDT clinicians to choice porphyrins and related compounds are not overwhelming, and certainly do not prevent consideration of photosensitizers based on other chromophoric systems. Indeed, hystochemistry is based on the differential staining of tissues, including tumor tissues, with a variety of organic dyes. It has to be said, that in many cases the proposed PDT sensitizers have simply been selected from what was available on the shelf, and have not been subjected to thoughtful structural variation and bioassay to sort out the best therapeutic candidate.

(i) Polymethine compounds

Polymethine dyes are compounds made up from an odd number of methine groups bound together by alternating single and double bonds.[86] Among these, cyanine dyes sre part of a synthetic dye family belonging to polymethine group and they were firstly synthesized over a century ago. Depending on the extension of the conjugated system and on the terminal substituents, their absorption covers the spectrum from NIR to UV. The cyanine dyes were originally developed in another field of applied photosensitization, that of photographic sensitizers,[87] but they are known to the biologists because they have many uses as fluorescent dyes, particularly in biomedical imaging. An example is merocyanine 540 (**2.48**) which has been used as fluorescent

axonal stain.[88] Lately, it has been advanced as phototherapeutic agent in the photodynamic inactivation of *Staphylococcus aureus* planktonic and biofilm cells,[89] and as photosensitizer in the treatment of malignant haemopoietic cells,[90] in different colorectal carcinoma cell lines,[90] in murine myeloid leukemia cells,[91] and in acute promyelocytic leukemia (HL-60) and common acute lymphoblastic leukemia antigen-positive non-T, non-B acute lymphoblastic leukemia (Reh) cell lines.[92] Comparative studies[93] in two myeloid leukemia cell lines in the mouse have revealed that *m*THPC (**2.4**) is significantly more potent and more selective in photokilling leukemia cells than is merocyanine 540 and that both *m*THPC and merocyanine 540 will induce apoptosis in leukemia cells, with the *m*THPC being observed to kill virtually all the cells in this way. Another interesting cyanine dye, indocyanine green (ICG, **2.49**), has been approved by the United States Food and Drug Administration since it has excellent safety records with very few side effects, and it is widely used in medical diagnosis since 1956.[94] ICG absorbs and emits in the near-infrared range of the spectrum (790-820 nm) and these spectroscopic properties are used to determine the liver function,[95] cardiac output,[96] and blood volume,[97] and in ophthalmologic angiography.[98] This large clinical history means that, if ICG was a useful PDT sensitizer, the route to regulatory approval would be much easier because of existing clinical experience. Indeed, the PDT effect on keratinocytes in cell culture has been investigated[99] and encouraging results from studies of the photodynamic effect in four different cell lines derived from human skin (SCL1 and SCL2 squamous cell carcinoma, HaCaT keratinocytes and N1 fibroblasts)[100] have led to a pilot study of ICG laser therapy of acne vulgaris.[101] Another interesting cyanine derivative is l-ethyl-2-{[3-ethyl-5-(3-methylbenzothiazolin-2-yliden)]-4-oxothiazolidin-2-ylidenemethyl)pyridium (MKT-077, **2.50**) which has been suggested as anticarcinoma agent in preclinical studies based on its selective mitochondrial accumulation.

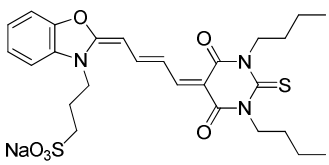

2.48 Merocyanine 540

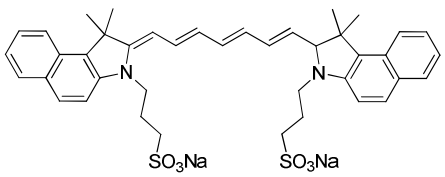

2.49 Indocyanine green (ICG)

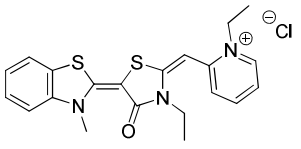

2.50 MKT-077

Scheme 2.16

Another family of polymethine compounds is represented by squaraine dyes, the

condensation product of electron-rich substrates and squaric.[102-105] These quadrupolar dyes are renown because of several desirable properties, including sharp and intense absorption in the visible and near infrared region,[106, 107] good photostability,[108] and high photoconductivity.[109] Squaraines have been extensively investigated since the mid 1960s for a large number of technological applications including xerography,[110] data storage,[111] light emitting field-effect transistors,[112] solar cells[113, 114] and nonlinear optics.[115] It has recently been shown that squaraines can also behave as very efficient two-photon absorbers,[116] fluorescent histological probes[117] and fluorescence patterning applications.[118] Due to their remarkable properties, squaraines have also been suggested as second generation sensitizers for PDT.[119-123] Since their relevance in this thesis work, their biological applications will be discussed in greater details later on.

(ii) Hypericin

Hypericin (**2.51**) is a naturally-occurring extended quinone with the absorption maximum at 590 nm in ethanol (ε = 41600) and Φ_Δ ~ 0.36 in this solvent. This substance has PDT activity against mammary carcinoma implants in athymic mice.[124] In a single case (mesothelioma) where it was applied superficially, it was not effective by itself, but appeared to act synergistically with HpD given subcutaneously.[125] Photovirucidal activity has also been recorded.[126]

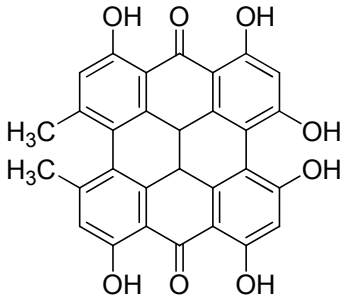

2.51 Hypericin

Scheme 2.17

(iii) Phenothiaziones

Many of the phenothiazine dyes, typified by methylene blue (**2.54**), the Azure stains and toluidine blue (**2.53**), are commercially available, and there is a considerable literature on the use of these dyes to stain and visualize cancerous lesions in vivo as an aid in diagnosis.[127] Phenothiazinium dyes have photomicrobicidal properties,[128] and have activity as PDT agents in in vitro experiments with different cancer cell lines.[129]

Nevertheless, the phenothiazinium dyes have not emerged as good PDT agents against cancer because they tend to be rapidly excreted and lack selectivity when injected. Recent studies on a more lipophilic phenothiazinium salt (**2.55**) have shown more promise. Administred i.v. at 10 mg kg-1 to Wistar rats with fibrosarrcoma implants, it was found that tumor/skin and tumor/muscle ratios were 9 and 4 respectively, after four 4 h. Fluorescence microscopy indicated that the phenothiazinium sensitizer was predominanty localized in vessel walls.

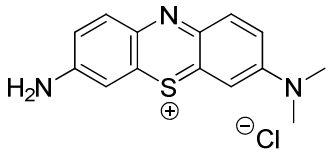

2.53 Toluidine blue

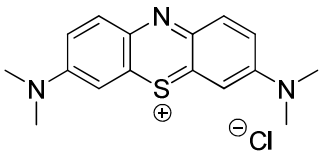

2.54 Methylene blue

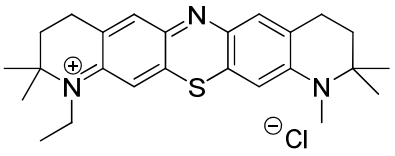

2.55

Scheme 2.18

(iv) Porphycenes

Porphycenes are isomers of porphyrins that, like the porphyrins, possess an aromatic system with 18 electrons. These compounds were first described by Vogel and were synthesized by McMurry coupling of bipyrrole dialdehydes.[130] Althoug the syntheses are often low-yielding from uncommon starting materials, the novelty of the system provides interest from the intellectual property point of view and many novel compounds have been prepared with PDT in mind. Cytopharm Inc in association with Glaxo-Wellcome are thought to be developing compounds of this series for PDT applications. The porphycene system has a porphyrin-like spectrum, but Band I is much more intense and it is shifted to the red. Porphycene has the absorption maximum at 630 nm (ε = 51900) in benzene and Φ_Δ ~ 0.15-0.40 depending on the substitution pattern. Reduction gives 2,3-dihydroporphycene, an analogue of chlorin, but Band I does not intensify as it does in the porphyrin series. Because of porphycene insolubility and hydrophobicity, several substituted amphiphilic porphycenes are being synthesized and evaluated, including the 2,7,12,17-tetrakis(2-metoxyethyl) derivative. Jori *et al.*[131] have investigated the pharmacokinetic in animal models for this class of compounds. They found that the more hydrophilic sensitizers show lower tumor uptake with lower selectivity, but distribution occurs rapidly. On the other hand, the more hydrophobic compounds equilibrate more slowly, but the concentration eventually reached are higher and there is more selectivity (Table 2.1).

Table 2.1: Retention times in reverse phase chromatography, plasma uptakes and tumor/muscle ratios for porphycenes[131]

Compound	Retention time [min]	Plasma $t_{½}$	[Tumor]/[Muscle]
2.56	1.0	0.02	2.0@20 min
2.57	1.3	0.02	2.8@20 min
2.58	9.7	6.26	26.3@3 h
2.59	6.6	0.37	19.0@24 h

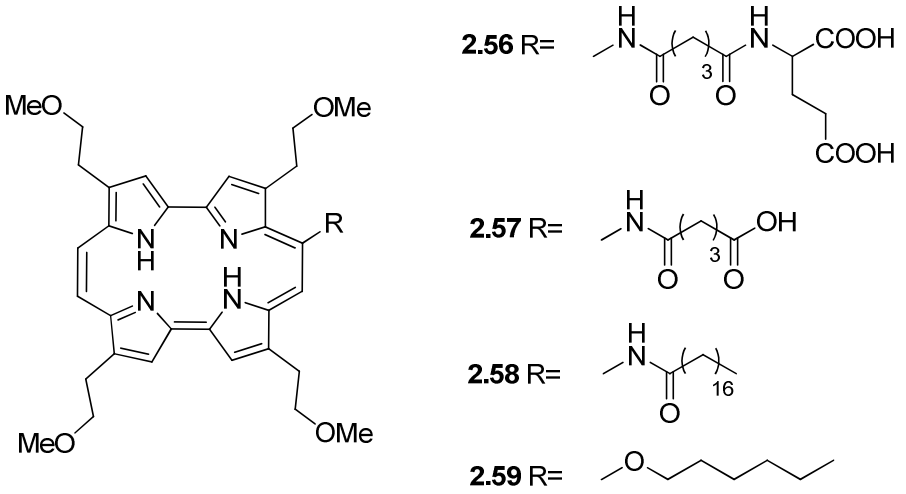

Scheme 2.19

(v) Texaphyrins

The texaphyrins have an expanded coordination with five nitrogen atoms, and it is metal complexes than the free base which appear to be making the running. The basic system is formed by condensing a diformyltripyrrane with a diamine compound.[132] When the diamine is an *o*-phenylelendiamine, or a similar molecule, the initially formed bis-azomethine is easily oxidized to the aromatic texaphyrin (**2.60**). The texaphyrins readily form metal complexes with metal ions , for example an eight-coordinate luterium(III) complex or a ten-coordinate lanthanum(III) (**2.61**) complex which both show phototumoricidal properties in vivo.[133] These complexes have a strong absorption band in the 600-900 nm region, the position of which can be tuned by suitable choice of substituents, including the metal. The texaphyrin nucleus is hydrophobic so that two

triethylene glycol chains have been attached to improve water-solubility and the free base derivative is metallated with lutetium acetate to give the amphiphilic lutetium texaphyrin being commercially developed under the proprietary name of "Lutrin" by Pharmacyclics in Sunnyvale, California. It has attractive properties, with the absorption maximum at 732 nm (ε = 42000 l mol^{-1} cm^{-1}), selectivity for tumor tissue, and a short drug-light interval (3 hours).

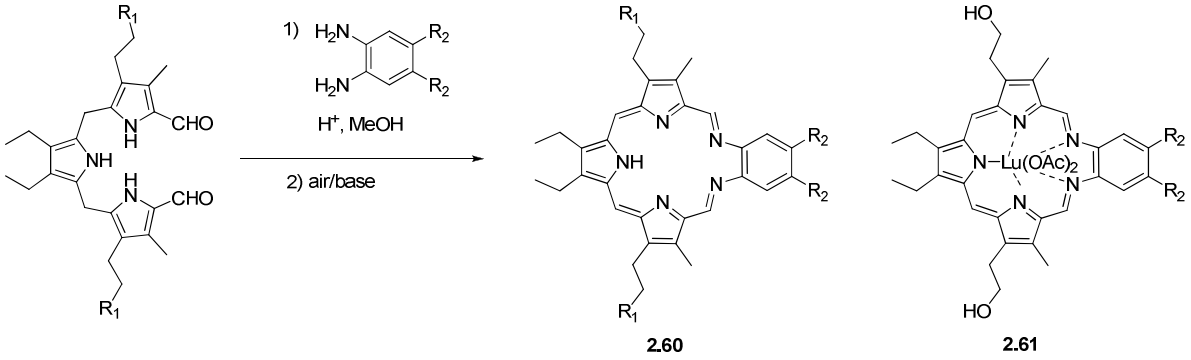

Scheme 2.20

(vi) Xanthenes

Researchers have often looked for new PDT sensitizers among compounds known for their biologically activity, although unrelated to PDT apparently. One example is xanthenes, a yellow organic heterocyclic compound used as a fungicide. Derivatives of xanthene are commonly referred to collectively as xanthenes, and are the basis of a class of dyes which includes fluorescein, eosins, and rhodamines. The fungicidal activity of some xanthenes has led them to be considered good singlet oxygen sensitizers opening their way to the earliest clinical experiments with eosin (**2.63**) by Jesionek and von Tappeneir between 1903 and 1905. Dougherty too started his PDT studies with fluorescein in 1974, but he quickly moved on to HpD because it was much more effective. Indeed, the available xanthenes are too water soluble to give a good clinical result, except perhaps by topical application. Given systematically they do not seem to show the localization and selectivity required. It is conceivable that they could do so if they were suitable substituted with lipophilic groups.

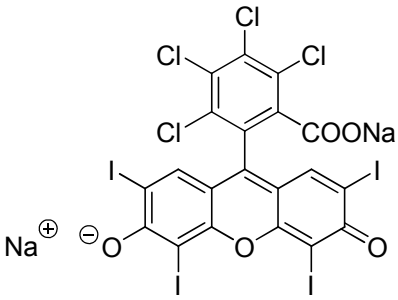

2.62 Rose bengal

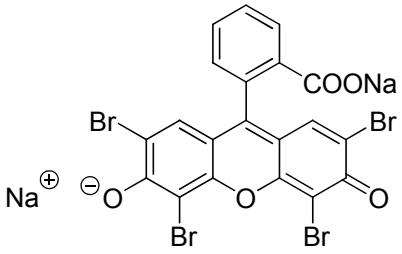

2.63 Eosin Y

Scheme 2.21

2.2.5 Third generation sensitizers

As discussed so far, first-generation PDT sensitizers, such as Photofrin®, exhibited prolonged patient photosensitivity (poor clearance) and lacked long wavelength absorption: important factors contributing to the limitation of these photosensitizers in PDT. The synthesis of improved second-generation photosensitizers moved towards modified tetrapyrrolic compounds, such as benzoporphyrin (Visudyne®), chlorin (Temoporfin®) and porphycene (ATMPn), which have a more intense long wavelength absorption. Metallated derivatives have also been synthesized (Al, AlPc) and investigated, although there is no consistent correlation between metallation and increased photodynamic activity. More recently, targeting strategies have been shown to increase the affinity of the photosensitizer for tumour tissue.[134] There have also been reports of selectively targeting subcellular compartments, including the mitochondria.[135] The biochemical usage of conjugated phosensitizers with appropriate targeting approaches have led to third-generation photosensitizers and some of the most promising results to date. Conjugation in this sense may be defined as the covalet attachment of the principal molecular backbone to a second molecular moiety which confers beneficial property on the molecular ensemble. Other examples comprise the pegylation of *m*-THPC by the attachment of polyethylene glycol residues to the four phenolic functions to improve water solubility, the functionalization of chlorins with estradiol to improve selectivity against breast carcinoma cells overexpressing the estrogen receptors by Montforts,[136] and the functionalization of chlorins with oligonucleotides which form specific complexes with suitable single-stranded and double-stranded polynucleotides, and site-direct photodamage to nucleic acid.[137] This work is also relevant to the current search for system with photovirucidal activity.

2.2.6. Prospects for the future

PDT has made considerable headway over the past twenty years, but it still excites suspicion because of its novelty characteristics. For example, the first regulatory approval in the United Kingdom for a PDT procedure was granted in 1999, six years after the first such approval in Canada. Like the Canadian approval, the UK one is carefully limited for Photofrin in the pallation of certain obstructing endobronchial lung cancers, but it represents a step forward in attitude. PDT is now in a position to join those techniques already in use in tumor treatment. Indeed, tumor phototherapy has several features which need to be considered when a method of treatment is being selected:

(i) it can be carried out safely, often on an out-patient surgical basis;

(ii) provided that care is taken to avoid subsequent exposure to strong illumination, it has few side effects. The generalized residual photosensitivity is a significant drawback, but a bearable one in contrast to the severe side effects associated with some forms of cancer chemotherapy. Although, second and third generation sensitizers may cause less generalized photosensitivity, or none at all;

(iii) because collagen appears to resist photochemical destruction, the general structure of the tissue is conserved and the healing and the cosmetic outcomes are favorable. This is often not the case for surgical intervention on tumors in delicate thin tissues, such as those of the nose and throat;

(iv) with small, maneuverable and cheap non-laser source (e.g., tungsten-halogen lamp, small arc xenon lamp, OLEDs) the procedure is inexpensive, although cost will depends on the cost of the drug. As an out-patient procedure it would be expected to reduce health costs in the Western world, but it can also be seen to be a practical low-cost procedure in Third World countries, as is being demonstrated in current trials in India;

(v) the success rate is satisfactory: if the treatment is unseuccessful, no lasting harm has been done. It does not debar subsequent surgical excision or other treatment should this become advisable. PDT with m-THPC does not induce resistance to chemotherapy, radiotherapy or further PDT in human breast cancer cells studied in vivo.

PDT is at its most powerful in the early detection and early treatment of tumors. It is not suitable for all tumors: a tumor has in the way of things human, often grown to a substantial size before the patient presents, and PDT does not lend itself to the treatment of large tumors. However, even then, two variant applications of PDT may be helpful:

(i) *intraoperative*, where after surgical excision of the tumor, the wound is subjected to PDT to kill any remaining patches of tumor tissue;

(ii) *palliative*, where structures, especially tubular ones (e.g., esophagus, bronchus) are cleared of tumor to ease congestion.

The rest of this section will be devoted to looking at the main second generation drugs which are in the experimental clinical phase, and to cast a glance to the future.

a) Photofrin®

The problems concerned with Photofrin® preparation has already been discussed in detail, but it is useful to rehearse some of the clinical details, to be compared with second generation drugs. Administration tipically involves a drug dose of about 20 mg kg-1, a drug interval of 48 hours, with irradiation at 630 nm. Photosensitization precautions are advised for 30 days. Photofrin is already in the market place, and has been licensed in Canada (Lederle), Europe (Beaufour-Ipsen) and in the United States (Sanofi). Example of major cancer treatment approved for Photofrin are the advanced stage esophageal cancer by Lightdale,[138] the abdominal non-small-cell lung cancer by Lam,[139] and the early stage lung cancer by Kato.[140] In the first case, in a multicenter randomized trial for the treatment of partially obstructing esophageal cancer, comparison was made with thermal ablation (Nd-YAG laser). The trial involved 236 patients. It was found that PDT has an advantage over the Nd-YAG laser treatment in that it caused fewer esophageal perforations, required fewer treatments, was found to be more comfortable by the patients and easier to carry by the clinicians. PDT scored less well than the reference laser ablation in that there were more adverse reactions, including some cases of mild sunburn not found with ablation. Overall, the median survival rate in the two groups was the same. A comparative trial involving 41 patients for the treatment of abdominal non-small-cell lung cancer by radiotherapy combined with PDT and radiotherapy alone showed that adding the PDT component increased the clearance of obstructed airways from 10%

to 70%. A trial of PDT against Nd-YAG laser treatment carried on 211 patients has shown several advantages for PDT, but generalized photosensitization is a problem when patients do not follow instructions. Where the two proceeding examples are palliative, Kato and his colleagues reported one of the most promising early stage type of treatment of lung cancer with Photofrin (75 patients). The response depends on tumor size, with a complete response of about 96% for tumor less than 5 mm in size, but only about 37% for tumor greater than 2 cm in size.

b) δ-ALA

The photosensitizer here is essentially endogenous protoporphyrin IX. This is emerging as an excellent photodianostic agent, but phototherapeutic applications are essentially limited to superficial lesions. [26, 141] However, the response rate of δ-ALA PDT in these superficial neoplasms is striking: in an analysis of 826 superficial basal carcinomas treated in hospitals in Canada and Europe, complete responses average 87%, with only 8% of lesions showing no response. Promising results have also been reported for other superficial lesions, including squamous cell carcinoma, Bowen's disease, mycosis fungoides and psoriasis. On the other hand, results for the effect of δ-ALA PDT on nodular basal cell carcinomas are less satisfactory. The dose of δ-ALA is much higher than that which is used with the preformed photosensitizers. When applied topically the dose is difficult to measure, but an oil-water emulsion containing 20% δ-ALA is frequently used, followed by a drug light interval of 3-8 hours. Intravenous injection employs about 30 mg kg^{-1}, while the oral dose is about 60 mg kg^{-1}. Long term photosensitivity is minimal. The topical treatment, which is non-invasive, can be repeated without difficulty if this is required. Pain, controllable with local anesthesia, may be experienced during the irradiation. δ-ALA, under the trade name Levulan, is in Phase III clinical trial for actinic keratoses, Phase II for bladder cancer photodiagnosis, acne, hair removal.

c) *m*THPC (**2.4**)

This compound is the most potent of the photosensitizers in commercial development, requiring drug doses and light fluencies such low as 0.1 mg kg^{-1} and 20 J cm^{-2}.[44, 45] The original clinical work was on 4 cases of malignant mesothieloma treated intraoperatively using a drug dose of 0.3 mg kg^{-1}, a drug light interval of 48 hours and a fluence of 10 J cm^{-2} at 650 nm.[142] Extensive clinical studies, under the

overall coordination of Scotia Pharmaceuticals Ltd., have concentrated on cancer of the upper aerodigestive tract, although there is also activity in prostate, pancreas, gynaeological and palliative applications. For example, clinicians in Lausanne described the treatment of early squamous cell carcinomas of the upper digestive tract of 27 patients in 1993. Treatment of 36 early tumors gave complete response, but complications included perforation of the esophageal wall in one case and residual photosensitization up to one week after drug administration. The same group has also studied the pharmacokinetics of *m*THPC in plasma in patients undergoing PDT, the drug being injected in water:polyethylene glygol 400:ethanol in proportion 5:3:2. Drug concentrations in plasma fell for about an hour, and then, remarkably, peaked after 10 hours. It is suggested that *m*THPC plasma levels monitored just before PDT may be used to adjust PDT light dosimetry. *m*THPC, under the trade name Foscan, is in Phase III clinical trial for ancers of upper digestive tract, prostate and others and palliative procedures).

d) Tin etiopurpurin (SnEt2, **2.64**)

This sensitizer is hydrophobic and it is injected as an emulsion in Cremophor.[143] Preliminary clinical trials have given encouraging results with cutaneous metastatic breast cancer, BCC and Kaposi's sarcoma. The drug has a drawback as far as residual photosensitization is concerned, since photoreaction is reported to persist in some patients for a month or more. Tin etiopurpurin, under the trade name Purlytin, is in Phase III clinical trial for wet AMD and Phase I for prostate cancer.

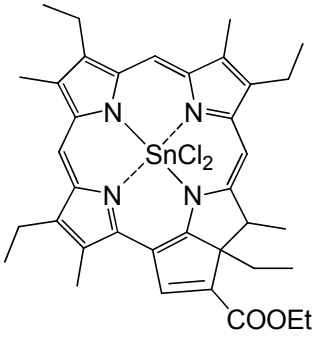

2.64 Tin etiopurpurin

Scheme 2.22

e) Mono-L-aspartylchlorin e_6 (MACE, **2.33**)

This drug is one of the earliest chlorins with proven PDT application. It is water

soluble, so can be administred in PBS, has a short drug-light interval, and residual skin photosensitivity is brief. MACE is believed to be undergoing in Japan for the treatment of lung cancer, but little information has been published.

f) 3-(1-hexyloxyethyl)-3-devinylpyropheophorbide *a* (**2.26**)

This water-insoluble sensitizer has been taken on by QLT Phototherapeutics where it has been administred in a detergent vehicle. It is an effective sensitizer, and leaves little or no residual skin photosensitivity.[144] This pyrophrophorbide *a*, under the trade name Photochlor, is in Phase I clinical trials.

g) Sulphonated aluminium phthalocyanine (Photosens, **2.42**)

The sulphonation of chloroaluminium phthalocyanine gives a mixture of sulphonic acids. A mixture of di- and trisulphonic acids has been employed by Stradnadko in Moscow for extensive clinical trials. Residual photosensitivity is thought to be a significant problem with this drug, which is not easily photobleached. The treatment appears to benefit from the use of ascorbic acid or sodium ascorbate (20-50 mg kg^{-1}) as an adjunct.

h) Benzoporphyrin derivative (BPDMA, **2.14**)

This in a clinical context refers to the mixture of mono acids derived from the compound in which the initial Diels-Alder addition has occurred on ring A of protoporphyrin dimethyl ester. It may be said to share with m-THPC the lead position amongst the second generation PDT sensitizers. Although it is reported to have attractive cancer PDT potential,[145] it is currently being advanced by QLT Photoherapeutics Inc. as a treatment for age-related macular degeneration. In spite of being a monocarboxylic acid, benzoporphyrin derivative is hydrophobic, and needs a delivery vehicle. Usually a liposomal preparation is chosen. The drug-light interval is conveniently short, and residual photosensitization is minimal. This benzoporphyrin derivative, under the proprietary name Verteporfin, has been in clinical trial for BCC, cutaneous metastases, and psoriasis. It has been approved the treatment of age-related macular degeneration (AMD) in patients with predominantly classic subfoveal choroidal neovascularization under the proprietary name of Visudyne (QLT Inc) by FDA in 2000.

i) Lutetium texaphyrin (**2.61**)

This tetrapyrrole has built-in hydrophilic chains, has water compatibility and fluorescence, and is an effective sensitizer which generates little residual photosensitivity after PDT. The phototherapy is painful, however, and this needs to be controlled with local anesthesia. With absorption at 732 nm, this sensitizer present an opportunity to photodegrade melanomas, and this is one of the clinical targets. It appears to be remarkably selective for tumors versus normal skin: cases are described where subcutaneous melanomas show complete response with little damage to overlying skin. Preliminary studies on a range of skin cancers gave 29% complete responses and 17% partial responses. This texaphyrin, under the proprietary name Lutrin, has been in phase I/II trials for breast cancer, melanoma, Kaposi's sarcoma.[146]

Five of the compounds referred to are chlorins: *m*THPC, MACE, $SnEt_2$, Photochlor and benzoporphyrin derivative. Clinical comparison between the various sensitizers are so far uncommon, and limited to small number of patients. For example, a study by Bown and his colleagues examined the effect of three different sensitizers in the treatment of various benign and malignant gastrointestinal tumors in the esophagus, duodenum and rectum in 22 patients.[147] Photofrin (i.v.) was used for 4 patients, oral δ-ALA for 16 patients, and *m*THPC (i.v.) for 2 patients. With δ-ALA, photonecrosis was only superficial (up to 1.8 mm), although it was said to improve at higher concentrations or with modified light dosimetry; with Photofrin and *m*THPC much deeper tumor photonecrosis was observed. It was found that Photofrin and *m*THPC worked better, but caused cutaneous photosensitivity, unlike δ-ALA, lasting up to 12 and 5 weeks, respectively. A comparison of various PDT sensitizers features is given in Table 2.2.

Table 2.2: Comparison of second generation PDT sensitizers

Compound	Irradiation wavelength [nm]	Φ_Δ	Drug dose [mg/kg]	Light dose [j/cm^2]	Treatment time (s)
δ-ALA	635	0.6	60	50-150	500-1500
*m*THPC	652	0.43	0.15	5-20	50-200
SnEt2	659	0.6	1.2	150-200	1500-2000
MACE	660	0.8	1.0	25-200	1500

Photosens	675	0.34	1.0	50-200	1500
BPDMA	690	0.7	4	150	1500
Lu Texaphyrin	732	0.11	1.0	150	1500

Undoubtedly new sensitizers will continue to appear, especially as other targets become apparent. It seems likely that the guidelines given in this section will become modified as the tendency emerges to tailor different sensitizers to specific cancers and specific diseases. It also seem likely that further efforts will be made (i) to harness photobleaching capability in the design of drug in order to minimized residual photosensitivity, and (ii) to prepare third generation sensitizers covalently attached to a a targeting system.

What appears to be happening now is that research scientists and clinicians with experience in PDT of cancer are indulging in some useful lateral thinking and asking question: what other diseases might be treated with phototherapy? The major prospects for other phototherapies are psoriasis, arthritis, age-related macular degeneration, atheromous plaques, photoangioplasty of peripheral arterial disease, and microorganism killing, for example cationic porphycenes show photomicrobicidal effects, while photovirucidal activity has been looked at intensively by Ben-Hur for the sterilization of transfused blood.

The possibilities for the future are not limitless, but they are extensive, largely because PDT has not been generally appreciated and cultivated in the past. Now that the value of PDT is becoming recognized, the outlook for future development appears to be very encouraging.

2.3 Photophysical aspects of PDT sensitizers

2.3.1 Basic photophysial aspects

In an interdisciplinary subject such as PDT we cannot go much firther without setting down the basic photophysics that is needed. Briefly, the ground state of a sensitizer ($^1M_0$) is its lowest-energy electronic state. It usually has two electrons with opposite spins in the highest occupy molecular orbital (HOMO) (i.e., a singlet state with a null total angular momentum). This system could evolved into an excited state ^1M_n by promoting one electron from the HOMO to the lowest unoccupied molecular orbital

(LUMO), for example by light absorption. In this process, the excited electron preserves its spin and the final state is a singlet state too. Independently on which state ^1M_n has been excited, it is rapidly radiationless deactivated to the first singlet excited state $^1M_1$, but for some azulene and thiocarbonyl derivatives. This higher energy state dynamically evolved to the initial state $^1M_0$ by light emission (fluorescence) and by radiationless deactivation without spin inversion (internal conversion), and to an excited state with an unitary total angular momentum ^3M_n (the triplet state) by radiationless deactivation with spin inversion (intersystem crossing). Analogously to the singlet state manifold, each ^3M_n relaxed to the first triplet excited state $^3M_1$ rapidly. This state is higher in energy than the ground state, but lower than $^1M_1$. $^3M_1$ further relaxes to the ground state by both radiationless deactivation (intersystem crossing) and light emission (phosphorescence). Since transitions between states with different total angular momentum are formally forbidden, the triplet state is longer lived with respect to the singlet excited state.

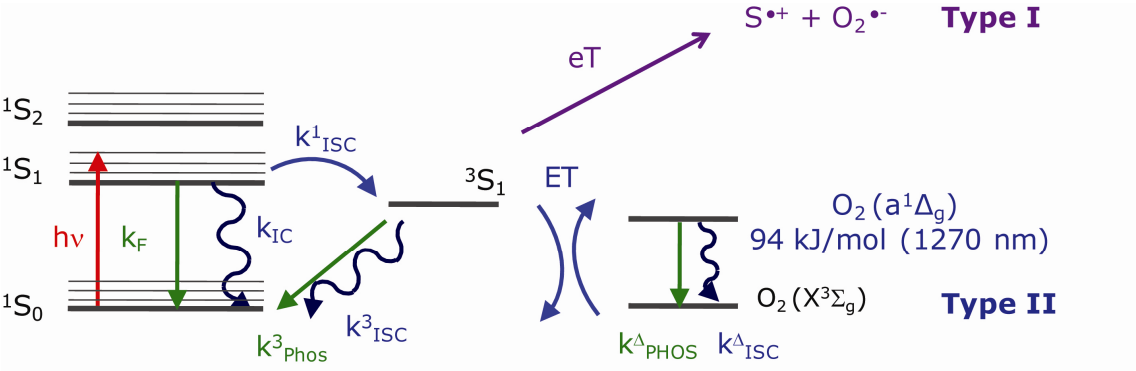

Figure 2.1: illustration of the photophysical and photochemical mechanism leading to cytotoxic species generation upon irradiation of the sensitizer (S).

The sensitizer long-lived excited states* can undergo two kinds of reactions (
Figure 2.1). Firstly, in a Type 1 reaction, it can react directly with a substrate, such as an unsaturated lipids (LOOHs derived from phospholipids and cholesterol),[148-151] a protein residue (e.g., cysteine and methionine are oxidized mainly to sulfoxides, histidine yields a thermally unstable endoperoxide, tryptophan give *N*-formylkynurenine, tyrosine can undergo phenolic oxidative coupling),[152] DNA (both at the nuclei bases and at the sugars that link the DNA strands by oxidation of the sugar linkages, or cross-linking of

* In many cases, the triplet states are the only ones mentioned as long-lived states, but there are few noticeable exceptions (i.e., the first excited state of pyrene has a lifetime up to 130 ns in the absence of oxygen).

DNA to protein),[153-155] and molecular oxygen, and transfer a proton or an electron to form a radical anion or radical cation, respectively. These radicals may further react in a chain process. Alternatively in a Type 2 reaction, the sensitizer long-lived excited state can transfer its energy to the triplet ground state of molecular oxygen, $O_2\left({}^3\Sigma_g^-\right)$, to produce the first excited state of molecular oxygen, singlet oxygen $O_2\left({}^1\Delta_g\right)$. Both Type 1 and Type 2 reactions can occur simultaneously, and the ratio between these processes depends on the photophysical properties the sensitizer and on the concentrations of substrate and oxygen. Type 1 pathways frequently involve initial production of superoxide radical anion ($O_2^{\cdot-}$) by electron transfer from the sensitizer long-lived excited state to molecular oxygen.[156, 157] The highly reactive superoxide can either react with itself to produce hydrogen peroxide (HOOH) and oxygen, a dismutation catalyzed by the enzyme superoxide dismutase (SOD), or it can undergo an acid-base reaction with water to give the superoxide radical (HOO·). This reactive species can ablate a hydrogen atom from a suitable target (RH) to give hydrogen peroxide and a radical (R·). Hydrogen peroxide is important in biological systems because it can pass readily through cell membranes and cannot be excluded from cells. Superoxide is also important as reducing agent in the reduction of metal ions (such as Fe^{3+}). This reaction is called the Fenton reaction and it has the highly reactive hydroxyl radical (HO·) as byproduct. Moreover, the reduced metal (Fe^{2+}) catalyzes the breakage of hydrogen peroxide to produce am equivalent of hydroxyl radical and one of hydroxide ion (HO-). Superoxide can also react with the hydroxyl radical to form singlet oxygen. With the term reactive oxygen species (ROS), we identified the superoxide radical anion ($O_2^{\cdot-}$), hydrogen peroxide (HOOH), the superoxide radical (HOO·), the hydroxyl radical (HO·). They are highly reactive species which damage is "diffusion rate-limited", therefore limited to a small region in space (< 1 μm) and time (< 1 μs). They can add to an organic substrate such as an unsaturated fatty acid to form a hydroxylated radical adduct. The hydroxyl radical can also oxidize the organic substrate by acting as electron acceptor. The resulting oxidized substrate is again a radical, and can react with other molecules in a chain reaction. For example, it could react with ground-state oxygen to produce a peroxyl radical (ROO·), which can react with other biological substrates in a chain reaction again. This type of chain reaction is common in the oxidative damage of fatty acids and other lipids. These ROS, together

with singlet oxygen produced via Type 2 pathway, are indeed oxidizing agents that can directly react with many biological molecules. Although all cells have some capability of repairing oxidative damage to proteins and DNA, excess damage can cause mutations or cell death. [152, 15158, 159]

2.3.4 Light delivery

One of the chief attractions of PDT as a therapy is the concept of dual selectivity. Collateral damage to normal tissue can be minimized by increasing the selective

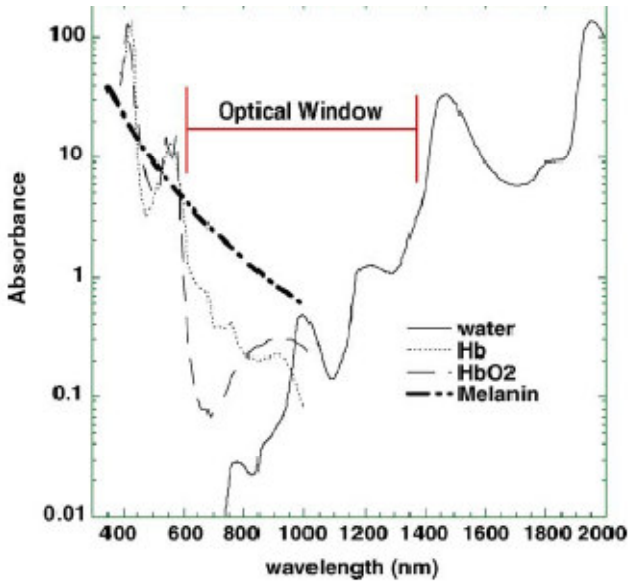

Figure 2.2: Representation of the tissue transparency window

accumulation of the sensitizer in the tumor tissue, and by delivering the light in a spatially confined and focused way. It is therefore important to be able to predict the spatial distribution of light in the target tissue. Light is either scattered or absorbed when it enters tissue and the extent of both processes depends on tissue type and light wavelength because the biological tissue is inhomogeneous and the presence of microscopic inhomogenities (macromolecules, cell organelles, organized cell structure, interstitial layers, etc.). Scattering is generally the most important factor in limiting light penetration into most tissues leading to spreading of a light beam and loss of directionality. Absorption is usually of lesser importance and it is largely due to endogenous tissue chromophores such as hemoglobin, myoglobin and cytochromes. The combination of absorption of lower wavelength light by the important tissue chromophores (oxy and deoxyhemoglobin and melanin) together with reduced light scattering at longer wavelengths and the occurrence of water absorption at wavelengths greater than 1300nm has led to the concept of the ‘‘optical window’’ in tissue (Figure 2.2). In terms of PDT the average effective penetration depth (intensity reduced to 37%) is about 1-3mm at 630 nm, the wavelength used for clinical treatment with Photofrin, while penetration is approximately twice that at 700-850 nm.[158, 159] The absorption of light by the sensitizer itself can limit tissue light penetration. This phenomenon has been termed “self-shielding” and is particularly pronounced with sensitizer that absorb very

strongly at the treatment wavelength.[160] Many sensitizer are prone to photobleaching.[161] This thought to happen when the singlet oxygen or other ROS produced upon illumination reacts with the sensitizer molecule itself in a way that reduces its efficiency for further photosensitization processes. Sensitizer of different chemical structures have widely varying photobleaching rates and in some cases (particularly that of PPIX) the first product of photobleaching is actually a better sensitizer than the starting molecule. Nevertheless photobleaching usually means loss of PDT reactivity but this may still have beneficial effects in term of post-treatment removal of the sensitizer and loss of photosensitivity.

2.4 Mechanism of action

In healthy aerobes, production of ROS is balanced with antioxidant defense system which optimize the levels of most ROS whilst still permitting enough to remain for their essential roles. When this delicate balance is pushed toward the ROS production, cellular damage occurs. Indeed, a disturbance in the prooxidant and antioxidant equilibrium in favor of the former can result from either direct oxidative damage (i.e., increased production of ROS, either by the endogenous system or by exogenous sensitizers) or by failure of repair or replacement systems (i.e., diminished antioxidants). Depending on the nature and on the extent of oxidative stress, cells respond in different ways:

a) Increased proliferation. Many cell types respond to mild oxidative stress by proliferating;
b) Adaption of the cell or organism by upregulation of the defense system which may completely protect against damage, protect against damage to some extent but not completely, or overprotect the cells.
c) Cell injury. This involves damage to some or all molecular targets: lipids, DNA, protein, carbohydrate, etc
d) Senescence. The cell survives but can no longer divide.
e) Cell death. After injury the cell may recover from the oxidative damage by repairing it or by replacing the damaged molecules; or it may survive with persistent oxidative damage; or, oxidative damage may trigger cell death mechanisms.

Indeed, the aim of a PDT sensitizer is to increase the oxidative stress by producing

either singlet oxygen or ROS to such an extent that the target cells die. One of the mechanism of damage to cellular targets by oxidative stress is the lipid peroxidation. This process was defined by Tappel as the oxidative deterioration of polyunsaturated lipids. Indeed, polyunsaturated fatty acids (PUFAs) contains multiple carbon-carbon double bonds which are readily oxidize by both ROS and singlet oxygen, although in a different way. The membranes that surround cells and organelles contain large amount of PUFA along with proteins. Their proximity implies that lipid peroxidation is very likely to damage membrane proteins as well as lipids. Moreover, the membrane structure is tightly related to the chemical structure and distribution of the PUFAs which is made of. For example, if we consider that when the number of double bonds in a fatty acid increases, its melting point drops, it is obvious that the membrane fluidity is largely due to the presence of PUFA sidechains. Damage to PUFAs tends to decrease the number of double bonds in favor of hydroxyl groups, decreasing in such way the membrane fluidity and the proper functioning of the biological membrane. From the chemical point of view, the initiation of lipid peroxidation is caused by addition of a ROS or, more usually, by hydrogen ablation from a methylene group by ROS.

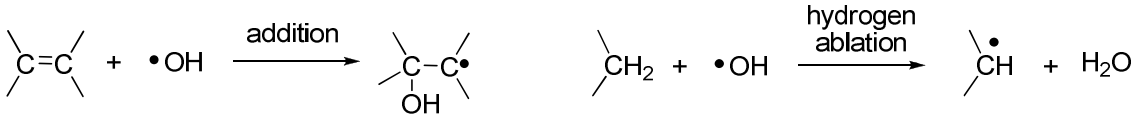

Scheme 2.23

In both cases, a carbon radical results. This is particularly true for allylic hydrogen which reduction potential ($PUFA^{\bullet}$/PUFA) has been estimated as about 0.6 V. Hence hydroxyl (●OH), hydroperoxyl (●OOH), alkoxyl (RO●) and peroxyl (ROO●) are thermodynamically capable of oxidizing PUFAs at allylic hydrogens. Indeed, the rate constant for reaction of ●OH with artificial lecithin bilayers has been measured as higher as $5 \times 10^8 M^{-1}s^{-1}$. By contrast the superoxide radical anion ($O_2^{\bullet -}$) is not sufficiently reactive to abstract an hydrogen from lipids; in any case, the negative charge preclude it from entering the lipid phase of membranes. However, the protonated, uncharged hydroperoxyl radical (●OOH) should enter membranes more easily and it is more reactive toward allylic hydrogens of some PUFAs (e.g., linoleic, lilenic and arachidonic acids) with rate constants although with rate constant much smaller ($\sim 2 \times 10^3 M^{-1}s^{-1}$). In addition, ●OOH can stimulate peroxidation by reaction with preformed lipid hydroperoxides to generate peroxyl radicals.

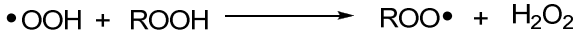

The most likely fate of the carbon radicals generated in the initial stage of lipid peroxidation under aerobic conditions is to combine with the molecular oxygen concentrated inside the lipophilic membranes to give a peroxyl radical (ROO●):

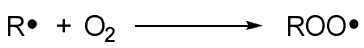

Peroxyl radical can abstract an hydrogen from an adjacent unsaturated fatty acid side-chain during the propagation stage of lipid peroxidation. The new carbon radicals formed can then react with molecular oxygen in a chain reaction to form new peroxyl radicals. A single initiation event thus has the potential to generate multiple peroxide molecules by a chain reaction (Scheme 2.24).

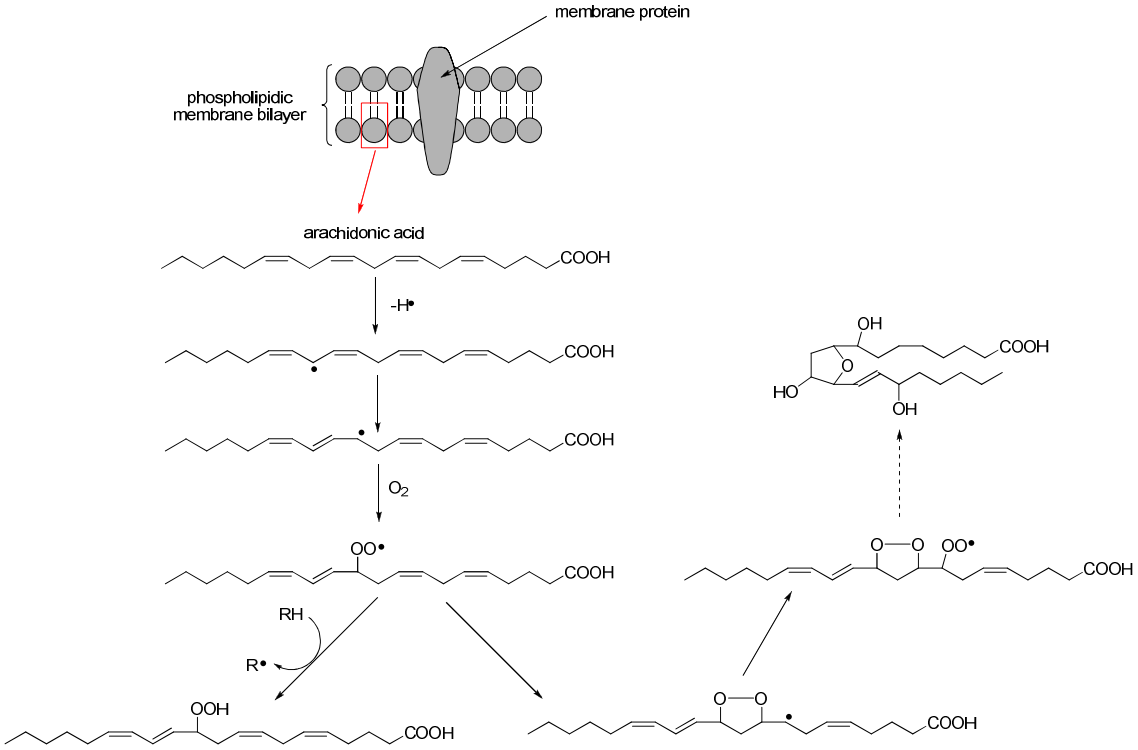

Scheme 2.24: Formation of hydroperoxides and cyclic peroxides from arachidonic acid.

Unlike ROS, singlet oxygen can react with carbon-carbon double bond with an hydrogen in an allylic position to give a hydroperoxide according to the so-called ene reaction (Scheme 2.25).

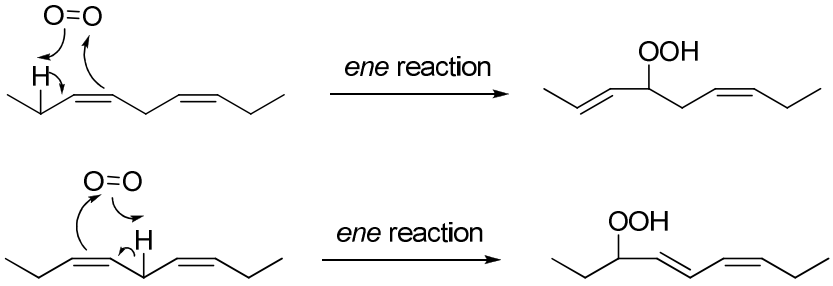

Scheme 2.25: the singlet oxygen *ene* reaction.

For example, reaction of singlet oxygen with linoleic acid gives four isomeric hydroperoxides, two conjugated 9-hydroperoxy-trans-10-cis-12- and 13-hydroperoxy-cis-9-trans-11- octadecadienoic acids and two unconjugated 10-hydroperoxy-trans-8cis-12- and 12-hydroperoxy-trans-9-cis-13-octadecadienoic acids. In contrast, the abstraction of hydrogen by peroxyl radicals of linoleic acid produces a mixture of four cis,trans and trans,trans 9-hydroperoxy-trans-10-cis-12- and 13-hydroperoxy-cis-9-trans-11-octadecadienoic acids (Scheme 2.26). Strictly speaking, singlet oxygen is not initiating peroxidation; unless the peroxides are decomposed to give peroxyl and alkoxyl radicals, a chain reaction will not begin.

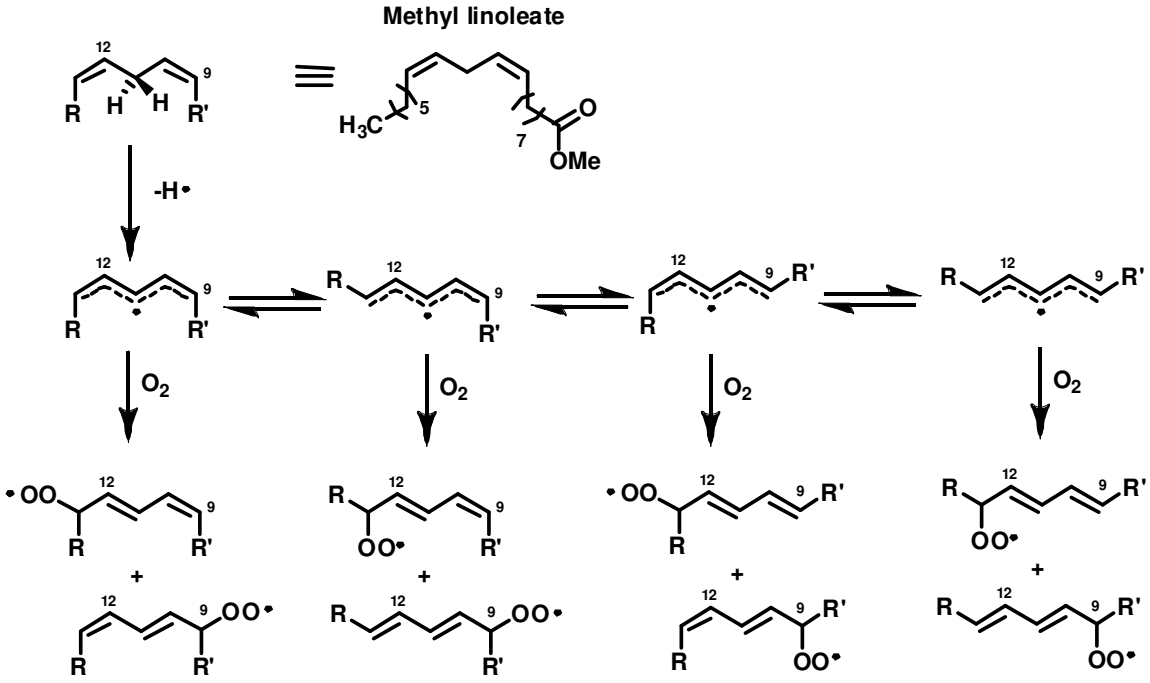

Scheme 2.26

2.5 Biological aspects of PDT sensitizers

The overall aim of photosensitizer bioassay is to provide a procedure which is suitable for clinical PDT. This is a complex process that does not requires uniquely the design of a photosensitizer able to produce singlet oxygen or reactive oxygen species efficiently, but also the development of efficient delivery strategies, a rationale for the subcellular accumulation dynamics, the correct evaluation of each dye farmacokinetics, the choice of an appropriate light source and light dose. Indeed, a perfect match is needed to replicate the photodynamic effect explicated by a sensitizer in solution, in cell

culture and tumor tissues too. It is therefore necessary use a number of preliminary screens and then move to a mammalian model with functioning organs and a vascular system to weed out unpromising photosensitizers and decide on the one explicating PDT activity. In this chapter some of the important biological aspects will be summarized, and some account given of the localization of sensitizers in biological systems.

2.5.1 Preliminary physical tests.

Some physical tests should be done to evaluate the performance of a potential PDT photosensitizer ex vivo and in vivo. Among these, the evaluation of the partition coefficient between water and 1-octanol (logP) provides useful information about the lipophilicity and hydrophilicity of the sensitizer. Singlet oxygen and reactive oxygen species quantum yields should be assigned too along with absorption (molar extinction coefficient) and emission characterization (fluorescence quantum yield). The excited state dynamics is often a crucial tool in the determination of the interaction between the sensitizer and the surrounding environment (molecular oxygen, biological molecules, macromolecules and membranes).

2.5.2 In vitro bioassays

In vitro bioassays are a good way to sort out photosensitizers reducing animal experiments. Bioassays could provide measurement of the pharmacological activity of new or chemically undefined substances, investigation of the function of endogenous mediators, determination of the side-effect profile, including the degree of drug toxicity, measurement of the concentration of known substances (alternatives to the use of whole animals have made this use obsolete). For example, a PDT drug should undergo two experiments before irradiation. First, a study of dark cytotoxicity, to pick out dyes that are not toxic in the absence of light. Second, a qualitative and quantitative study of photosensitizer uptake by tumor cells, by means of confocal fluorescence microscopy to assess subcellular localization and cytofluorimetry to assess the dye concentration in the cellular medium. After irradiation, the photochemical-induced cell kill is being determined against appropriate dark controls. Quantitative cell kill may be determined either by the staining of the dead cells with a dyestuff (e.g., with propidium iodide), followed by counting under a microscope; or by dilution and sub-culture, and counting the new colonies (clonogenic assay). Two in vitro procedures deserve special mention.

(i) Multicellular Tumor Spheroids (MTS) depends on measuring the ability of a photosensitizer to halt the rate growth of a model microtumor. Some tumor cell lines can be cultured as monolayers, and then induced to form small spheres (multicellular tumor spheroids) which continue to grow in a spherical shape. They develop a necrotic center, and in this respect they are thought to be good models for much larger tumors. Such spheroids are placed in growth medium in multi-well plates, and volume is measured with time in the presence and absence of photosensitizer and light. Activity is indicated by a diminution in the rate of growth of the spheroid volume compared with controls.

(ii) MTT assay. This assay is based on 3-(4,5-dimethylthiazol-2-yl)-2,5-diphenyl-2*H*-tetrazolium bromide. Metabolically active mitochondria reduce MTT, which is yellowish, to the corresponding formazan, which is blue. If it is accepted that metabolically active mitochondria signify a living cell, then this offers a convenient and rapid spectroscopic method for estimating cell death.

2.5.3 In vivo bioassays

Assays involving animals are subject to strict regulatory control of both the scientist and the laboratory. Since the results are subject to biological variation it is necessary to have several animals in each group in order to give a reliable mean value. The model tumor may be produced by induction or by subcutaneous or intramuscular transplantation of cells from an established tumor cell line. Animals are selected with tumor of approximately the same size, and treated with the sensitizer. Significantly variables are the drug-light interval, the drug dose, the light fluence, the excitation wavelength. The first hurdle in in vivo assays is to find activity, that is to find a sensitizer of low dark toxicity which efficiently causes tumor photodestruction. Tumor diminution may be measured in a variety of ways. One way is to measure the decrease in the rate of growth of the tumor, by estimating tumor volume at given times after irradiation. A fundamental requirement for PDT drug is tumor selectivity. The second hurdle is selectivity, that is to find a sensitizer that selectively photodamage tumor tissue with respect to normal tissue. There are two objectives here: (i) to diminish damage to normal peritumor tissue, since the area surrounding the tumor will be inevitably receive some irradiation, and (ii) to reduce long term general photosensitivity. Sensitivity could be assessed by subjecting normal tissue in a

sensitized tumor-bearing animal to the same light conditions as the tumor. It is then possible to establish simple indices for damage to normal and tumor tissues, and to plot dose-response curves.[162] Indeed, a PDT procedure requires to reach a fair compromise between sensitizer dose, light conditions, and normal vs. tumor tissue damage indexes.

2.5.4 Subcellular localization

Being singlet oxygen and ROS short-lived species, the damage photoinduced by the sensitizer is circumscribed in its submicrometric neighborhood. It is therefore vital to assess and guide the location of the photosensitizer toward sensible subcellular targets. Indeed, the singlet oxygen lifetime in a biological environment was found to be close to 3 μs. Considering a diffusion coefficient of 2×10^{-5} cm^2s^{-1}, the distance traveled by singlet oxygen in the biological environment is about 268 nm (root-mean-square radial displacement).[163] For radical chain reactions the sphere of reaction could be slightly larger but still within the vicinity of the sensitizer molecule, so photodamage to biological targets could occur quite close to the sensitizer localization area.

Several factors control specificity, selectivity and visibility of the outcome in any staining procedure using dyes. Local concentration of the tissue target often determines the sensitizer concentration, as does the fine structure within the object being stained, which may facilitate or impede diffusion of dyes. Several contributions to affinity control the specificity of staining. These include: (i) electrical forces, which result in accumulation of dye ions in regions of oppositely charged tissue polyions; (ii) weaker short-range attractions (hydrogen bonding, van der Waals forces or (iii) hydrophobic bonding, depending on the solvent) hold dyes ions in contact with their biomacromolecular targets; nonionic forces can also influence the electronic properties of stained sites by either the solvatochromic effect or aggregation; (iv) covalent bonds between dye and tissue result in the strongest binding, such as in methods using Schiff's reagent and possibly also some mordant dyes. The rate at which a reagent gains access to or is removed from targets affects its concentration in cells or tissues. According to Horobin,[164] selective tracking of different organelles within living cells could be predicted by quantitative structure-activity relations (QSAR) of such reagents. Accounts of affinity can focus on the biomolecules constituting cellular structures and emphasize intermolecular forces, such as:

(i) *Electrical interactions*. Interaction of dye ions with tissue polyanions is

substantially influenced by the signs of the electrical charges on the dye and the biomacromolecule. For example, most proteins carry an overall positive charge under acidic conditions and are therefore nonspecifically stained by acid dyes ($Z < 0$) under basic conditions. Tissue polyanions including DNA, ribosomal RNA, and anionic glycosaminoglycans are stained by basic dyes ($Z > 0$) under acidic conditions. The electric charge on unionizable dyes contributes to affinity and controls staining selectivity similarly.

(ii) *Non-coulombic dye–tissue attractions*. Binding of acid and basic dyes to tissue sections is also aided by van der Waals attractions. These non-coulombic forces include short-range forces such as dipole and induced dipole attractions and dispersion forces. These are significant with reagents possessing large aromatic systems. Other non-coulombic specimen-stain interactions can contribute to affinity. Hydrogen bonding involves formation of weak bonds between hydrogen and adjacent electronegative atoms, usually oxygen or nitrogen and plays a vital role in non aqueous environment. Charge transfer phenomena involve partial transfer of charge between electron donor and electron acceptor molecules, resulting in a complex with electronic properties different than the starting material ones. Such effects arise in Romanowsky-Giemsa staining, where azure B and eosin Y molecules accept or donate an electron from or to chromosomes, nuclear chromatin and certain other sites resulting in formation of a complex with an intense magenta color, respectively. The staining phenomenon termed metachromasia appears when highly charged flexible biopolymers provide templates that encourage dye aggregation. In such aggregates, dye ions bind together by short-range forces to give a new electronic entity with new spectral properties.

(iii) *Hydrophobic bonding and other hydrophobic effects*. This phenomenon occurs widely and involves any dye or staining reagent with hydrophobic groupings associating with hydrophobic portions of either the biological substrates or adjacent dye molecules. In the latter case we refer to as metachromasia. Usually, in metachromasia the aromatic rings of basic dyes constitute the hydrophobic domains in aqueous systems. The widespread contribution of hydrophobic bonding to the affinities of routine stains is shown by the routine use of 70% alcohol or 10% DMSO as a differentiating

solvent.

(iv) *Staining involving covalent bond formation*. Two of the most widely employed stains involving covalent bond formation with the specimens are the periodic acid-Schiff (PAS) stain for polysaccharides and the Feulgen stain for DNA. These bonds contribute to staining affinities, and the chemistry of formation defines the selectivity. Both procedures use Schiff's reagent, the reaction product of fuchsine and sodium bisulfite, which combines with aldehyde groups to form a colored product. The different selectivities of the two methods arise from the different reactions used to generate aldehydes. In the PAS method, specimens are treated with an oxidizing agent that generates aldehydes from the sugar residues in polysaccharides. In the Feulgen technique, specimens are subjected to acid hydrolysis, which generates aldehydes from DNA. Other procedures involving formation of stain-specimen covalencies include the thiol-reactive dye, mercury orange, and the protein and polysaccharide reactive procion dyes. Other widely applied methods involve formation of coordinate bonds between an organic grouping and a metal ion. Examples include staining of tissue calcium ions by forming chelates with alizarin red S.

Compounds that accumulate in a given structure by a given mechanism show similar patterns of electric charge (Z), of acid or base strength (pK_a), of hydrophilicity/lipophilicity (evaluated by means of the logP value), of extent of conjugated bond systems (conjugated bond numbers). For instance, small lipophilic cations of strong bases (e.g., rhodamine 123 which has $Z > 0$, $5 > \log P > 0$, and CBN < 40) accumulate in mitochondria, whereas small hydrophilic cations of weak bases (e.g., neutral red which has $Z > 0$, $\log P < -5$, $pK_a \sim 7$, CBN < 40) accumulate in lysosomes. Such relationships can be expressed numerically as quantitative structure activity relations (QSAR). Decision rules based on QSAR, including some relating to the fluorescent probes already mentioned, is given in Table 3.13. These molecular parameters permit the control of sensitiser uptake by cancer tissue to be effective for PDT. Confocal laser scanning fluorescence microscopy has made the determination of intracellular location of sensitizer much easier, and gives more sensitivity and better spatial resolution than earlier non-confocal techniques.[165, 166]

a) *Lysosomes*: in 1993 lysosomes were proposed to be a critical intracellular target for localization of sensitizers.[166] However, succeeding studies[166, 167] have found that although lysosomally localized sensitizer can lead to cell killing upon illumination, the relative efficacy is significantly lower than that seen with sensitizer localized in mitochondria and other organelles. This may be due to the tendency of sensitizer with greater degrees of aggregation to accumulate in lysosomes. Woodburn et al.[167] studied intracellular localization, in V79 Chinese hamster lung fibroblasts and C6 glioma cells, of a series of porphyrins derived from haematoporphyrin and PpIX with side chains chemically modified to give hydrophobic and anionic or cationic residues at physiological pH. Compounds were selected to represent all combinations of these characteristics and it was found that those with a net cationic character localized in mitochondria, while those with net anionic character localized in lysosomes. Nagata et al.[168] showed that the chlorin-based sensitizers, ATX-S10 (Na) had a primary site of accumulation in lysosomes but cells underwent apoptosis upon illumination doses leading to 70% cell death, suggesting that apoptotic pathways may be activated via mitochondrial destabilization following the damage of lysosomes by PDT. Berg et al.[168, 169] used the photochemical internalization technique to incorporated a macromolecule that needed to be delivered into the cell cytoplasm and a aluminum phthalocyanine disulfonate in the lysosomal membrane. On delivery of the correct amount of light the lysosome was ruptured by photochemical damage to its membrane thus releasing the intact macromolecule into the cytoplasm. The initial lysosomal localization may redistribute due to photodynamic action. Indeed, it was found that exposure of cells preincubated with anionic porphyrins resulted in relocalization of the sensitizers from the lysosomes to the cytoplasm and the the nucleus upon photodynamic permeabilization of the lysosomal membrane.[170, 171] Many workers have proposed delivery strategies entailing active targeting to a cell-type specific receptor. This is often accomplished by covalently linking a sensitizer molecules to the specific ligand of the receptor (e.g., carbohydrates, vitamins, proteins, antibodies, fatty acids). When most of these receptors bind their natural ligand to which is covalently attached the sensitizer, the entire construct is internalized into the cell and follows the endosomal-lysosomal pathway discussed above. In many cases sensitizer delivered by this method

gives the most specific lysosomal fluorescence seen in PDT. An example of this is given by the class A scavenger receptors whose expression is specific to mature macrophages is targeted by a conjugate between maleylated albumin and chlorin (e6) delivered to the J774 mouse macrophage tumor cell line (Figure 2.3: In vivo confocal fluorescence images of an orthotopic rat prostate tumor injected with the e6. (A) The image captured 10 min after i.v. injection and (B) same region of the tumor captured 75 min post-injection. Scale bar is 100 µm.).[171] The maleylated albumin is endocytosed after binding to its receptor and the PS ends up specifically localized in lysosomes.

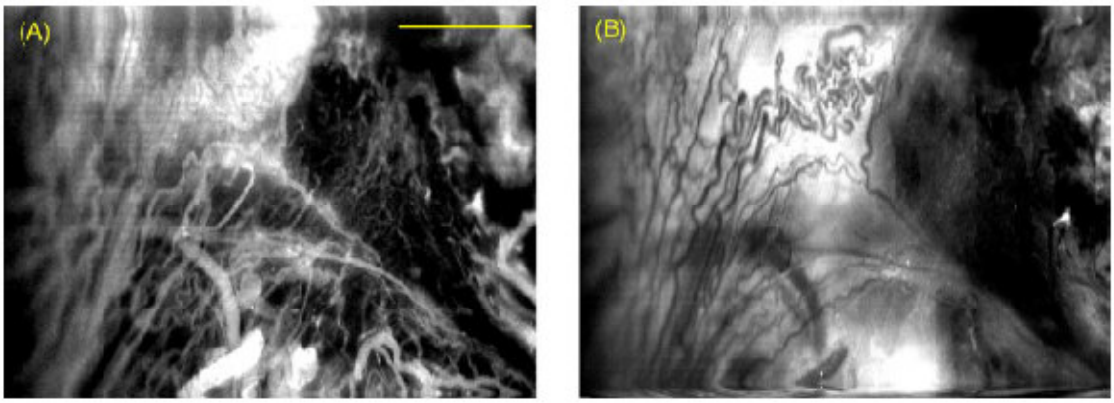

Figure 2.3: In vivo confocal fluorescence images of an orthotopic rat prostate tumor injected with the e6. (A) The image captured 10 min after i.v. injection and (B) same region of the tumor captured 75 min post-injection. Scale bar is 100 µm.

b) *Mitochondria: m*itochondria have been found to be a very important subcellular target in PDT.[172] This is related to the central role plays by mitochondrial in the cell cycle. Indeed, mitochondria are the "cellular power plants" because they generate most of the cell's chemical energy, stored as adenosine triphosphate (ATP). In addition, mitochondria are involved in a range of other processes, such as signaling, cellular differentiation, cell death, as well as the control of the cell cycle and cell growth. Benzoporphyrin derivative (**2.14**) is one of the well-studied mitochondrial sensitizer.[173] Two meso-tetraphenylporphyrin derivatives bearing adjacent: 5,10-di[4-*N*-trimethylaminophenyl]-15,20-diphenylporphyrin (DADP-*a*) or opposite: 5,15-di[4-(*N*-trimethylaminophenyl)-10,20-diphenylporphyrin (DADP-*o*) cationic ammonium groups on two of the *para*-phenyl positions were compared in study by Kessel et al.[174] DADP-*a* localized in mitochondria, while DADP-*o* (a much more symmetric molecule) localized in lysosomes, and led to extensive lysosomal photodamage after irradiation. Oseroff et al. evaluated 10 rhodamine and cyanine dyes as carcinoma-specific

mitochondrial sensitizers in vitro. The most effective, *N*,*N*-bis(2-ethyl-1,3-dioxolane)kryptocyanine, caused marked, light-dependent killing of human bladder, squamous, and colon carcinoma cell lines after 30-min incubations at 1-0.01 μM but was minimally toxic to human keratinocytes and to normal monkey kidney epithelial cells. Dummin et al.[175] prepared cationic zinc (II) phthalocyanines with lipophilic side-chains and showed they specifically accumulated in the inner mitochondrial membranes. On irradiation of the incubated HeLa cells, the cristae were completely destroyed. It was known previously that Pc4 localized in mitochondria and Golgi complexes and ER.[166, 176] At early times (0-1 h) after introduction of Pc 4 to LY-R cells, the dye was found in the mitochondria, lysosomes and Golgi apparatus, as well as other cytoplasmic membranes, but not in the plasma membrane or the nucleus. Over the next 2 h, there was some loss of Pc 4 from the lysosomes but an accumulation in the Golgi apparatus and the mitochondria. The exact binding site of Pc4 was discovered only recently. Pc 4-PDT photodamaged Bcl-2 and Bcl-xL, antiapoptotic proteins interacting with the permeability transition pore complex that forms at contact sites between the inner and outer mitochondrial membranes. These complexes and the inner membrane are unique in containing the phospholipid cardiolipin. Nonyl-acridine orange (NAO) is a specific probe of cardiolipin and Morris et al. showed evidence for fluorescence resonance energy transfer from NAO to Pc 4, defining a binding site for the photosensitizer.

c) *Plasma membrane*

Compounds that localize in plasma membranes of cultured cells are relatively uncommon in the PDT field. Aveline and Redmond[177] showed that deuteroporphyrin IX (DP) and its monobromo and dibromo derivatives localized preferentially in the plasma membrane of L1210 cells. Photofrin shows a dynamic distribution in human carcinoma cells: the plasma membranes are the main target sites of Photofrin after a brief (3 h) incubation, while the Golgi complex is affected after prolonged (24 h) incubation.[178] The effects of PDT on cells with plasma membrane-localized Photofrin was found to be a cessation of proliferation post PDT at dose less than 7 μg/ml, and plasma membrane disruption and cell swelling at higher dose (28 μg/ml).

d) Golgi apparatus and endoplasmic reticulum

Teiten et al.[179] studied Foscan subcellular localization in the MCF-7 human adenocarcinoma cell line by means of confocal microscopy and microspectrofluorometry. The fluorescence topographic revealed that Foscan presents low localization in lysosomes in mitochondria and a marked accumulation in the endoplasmic reticulum (ER) and in the Golgi apparatus.

2.5.5 In vivo localization

a) In vivo localization

Many methods are available for examining the sensitizer localization in whole animals or humans. Fluorescence measurements and radiocounting provide reliable results both in dissected biological sample and in the intact tissue. Within an individual tissue, the localization of the photosensitizer is afflicted by the nature of the different compartments.[180] For example, HpD and water soluble dyes localize in a mouse mammary tumor mainly in the stroma, which constitutes a significant compartment in most solid tumors. On the other end, lipophilic sensitizers which are able to penetrate the tumor cellular membranes tend to be more effective photonecrotic agents. The situation is more complicated when we consider the whole living organism. Most photosensitizers are found in high concentrations in the metabolically vigorous tissues, such as liver, spleen, kidneys, lungs. What is of particular interest is a high ratio of photosensitizer concentration in tumor with respect to concentrations in all other tissues. For example, in Figure 2.4: Tissue/tumor concentration ratios for $AlPcS_4$, AlPc, $TPPS_4$, *m*THPP, PpIX from δ-ALA, and Photofrin in normal and tumor tissues of mice bearing mouse mammary carcinoma C3H/Tif. are represented some tissue/tumor ratios for normal and tumor tissues determined by fluorimetry in mice bearing a C3H/Tif mouse mammary carcinoma 24 h after administration of different photosensitizers. Obviously, the drug uptake depends on the sensitizer molecular structure. Elimination of photosensitizers from the organism depends very much on chemical structure. $AlPcS_4$ and other water-soluble sensitizers are excreted mainly in the urine, while the less soluble *m*-THPC and Photofrin is eliminated mainly in feces as assessed by radioactive labeling studies.

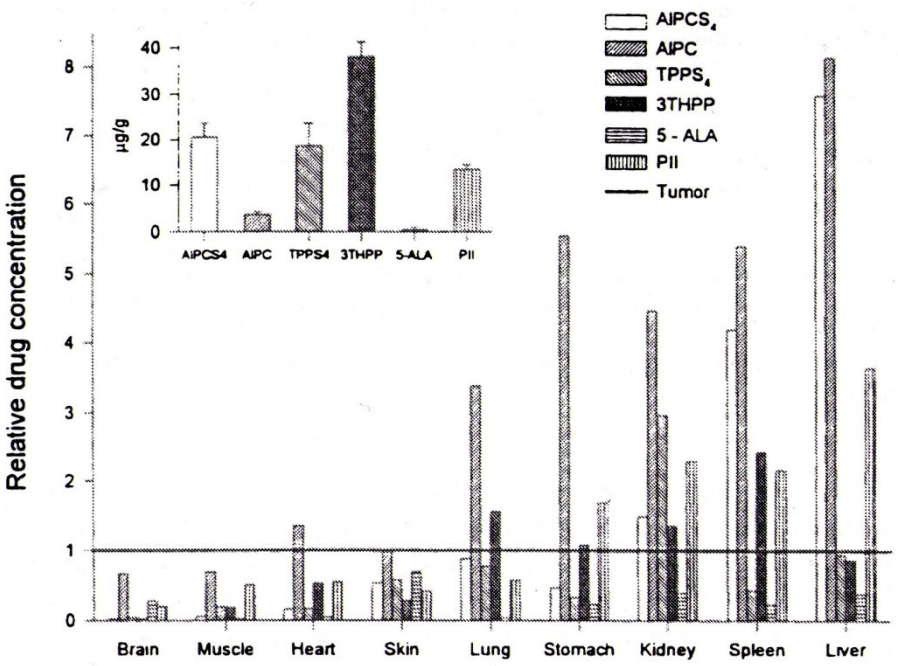

Figure 2.4: Tissue/tumor concentration ratios for $AlPcS_4$, AlPc, $TPPS_4$, *m*THPP, PpIX from δ-ALA, and Photofrin in normal and tumor tissues of mice bearing mouse mammary carcinoma C3H/Tif.

b) Sensitizer pharmacokinetics and biodistribution

When a sensitizer is injected into the bloodstream, it binds to various serum proteins and this can affect its phamacokinetics and distribution. Different sensitizers can have very different pharmacokinetics and this can directly affect the illumination parameters. Intravenously injected sensitizers undergo a transition from being bound to serum proteins, then bound to endothelial cells, then bound to the adventitia of the vessels, then bound either to the extracellular matrix or to the cells within the tumor, and finally to being cleared from the tumor by lymphatics or blood vessels, and excreted either by the kidneys or the liver. The effect of PDT on the tumor largely depends at which stage of this continuous process light is delivered.

The anti-tumor effects of PDT are divided into three main mechanisms:

a) Powerful anti-vascular effects can lead to thrombosis and hemorrhage in tumor blood vessels that subsequently lead to tumor death via deprivation of oxygen and nutrients.
b) Direct tumor cell death by apoptosis or necrosis can occur if the sensitizer has been allowed to be taken up by tumor cells.
c) Finally the acute inflammation and release of cytokines and stress response proteins induced in the tumor can lead to an influx of leukocytes that can both contribute to tumor destruction as well as to stimulate the immune system to

recognize and destroy tumor cells even at distant locations.

We now come to consider the mechanisms that operate when PDT is carried out in vivo. The vast explosion of biomedical research in recent decades has led to the ready availability of multiple animal models of cancer. The choice of the most appropriate animal model of cancer to test PDT is complex and multifactorial and is often not rationally justified. However, the fact that practical light delivery to the tumor is an integral part of PDT means that the majority of reported studies have used subcutaneous tumors.

As previously stated, when a sensitizer is injected into the bloodstream, it must come to equilibrium with the components of the circulating blood, depending on the delivery solvent or vehicle that is used for the injection. This can involve the sensitizer disaggregating from itself or its delivery vehicle and binding instead to either various protein components of serum or circulating cells (e.g., erythrocytes and leukocytes).[181] It is reasonable that the different size and physiological characteristics of blood vessels in the tumor and normal tissues, governs to a great extent where the drug localizes. The sensitizer will then extravasate through the wall of the blood vessel and diffuse throughout the parenchyma of the tumor. Finally, the chromophore will be eliminated from the tissue by lymphatic drainage and excreted from the body. For the majority of sensitizer in clinical use (i.e., Photofrin), excretion is from the liver into the bile and thence to the intestine where it is lost via fecal elimination. Measurement of pharmacokinetics requires sequential measurements of sensitizer concentration in tissue in order to construct temporal profiles that can be compared for different drugs. This procedure require a method to quantify the sensitizer concentration. To this aim, a non-invasive approach with fiber-based fluorescence detection systems is used to monitor continuously the variation over time of a fluorescence signal correlated to the sensitizer concentration.[182, 183]

For example, there has been a wide variation in pharmacokinetics reported for Photofrin in clinical and preclinical use. Bellnier and Dougherty[184] studied pharmacokinetics of Photofrin in patients scheduled to undergo PDT for the treatment of carcinoma of the lung or the skin. They found a triexponential three-compartment pharmacokinetic model 16 h, 7.5 days, and 155.5 days half-lives. Detectable Photofrin fluorescence was shown to persist in the serum for longer than one year. Pharmacokinetic studies in different sensitizers report on lifetimes of 7.77 and 596 h for 2-[1-hexyloxyethyl]-2-devinyl pyropheophorbide-*a*,[185] of 0.5, 7and 80 h for Foscan,[186] 10 min and 20 h for Pc4,[187, 188]

and 2 min and 1.3 h for the palladium bacteriopheophorbide TOOKAD.[187] These dramatic changes in the pharmacokinetics reflect the way a specific sensitizer reaches the tumor tissue after injection and its selectivity for the tumor itself.[189] Indeed, most sensitizers behave as macromolecules when injected into the bloodstream, either because they bind to protein (e.g., albumin, HDL, LDL and VLDL)[190-192] or because they form intermolecular aggregates. However, even this study has been complicated by the fact that the most lipophilic sensitizer are poorly soluble or insoluble in aqueous media and need to be delivered with proper delivery agents. Many progress has been made since the first observations that porphyrins and their derivatives localize in tumors when injected into the bloodstream.[193] A review by Boyle and Dolphin[194] collected tumor-normal tissue ratios for many experimental studies of sensitizers in animal models. Nevertheless. the complexity of comparing different sensitizer structures, different tumor models, and different procedures does not help in defining simple rules to control the tendency of a given sensitizer to preferentially localize in tumors and other specific organs and anatomical sites.[193-197] Though, three classes of photosensitizers, which have tumor localizing properties can be delineated:

(a) hydrophilic compounds (e.g., and tetra-sulfonated derivatives of tetraphenylporphine and chloroaluminum phthalocyanine) which are primarily bound to albumin and globulins;

(b) amphiphilic asymmetric sensitizer (e.g., adjacent disulfonate derivatives of tetraphenylporphine and chloroaluminum phthalocyanine, benzoporphyrin derivative monoacid, LuTex and MACE), which insert into the outer phospholipid and apoprotein layer of lipoprotein particles;

(c) hydrophobic compounds (e.g., unsubstituted phthalocyanines (ZnPC, ClAlPC) naphthalocyanines (isoBOSINC), SnET2), which require a solubilization vehicle such as liposomes,[198-201] natural or synthetic lipoproteins,[197, 202-204] and the castor oil derivative Cremophor EL.[205, 206]

To better understand the mechanisms underlying delivery strategies, it is appropriate to make a distinction between selective accumulation and selective retention. A fast pharmacokinetics is a symptom of selective accumulation in the tumor, while a lower pharmacokinetics is more likely due to selective retention. In the first case, the increased vascular permeability to macromolecules typical of tumor neovasculature is mainly responsible for the preferential extravasation of the sensitizer frequently bind to albumin, which size and Stokes radius are ideal to pass through the “pores” in the

endothelium of the tumor microvessels.[207] The selective retention of sensitizer in tumors has been the subject of much speculation.[197] One of this theory relies on the overexpression of the LDL (apo B/E) receptor by cancer cells.[197, 208] In this way rapidly growing malignant cells supply the amount of lipids (i.e., cholesterol) necessary for the rapid turnover of cellular membranes. Another theory count on the hindered macromolecule extravasion by the poorly developed lymphatic drainage vascular system of tumor tissues.[209]

2.5.6 Mechanisms of tumor destruction

Increasing research is directed towards understanding the mechanisms involved in PDT at both the molecular, cellular and tissue levels. It is expected that it may be possible to more accurately predict response to treatment when sufficient knowledge has been accumulated. Indeed, the discovery of programmed cell death or apoptosis has revolutionized the field of cytotoxic therapies in general and PDT in particular. PDT, on the other hand, tends to operate via an acute stress response involving mitochondrial damage, cytochrome *c* release and formation of an apotosome involving caspase. A second discovery that has had major impact on cell-based PDT research is the field of transcription factors. These are proteins that are often induced by acute insults and bind to certain regions on DNA and therefore lead to transcription of genes and the consequent production of a multitude of proteins that affect cell function and cell death or survival. The search which more closely define the molecular targets of PDT is inherently complex. Different cell types, different PS and different incubation and illumination conditions can all significantly alter the outcome of PDT. The question of whether there are particular cellular proteins that are more susceptible to oxidation by singlet oxygen or other PDT-generated ROS is just starting to be addressed. This question is closely related to the intracellular localization of the sensitizer.

2.5.7 Mechanisms of cell death in PDT

Recent research has elucidated many pathways whereby mammalian cells can die, and some of the ways that PDT can initiate these processes. The concentration, physicochemical properties and subcellular location of the sensitizer, the concentration of oxygen,[210-212] the appropriate wavelength and intensity of the light, and the cell type specific properties may all influence the mode and extent of cell death.

a) Modes of cell death

Kerr was the first to provide evidence[213] that cells may undergo at least two distinct

types of cell death. The first type is necrosis, a form of degeneration affecting extensive cell populations, characterized by cytoplasm swelling, proteolytic activity, destruction of organelle and plasma membranes, leading to the release of intracellular contents and inflammation. Necrosis has generally been considered an unprogrammed process. A different type of cell death, apoptosis, involves single cells usually surrounded by healthy-looking neighbors. In vitro, apoptotic cells are ultimately fragmented into multiple membrane-enclosed spherical vesicles, while in vivo, these apoptotic bodies are scavenged by phagocytes, that prevent inflammation. Apoptosis usually requires transcriptional activation of specific genes and activation of caspases. This situation is further complicated by alternative and concomitant modes of cell death. These include mitotic cell death,[214] programmed necrosis,[215] the cysteine cathepsin mediated lysosomal death pathway,[216] and autophagic cell death.[217] Among the biological stimulus that trigger cell death, caspases are interesting target for PDT because they employ an oxidable cysteine residue at the active site.[218] Effector caspases determines the features of apoptotic cell death by proteolytic cleavage of cellular substrates.[219] Indeed, cell death can be initiated by three different pathways involving caspase 8 (death receptor activation), the endoplasmic reticulum stress pathway involving activation of caspase 12, and the mitochondrial pathway, in which release of proteins (including cytochrome *c*) by mitochondria into the cytoplasm leads to activation of caspase 9 and downstream cleavage of caspase 3, 7 or 6. Effector caspases cleave and inactivate proteins that protect living cells from apoptosis, such as the anti-apoptotic Bcl-2 family protein, which promotes apoptosis via the mitochondria.[220]

Figure 2.5: Cellular signaling pathways leading to apoptosis in cells after PDT.[221]

b) Apoptosis and necrosis after PDT

Because of the intense interest involving cell death mechanisms, workers in the field of PDT have looked at the occurrence of apoptosis and necrosis both in vitro and in vivo.[222]

Figure 2.1 illustrates some of the cellular and molecular signaling pathways that have been determined to occur in cells treated with PDT in vitro. Agarwal et al. were the first to report apoptosis after PDT with chloroaluminum phthalocyanine in mouse lymphoma L5178Y cells.[223] Photosensitizers localized in the plasma membrane can rapidly switch the balance towards necrotic cell death likely causing loss of plasma membrane integrity and rapid depletion of intracellular ATP.[224] It is also possible that high doses of PDT can photochemically inactivate essential enzymes (by protein cross-linking)[225] and other components of the apoptotic cascade such as caspases. Pc4 localizes in the mitochondria inner membrane which is distinctive in containing cardiolipin, a diphosphatidylglycerol derivative with four unsaturated 18-carbon fatty alkyl chains. Cardiolipin photooxidation may impair membrane integrity and impermeability inducing apoptosis by Bcl-2 and Bcl-xL deactivation. In a different study it has been shown that Lutex binds to lysosomes of EMT6 cells in vitro and to produce apoptosis in EMT6 tumors in vivo, indicating that lysosomally bound PSs can induce apoptosis upon

photoactivation.[226] Thibaut et al.[227] used apoptosis inhibitors to study PDT of murine melanoma B16-A45 cells and mTHPC. Although all inhibitors tested blocked PDT-induced apoptosis, none produced a significant modification of the phototoxic effect of mTHPC on B16 cells. It has been suggested that apoptosis and necrosis share common initiation pathways and that the final outcome is determined by the presence of an active caspase. This implies that apoptosis inhibition reorients cells to necrosis, i.e. those cells sufficiently damaged by PDT appear to be killed, regardless of the mechanism involved. Mitochondria were shown to be the main targets of mTHPC in some reports.[228] PDT of mTHPC-sensitized murine leukemia cells caused rapid appearance of the apoptogenic protein cytochrome *c* in the cytosol.

HPD/Photofrin PDT on cells can result in either apoptosis or necrosis of target cells.[151, 227, 229] Indeed, biochemical analysis indicated that HpD/PF PDT elicited lipid peroxidation and enzyme inactivation on plasma membranes, as well as mitochondria damage and inactivation of mitochondrial enzymes.[151]

The situation is more complicated when we change the prospective from the single cell to the tissue. Dahle et al.[230] showed that during in vitro PDT some cells die by direct effect, but adjacent cells suffer lethal cell damage which is propagated through a signaling chain, termed the bystander effect. Treatment of MDCK II cells with tetra(3-hydroxyphenyl)porphyrin induces a rapid apoptotic response characterized by an overabundance of microcolonies that had responded to the treatment as a single unit, in which either all or no cells were dead, indicating that the cells are not inactivated independently. Moreover, the degree of bystander effect was higher for cells dying by necrosis than for cell dying by apoptosis. The cell death topic is always evolving. Indeed, it is not trivial to assess the extent of cell damage and to set the point of no return of cell recovery. Cells are dynamic, complex objects which inrta- and inter-signaling pathways are far to be understood and manipulated.

2.6 Biological application of squaraine dyes

Squaraine dyes are ideal candidates for fluorescence detection in biomedical applications. They possess a sharp and intense absorption, with molar extinction coefficient up to 300000 l mol^{-1} cm^{-1}, and an emission band in the near-IR region, where the autofluorescence from biological samples is minimal. Squaraines are characterized by a very small Stokes shift as expected from polymethine molecules. Their peculiar quadrupolar structure with an electronpoor central moiety ensure greater photostability

and lower photobleaching rates with respect to open-chain cationic cyanines, such as Cy5 or Alexa 647. Squaraines have been extensively used as the signaling units in chemosensors and chemodosimeters because of their absorbance and fluorescence spectra and fluorescence quantum yields which get perturbed with the polarity of the medium, temperature, pH, and other additives. Indeed, the intense absorption and the emission arising from charge transfer transitions during electronic excitation are highly environmentally sensitive.[231] Therefore, squaraine dyes can signal the binding event in the form of measurable changes in their optical properties. For example, the indolenine-based squaraines **2.65a** and **2.66a** have been proved to respond to the alterations in the hydrophobicity of bilayer membranes by a significant increase of their fluorescence intensity and red-shift of emission maximum on going from aqueous to lipidic environment.[232]

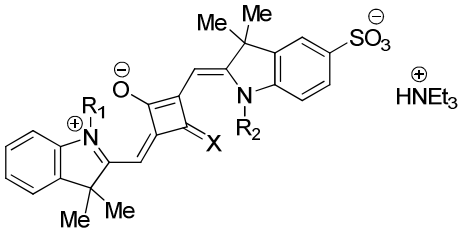

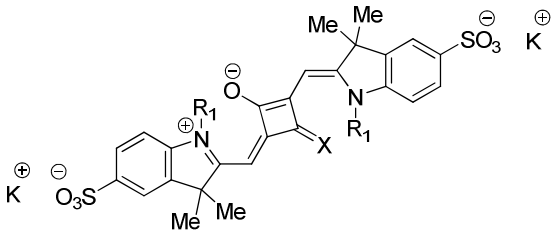

2.65a	X=O	R_1=Me	R_2=$(CH_2)_5COOH$
2.65b	X=$C(CN)_2$	R_1=Me	R_2=$(CH_2)_5COOH$
2.65c	X=S	R_1=Me	R_2=$(CH_2)_5COOH$
2.65d	X=$C(CN)_2$	R_1=$(CH_2)_3COOH$	R_2=Et
2.67a	X=O	R_1=Me	R_2=$(CH_2)_5COOSu$
2.67b	X=$C(CN)_2$	R_1=Me	R_2=$(CH_2)_5COOSu$
2.67c	X=S	R_1=Me	R_2=$(CH_2)_5COOSu$
2.67d	X=$C(CN)_2$	R_1=$(CH_2)_3COOSu$	R_2=Et

2.66a	X=O	R_1=$(CH_2)_3COOH$
2.66b	X=$C(CN)_2$	R_1=$(CH_2)_3COOH$
2.66c	X=S	R_1=$(CH_2)_3COOH$
2.68a	X=O	R_1=$(CH_2)_3COOSu$
2.68b	X=$C(CN)_2$	R_1=$(CH_2)_3COOSu$
2.68c	X=S	R_1=$(CH_2)_3COOSu$

Scheme 2.27

Another example is represented by bis(2,4,6-trihydroxy)phenylsquaraine, which fluorescence quantum yield of <0.002 in aqueous media undergoes a 90-fold enhancement by encapsulation within the lipophilic core of β-cyclodextrin.[233] Being the fluorescence quantum yield an expression of the singlet excited state lifetime, squaraine dyes also show potential as molecular probes in fluorescence lifetime (FLT) based applications.[234] Terpetschnig reported on the spectroscopic properties of the water-soluble indolenine-based squaraines **2.65-2.68** before and after conjugation with bovine serum albumin (BSA).[235] Indeed, these dyes exhibit lower fluorescence quantum yields (Φ_f ~ 0.02-0.10) and shorter fluorescence lifetimes in water (from 0.15 to 0.29 ns for the

free non-symmetrical squaraines **2.65,2.67** and from 0.41 to 0.84 ns for the symmetrical ones **2.66,2.68**) but they show increased brightness (Φ_f ~ 0.13-0.45) and fluorescence lifetimes upon covalent attachment to BSA (from 1.30 to 3.32 ns for **2.65,2.67** and from 1.84 to 3.26 ns for **2.66,2.68**). These properties make them suitable labels for fluorescence binding assays where the binding event is detected by either a change of the fluorescence lifetime or the intensity. Ros-Lis et al. reported a method for the detection of cyanide[236] and thiols[237] based on the reactivity of the electrophilic core of the aniline-based squaraines **2.69** towards this nucleophiles, leading to color bleaching and fluorescence quenching. A similar approach was used by Ajayaghosh et al. in the detection of low molecular weight amino thiols in human blood plasma (HBP).[238] They reported the chemically activable squaraine dye **2.70** that break its conjugation by nucleophilic attack by a thiol exhibiting remarkable changes in absorption and emission.

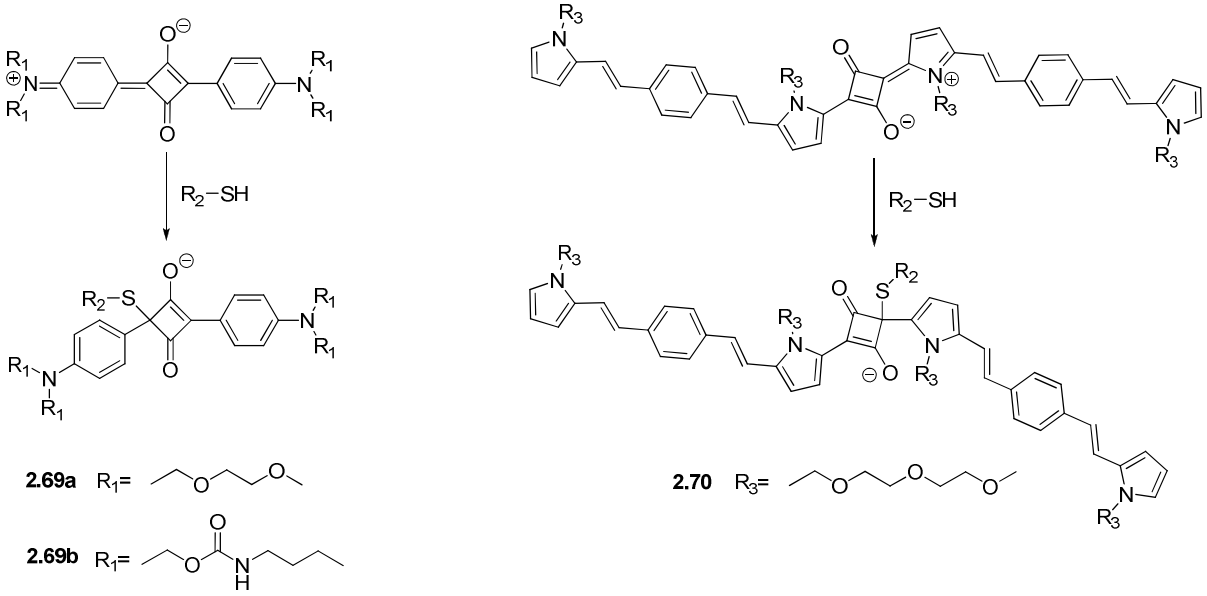

Scheme 2.28

The ease of chemical modification of the squaraine backbone permits the ready incorporation of different reactive functionalities in order to study their interaction with biological targets and the tuning of optical properties.[239] For this reason, squaraine dyes have been widely used as fluorescent protein labels.[240] Oswald et al. modified squaraine dyes with succinimidyl esters and linked covalently them to BSA and human serum albumin (HSA) proteins.[241] The activation to the *N*-hydroxysuccinimide (NHS) ester is achieved by reaction of the carboxy-substituted compound with NHS and dicyclohexylcarbodiimide (DCC) in an inert, dry solvent (e.g. acetonitrile, DMF or DMSO) or by reaction with a small excess of TSTU and DIPEA in dry DMF at room

temperature. The fluorescence quantum yields of the dyes increased from 0.15 to 0.6-0.7 when attached to protein allowing measurements in whole blood at detection limits twice as low as alternate assays employing Cy5. These excellent results has led to the development of Seta dyes, a group of commercially available dyes based on squaraines. Among these, two succinimidyl esters Square-670-NHS and Seta-635-NHS were conjugated to lysozyme (Lz) to explore protein-lipid interactions.[242] Indeed, fluorescence intensity of Square-670-Lz was found to decrease upon association with lipid bilayers, while the fluorescence intensity of Seta-635-Lz displayed more complex behavior depending on lipid-to-protein molar ratio. Moreover a model system Seta-633-biotin was prepared and the biotin/antibiotin interaction was demonstrated by fluorescence lifetime analysis.[243] Furthermore, Terpetschnig et al.[239] studied the interaction of ten squarylium dyes with BSA in the free form and as conjugates. In this case, the symmetrical indolenine-based squaraines displayed a 28-fold fluorescence intensity increase upon proteins binding. A similar work by Welder et al.[244] described the interaction of 3-oxosubstituted squaraines in presence of various proteins. They concluded that both the symmetrical and unsymmetrical squarylium dyes showed enhancement of fluorescence intensity upon noncovalent interactions with proteins such as HSA, β-lactoglobulin A and trypsinogen. More recently, Yarmoluk et al.[245] synthesized and evaluated structure-properties relationships in the series of 3-oxo- and 3-dicyanomethylene squaraines containing indolenine, benzothiazole and benzoxazole moieties **2.71-2.72** for detection of a variety of proteins such as bovine BSA, HSA, ovalbumin, avidin from hen egg white (AVI), and hydrolases such as trypsine and lysozyme. All investigated squaraines show considerable emission increase in the presence of BSA only; fluorescence enhancing of the dyes in the presence of other albumins (HSA and ovalbumin) is significantly lower, while in the presence of hydrolases lysozyme or trypsin studied squaraines either insignificantly increased or even decreased their fluorescence intensity.

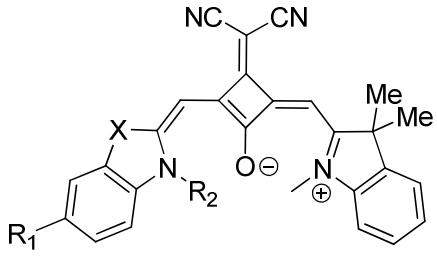

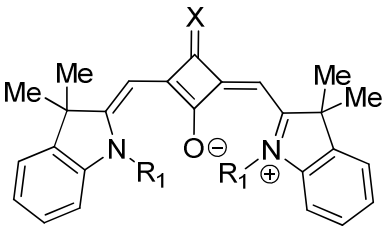

2.71a	X=O	R_1=H	R_2=Me	**2.72a**	X=NHBu	R_1=Me
2.71b	X=S	R_1=H	R_2=Me	**2.72b**	X=NHBu	R_1=Et
2.71c	X=$C(CH_3)_2$	R_1=Me	R_2=$(CH_2)_5COOH$	**2.72c**	X=NEt_2	R_1=Me
2.71d	X=$C(CH_3)_2$	R_1=$SO_3^{\ominus}$	R_2=$(CH_2)_5COOH$	**2.72d**	X=$C(CN)_2$	R_1=$Me^{\ominus}$

Scheme 2.29

Thomas et al. described the synthesis and glucose-biosensing performance of aniline- and benzothiazolium-based squaraines functionalized with a thiol-reactive iodoacetyl group when conjugated to mutants of the D-glucose/D-galactose-binding protein (GGBP).[246, 247] They found that the fluorescence intensity of the dye underwent significant changes in the presence of glucose, because of polarity changes in the squaraine binding site.

Squaraine dyes have also been successfully employed as second generation photosensitizers for photodynamic therapy (PDT). This well-established medical treatment involves the insurgence of cytotoxic species in the cellular environment following irradiation of a suitable dye with visible light in the presence of molecular oxygen. Due to their intense absorption and emission properties in the transparency window of biological tissue (600-900 nm), many squaraine families have been look for potential applications in PDT. Among these squaraines deriving from heteoaryl anhydrobases,[121, 122, 248] aniline,[249] pyrrole,[123, 250] indolizine,[123] quinoline,[251] and trihydroxybenzene[252, 253] derivatives have been reported. Despite the huge effort in the synthesis, few of these dyes have been further investigated in cell lines and animal bearing tumors. Ramaiah et al.[252] have reported that the halogenation of trihydroxy-based squaraines is essential to exploit the PDT efficacy in AS52 Chinese hamster ovary cells. Indeed, the tetraiodo-derivative **2.73** caused a considerable reduction of tumor volume in mice bearing a skin tumor.[254]

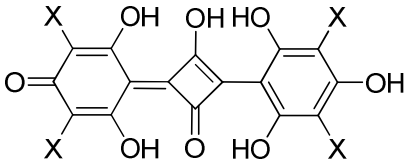

2.73a X=H
2.73b X=I
2.73c X=Br

Moreover, some of us tested the photosensitizing properties of benzothiaziole-based mono- and bis-squaraines in four different cancer cell lines. We found that in the dark these squaraines are largely nontoxic, but when they are irradiated with white light at a fluence of 15 J/cm^2, they promote a strong photodynamic effect that causes cell death in all tested cells. Since the transport of the sensitizer through cell membrane is critical to its effectiveness, different strategies have been studied in this regard. Good water solubility and resistance to the formation of ground state interactions are indeed desirable properties for biological fluorescent labels and PDT sensitizers. Though, squaraine dyes are generally not soluble in water. Their solubility have been increased by the introduction of polar functional groups, such as the sulfonate group,[235, 245] carbohydrates,[251] quaternary ammonium groups,[234] the carboxyl group,[234] polyethylene glycol residues,[123, 255, 256] hydroxyl groups,[257] and phosphonic group.[258] Other strategies take advantage of the strong affinity of some squaraines (i.e, trihydroxybenzene-based squaraines) with BSA[257] and of the synthesis of cholesterol conjugated dyes[251] to enhance cell permeability and perform their photodynamic effect. The low solubility of squaraines afflict also their propensity to aggregate, which reduces the amount of reactive oxygen species generated. The sterically protected squaraine-rotaxanes are indeed more resistant to aggregation, photooxidation, and chemical bleaching by biological nucleophiles, while retaining their photophysical behavior.[249]

Bibliography

1. Raab, O., Ueber die Wirkung fluorescirender Stoffe auf Infusorien. *Z Biol* **1900,** *39*, 524-546.

2. Von Tappeiner, H.; Jodlbauer, A., Über die Wirkung der photodynamischen (fluorescierenden) Stoffe auf Protozoen und Enzyme. *Dtsch Arch Klin Med* **1904,** *80*, 427-87.

3. Jodlbauer, A.; von Tappeiner, H., Die Beteiligung des Sauerstoffs bei der Wirkung fluorescierender Stoffe. *Dtsch. Arch. Klin. Med* **1905,** *82*, 520-546.

4. Hausmann, W., Die sensibilisierende Wirkung des hämatoporphyrins. *Biochem* **1911,** *30*, 276-316.

5. Pfeiffer, H., Der Nachweis photodynamischer Wirkungen fluoreszierender Stoffe am lebenden Warmblüter. *Handbuch der Biochemischen Arbeitsmethoden. Urban und Schwarzenberg, Berlin* **1911**, 563-571.

6. Meyer-Betz, F., Untersuchungen über die biologische (photodynamische) Wirkung des Hämatoporphyrins und anderer Derivate des Blut-und Gallenfarbstoffs. *Dtsch Arch Klin Med* **1913,** *112*, 476-503.

7. Policard, A., Etude sur les aspects offerts par des tumeurs experimentales examinees a la lumiere de Wood. *CR Soc Biol* **1924,** *91*, 1423-1424.

8. Fischer, H.; Hilmer, H.; Lindner, F.; Puetzer, B., Zur kenntnis der naturlichen porphyrine: chemische befund bei einem fall von porphyrinurie (Petry). *Hoppe Seylers Z Physiol Chem* **1925,** *150*, 44.

9. Korbler, J., Untersuchung von Krebsgewebe im fluoreszenzerregenden Licht. *Strahlentherapie* **1931,** *41*, 510–518.

10. Schwartz, S., Absolon K, Vermund H. Some relationship of porphyrins, x-rays and tumors. *Bull Univ Minnesota Med Sch* **1955,** *27*, 7-13.

11. Dougherty, T., Photosensitizers: therapy and detection of malignant tumors. *Photochemistry and Photobiology* **1987,** *45*, 879-889.

12. Moan, J.; Christensen, T.; Sommer, S., The main photosensitizing components of hematoporphyrin derivative. *Cancer letters* **1982,** *15* (2), 161.

13. Moan, J.; Sandberg, S.; Christensen, T.; Elander, S., Hematoporphyrin derivative: chemical composition, photochemical and photosensitizing properties. *Advances in experimental medicine and biology* **1983,** *160*, 165.

14. Moan, J.; Sommer, S., Uptake of the components of hematoporphyrin derivative by cells and tumours. *Cancer letters* **1983,** *21* (2), 167.

15. Dougherty, T., A brief history of clinical photodynamic therapy development at Roswell Park Cancer Institute. *Journal of Clinical Laser Medicine & Surgery* **1996,** *14* (5), 219-221.

16. Winkelman, J., The distribution of tetraphenylporphinesulfonate in the tumor-bearing rat. *Cancer research* **1962,** *22* (5 Part 1), 589.

17. Ben-Hur, E.; Rosenthal, I., Photosensitized inactivation of Chinese hamster cells by phthalocyanines. *Photochemistry and Photobiology* **1985,** *42* (2), 129-133.

18. Moan, J., Porphyrin photosensitization and phototherapy. *Photochemistry and Photobiology* **1986,** *43* (6), 681-690.

19. PAQUETTE, B.; ALI, H.; LANGLOIS, R.; LIER, J., Biological activities of phthalocyanines-VIII. Cellular distribution inV-79 Chinese hamster cells and phototoxicity of selectively sulfonated aluminum phthalocyanines. *Photochemistry and Photobiology* **1988,** *47* (2), 215-220.

20. BERG, K.; BOMMER, J.; MOAN, J., Evaluation of sulfonated aluminum phthalocyanines for use in photochemotherapy. A study on the relative efficiencies of photoinactivation. *Photochemistry and Photobiology* **1989,** *49* (5), 587-594.

21. Peng, Q.; Farrants, G.; Madslien, K.; Bommer, J.; Moan, J.; Danielsen, H.;

Nesland, J., Subcellular localization, redistribution and photobleaching of sulfonated aluminum phthalocyanines in a human melanoma cell line. *International Journal of Cancer* **1991,** *49* (2).

22. Berenbaum, M.; Akande, S.; Bonnett, R.; Kaur, H.; Ioannou, S.; White, R.; Winfield, U., meso-Tetra (hydroxyphenyl) porphyrins, a new class of potent tumour photosensitisers with favourable selectivity. *British journal of cancer.* **1986,** *54* (5), 717-725.

23. Dougherty, T.; Gomer, C.; Henderson, B.; Jori, G.; Kessel, D.; Korbelik, M.; Moan, J.; Peng, Q., Photodynamic therapy. *J. Natl. Cancer Inst.* **1998,** *90* (12), 889-905.

24. Peng, Q.; Berg, K.; Moan, J.; Kongshaug, M.; Nesland, J., 5-Aminolevulinic acid-based photodynamic therapy: principles and experimental research. *Photochemistry and Photobiology* **1997,** *65* (2), 235-251.

25. Malik, Z.; Lugaci, H., Destruction of erythroleukaemic cells by photoactivation of endogenous porphyrins. *British journal of cancer* **1987,** *56* (5), 589.

26. Kennedy, J.; Pottier, R.; Pross, D., Photodynamic therapy with endogenous protoporphyrin IX: basic principles and present clinical experience. *Journal of photochemistry and photobiology. B, Biology* **1990,** *6* (1-2), 143.

27. Morone, M.; Beverina, L.; Abbotto, A.; Silvestri, F.; Collini, E.; Ferrante, C.; Bozio, R.; Pagani, G., Enhancement of Two-Photon Absorption Cross-Section and Singlet-Oxygen Generation in Porphyrins upon [beta]-Functionalization with Donor Acceptor Substituents. *Org. Lett* **2006,** *8* (13), 2719-2722.

28. Sastre, A.; Torres, T.; Hanack, M., Synthesis of novel unsymmetrical monoaminated phthalocyanines. *Tetrahedron Letters* **1995,** *36* (46), 8501-8504.

29. Claessens, C.; Hahn, U.; Torres, T., Phthalocyanines: From outstanding electronic properties to emerging applications. *Chemical Record* **2008,** *8* (2), 75.

30. Nonell, S.; Rubio, N.; Rey, B.; Torres, T., Synthesis, optical absorption and photophysical properties of cone-shaped subnaphthalocyanine. *Journal of the Chemical Society, Perkin Transactions 2* **2000,** *2000* (6), 1091-1094.

31. Martí, C.; Nonell, S.; Nicolau, M.; Torres, T., Photophysical properties of neutral and cationic tetrapyridinoporphyrazines. *Photochemistry and Photobiology* **2000,** *71* (1), 53-59.

32. Claessens, C.; de la Torre, G.; Torres, T. In *The singular optical properties of phthalocyanines: from photosensitizers for photodynamic therapy to nonlinear optical applications (Invited Paper)*, 2005; p 379.

33. Schumm, O., Bemerkung zu dem Vortrag von Hans Fischer: Uber Porphyrine und ihre Synthesen. *Berichte der deutschen chemischen Gesellschaft (A and B Series)* **1928,** *61* (4).

34. Bonnett, R.; McManus, K., Approaches to the stepwise synthesis of benzoporphyrins and phthalocyanines. Part 1. Synthesis of *opp*-dibenzoporphyrins (dibenzo [*g*,*q*] porphyrins). *Journal of the Chemical Society, Perkin Transactions 1* **1996,** *1996* (20), 2461-2466.

35. Grigg, R.; Johnson, A.; Kenyon, R.; Math, V.; Richardson, K., The cyclisation of 1-bromo-19-methyl-and 1, 19-dimethyl-1, 19-dideoxybiladiene-ac dihydrobromides. *Journal of the Chemical Society C: Organic* **1969,** *1969* (2), 176-182.

36. Woodward, R.; Ayer, W.; Beaton, J.; Bickelhaupt, F.; Bonnett, R.; Buchschacher, P.; Closs, G.; Dutler, H.; Hannah, J.; Hauck, F., The total synthesis of chlorophyll a. *Tetrahedron* **1990,** *46* (22), 7599-7659.

37. Tarlton, E. J.; MacDonald, S. F.; Baltazzi, E., Uroporphyrin 31. *Journal of the American Chemical Society* **2002,** *82* (16), 4389-4395.

38. Adler, A. D.; Longo, F. R.; Finarelli, J. D.; Goldmacher, J.; Assour, J.; Korsakoff, L., A simplified synthesis for *meso*-tetraphenylporphine. *The Journal of Organic Chemistry* **1967,** *32* (2), 476-476.

39. Rothemund, P., Formation of porphyrins from pyrrole and aldhehydes. *Journal of the American Chemical Society* **2002,** *57* (10), 2010-2011.

40. Ono, N.; Miyagawa, H.; Ueta, T.; Ogawa, T.; Tani, H., Synthesis of 3, 4-diarylpyrroles and conversion into dodecaarylporphyrins; a new approach to porphyrins with altered redox potentials. *Journal of the Chemical Society, Perkin Transactions 1* **1998,** *1998* (10), 1595-1602.

41. Lindsey, J. S.; Schreiman, I. C.; Hsu, H. C.; Kearney, P. C.; Marguerettaz, A. M., Rothemund and Adler-Longo reactions revisited: synthesis of tetraphenylporphyrins under equilibrium conditions. *The Journal of Organic Chemistry* **2002,** *52* (5), 827-836.

42. Bonar-Law, R. P., Porphyrin Synthesis in Surfactant Solution: Multicomponent Assembly in Micelles. *The Journal of Organic Chemistry* **1996,** *61* (11), 3623-3634.

43. Winkelman, J., The Distribution of Tetraphenylporphinesulfonate in the Tumor-bearing Rat. *Cancer Res* **1962,** *22* (5_Part_1), 589-596.

44. Bonnett, R.; White, R.; Winfield, U.; Berenbaum, M., Hydroporphyrins of the meso-tetra (hydroxyphenyl) porphyrin series as tumour photosensitizers. *Biochem J* **1989,** *261* (1), 277-80.

45. Dilkes, M.; DeJode, M.; Rowntree-Taylor, A.; McGilligan, J.; Kenyon, G.; McKelvie, P., m-THPC photodynamic therapy for head and neck cancer. *Lasers in Medical Science* **1996,** *11* (1), 23-29.

46. Mironov, A.; Efremov, A.; Efremova, O.; Bonnett, R.; Martinez, G., Chlorins with an exocyclic -lactone ring and their derivatives. *Journal of the Chemical Society, Perkin Transactions 1* **1998,** *1998* (21), 3601-3608.

47. Kennedy, J.; Pottier, R., Endogenous protoporphyrin IX, a clinically useful photosensitizer for photodynamic therapy. *Journal of photochemistry and photobiology. B, Biology* **1992,** *14* (4), 275.

48. Kennedy, J. C.; Marcus, S. L.; Pottier, R. H., Photodynamic Therapy (PDT) and Photodiagnosis (PD) Using Endogenous Photosensitization Induced by 5-Aminolevulinic Acid (ALA): Mechanisms and Clinical Results. *Journal of Clinical Laser Medicine & Surgery* **1996,** *14* (5), 289-304.

49. Qian Peng; Trond Warloe; Kristian Berg; Johan Moan; Magne Kongshaug; Karl-Erik Giercksky; Jahn M. Nesland, 5-Aminolevulinic acid-based photodynamic therapy. *Cancer* **1997,** *79* (12), 2282-2308.

50. Tabata, K.; Ogura, S.-i.; Okura, I., Photodynamic Efficiency of Protoporphyrin IX: Comparison of Endogenous Protoporphyrin IX Induced by 5-Aminolevulinic Acid and Exogenous Porphyrin IX. *Photochemistry and Photobiology* **1997,** *66* (6), 842-846.

51. Gurinovich, G.; Zorina, T.; Melnov, S.; Melnova, N.; Gurinovich, I.; Grubina,

L.; Sarzhevskaya, M.; Cherenkevich, S., Photodynamic activity of chlorin e 6 and chlorin e 6 ethyelenediamide in vitro and in vivo. *Journal of photochemistry and photobiology. B, Biology* **1992,** *13* (1), 51-57.

52. Pandey, R.; Bellnier, D.; Smith, K.; Dougherty, T., Chlorin and porphyrin derivatives as potential photosensitizers in photodynamic therapy. *Photochemistry and Photobiology* **1991,** *53* (1), 65-72.

53. Adams, K.; Berenbaum, M.; Bonnett, R.; Nizhnik, A.; Salgado, A.; Vallés, M., Second generation tumour photosensitisers: the synthesis and biological activity of octaalkyl chlorins and bacteriochlorins with graded amphiphilic character. *Journal of the Chemical Society, Perkin Transactions 1* **1992,** *1992* (12), 1465-1470.

54. Zenkevich, E.; Sagun, E.; Knyukshto, V.; Shulga, A.; Mironov, A.; Efremova, O.; Bonnett, R.; Songca, S. P.; Kassem, M., Photophysical and photochemical properties of potential porphyrin and chlorin photosensitizers for PDT. *Journal of Photochemistry and Photobiology B: Biology* **1996,** *33* (2), 171-180.

55. Kessel, D.; Woodburn, K.; Gomer, C. J.; Jagerovic, N.; Smith, K. M., Photosensitization with derivatives of chlorin p6. *Journal of Photochemistry and Photobiology B: Biology* **1995,** *28* (1), 13-18.

56. Kozyrev, A. N.; Zheng, G.; Lazarou, E.; Dougherty, T. J.; Smith, K. M.; Pandey, R. K., Syntheses of emeraldin and purpurin-18 analogs as target-specific photosensitizers for photodynamic therapy. *Tetrahedron Letters* **1997,** *38* (19), 3335-3338.

57. Lee, S.; Jagerovic, N.; Smith, K., Use of the chlorophyll derivative, purpurin-18, for syntheses of sensitizers for use in photodynamic therapy. *Journal of the Chemical Society. Perkin transactions. I* **1993,** (19), 2369-2377.

58. Mironov, A. F.; Lebedeva, V. S., Cyclic N-hydroxyimides in a series of chlorins and porphyrins. **1998,** *39*, 905-908.

59. Mironov, A. F.; Efremov, A. V.; Efremova, O. g. A.; Bonnett, R., Novel Chlorins with a δ-Lactone Ring fused at Ring D. *Tetrahedron Letters* **1997,** *38* (38), 6775-6778.

60. Kozyrev, A.; Pandey, R., LiOH promoted allomerization of pyropheophorbide a. A convenient synthesis of 13^2-oxopyropheophorbide *a* and its unusual enolization. *Chemical Communications* **1998,** *1998* (4), 481-482.

61. Nelson, J. S.; Roberts, W. G.; Berns, M. W., *In Vivo* Studies on the Utilization of Mono-L-aspartyl Chlorin (NPe6) for Photodynamic Therapy. *Cancer Res* **1987,** *47* (17), 4681-4685.

62. Gomi, S.; Nishizuka, T.; Ushiroda, O.; Uchida, N.; Takahashi, H.; Sumi, S., The structures of mono-L-aspartyl chlorin e_6 and its related compounds. *Heterocycles* **1998,** *48* (11), 2231-2243.

63. Gerlach, B.; Montforts, F., Azachlorins: Synthesis of a novel type of hydroporphyrins from the bile pigment bilirubin. *Liebigs Annalen* **1995,** (8).

64. Linstead, R.; Weiss, F., Phthalocyanines and related compounds-Part XX. Further investigations on tetrabenzoporphin and allied substances. *J Chem Soc* **1950**, 2975-2981.

65. Bender, C.; Bonnett, R.; Smith, R., The chemistry of 1, 3, 4, 7-

tetramethylisoindole and a route to the tetrabenzporphyrin system. *Journal of the Chemical Society C: Organic* **1970,** *1970* (9), 1251-1257.

66. Clezy, P.; Fookes, C.; Mirza, A., The chemistry of pyrrolic compounds. XXXVII. Monobenzoporphyrins: The rhodoporphyrin of petroleum deposits. *Australian Journal of Chemistry* **1977,** *30* (6), 1337-1347.

67. Tomé, A.; Lacerda, P.; Neves, M.; Cavaleiro, J., *meso*-Arylporphyrins as dienophiles in Diels–Alder reactions: a novel approach to the synthesis of chlorins, bacteriochlorins and naphthoporphyrins. *Chemical Communications* **1997,** *1997* (13), 1199-1200.

68. Nguyen, L. T.; Senge, M. O.; Smith, K. M., Simple Methodology for Syntheses of Porphyrins Possessing Multiple Peripheral Substituents with an Element of Symmetry. *The Journal of Organic Chemistry* **1996,** *61* (3), 998-1003.

69. Valles, M. A.; Biolo, R.; Bonnett, R.; Canete, M.; Gomez, A. M.; Jori, G.; Juarranz, A.; McManus, K. A.; Okolo, K. T.; Soncin, M.; Villanueva, A. In *Benzoporphyrins as photosenitizers for the photodynamic therapy of cancer*, Photochemotherapy: Photodynamic Therapy and Other Modalities, Barcelona, Spain, SPIE: Barcelona, Spain, 1996; pp 11-22.

70. Linstead, R., 212. Phthalocyanines. Part I. A new type of synthetic colouring matters. *Journal of the Chemical Society (Resumed)* **1934,** *1934*, 1016-1017.

71. Byrne, G.; Linstead, R.; Lowe, A., 213. Phthalocyanines. Part II. The preparation of phthalocyanine and some metallic derivatives from o-cyanobenzamide and phthalimide. *Journal of the Chemical Society (Resumed)* **1934,** *1934*, 1017-1022.

72. Dent, C.; Linstead, R.; Lowe, A., 217. Phthalocyanines. Part VI. The structure of the phthalocyanines. *Journal of the Chemical Society (Resumed)* **1934,** *1934*, 1033-1039.

73. Robertson, J., 136. An X-ray study of the structure of the phthalocyanines. Part I. The metal-free, nickel, copper, and platinum compounds. *Journal of the Chemical Society (Resumed)* **1935,** *1935*, 615-621.

74. Leznoff, C.; Hu, M.; Nolan, K., The synthesis of phthalocyanines at room temperature. *Chemical Communications* **1996,** *1996* (10), 1245-1246.

75. Wöhrle, D.; Muller, S.; Shopova, M.; Mantareva, V.; Spassova, G.; Vietri, F.; Ricchelli, F.; Jori, G., Effect of delivery system on the pharmacokinetic and phototherapeutic properties of bis (methyloxyethyleneoxy) silicon-phthalocyanine in tumor-bearing mice. *Journal of Photochemistry & Photobiology, B: Biology* **1999,** *50* (2-3), 124-128.

76. Shopova, M.; Mantareva, V.; Krastev, K.; Hadjiolov, D.; Mil-ev, A.; Spirov, K.; Jori, G.; Ricchelli, F., Comparative pharmacokinetic and photodynamic studies with zinc (II) phthalocyanine in hamsters bearing an induced or transplanted rhabdomyosarcoma. *J. Photochem. Photobiol. B* **1992,** *16*, 83-89.

77. Fabric, C.; Ometto, C.; Milanesi, C.; Jori, G.; Cook, M.; Russell, D., Tumour-localizing and tumour-photosensitizing properties of zinc (II)-octapentyl-phthalocyanine. *Journal of Photochemistry & Photobiology, B: Biology* **1997,** *39* (3), 279-284.

78. Griffiths, J.; Schofield, J.; Wainwright, M.; Brown, S. B., Some observations on the synthesis of polysubstituted zinc phthalocyanine sensitisers for photodynamic

therapy. *Dyes and Pigments* **1997,** *33* (1), 65-78.

79. Stranadko, E.; Skobelkin, O.; Litwin, G.; Astrakhankina, T. In *Clinical photodynamic therapy of malignant neoplasms [2325-32]*, SPIE INTERNATIONAL SOCIETY FOR OPTICAL: 1994; pp 240-240.

80. Stranadko, E.; Skobelkin, O.; Vorozhtsov, G.; Mironov, A.; Beshleul, S.; Markitchev, N.; Riabov, M. In *Photodynamic therapy of cancer: five-year clinical experience*, 1997; p 253.

81. Hu, M.; Brasseur, N.; Yildiz, S. Z.; van Lier, J. E.; Leznoff, C. C., Hydroxyphthalocyanines as Potential Photodynamic Agents for Cancer Therapy. *Journal of Medicinal Chemistry* **1998,** *41* (11), 1789-1802.

82. Lukyanets, E., Phthalocyanines as photosensitizers in the photodynamic therapy of cancer. *Journal of Porphyrins and Phthalocyanines* **1999,** *3* (67), 424-432.

83. Zaidi, S. I. A.; Agarwal, R.; Eichler, G.; Rihter, B. D.; Kenney, M. E.; Mukhtar, H., Photodynamic effects of new silicon phthalocyanines: in vitro studies using rat hepatic microsomes and human erythrocyte ghosts as model membrane sources. *Photochemistry and Photobiology* **1993,** *58* (2), 204-210.

84. Shopova, M.; Woehrle, D.; Mantareva, V.; Mueller, S., Naphthalocyanine Complexes as Potential Photosensitizers for Photodynamic Therapy of Tumors. *Journal of Biomedical Optics* **1999,** *4*, 276.

85. Biolo, R.; Jori, G.; Soncin, M.; Pratesi, R.; Vanni, U.; Rihter, B.; Kenney, M.; Rodgers, M., Photodynamic therapy of B16 pigmented melanoma with liposome-delivered Si (IV)-naphthalocyanine. *Photochemistry and Photobiology* **1994,** *59* (3), 362-365.

86. Kachkovski, A. D.; Dekhtyar, M. L., Electronic properties of polymethine compounds : 2. Electron Donor Ability and Relative Stability. *Dyes and Pigments* **1993,** *22* (2), 83-97.

87. Zhu, Z., Thirty-five years of studies on the chemistry of polymethine cyanine dyes. *Dyes and Pigments* **1995,** *27* (2), 77-111.

88. Cohen, L.; Salzberg, B.; Davila, H.; Ross, W.; Landowne, D.; Waggoner, A.; Wang, C., Changes in axon fluorescence during activity: molecular probes of membrane potential. *Journal of Membrane Biology* **1974,** *19* (1), 1-36.

89. Lin, H.-Y.; Chen, C.-T.; Huang, C.-T., Use of Merocyanine 540 for Photodynamic Inactivation of *Staphylococcus aureus* Planktonic and Biofilm Cells. *Appl. Environ. Microbiol.* **2004,** *70* (11), 6453-6458.

90. Meagher, R. C.; Sieber, F.; Spivak, J. L., Susceptibility to merocyanine 540-mediated photosensitization: A differentiation marker on murine hematopoietic progenitor cells. *Journal of Cellular Physiology* **1983,** *116* (1), 118-124.

91. Chen, J.; Cheung, N.; Fung, M.; Wen, J.; Leung, W.; Mak, N., Subcellular Localization of Merocyanine 540 (MC540) and Induction of Apoptosis in Murine Myeloid Leukemia Cells. *Photochemistry and Photobiology* **2000,** *72* (1), 114-120.

92. Atzpodien, J.; Gulati, S. C.; Clarkson, B. D., Comparison of the Cytotoxic Effects of Merocyanine-540 on Leukemic Cells and Normal Human Bone Marrow. *Cancer Res* **1986,** *46* (10), 4892-4895.

93. Chen, J. Y.; Mak, N. K.; Wen, J. M.; Leung, W. N.; Chen, S. C.; Fung, M. C.;

Cheung, N. H., A Comparison of the Photodynamic Effects of Temoporfin (mTHPC) and MC540 on Leukemia Cells: Efficacy and Apoptosis. *Photochemistry and Photobiology* **1998,** *68* (4), 545-554.

94. Fox, I.; Brooker, L.; Heseltine, D.; Wood, E., A new dye for continuous recording of dilution curves in whole blood independent of variations in blood oxygen saturation. *Circulation* **1956,** *14*, 937-938.

95. Cherrick, G.; Stein, S.; Leevy, C.; Davidson, C., Indocyanine green: observations on its physical properties, plasma decay, and hepatic extraction. *Journal of Clinical Investigation* **1960,** *39* (4), 592.

96. Fox, I., History and developmental aspects of the indicator-dilution technic. *Circulation Research* **1962,** *10* (3), 381-392.

97. Bradley, E. C.; Barr, J. W., Determination of blood volume using indocyanine green (Cardio-Green®) dye. *Life Sciences* **1968,** *7* (17), 1001-1007.

98. Kulvin, S.; Stauffer, L.; Kogure, K.; David, N., Fundus Angiography in Man by Intracarotid Administration of Dye. *Southern Medical Journal* **1970,** *63* (9), 998.

99. Fickweiler, S.; Szeimies, R.-M.; Bäumler, W.; Steinbach, P.; Karrer, S.; Goetz, A. E.; Abels, C.; Hofstädter, F., Indocyanine green: Intracellular uptake and phototherapeutic effects in vitro. *Journal of Photochemistry and Photobiology B: Biology* **1997,** *38* (2-3), 178-183.

100. Abels, C.; Fickweiler, S.; Weiderer, P.; Bäumler, W.; Hofstädter, F.; Landthaler, M.; Szeimies, R., Indocyanine green (ICG) and laser irradiation induce photooxidation. *Archives of Dermatological Research* **2000,** *292* (8), 404-411.

101. Tuchin, V.; Genina, E.; Bashkatov, A.; Simonenko, G.; Odoevskaya, O.; Altshuler, G., A pilot study of ICG laser therapy of acne vulgaris: photodynamic and photothermolysis treatment. *Lasers in surgery and medicine* **2003,** *33* (5).

102. Treibs, A.; Jacob, K., Cyclotrimethine Dyes Derived from Squaric Acid. *Angewandte Chemie International Edition in English* **1965,** *4* (8), 694.

103. Maahs, G.; Hegenberg, P., Syntheses and Derivatives of Squaric Acid. *Angewandte Chemie International Edition in English* **1966,** *5* (10), 888-893.

104. H.-E. Sprenger; Ziegenbein, W., Cyclobutendiylium-Farbstoffe. *Angewandte Chemie* **1968,** *80* (14), 541-546.

105. Schmidt, A. H., Reaktionen von Quadrature und Quadrature-Derivaten. *Synthesis* **1980,** *1980* (12), 961-994.

106. Law, K.-Y., Squaraine chemistry: effects of structural changes on the absorption and multiple fluorescence emission of bis[4-(dimethylamino)phenyl]squaraine and its derivatives. *The Journal of Physical Chemistry* **1987,** *91* (20), 5184-5193.

107. Law, K.-Y., Squaraine chemistry: effects of solvent and temperature on the fluorescence emission of squaraines. *Journal of Photochemistry and Photobiology A: Chemistry* **1994,** *84* (2), 123-132.

108. Law, K.-Y., Squaraine Chemistry. Absorption, Fluorescence Emission, and Photophysics of Unsymmetrical Squaraines. *The Journal of Physical Chemistry* **1995,** *99* (24), 9818-9824.

109. Law, K. Y.; Facci, J.; Balley, F.; Yanus, J., Squaraine chemistry: solution

electrochemistry and its use in assessing the relative photosensitivity of squaraines in bilayer xerographic devices. *Journal of imaging science* **1990,** *34* (2), 31-38.

110. Law, K. Y., Organic photoconductive materials: recent trends and developments. *Chemical Reviews* **1993,** *93* (1), 449-486.

111. Emmelius, M.; Pawlowski, G.; Vollmann, H. W., Materialien für die optische Datenspeicherung. *Angewandte Chemie* **1989,** *101* (11), 1475-1502.

112. Smits, E. C. P.; Setayesh, S.; Anthopoulos, T. D.; Buechel, M.; Nijssen, W.; Coehoorn, R.; Blom, P. W. M.; de Boer, B.; de Leeuw, D. M., Near-Infrared Light-Emitting Ambipolar Organic Field-Effect Transistors. *Advanced Materials* **2007,** *19* (5), 734-738.

113. Yum, J.-H.; Walter, P.; Huber, S.; Rentsch, D.; Geiger, T.; Nuesch, F.; De Angelis, F.; Gratzel, M.; Nazeeruddin, M. K., Efficient Far Red Sensitization of Nanocrystalline TiO_2 Films by an Unsymmetrical Squaraine Dye. *Journal of the American Chemical Society* **2007,** *129* (34), 10320-10321.

114. Silvestri, F.; Irwin, M. D.; Beverina, L.; Facchetti, A.; Pagani, G. A.; Marks, T. J., Efficient Squaraine-Based Solution Processable Bulk-Heterojunction Solar Cells. *Journal of the American Chemical Society* **2008,** *130* (52), 17640-17641.

115. Chen, C.-T.; Marder, S. R.; Cheng, L.-T., Syntheses and Linear and Nonlinear Optical Properties of Unsymmetrical Squaraines with Extended Conjugation. *Journal of the American Chemical Society* **1994,** *116* (7), 3117-3118.

116. Scherer, D.; Dörfler, R.; Feldner, A.; Vogtmann, T.; Schwoerer, M.; Lawrentz, U.; Grahn, W.; Lambert, C., Two-photon states in squaraine monomers and oligomers. *Chemical Physics* **2002,** *279* (2-3), 179-207.

117. Xiang, Z.; Nesterov, E. E.; Skoch, J.; Lin, T.; Hyman, B. T.; Swager, T. M.; Bacskai, B. J.; Reeves, S. A., Detection of Myelination Using a Novel Histological Probe. *J. Histochem. Cytochem.* **2005,** *53* (12), 1511-1516.

118. L.-H. Liu, K. N., R. Pansu, J.-J. Vachon, P. Tauc, E. Ishow,, Fluorescence Patterning through Photoinduced Migration of Squaraine-Functionalized Azo Derivatives. *Advanced Materials* **2007,** *19* (3), 433-436.

119. Ramaiah, D.; Joy, A.; Chandrasekhar, N.; Eldho, N. V.; Das, S.; George, M. V., Halogenated Squaraine Dyes as Potential Photochemotherapeutic Agents. Synthesis and Study of Photophysical Properties and Quantum Efficiencies of Singlet Oxygen Generation*. *Photochemistry and Photobiology* **1997,** *65* (5), 783-790.

120. Ramaiah, D.; Eckert, I.; Arun, K. T.; Weidenfeller, L.; Epe, B., Squaraine Dyes for Photodynamic Therapy: Study of Their Cytotoxicity and Genotoxicity in Bacteria and Mammalian Cells. *Photochemistry and Photobiology* **2002,** *76* (6), 672-677.

121. Santos, P. F.; Reis, L. V.; Almeida, P.; Oliveira, A. S.; Vieira Ferreira, L. F., Singlet oxygen generation ability of squarylium cyanine dyes. *Journal of Photochemistry and Photobiology A: Chemistry* **2003,** *160* (3), 159-161.

122. Santos, P. F.; Reis, L. V.; Duarte, I.; Serrano, J. P.; Almeida, P.; Oliveira, A. S.; Vieira Ferreira, L. F., Synthesis and Photochemical Evaluation of Iodinated Squarylium Cyanine Dyes. *Helvetica Chimica Acta* **2005,** *88* (5), 1135-1143.

123. Beverina, L.; Crippa, M.; Landenna, M.; Ruffo, R.; Salice, P.; Silvestri, F.; Versari, S.; Villa, A.; Ciaffoni, L.; Collini, E.; Ferrante, C.; Bradamante, S.; Mari, C.

M.; Bozio, R.; Pagani, G. A., Assessment of Water-Soluble π-Extended Squaraines as One- and Two-Photon Singlet Oxygen Photosensitizers: Design, Synthesis, and Characterization. *Journal of the American Chemical Society* **2008,** *130* (6), 1894-1902.

124. Thomas, C.; Pardini, R., Oxygen dependence of hypericin-induced phototoxicity to EMT6 mouse mammary carcinoma cells. *Photochemistry and Photobiology* **1984,** *39* (6), 831-837.

125. Koren, H.; Schenk, G. M.; Iindra, R. H.; Alth, G.; Ebermann, R.; Kubin, A.; Koderhold, G.; Kreitner, M., Hypericin in phototherapy. *Journal of Photochemistry and Photobiology B: Biology* **1996,** *36* (2), 113-119.

126. Lavie, G.; Mazur, Y.; Lavie, D.; Prince, A.; Pascual, D.; Liebes, L.; Levin, B.; Meruelo, D., Hypericin as an inactivator of infectious viruses in blood components. *Transfusion* **1995,** *35* (5), 392-400.

127. Peng, Q.; Brown, S.; Moan, J.; Nesland, J.; Wainwright, M.; Griffiths, J.; Dixon, B.; Cruse-Sawyer, J.; Vernon, D., Biodistribution of a methylene blue derivative in tumor and normal tissues of rats. *Journal of photochemistry and photobiology. B, Biology* **1993,** *20* (1), 63.

128. Wainwright, M.; Phoenix, D.; Marland, J.; Wareing, D.; Bolton, F., A study of photobactericidal activity in the phenothiazinium series. *FEMS immunology and medical microbiology* **1997,** *19* (1), 75-80.

129. Wainwright, M.; Giddens, R. M., Phenothiazinium photosensitisers: choices in synthesis and application. *Dyes and Pigments* **2003,** *57* (3), 245-257.

130. Vogel, E.; Köcher, M.; Schmickler, H.; Lex, J., Porphycene - a Novel Porphin Isomer. *Angewandte Chemie International Edition in English* **1986,** *25* (3), 257-259.

131. Segalla, A.; Fedeli, F.; Reddi, E.; Jori, G.; Cross, A., Effect of chemical structure and hydrophobicityon the pharmacokinetic properties of porphycenes in tumour-bearing mice. *International Journal of Cancer* **1997,** *72* (2).

132. Sessler, J. L.; Hemmi, G.; Mody, T. D.; Murai, T.; Burrell, A.; Young, S. W., Texaphyrins: Synthesis and Applications. *Accounts of Chemical Research* **1994,** *27* (2), 43-50.

133. Sessler, J. L.; Miller, R. A., Texaphyrins: New drugs with diverse clinical applications in radiation and photodynamic therapy. *Biochemical Pharmacology* **2000,** *59* (7), 733-739.

134. Hudson, R.; Carcenac, M.; Smith, K.; Madden, L.; Clarke, O. J.; Pelegrin, A.; Greenman, J.; Boyle, R. W., The development and characterisation of porphyrin isothiocyanate-monoclonal antibody conjugates for photoimmunotherapy. *Br J Cancer* **2005,** *92* (8), 1442-1449.

135. Dummin, H.; Cernay, T.; Zimmermann, H. W., Selective photosensitization of mitochondria in HeLa cells by cationic Zn(II)phthalocyanines with lipophilic side-chains. *Journal of Photochemistry and Photobiology B: Biology* **1997,** *37* (3), 219-229.

136. Montforts, F.-P.; Meier, A.; Scheurich, G.; Haake, G.; Bats, J. W., Chlorins Designed for Photodynamic Tumor Therapy and as Model Systems for Photosynthesis. *Angewandte Chemie International Edition in English* **1992,** *31* (12), 1592-1594.

137. Boutorine, A. S.; Brault, D.; Takasugi, M.; Delgado, O.; Helene, C., Chlorin-Oligonucleotide Conjugates: Synthesis, Properties, and Red Light-Induced

Photochemical Sequence-Specific DNA Cleavage in Duplexes and Triplexes. *Journal of the American Chemical Society* **1996,** *118* (40), 9469-9476.

138. Lightdale, C.; Heier, S.; Marcon, N.; MCAUGHAN, J.; Gerdes, H.; Overholt, B.; Sivak, M.; Stiegmann, G.; Nava, H., Photodynamic therapy with porfimer sodium versus thermal ablation therapy with Nd: YAG laser for palliation of esophageal cancer: a multicenter randomized trial. *Gastrointestinal endoscopy* **1995,** *42* (6), 507-512.

139. Lam, S.; Grafton, C.; Coy, P.; Voss, N. In *Combined photodynamic therapy using Photofrin and radiotherapy versus radiotherapy alone in patients with inoperable obstructive nonsmall-cell bronchogenic carcinoma [1616-07]*, SPIE INTERNATIONAL SOCIETY FOR OPTICAL: 1991; pp 20-20.

140. Kato, H.; Okunaka, T.; Shimatani, H., Photodynamic therapy for early stage bronchogenic carcinoma. *Journal of Clinical Laser Medicine & Surgery* **1996,** *14* (5), 235-238.

141. Peng, Q.; Warloe, T.; Berg, K.; Moan, J.; Kongshaug, M.; Giercksky, K.; Nesland, J., 5-Aminolevulinic acid-based photodynamic therapy. Clinical research and future challenges. *Cancer* **1997,** *79* (12), 2282.

142. Ris, H.; Altermatt, H.; Inderbitzi, R.; Hess, R.; Nachbur, B.; Stewart, J.; Wang, Q.; Lim, C.; Bonnett, R.; Berenbaum, M., Photodynamic therapy with chlorins for diffuse malignant mesothelioma: initial clinical results. *British journal of cancer* **1991,** *64* (6), 1116.

143. Razum, N.; Snyder, A.; Doiron, D. In *SnET2: clinical update*, 1996; p 43.

144. Pandey, R. K.; Sumlin, A. B.; Constantine, S.; Aoudia, M.; Potter, W. R.; Bellnier, D. A.; Henderson, B. W.; Rodgers, M. A.; Smith, K. M.; Dougherty, T. J., Alkyl Ether Analogs of Chlorophyll-*a* Derivatives: Part 1. Synthesis, Photophysical Properties and Photodynamic Efficacy. *Photochemistry and Photobiology* **1996,** *64* (1), 194-204.

145. Richter, A.; Kelly, B.; Chow, J.; Liu, D.; Towers, G.; Dolphin, D.; Levy, J., Preliminary studies on a more effective phototoxic agent than hematoporphyrin. *Journal of the National Cancer Institute* **1987,** *79* (6), 1327.

146. Renschler, M.; Yuen, A.; Panella, T., Photodynamic therapy trials with lutetium texaphyrin. *Photochem Photobiol* **1997,** *65*, 475.

147. Mìkvy, P.; Messmann, H.; Regula, J.; Conio, M.; Pauer, M.; Millson, C.; MacRobert, A.; Bown, S., Photodynamic therapy for gastrointestinal tumors using three photosensitizers--ALA induced PPIX, Photofrin and MTHPC. A pilot study. *Neoplasma* **1998,** *45* (3), 157.

148. Girotti, M., 198 . Mechanism of lipid peroxidation. *Free Rad. Biol Med 1*, 87-95.

149. Girotti, A., Mechanisms of photosensitization. *Photochemistry and Photobiology* **1983,** *38* (6), 745-751.

150. Bachowski, G.; Korytowski, W.; Girotti, A., Characterization of lipid hydroperoxides generated by photodynamic treatment of leukemia cells. *Lipids* **1994,** *29* (7), 449-459.

151. Bachowski, G.; Pintar, T.; Girotti, A., Photosensitized lipid peroxidation and enzyme inactivation by membrane-bound merocyanine 540: reaction mechanisms in the absence and presence of ascorbate. *Photochem. Photobiol* **1991,** *53*, 481-491.

152. Grune, T.; Klotz, L.; Gieche, J.; Rudeck, M.; Sies, H., Protein oxidation and proteolysis by the nonradical oxidants singlet oxygen or peroxynitrite. *Free Radical Biology and Medicine* **2001,** *30* (11), 1243-1253.

153. Buchko, G.; Wagner, J.; Cadet, J.; Raoul, S.; Weinfeld, M., Methylene blue-mediated photooxidation of 7, 8-dihydro-8-oxo-2 -deoxyguanosine. *BBA-Gene Structure and Expression* **1995,** *1263* (1), 17-24.

154. Buchko, G.; Cadet, J.; Ravanat, J.; Labataille, P., Isolation and Characterization of a New Product Produced by Ionizing Irradiation and Type I Photosensitization of 2'-deoxyguanosine in Oxygen-saturated aqueous Solution:(2S)-2, 5'-anhydro-1-(2'-deoxy--d-erythro-pentofuranosyl)-5-guanidinylidene-2-hydroxy-4-oxoimidazolidine. *International Journal of Radiation Biology* **1993,** *63* (6), 669-676.

155. Ravanat, J.; Cadet, J., Reaction of singlet oxygen with 2'-deoxyguanosine and DNA. Isolation and characterization of the main oxidation products. *Chemical research in toxicology* **1995,** *8* (3), 379-388.

156. Bilski, P.; Motten, A.; Bilska, M.; Chignell, C., The photooxidation of diethylhydroxylamine by rose bengal in micellar and nonmicellar aqueous solutions. *Photochemistry and Photobiology* **1993,** *58*, 11-11.

157. Ma, J.; Jiang, L., Photogeneration of singlet oxygen ($^1O_2$) and free radicals (Sen -, O_2-) by tetra-brominated hypocrellin B derivative. *Free Radical Research* **2001,** *35* (6), 767-777.

158. Svaasand, L., Optical dosimetry for direct and interstitial photoradiation therapy of malignant tumors. *Progress in clinical and biological research* **1984,** *170*, 91.

159. Wilson, B. C.; Jeeves, W. P.; Lowe, D. M., In vivo and post mortem measurements of the attenuation spectra of light in mammalian tissues. *Photochemistry and Photobiology* **1985,** *42* (2), 153-162.

160. Dougherty, T.; Potter, W., Of what value is a highly absorbing photosensitizer in PDT? *Journal of photochemistry and photobiology. B, Biology* **1991,** *8* (2), 223.

161. Spikes, J.; Bommer, J., Photobleaching of mono-L-aspartyl chlorin e~ 6 (NPe6): a candidate sensitizer for the photodynamic therapy of tumors. *Photochemistry and Photobiology* **1993,** *58*, 346-346.

162. Berenbaum, M.; Bonnett, R.; Chevretton, E.; Akande-Adebakin, S.; Ruston, M., Selectivity of meso-tetra(hydroxyphenyl) porphyrins and chlorins and of photofrin II in causing photodamage in tumour, skin, muscle and bladder. The comcept of cost-benefit in analysing the results. *Lasers in Medical Science* **1993,** *8* (4), 235-243.

163. Skovsen, E.; Snyder, J. W.; Lambert, J. D. C.; Ogilby, P. R., Lifetime and Diffusion of Singlet Oxygen in a Cell. *The Journal of Physical Chemistry B* **2005,** *109* (18), 8570-8573.

164. Horobin, R., Biological staining: mechanisms and theory. *Biotechnic and Histochemistry* **2002,** *77* (1), 3-13.

165. Wilson, B. C.; Olivo, M.; Singh, G., Subcellular Localization of Photofrin and Aminolevulinic Acid and Photodynamic Cross-Resistance in Vitro in Radiation-Induced Fibrosarcoma Cells Sensitive or Resistant to Photofrin-Mediated Photodynamic Therapy. *Photochemistry and Photobiology* **1997,** *65* (1), 166-176.

166. Morris, R.; Azizuddin, K.; Lam, M.; Berlin, J.; Nieminen, A.; Kenney, M.;

Samia, A.; Burda, C.; Oleinick, N., Fluorescence resonance energy transfer reveals a binding site of a photosensitizer for photodynamic therapy. *Cancer research* **2003,** *63* (17), 5194.

167. MacDonald, I.; Morgan, J.; Bellnier, D.; Paszkiewicz, G.; Whitaker, J.; Litchfield, D.; Dougherty, T., Subcellular localization patterns and their relationship to photodynamic activity of pyropheophorbide-a derivatives. *Photochemistry and Photobiology* **1999,** *70*, 789-797.

168. Nagata, S.; Obana, A.; Gohto, Y.; Nakajima, S., Necrotic and apoptotic cell death of human malignant melanoma cells following photodynamic therapy using an amphiphilic photosensitizer, ATX-S10 (Na). *Lasers in surgery and medicine* **2003,** *33* (1), 64-70.

169. Høgset, A.; Prasmickaite, L.; Selbo, P.; Hellum, M.; Engesæter, B.; Bonsted, A.; Berg, K., Photochemical internalisation in drug and gene delivery. *Advanced drug delivery reviews* **2004,** *56* (1), 95-115.

170. Berg, K.; Madslien, K.; Bommer, J.; Oftebro, R.; Winkelman, J.; Moan, J., Light induced relocalization of sulfonated meso-tetraphenylporphines in NHIK 3025 cells and effects of dose fractionation. *Photochem. Photobiol* **1991,** *53* (2), 203-10.

171. Peng, Q.; Farrants, G.; Madslien, K.; Bommer, J.; Moan, J.; Danielsen, H.; Nesland, J., Subcellular localization, redistribution and photobleaching of sulfonated aluminum phthalocyanines in a human melanoma cell line. *Int. J. Cancer* **1991,** *49* (2), 290–295.

172. Morgan, J.; Oseroff, A., Mitochondria-based photodynamic anti-cancer therapy. *Advanced drug delivery reviews* **2001,** *49* (1-2), 71-86.

173. Runnels, J.; Chen, N.; Ortel, B.; Kato, D.; Hasan, T., BPD-MA-mediated photosensitization in vitro and in vivo: cellular adhesion and 1 integrin expression in ovarian cancer cells. *British journal of cancer* **1999,** *80* (7), 946.

174. Kessel, D.; Luguya, R.; Vicente, M., Localization and Photodynamic Efficacy of Two Cationic Porphyrins Varying in Charge Distribution¶. *Photochemistry and Photobiology* **2003,** *78* (5), 431-435.

175. Dummin, H.; Cernay, T.; Zimmermann, H., Selective photosensitization of mitochondria in HeLa cells by cationic Zn (II) phthalocyanines with lipophilic side-chains. *Journal of Photochemistry & Photobiology, B: Biology* **1997,** *37* (3), 219-229.

176. Trivedi, N.; Wang, H.; Nieminen, A.; Oleinick, N.; Izatt, J., Quantitative analysis of Pc 4 localization in mouse lymphoma (LY-R) cells via double-label confocal fluorescence microscopy. *Photochemistry and Photobiology* **2000,** *71* (5), 634-639.

177. Aveline, B.; Redmond, R., Can cellular phototoxicity be accurately predicted on the basis of sensitizer photophysics? *Photochemistry and Photobiology* **1999,** *69*, 306-316.

178. Hsieh, Y.; Wu, C.; Chang, C.; Yu, J., Subcellular localization of Photofrin® determines the death phenotype of human epidermoid carcinoma A431 cells triggered by photodynamic therapy: When plasma membranes are the main targets. *Journal of Cellular Physiology* **2003,** *194* (3), 363-375.

179. Teiten, M.; Bezdetnaya, L.; Morliere, P.; Santus, R.; Guillemin, F., Endoplasmic reticulum and Golgi apparatus are the preferential sites of Foscan® localisation in cultured tumour cells. *British journal of cancer* **2003,** *88* (1), 146.

180. Moan, J.; Peng, Q.; Iani, V.; Ma, L.; Horobin, R.; Berg, K.; Kongshaug, M.; Nesland, J. In *Biodistribution, pharmacokinetic, and in-vivo fluorescence spectroscopic studies of photosensitizers*, Proc. SPIE - Int. Soc. Opt. Eng., 1996; p 234.

181. MAUGAIN, E.; SASNOUSKI, S.; ZORIN, V.; MERLIN, J.; GUILLEMIN, F.; BEZDETNAYA, L., Foscan®-based photodynamic treatment in vivo: Correlation between efficacy and Foscan accumulation in tumor, plasma and leukocytes. *Oncology reports* **2004,** *12* (3), 639-645.

182. Bellnier, D.; Greco, W.; Parsons, J.; Oseroff, A.; Kuebler, A.; Dougherty, T., An assay for the quantitation of Photofrin (R) in tissues and fluids. *Photochemistry and Photobiology* **1997,** *66* (2), 237-244.

183. Frisoli, J.; Tudor, E.; Flotte, T.; Hasan, T.; Deutsch, T.; Schomacker, K., Pharmacokinetics of a fluorescent drug using laser-induced fluorescence. *Cancer research* **1993,** *53* (24), 5954.

184. Bellnier, D.; Dougherty, T., A preliminary pharmacokinetic study of intravenous Photofrin® in patients. *Journal of Clinical Laser Medicine & Surgery* **1996,** *14* (5), 311-314.

185. Bellnier, D.; Greco, W.; Loewen, G.; Nava, H.; Oseroff, A.; Pandey, R.; Tsuchida, T.; Dougherty, T., Population pharmacokinetics of the photodynamic therapy agent 2-[1-hexyloxyethyl]-2-devinyl pyropheophorbide-a in cancer patients. *Cancer research* **2003,** *63* (8), 1806.

186. Jones, H.; Vernon, D.; Brown, S., Photodynamic therapy effect of m-THPC (Foscan®) in vivo: correlation with pharmacokinetics. *British journal of cancer* **2003,** *89* (2), 398.

187. Brun, P.; DeGroot, J.; Dickson, E.; Farahani, M.; Pottier, R., Determination of the in vivo pharmacokinetics of palladium-bacteriopheophorbide (WST09) in EMT6 tumour-bearing Balb/c mice using graphite furnace atomic absorption spectroscopy. *Photochemical & Photobiological Sciences* **2004,** *3* (11-12), 1006-1010.

188. Egorin, M.; Zuhowski, E.; Sentz, D.; Dobson, J.; Callery, P.; Eiseman, J., Plasma pharmacokinetics and tissue distribution in CD2F1 mice of Pc4 (NSC 676418), a silicone phthalocyanine photodynamic sensitizing agent. *Cancer chemotherapy and pharmacology* **1999,** *44* (4), 283-294.

189. Reddi, E., Role of delivery vehicles for photosensitizers in the photodynamic therapy of tumours. *Journal of Photochemistry & Photobiology, B: Biology* **1997,** *37* (3), 189-195.

190. Kessel, D.; Morgan, A.; Garbo, G., Sites and efficacy of photodamage by tin etiopurpurin in vitro using different delivery systems. *Photochem. Photobiol* **1991,** *54*, 193–196.

191. Kongshaug, M.; Moan, J.; Brown, S., The distribution of porphyrins with different tumour localising ability among human plasma proteins. *British journal of cancer* **1989,** *59* (2), 184.

192. Maziere, J.; Santus, R.; Morliere, P.; Reyftmann, J.; Candide, C.; Mora, L.; Salmon, S.; Maziere, C.; Gatt, S.; Dubertret, L., Cellular uptake and photosensitizing properties of anticancer porphyrins in cell membranes and low and high density lipoproteins. *Journal of photochemistry and photobiology. B, Biology* **1990,** *6* (1-2), 61.

193. Hamblin, M.; Newman, E., On the mechanism of the tumour-localising effect in

photodynamic therapy. *Journal of photochemistry and photobiology. B, Biology* **1994,** *23* (1), 3.

194. Boyle, R.; Dolphin, D., Structure and biodistribution relationships of photodynamic sensitizers. *Photochemistry and Photobiology* **1996,** *64* (3), 469-485.

195. Larroque, C.; Pelegrin, A.; Van Lier, J., Serum albumin as a vehicle for zinc phthalocyanine: photodynamic activities in solid tumour models. *British journal of cancer* **1996,** *74* (12), 1886.

196. Jori, G. In *In vivo transport and pharmacokinetic behavior of tumour photosensitizers*, 1989; p 78.

197. Jori, G.; Reddi, E., The role of lipoproteins in the delivery of tumour-targeting photosensitizers. *The International journal of biochemistry* **1993,** *25* (10), 1369.

198. Ginevra, F.; Biffanti, S.; Pagnan, A.; Biolo, R.; Reddi, E.; Jori, G., Delivery of the tumour photosensitizer zinc (II)-phthalocyanine to serum proteins by different liposomes: studies in vitro and in vivo. *Cancer letters* **1990,** *49* (1), 59.

199. Jiang, F.; Lilge, L.; Logie, B.; Li, Y.; Chopp, M., Photodynamic therapy of 9L gliosarcoma with liposome-delivered photofrin. *Photochemistry and Photobiology* **1997,** *65*, 701-706.

200. Richter, A.; Waterfield, E.; Jain, A.; Canaan, A.; Allison, B.; Levy, J., Liposomal delivery of a photosensitizer, benzoporyphyrin derivative monoacid ring A (BPD), to tumor tissue in a mouse tumor model. *Photochemistry and Photobiology* **1993,** *57*, 1000-1000.

201. Polo, L.; Segalla, A.; Jori, G.; Bocchiotti, G.; Verna, G.; Franceschini, R.; Mosca, R.; De Filippi, P., Liposome-delivered 131I-labelled Zn (II)-phthalocyanine as a radiodiagnostic agent for tumours. *Cancer letters* **1996,** *109* (1-2), 57-61.

202. Korbelik, M., Low density lipoprotein receptor pathway in the delivery of Photofrin: how much is it relevant for selective accumulation of the photosensitizer in tumors? *Journal of photochemistry and photobiology. B, Biology* **1992,** *12* (1), 107-109.

203. Barel, A.; Jori, G.; Perin, A.; Romandini, P.; Pagnan, A.; Biffanti, S., Role of high-, low-and very low-density lipoproteins in the transport and tumor-delivery of hematoporphyrin in vivo. *Cancer letters* **1986,** *32* (2), 145.

204. Morliere, P.; Kohen, E.; Reyftmann, J.; Santus, R.; Kohen, C.; Maziere, J.; Goldstein, S.; Mangel, W.; Dubertret, L., Photosensitization by porphyrins delivered to L cell fibroblasts by human serum low density lipoproteins. A microspectrofluorometric study. *Photochemistry and Photobiology* **1987,** *46* (2), 183.

205. Woodburn, K.; Sykes, E.; Kessel, D., Interactions of Solutol HS 15 and Cremophor EL with plasma lipoproteins. *International Journal of Biochemistry and Cell Biology* **1995,** *27* (7), 693-699.

206. Woodburn, K.; Chang, C.; Lee, S.; Henderson, B.; Kessel, D., Biodistribution and PDT efficacy of a ketochlorin photosensitizer as a function of the delivery vehicle. *Photochemistry and Photobiology* **1994,** *60* (2), 154.

207. YUAN, F.; Leunig, M.; Berk, D.; Jain, R., Microvascular permeability of albumin, vascular surface area, and vascular volume measured in human adenocarcinoma LS 174 T using dorsal chamber in SCID mice. *Microvascular research(Print)* **1993,** *45* (3), 269-289.

208. Allison, B.; Pritchard, P.; Levy, J., Evidence for low-density lipoprotein receptor-mediated uptake of benzoporphyrin derivative. *British journal of cancer* **1994,** *69* (5), 833.

209. Roberts, W.; Hasan, T., Role of neovasculature and vascular permeability on the tumor retention of photodynamic agents. *Cancer research* **1992,** *52* (4), 924.

210. Henderson, B.; Dougherty, T., How does photodynamic therapy work. *Photochem Photobiol* **1992,** *55* (1), 145-157.

211. Dewhirst, M.; Kimura, H.; Rehmus, S.; Braun, R.; Papahadjopoulos, D.; Hong, K.; Secomb, T., Microvascular studies on the origins of perfusion-limited hypoxia. *The British Journal of Cancer. Supplement* **1996,** *27*, S247.

212. Tromberg, B.; Orenstein, A.; Kimel, S.; Barker, S.; Hyatt, J.; Nelson, J.; Berns, M., In vivo tumor oxygen tension measurements for the evaluation of the efficiency of photodynamic therapy. *Photochemistry and Photobiology* **1990,** *52* (2), 375.

213. Kerr, J.; Wyllie, A.; Currie, A., Apoptosis: a basic biological phenomenon with wide-ranging implications in tissue kinetics. *British journal of cancer* **1972,** *26* (4), 239.

214. Castedo, M.; Perfettini, J.; Roumier, T.; Andreau, K.; Medema, R.; Kroemer, G., Cell death by mitotic catastrophe: a molecular definition. *Oncogene* **2004,** *23* (16), 2825-2837.

215. Bizik, J.; Kankuri, E.; Ristimäki, A.; Taieb, A.; Vapaatalo, H.; Lubitz, W.; Vaheri, A., Cell–cell contacts trigger programmed necrosis and induce cyclooxygenase-2 expression. *Cell Death & Differentiation* **2003,** *11* (2), 183-195.

216. Leist, M.; Jaattela, M., Triggering of apoptosis by cathepsins. *Cell Death and Differentiation* **2001,** *8* (4), 324-326.

217. Yu, L.; Lenardo, M.; Baehrecke, E., Autophagy and caspases: a new cell death program. *Cell cycle (Georgetown, Tex.)* **2004,** *3* (9), 1124.

218. Leist, M.; Jaattela, M., Four deaths and a funeral: from caspases to alternative mechanisms. *Nature Reviews Molecular Cell Biology* **2001,** *2* (8), 589-598.

219. Stroh, C.; Schulze-Osthoff, K., Death by a thousand cuts: an ever increasing list of caspase substrates. *Cell Death and Differentiation* **1998,** *5* (12), 997.

220. Martinou, J.; Green, D., Breaking the mitochondrial barrier. *Nature Reviews Molecular Cell Biology* **2001,** *2* (1), 63-67.

221. Castano, A. P.; Demidova, T. N.; Hamblin, M. R., Mechanisms in photodynamic therapy: part two--cellular signaling, cell metabolism and modes of cell death. *Photodiagnosis and Photodynamic Therapy* **2005,** *2* (1), 1-23.

222. Oleinick, N.; Morris, R.; Belichenko, I., The role of apoptosis in response to photodynamic therapy: what, where, why, and how. *Photochemical & Photobiological Sciences* **2002,** *1* (1), 1-21.

223. Agarwal, M.; Clay, M.; Harvey, E.; Evans, H.; Antunez, A.; Oleinick, N., Photodynamic therapy induces rapid cell death by apoptosis in L5178Y mouse lymphoma cells. *Cancer research* **1991,** *51* (21), 5993.

224. Kessel, D.; Poretz, R., Sites of photodamage induced by photodynamic therapy with a chlorin e6 triacetoxymethyl ester (CAME). *Photochemistry and Photobiology* **2000,** *71* (1), 94-96.

225. Lavie, G.; Kaplinsky, C.; Toren, A.; Aizman, I.; Meruelo, D.; Mazur, Y.; Mandel, M., A photodynamic pathway to apoptosis and necrosis induced by dimethyl tetrahydroxyhelianthrone and hypericin in leukaemic cells: possible relevance to photodynamic therapy. *British journal of cancer* **1999,** *79* (3/4), 423.

226. Woodburn, K.; Fan, Q.; Miles, D.; Kessel, D.; Luo, Y.; Young, S., Localization and efficacy analysis of the phototherapeutic lutetium texaphyrin (PCI-0123) in the murine EMT6 sarcoma model. *Photochemistry and Photobiology* **1997,** *65* (3), 410.

227. Dellinger, M., Apoptosis or necrosis following Photofrin (R) photosensitization: Influence of the incubation protocol. *Photochemistry and Photobiology* **1996,** *64* (1), 182-187.

228. Chen, J.; Mak, N.; Yow, C.; Fung, M.; Chiu, L.; Leung, W.; Cheung, N., The Binding Characteristics and Intracellular Localization of Temoporfin (m THPC) in Myeloid Leukemia Cells: Phototoxicity and Mitochondrial Damage¶. *Photochemistry and Photobiology* **2000,** *72* (4), 541-547.

229. He, X.; Sikes, R.; Thomsen, S.; Chung, L.; Jacques, S., Photodynamic therapy with photofrin II induces programmed cell death in carcinoma cell lines. *Photochemistry and Photobiology* **1994,** *59* (4), 468.

230. Dahle, J.; Kaalhus, O.; Moan, J.; Steen, H., Cooperative effects of photodynamic treatment of cells in microcolonies. *Proceedings of the National Academy of Sciences of the United States of America* **1997,** *94* (5), 1773.

231. Bigelow, R.; Freund, H., An MNDO and CNDO/S (S+ DES CI) study on the structural and electronic properties of a model squaraine dye and related cyanine. *Chem. Phys* **1986,** *107* (2-3), 159–174.

232. Ioffe, V.; Gorbenko, G.; Domanov, Y.; Tatarets, A.; Patsenker, L.; Terpetsching, E.; Dyubko, T., A new fluorescent squaraine probe for the measurement of membrane polarity. *Journal of Fluorescence* **2006,** *16* (1), 47-52.

233. Das, S.; Thomas, K.; George, M.; Kamat, P., Fluorescence enhancement of bis (2, 4, 6-trihydroxyphenyl) squaraine anion by 2: 1 host–guest complexation with -cyclodextrin. *Journal of the Chemical Society, Faraday Transactions* **1992,** *88* (23), 3419-3422.

234. Chen, H.; Farahat, M.; Law, K.; Whitten, D., Aggregation of surfactant squaraine dyes in aqueous solution and microheterogeneous media: Correlation of aggregation behavior with molecular structure. *J. Am. Chem. SOC* **1996,** *118* (11), 2584-2594.

235. Tatarets, A. L.; Fedyunyayeva, I. A.; Dyubko, T. S.; Povrozin, Y. A.; Doroshenko, A. O.; Terpetschnig, E. A.; Patsenker, L. D., Synthesis of water-soluble, ring-substituted squaraine dyes and their evaluation as fluorescent probes and labels. *Analytica Chimica Acta* **2006,** *570* (2), 214-223.

236. Ros-Lis, J.; Martínez-Máñez, R.; Soto, J., A selective chromogenic reagent for cyanide determination. *Chemical Communications* **2002,** *2002* (19), 2248-2249.

237. Ros-Lis, J. V.; Garcia, B.; Jimenez, D.; Martinez-Manez, R.; Sancenon, F.; Soto, J.; Gonzalvo, F.; Valldecabres, M. C., Squaraines as Fluoro-Chromogenic Probes for Thiol-Containing Compounds and Their Application to the Detection of Biorelevant Thiols. *Journal of the American Chemical Society* **2004,** *126* (13), 4064-4065.

238. Sreejith, S.; Divya, K.; Ajayaghosh, A., A near-infrared squaraine dye as a latent

ratiometric fluorophore for the detection of aminothiol content in blood plasma. *Angewandte Chemie (International ed. in English)* **2008,** *47* (41), 7883.

239. Terpetschnig, E.; Szmacinski, H.; Ozinskas, A.; Lakowicz, J. R., Synthesis of Squaraine-N-Hydroxysuccinimide Esters and Their Biological Application as Long-Wavelength Fluorescent Labels. *Analytical Biochemistry* **1994,** *217* (2), 197-204.

240. Patonay, G.; Salon, J.; Sowell, J.; Strekowski, L., Noncovalent labeling of biomolecules with red and near-infrared dyes. *Molecules* **2004,** *9* (3), 40–49.

241. Oswald, B.; Patsenker, L.; Duschl, J.; Szmacinski, H.; Wolfbeis, O. S.; Terpetschnig, E., Synthesis, Spectral Properties, and Detection Limits of Reactive Squaraine Dyes, a New Class of Diode Laser Compatible Fluorescent Protein Labels. *Bioconjugate Chemistry* **2000,** *11* (3), 438-438.

242. Ioffe, V.; Gorbenko, G.; Kinnunen, P.; Tatarets, A.; Kolosova, O.; Patsenker, L.; Terpetschnig, E., Tracing Lysozyme-Lipid Interactions with Long-Wavelength Squaraine Dyes. *Journal of Fluorescence* **2007,** *17* (1), 65-72.

243. Povrozin, Y.; Kolosova, O.; Obukhova, O.; Tatarets, A.; Sidorov, V.; Terpetschnig, E.; Patsenker, L., Seta-633-A NIR Fluorescence Lifetime Label for Low-Molecular-Weight Analytes. *Bioconjugate Chemistry* **2009**.

244. Welder, F.; Paul, B.; Nakazumi, H.; Yagi, S.; Colyer, C. L., Symmetric and asymmetric squarylium dyes as noncovalent protein labels: a study by fluorimetry and capillary electrophoresis. *Journal of Chromatography B* **2003,** *793* (1), 93-105.

245. Volkova, K. D.; Kovalska, V. B.; Tatarets, A. L.; Patsenker, L. D.; Kryvorotenko, D. V.; Yarmoluk, S. M., Spectroscopic study of squaraines as protein-sensitive fluorescent dyes. *Dyes and Pigments* **2007,** *72* (3), 285-292.

246. Thomas, J.; Sherman, D. B.; Amiss, T. J.; Andaluz, S. A.; Pitner, J. B., Synthesis and Biosensor Performance of a Near-IR Thiol-Reactive Fluorophore Based on Benzothiazolium Squaraine. *Bioconjugate Chemistry* **2007,** *18* (6), 1841-1846.

247. Pitner, J.; Thomas, K.; Sherman, D.; Alarcon, J.; Mohiuddin, G.; Kyler, K.; Venepalli, B. In *Design and synthesis of a squaraine dye for long wavelength fluorescence-based biosensors*, Proceedings of SPIE, 2005; p 24.

248. Santos, P. F.; Reis, L. V.; Almeida, P.; Serrano, J. P.; Oliveira, A. S.; Vieira Ferreira, L. F., Efficiency of singlet oxygen generation of aminosquarylium cyanines. *Journal of Photochemistry and Photobiology A: Chemistry* **2004,** *163* (1-2), 267-269.

249. Arunkumar, E.; Sudeep, P.; Kamat, P.; Noll, B.; Smith, B., Singlet oxygen generation using iodinated squaraine and squaraine-rotaxane dyes. *New Journal of Chemistry* **2007,** *31* (5), 677-683.

250. Bonnett, R.; Motevalli, M.; Siu, J., Squaraines based on 2-arylpyrroles. *Tetrahedron* **2004,** *60* (40), 8913-8918.

251. Jyothish, K.; Avirah, R. R.; Ramaiah, D., Synthesis of New Cholesterol- and Sugar-Anchored Squaraine Dyes: Further Evidence of How Electronic Factors Influence Dye Formation. *Organic Letters* **2005,** *8* (1), 111-114.

252. Ramaiah, D.; Eckert, I.; Arun, K.; Weidenfeller, L.; Epe, B., Squaraine dyes for photodynamic therapy: study of their cytotoxicity and genotoxicity in bacteria and mammalian cells. *Photochemistry and Photobiology* **2002,** *76* (6), 672-677.

253. Ramaiah, D.; Eckert, I.; Arun, K.; Weidenfeller, L.; Epe, B., Squaraine Dyes for

Photodynamic Therapy: Mechanism of Cytotoxicity and DNA Damage Induced by Halogenated Squaraine Dyes Plus Light (> 600 nm)¶. *Photochemistry and Photobiology* **2004,** *79* (1), 99-104.

254. Gayathri Devi, D.; Cibin, T. R.; Ramaiah, D.; Abraham, A., Bis(3,5-diiodo-2,4,6-trihydroxyphenyl)squaraine: A novel candidate in photodynamic therapy for skin cancer models in vivo. *Journal of Photochemistry and Photobiology B: Biology* **2008,** *92* (3), 153-159.

255. Chenthamarakshan, C. R.; Eldo, J.; Ajayaghosh, A., Squaraine Dye Based Molecular Wires Containing Flexible Oxyethylene Chains as Sensors. Enhanced Fluorescence Response on Li+ Recognitionâ€ *Macromolecules* **1999,** *32* (18), 5846-5851.

256. Chenthamarakshan, C. R.; Ajayaghosh, A., Enhanced sensitivity and selectivity in lithium ion recognition property of an oligomeric squaraine dye based fluorescent sensor. *Tetrahedron Letters* **1998,** *39* (13), 1795-1798.

257. Jisha, V. S.; Arun, K. T.; Hariharan, M.; Ramaiah, D., Site-Selective Binding and Dual Mode Recognition of Serum Albumin by a Squaraine Dye. *Journal of the American Chemical Society* **2006,** *128* (18), 6024-6025.

258. Reddington, M. V., Synthesis and Properties of Phosphonic Acid Containing Cyanine and Squaraine Dyes for Use as Fluorescent Labels. *Bioconjugate Chemistry* **2007,** *18* (6), 2178-2190.

3. Analysis, design, interpretations of results

3.1 Exploiting squaraine synthesis

The synthesis of squaraine involves the reaction of a nucleophile with either squaric acid or its derivatives to yield a conjugated quadrupolar dye constituted by two electronrich terminal and an electronpoor core.[1-5] This peculiar structure is responsible for the electronic transitions in the NIR region that characterize squarylium dyes. Some of the electronrich substrates that react with squaric acid and its derivatives are electronrich benzene (i.e., 1,3,5-trihydroxybenzene), heteroaryl anhydrobases derivating from indoleninium, benzothiazolium, benzofuranium salts, and derivatives of pyrrole, aniline and thiophene. The condensation reactions are usually performed in protic solvents such as acetic acid or *n*-alkanols (i.e., buthanol or 2-propnaol). Mixtures of these with aromatic hydrocarbons (i.e., toluene) are used to azeotropically removed the condensation water. The synthesis of symmetric squaraine requires two equivalents of the nucleophile and one of squaric acid. It is assumed that the first equivalent condensates with squaric acid to give a reactive intermediates diacetoxy or dialkyl squarates of the general formula $Q(OR)_2$.[6, 7] Depending on the nucleophilicity of the reagents and on the condition applied, both 1,3-linking and 1,2-linking of its nucleophilic group at the squaric moiety could be achieved, though the most stable and interesting condensation products are the former one. Unsymmetrically squaraines substituted with two different terminal groups have also received a special interest.[8, 9] Indeed, some unsymmetrical squaraines exhibit large second order hyperpolarizabilities which allow their use for non-linear optical materials.[10-12] Although for the synthesis of these unsymmetrically substituted compounds the simultaneous condensation of squaric acid with two different nucleophiles seems to be the simplest way, it does not usually work. This is due to the fact that all the possible symmetrically and unsymmetrically substituted products were obtained and their separation requires a high expense on time and materials. Moreover, emisquaric acid are not easily available from their reaction between squaric acid and a nucleophile by a 1:1 condensation step. The most useful method for preparing emisquaric acids consists in the reaction of an ester of squaric acid (i.e., ethyl[13] or butyl[14] squarate) or of the acyl chloride of squaric acid[15] with a nucleophilic component. The products so obtained can be hydrolyzed to the corresponding emisquaric acids by heating them in aqueous acetic acid. The reaction of the emisquaric acid with an equivalent of an electronrich compound yields the desire

unsymmetrical squaraine.

Squaraine synthesis, though straightforward from the conceptual point of view, require a careful planning. Indeed, we have to deal with two subtle synthetic challenges: firstly, how to avoid both singlet oxygen and ROS production by the initially formed sensitizer in the reaction mixture. This underestimated problem can be responsible for the partial degradation of both reagents and products during the sensitizer synthesis. Then, we have to deal with the formation of a mixture of the squaric acid 1,3- and 1,2-condensation products. The 1,3-squaraine is the desired one, but it is not often easily separated by the less stable 1,2-one and its degradation products. Moreover, squaraine dyes are often poorly soluble in organic solvents and their characterization requires lots of time and effort. Keeping in mind these brief comments, we approached squaraine synthesis with two different strategies: a) we design and improve an existing apparatus to perform microwave-assisted reaction under azeotropic conditions in the dark and under nitrogen atmosphere (Figure 3.1).

Figure 3.1: synthetic experimental setup

The microwave-assisted heating helped us in reducing the reaction time from 18-24 h, in the case of conventional heating (i.e., an oil bath) to 2-6 h by improving the azeotropic distillation rate; b) we used boiling pyridine and dark brown glassware for the synthesis of some anhydrobase derivative squaraines. Especially in the latter case we achieve reaction yield up to 60% for the pure product as reported in greater detail in Chapter 4. Another interesting feature that worth mention is the versatility of squaraine

synthesis. Indeed, many different electronrich substrates condensate with squaric acid ensuring the fine tuning of squaraine molecular structure. In this regard, we here discuss three examples of molecular engineering: 1) how we control the electronic properties of squarylium dyes by chosing the appropriate heterocycle moieties; 2) how we tuned solubility and inserted specific functionalities in a given structure without affecting the overall electronic properties; 3) how we synthesized pre-functionalized and post-functionalizable squaraines to improve their bioavability as PDT sensitizers.

3.1.1 Molecular engineering of electronic properties for squaraine dyes

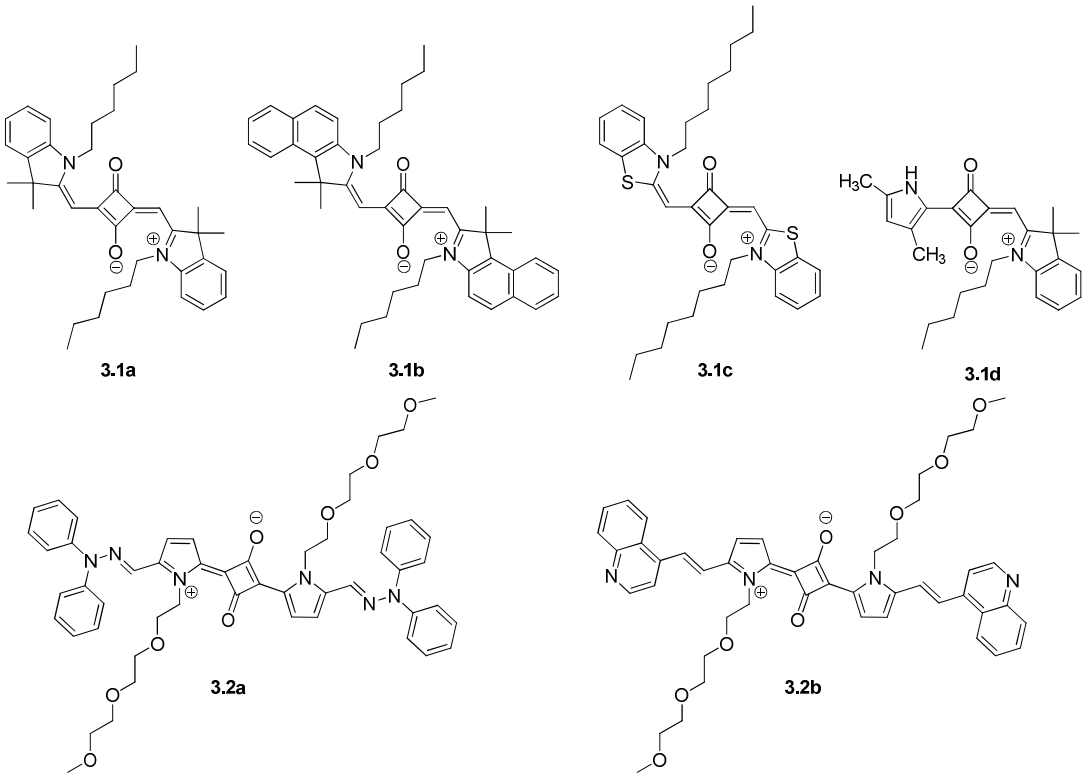

Scheme 3.1

Squaraines **3.1a** and **3.1b** were obtained microwave-assisted condensation starting from the appropriate heteroaryl anhydrobase precursor, imidazole and squaric acid in a 2-PrOH/toluene mixture for 2-4 h. Squaraines **3.1c** and **3.1d** were prepared following the methods described by Santos et al.[16] and by Treibs et al.,[17] respectively. Derivatives **3.2a** and **3.2b** were obtained were obtained as previously described by refluxing the appropriate arylhydrazonomethylpyrroles or bisheteroarylethane and squaric acid in a BuOH/toluene mixture for 1-3 h, according to a published procedure from our laboratory.[18] The series of anhydrobase derivatives is intended for photopysical studies (see Section 3.2), hence the functionalization with alkyl chains that improve solubility in organic solvents. We functionalized the pyrrole derivatives with glycolic chains to

improve water-solubility in one of the first attempt to use them as PDT sensitizer. From the same point of view, we studied two different strategies to increase the singlet oxygen quantum yield with respect to **3.1a**: (a) the ring fusion effect in **3.1b** and (b) the role of sulfur in **3.1c** as a heavy atom to facilitate intersystem crossing (as opposed to the much used, but not completely biologically friendly, halogen atoms). We also characterized the non symmetric derivative **3.1d** to investigate how the presence of a net dipole moment influences the interaction with molecular oxygen. This class of heteroaryl anhydrobase squaraines possesses sharp and intense main absorption bands in the region above 600 nm. The emission is symmetric in energy (Figure xxx) and is characterized by a very small Stokes shift as expected from polymethine molecules.[19] The bathochromic shift observed for **3.1b** is consistent with the extension of the π–conjugated system, while the bathochromic shift observed for **3.1c** reflects the stabilization effect due to the sulphur push character on the positive charge delocalized along the squarylium backbone. The hypsochromic shift observed for **3.1d** is consistent with the desymmetrization effect previously described.[20] With regard to derivatives **3.2a,b** we chose to extend the conjugation length by the introduction of an hydrazonic moiety and an electron-deficient heteroaromatic ring in order to exploit the effect of the oxidation potential on singlet oxygen generation. The data reported in Table 3.1 for the pyrrole derivatives are in agreement with the introduction of a further mild electron donating and electron withdrawing groups (respectively a hydrazone or quinoline moiety) on the structure terminals. These modifications also involve a broadening of the electronic transitions and an increase in the Stokes shift. These indications are particularly relevant when we try to match the sensitizer absorption with the transparency window of biological tissues (600-900 nm).

3.1.2 Molecular engineering of squaraine functionalities

In order to demonstrate the readiness of squaraine tailoring, we explored the synthetic possibilities arising from the condensation of the emisquaraine 3-(3,5-dimethyl-1*H*-pyrrol-2-yl)-4-hydroxycyclobut-3-ene-1,2-dione (**3.3**) with different anhydrobases derivatives* in a 2-PrOH/toluene mixture for 6-8 h (Scheme 3.2).

* Due to their low stability, the anhydrobases are generated in situ by reaction of the appropriate arylazonium salt with imidazole.

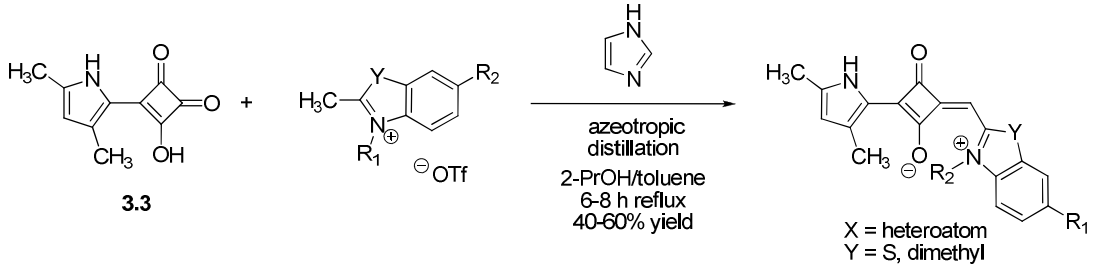

Scheme 3.2

Specifically, we inserted in the squaraine backbone: a) an alkyl chains (**3.1d**), to improve solubility in organic solvent; b) a sulphonate group to increase water solubility (**3.4**); c) a carboxylic acid (**3.5**) that could either associates to biological targets by hydrogen bonding (i.e., collagen[21]) or acts as functionalization site; c) cholesterol (**3.7**), which benefits are discussed later on; and d) a phthalimide group (**3.6**) that could be deprotected to amine.

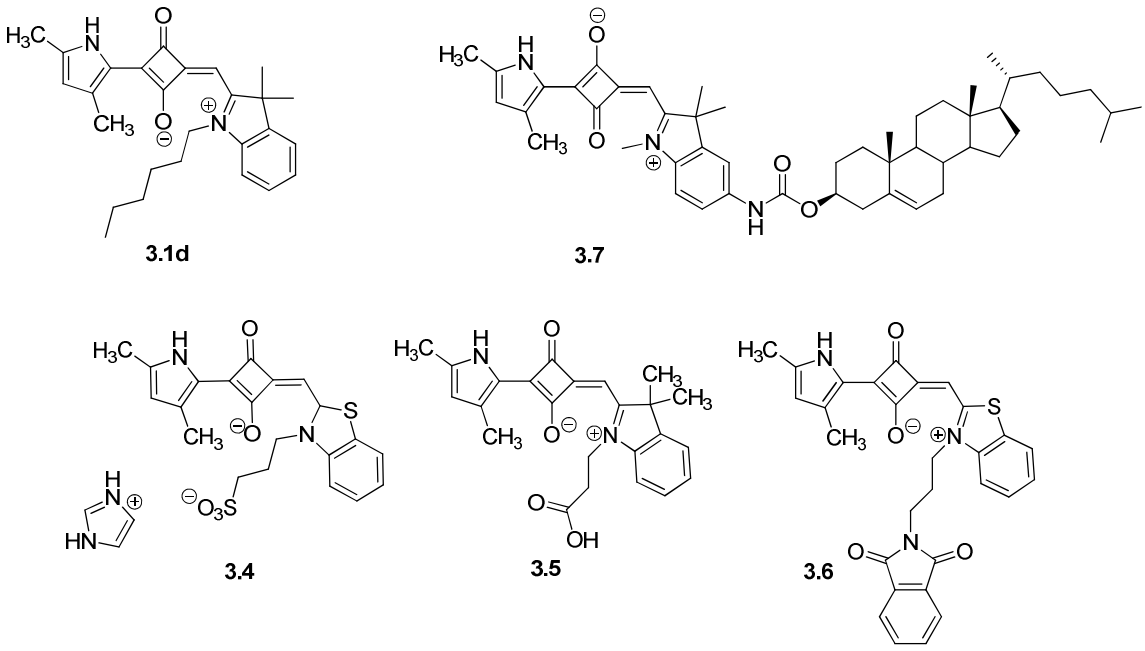

Scheme 3.3

Despite the remarkable differences in solubility these dyes possess, their electronic properties are not affected as evident from the $E_{0,0}$ energies reported in Table 3.1. This result confirm that squaraine dyes offer the great advantage of tunability with respect to other sensitizers. Indeed, we are able to design and synthesized squaraines with different functionalities without affecting the electronic properties of the molecular scaffold.

Table 3.1 Spectroscopic Properties of some Squaraines in Air-Equilibrated Solvents.

Compound	Substituent	$\lambda_{abs,max}$ [a] /nm (solvent)	$E_{0,0}$ [b] /kJ mol^{-1}
3.1d	hexyl	605 (toluene)	197.7
3.4	sulfonate	572 (DMSO)	209.1
3.5	carboxylic acid	598 (2-PrOH)	200.0
3.7	cholesteryl	613 (THF)	195.1
3.6	*N*-propylphthalimide	612 (CH_2Cl_2)	195.5

[a] Wavelength of absorption band maximum. Error of ± 0.5 nm. [b] S_0-S_1 energy.

3.1.3 Molecular engineering of bioavailability

Among all the possible functionalities, we chose to take advantage of cholesterol to improve squaraine bioavailability. As discussed in Chapter 2, every sensitizer need to be delivered with a specific agent, and liposomes are a suitable choice to improve the drug pharmacokinetics and increase the accumulation in the tumor tissues. Moreover, a lipophilic dye can penetrate the cellular membranes easier than a hydrophilic one (i.e., a sensitizer with a sulphonate group). Therefore, we provided a strategy to readily synthesize large amount of indolenine and benzothiazole cholesterol derivatives (**3.11** and **3.15**). This was done by nitration of the heteroaryl compound in a sulphonitric mixture at 0°C overnight followed by reduction of the nitro group with stannous chloride in refluxing ethyl acetate for 4 hours. The amine derivative obtained reacts with cholesteryl chloroformate both in a phase transfer catalysis and in an esterification reaction in the presence of triethylamine to afford the carbamate with high yields. The quantitative alkylation was achieved by reaction with methyl triflate. In this way, up to 12 grams of the benzothiazolium cholesteryl derivative and 10 grams of the indolenine one were obtained.

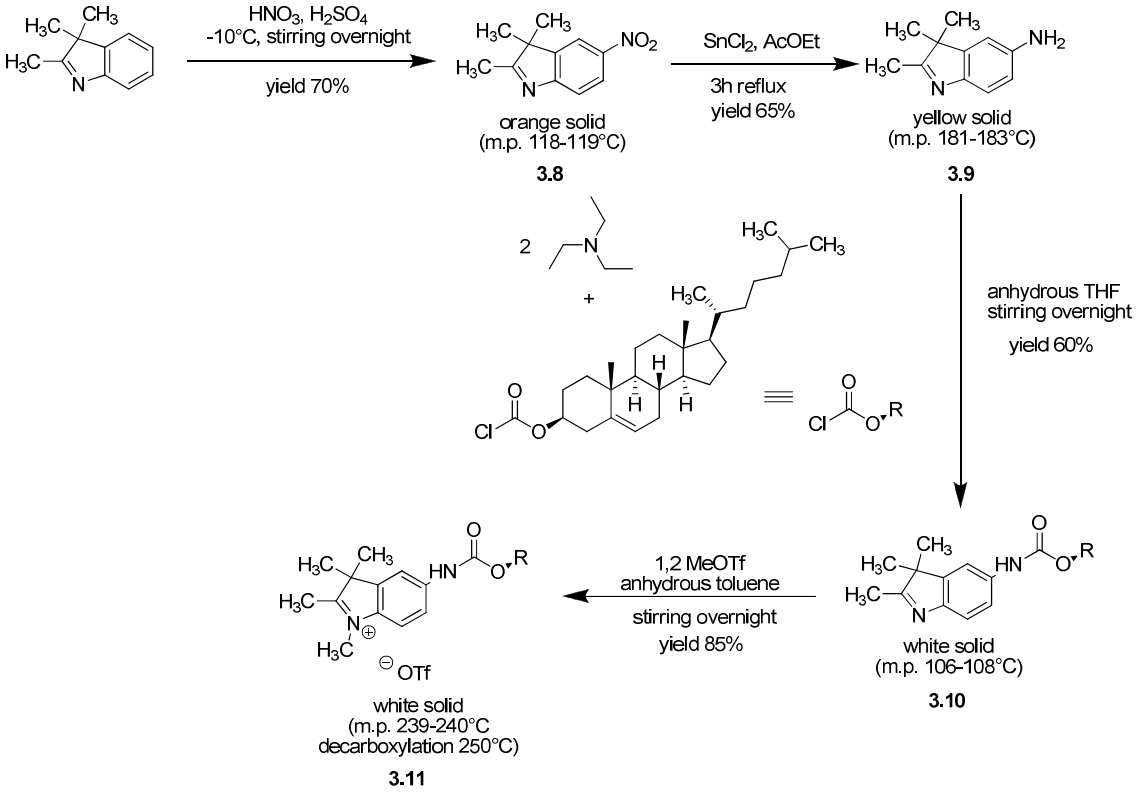

Scheme 3.4

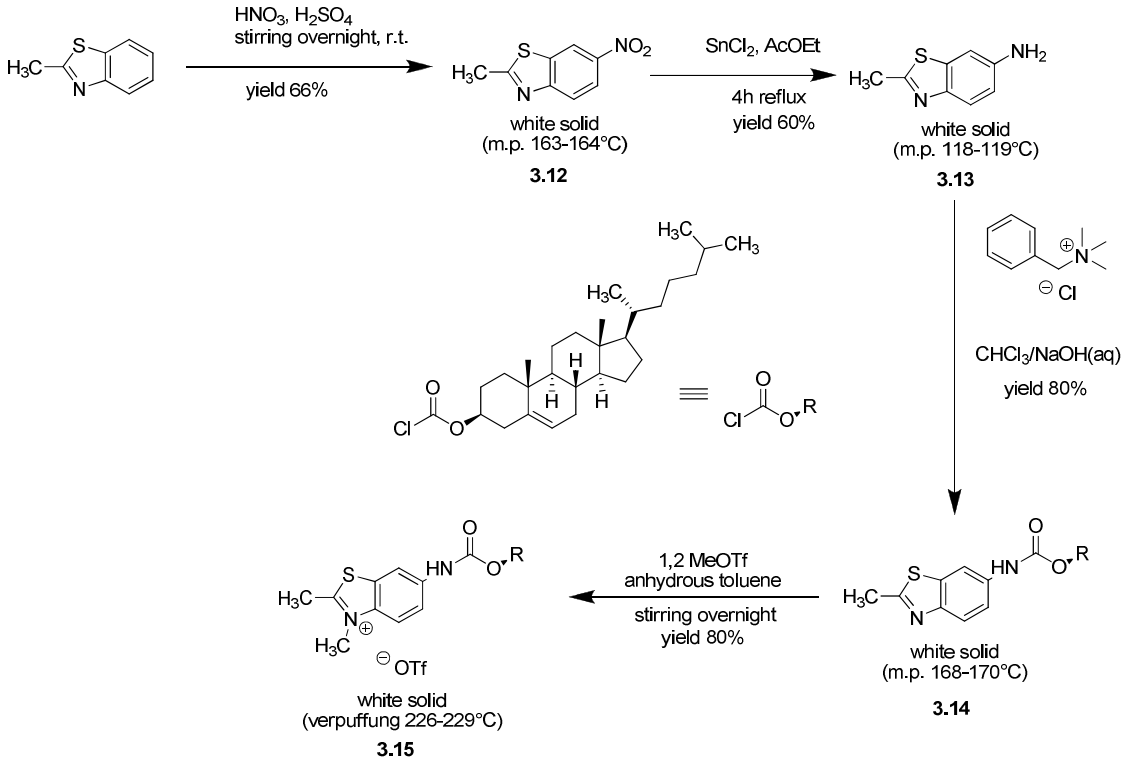

Scheme 3.5

These salts were used in the reaction with an appropriate emisquaraine and imidazole to yield the corresponding squaraine. Thanks to this strategy we synthesized six novel

cholesterol functionalized squaraine dyes in good amounts, five of which unsymmetrical. Moreover, we here presented two unprecedented thiophene-based emisquaraines opening the way to new class of thiophene-based squaraines. Of particular interest are the two bioconjugated analogous of the cell-killer archetype **3.1c**. Indeed, we designed these molecules to increase their compatibility within the lipophilic core of liposomes and LDL and enhance the tumor tissue selectivity and retention for the squaraine-delivery agent system.

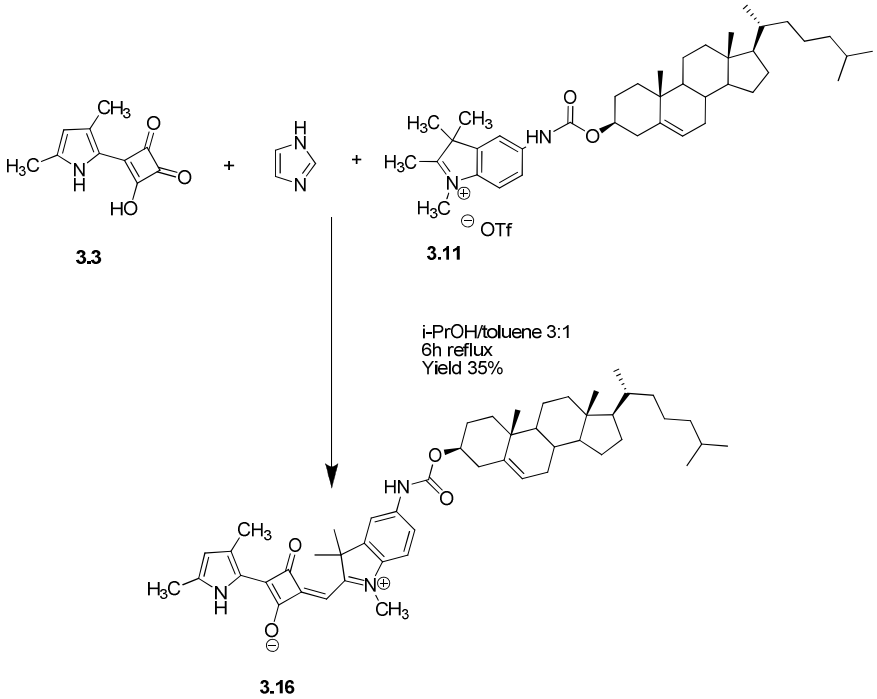

Scheme 3.6

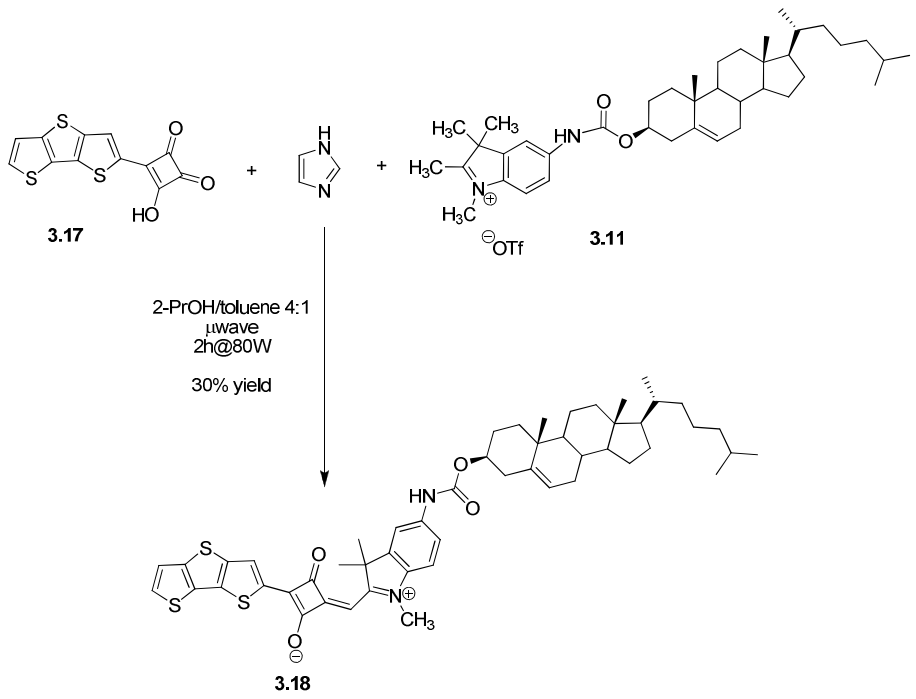

Scheme 3.7

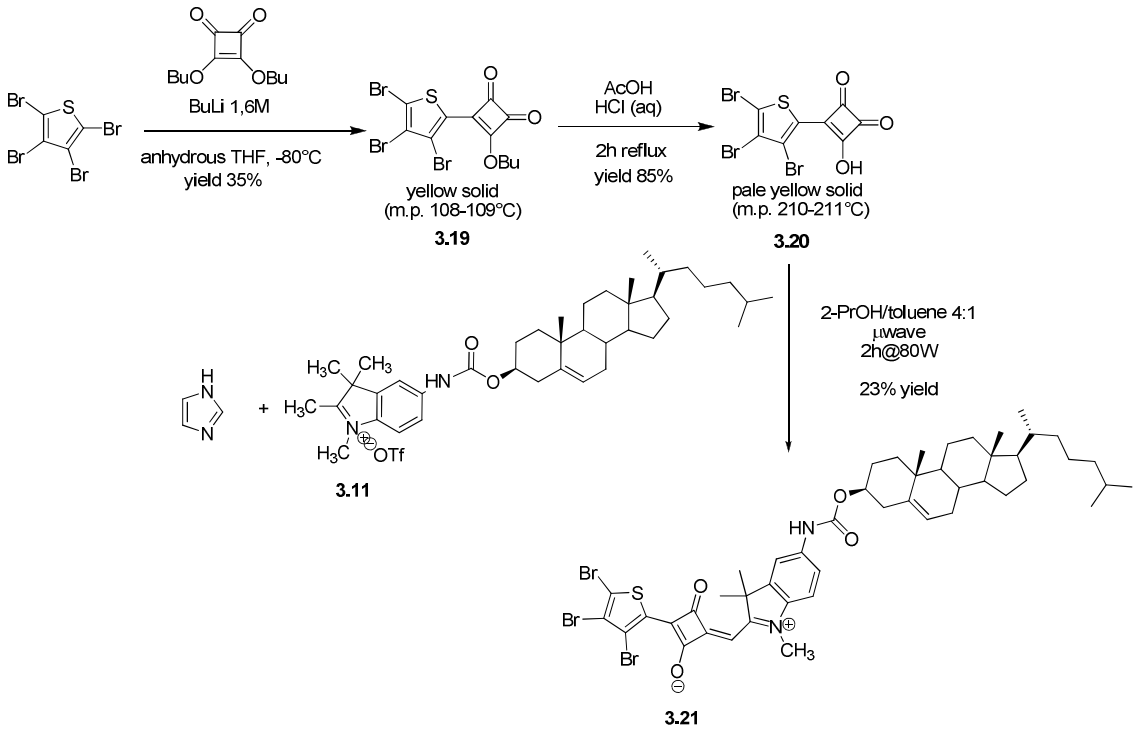

Scheme 3.8

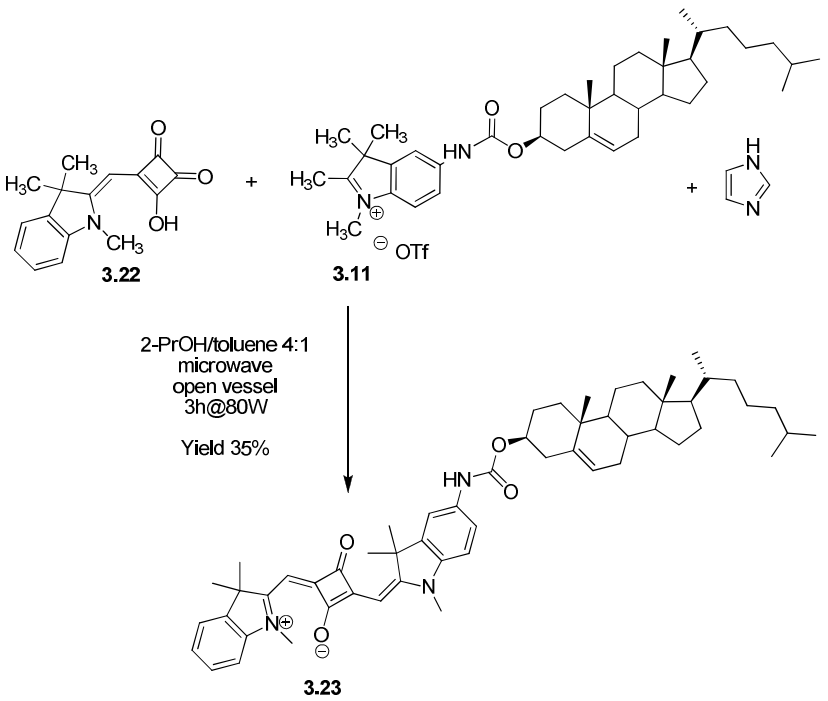

Scheme 3.9

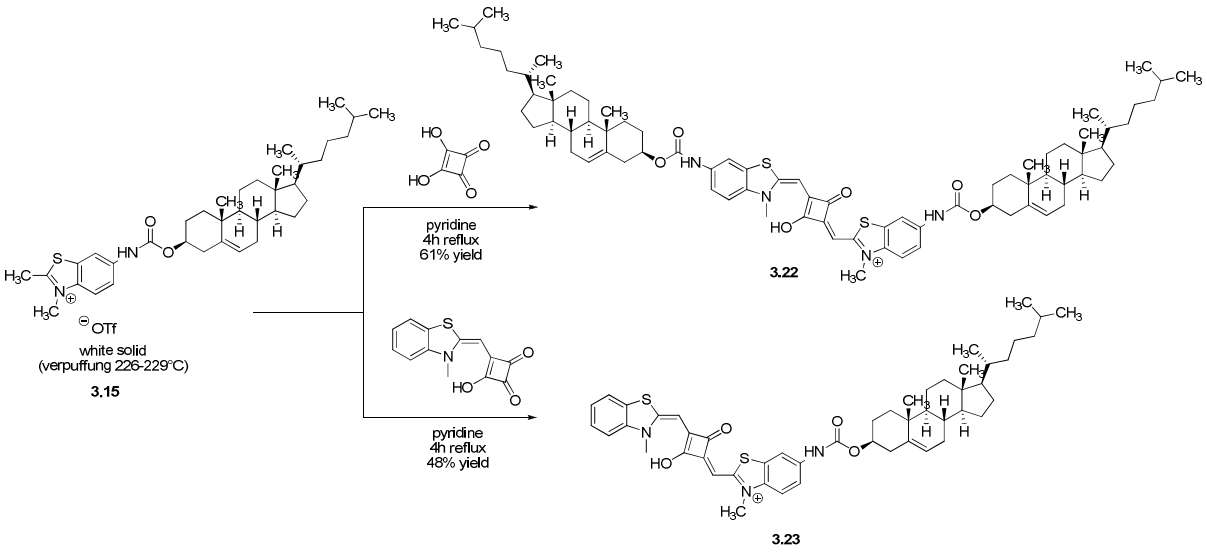

Scheme 3.10

The last example here reported shows the synthesis of a post-functionalizable squaraine. The demand for such a compound arises from the reactivity of squaraines toward nucleophiles. Indeed, thiols, amine, and to less extent other nucleophilic agents add irreversibly with the carbon of the squaric core in position 2 in a way similar to the Mannich addition. As a result, the chemical identity and the electronic conjugation of the squaraine is disrupted. Unfortunately, many biological systems suitable as tumor trackers (e.g., folic acid) contain such nucleophilic moieties, incompatible with the

squaraine synthesis. The development of a readily post-functionalizable sensitizer and a mild bioconjugation procedure with biological agents is therefore necessary. Following, we present an unsymmetrical indolenine-based squaraine with a functionalizable hydroxyl group on one of the benzene ring **3.27**. The synthesis involves the Fisher synthesis of 5-methoxy-2,3,3-trimethyl-3*H*-indole, deprotection of the metoxy group with BBr_3 in dichloromethane, alkylation in methyl iodide at room temperature over three days and condensation with the emisquaraine in pyridine. The desired product was collected by filtration after pouring in acidic water the reaction mixture as metallic green solid. This simple procedure allows the synthesis of a post-functionalizable squaraine in large amount (up to 300 mg), when compared to porphyrin-based sensitizers.

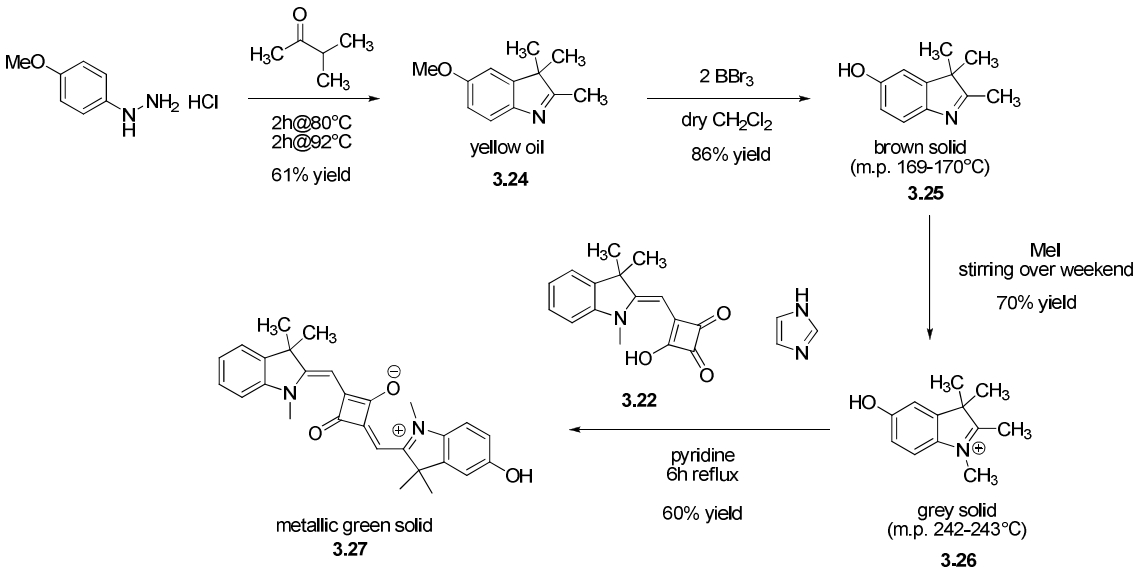

Scheme 3.11

3.2 Photophysics of Squaraine Dyes: Role of Charge-transfer in Singlet Oxygen Production and Removal

Because of the many demanding requirements of modern PDT sensitizers, we felt important to investigate with greater effort the photophysical behavior of heterocycle-based π-extended squaraines to lay foundations for future studies on the possible oxygen-mediated mechanism leading to cellular phototoxicity. We report herein the synthesis, the photophysical and electrochemical characterization of selected members of two classes of squaraines (including direct measurements of quantum yields of

singlet oxygen phosphorescence and triplet state formation). These are identified by their different Arabic numbers while letters identify their different substituents or skeletons (Scheme 3.1). All derivatives were characterized both in toluene and in acetonitrile. Table 3.1 shows the UV-vis absorption characteristics of the squaraines studied, while the representative spectra of **3.1a** in toluene are shown in Figure 3.2.

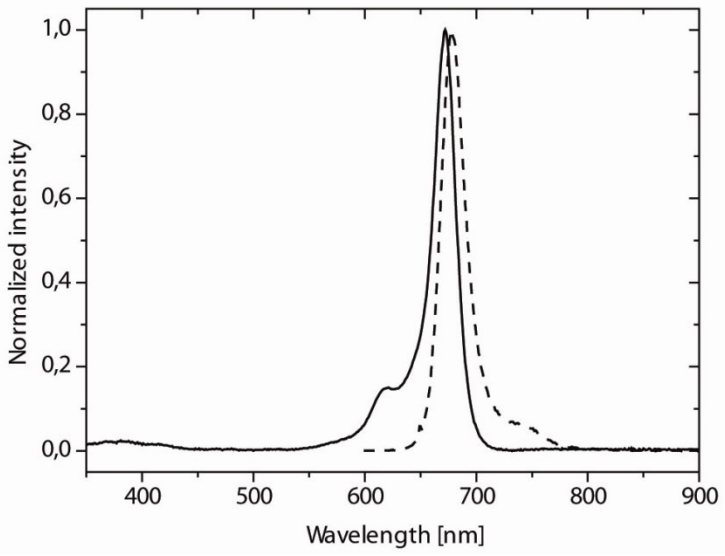

Figure 3.2: One-photon absorption (solid line) and fluorescence (dashed line) spectra of 3.1a in toluene.

Table 3.2: Spectroscopic properties of family 3.1 and 3.2 squaraines.

compound	solvent	$\lambda_{abs,max}$ [a]	$\lambda_{em,max}$ [b]	Stokes shift[c]	ε [d]	$E_{0,0}$ [e]
3.1a	Toluene	641	649	192	250000	15504
	Acetonitrile	634	643	221	235000	15662
3.1b	Toluene	672	678	132	275000	14815
	Acetonitrile			[f]		
3.1c	Toluene	682	705	478	295000	14420
	Acetonitrile	663	675	268	280000	14950
3.1d	Toluene	605	612	189	230000	16434
	Acetonitrile	593	602	252	195000	16737

3.2a	Toluene	729	750	384	300000	13523
	Acetonitrile	719	748	539	280000	13633
3.2b	Toluene	707	728	408	286000	13937
	Acetonitrile	683	713	616	264000	14327

[a]Absorption maximum wavelength, in nm ± 0.5. [b]Emission maximum wavelength, in nm ± 0.5. [c]Stokes shift, in cm^{-1} ±30. [d]Extinction molar coefficient, in l mol^{-1} cm^{-1}, estimated error 10%. [e]Optical gap, in cm^{-1} ±30. [f]Strong ground state aggregation.

For molecules derived from heteroaryl anhydrobases **3.1a-d**, this class of squaraines possesses sharp and intense main absorption bands in the region above 600 nm. The emission is symmetric in energy (Figure 3.2) and is characterized by a very small Stokes shift as expected from polymethine molecules.[19] This in turn implies that these dyes are extremely sensitive to inner-filter effects where a fraction of the emitted light will be re-absorbed by the sample, an artifact that can severely influences any attempt to measure emission quantum yields. For the present work we chose to excite each dye in both the blue region (380-400 nm), where the absorption is very low, and in the red region (640-680 nm) where the absorption is the most intense. For each molecule, it is important to stress that the whereas the magnitudes of the two emission spectra were markedly different due to the inner-filter effect the spectral shape was unaffected. This indicates that in both cases emission originates from the lowest vibrationally relaxed singlet state (i.e. we observe no deviation from Kasha's rule).

Both absorption and the emission are essentially non solvatochromic, however the Stokes shift is, with the exception of **3.1c**, largest in acetonitrile as expected as this is a highly polar solvent. The bathochromic shift observed for **3.1b** is consistent with the extension of the π–conjugated system, while the bathochromic shift observed for **3.1c** reflects the stabilization effect due to the sulphur push character on the positive charge delocalized along the squarylium backbone. The hypsochromic shift observed for **3.1d** is consistent with the desymmetrization effect previously described.[20]

The data reported in Table 3.2 for the pyrrole derivatives **3.2a** and **3.2b** are in agreement with the introduction of a further mild electron donating and electron withdrawing groups (respectively a hydrazone or quinoline moiety) on the structure terminals. These modifications also involve a broadening of the electronic transitions

and an increase in the Stokes shift.

3.2.1 Fluorescence yields and lifetimes

Fluorescence quantum yields (Φ_F) were determined relative to a standard (zinc-phthalocyanine in pyridine, for which $\Phi_F = 0.30$) using well-established procedures.[22] The integrated intensities were recorded at different absorbances, and we accounted for differences in the light collection efficiency due to different refractive indexes.[23] The data reported in Table 3.2 show the solvent plays a dramatic role in the photophysics of this polymethine dyes. All the symmetric squaraines exhibit only a small negative solvatochromism in the absorption and emission level while the fluorescence quantum yields drops more than four times on going from toluene to acetonitrile (Table 3.3).

Table 3.3: Fluorescence quantum yields, Φ_F, for various squaraine dyes in air-saturated toluene and acetonitrile[a]

Solvent	*Compound*					
	3.1a	**3.1b**	**3.1c**	**3.1d**	**3.2a**	**3.2b**
Toluene	0.29 ± 0.06 [b] (0.052 ± 0.002 [e])	0.51 ± 0.06 [c] (0.068 ± 0.002 [e])	0.85 ± 0.10 [d] (0.088 ± 0.005 [e])	0.13 ± 0.04 [f]	0.054 ± 0.010 [g]	0.06 ± 0.02 [h]
Acetonitrile	0.068 ± 0.018 [b]	/	0.21 ± 0.02 [d]	0.022 ± 0.007 [f]	< 0.005 [g]	< 0.005 [h]

[a] estimated error ± 10%. [b] Irradiation at 640 nm. [c] Irradiation at 672 nm. [d] Irradiation at 682 nm. [e] Irradiation at 380 nm. [f] Irradiation at 600 nm. [g] Irradiation at 730 nm. [h] Irradiation at 700 nm.

This is consistent with the fact that the electronic transition in symmetric polymethine dyes is associated with an intramolecular charge-transfer between donor and acceptor groups, producing an excited state with a dipole moment (μ_e) similar to that in the ground state (μ_g).[19] Nevertheless, the coexistence on the same molecule of two electronrich moieties and an electronrich core may involve the stabilization of an intramolecular charge-transfer state coupled radiationlessly to the ground state in polar solvents. The fluorescence quantum yield tends to increase on going from the pyrrole derivatives to the indolenine ones and then to the benzothiazolium one. We ascribe this behavior to an increased structural rigidity that could inhibit the vibronic contribution to the deactivation of the first excited state.

The wavelength of excitation is also very important. Not surprisingly we found higher values of Φ_F when irradiating in the near-IR region as opposed to in the blue region, due to the outstanding spectroscopic feature of these compounds. Indeed, part of the absorbed radiation in the near UV (*i.e.* blue region) will be re-emitted as

fluorescence and then it will be re-absorbed by adjacent molecule as a result of the extremely intense band in the NIR and the small Stokes shift. In short, exciting the chromophores in the blue band causes an artificial decrease in fluorescence quantum yield which severely can affect data interpretation. This is also true for acquiring singlet oxygen quantum yields. As such accurate data is obtained following excitation into the main absorption band around approx. 650 nm.

To get more information than is available from the steady-state data, we checked the fluorescence lifetimes of the presented squaraines. The data collected were in all cases fitted accurately with a single exponential decay and are reported in Table 3.4. The fluorescence lifetimes in toluene follow the same trend as the fluorescence quantum yield for all the squaraines. In fact, a plot of τ_F versus Φ_F yield a straight line, Figure 3.3, indicating very similar values of the radiative rate constant, k_r, for the compounds (as $k_r = \Phi_F/\tau_F$ is simply the slope from Figure 3.3). This indicates that, from both a comformational and transitional point of view, the emissive states of all dyes are very similar.[24]

Table 3.4: Fluorescence lifetime (τ_F) and radiative rate constant, k_r, for various squaraine dyes in air-equilibrated toluene.

	3.1a	**3.1b**	**3.1c**	**3.1d**	**3.2a**	**3.2b**
τ_F (ns)	2.84 ± 0.02	4.22 ± 0.03	6.54 ± 0.07	1.55 ± 0.01	1.04 ± 0.02	< 1

When we tried to repeat the measure in acetonitrile we found substantially weak responses with kinetics too short to be unambiguously separated from the signal. This is fully consistent with the intervention of non-radiative excited charge-transfer states strongly coupled to the ground state these dyes which efficiently deactivates the singlet excited state in polar solvents.

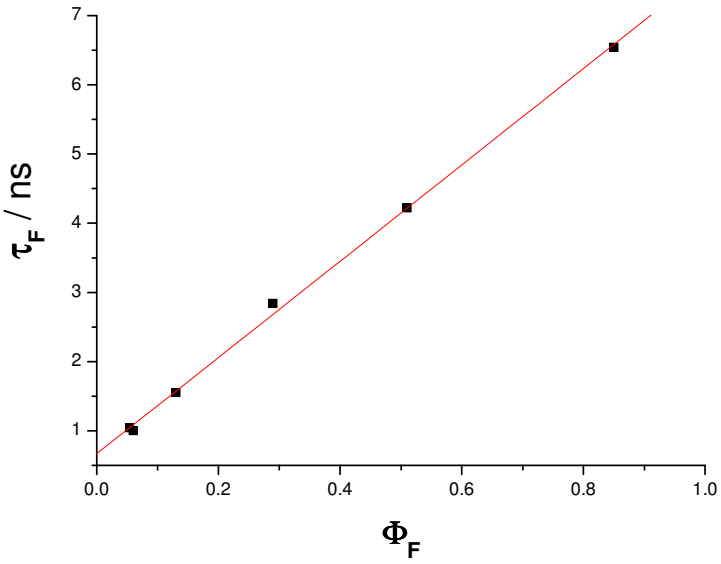

Figure 3.3: Plot of the fluorescence quantum yield against the fluorescence lifetime.

3.2.2 Singlet oxygen quantum yields (Φ_Δ)

Despite comparably long fluorescence lifetimes in air, the first excited singlet state for the molecules studied are still too short to be appreciably quenched by ground state oxygen under air-saturated conditions, and as such the triplet state is the precursor of singlet oxygen. Experiments were performed in toluene using both blue and red light for excitation, and the collected Φ_Δ values are summarized in Table 3.5. For molecules **3.1d, 3.2a and 3.2b** the signals were very low, yet detectable, and the estimated upper limit of Φ_Δ for these compounds is 0.005 in toluene. In acetonitrile all compounds gave Φ_Δ < 0.005, except **3.1b** and **3.1c** which aggregated sufficiently to prevent a quantification.

Table 3.5: Singlet oxygen quantum **yield (Φ_Δ) for various squaraine dyes in air-equilibrated toluene after excitation in the near-infrared band and in the blue band.**

λ_{ex} [a]	Φ_Δ [b]		
	1a	**1b**	**1c**
BLUE	0.018 ± 0.004 [c]	0.021 ± 0.008 [c]	0.05 ± 0.02 [c]
NIR	0.010 ± 0.004 [d]	0.006 ± 0.001 [d]	0.012 ± 0.004 [d]

[a] Excitation region. [b] Singlet oxygen quantum yield; estimated error ± 10%. [c] Irradiation at 395 nm. [d] Irradiation at 655 nm.

Generally we find that these squaraine dyes are very poor singlet oxygen photosensitizers. The results here presented are not in agreement with substantially higher singlet oxygen quantum yields reported previously with different experimental setup and procedures for squaraine dyes,[25-28] but are in agreement with the results reported for polymethine dyes.[29, 30] It is nonetheless evident that the symmetric anhydrobase derivatives are better singlet oxygen generators than the pyrrole derivatives, so that we will hereafter focus on compound **3.1a-c**.

To rationalize the difference between our and previously reported values, we again additionally performed the experiment irradiating in the near UV band in air-equilibrated toluene using perinaphthenone in toluene, $\Phi_\Delta = 0.95 \pm 0.05$,[31] as standard. Just as with the fluorescence quantum yields we see a marked difference between the two excitation regions. However, for Φ_Δ we obtain the largest values irradiating in the blue, as the fluorescence yield in this case is artificially small due to the inner filter effect. In turn a larger fraction of the excited molecules will intersystem cross to the triplet manifold as subsequently generate singlet oxygen. As such, we attributed this self-promoting singlet oxygen generation to the inner filter effect.[22] It is important to recognize that the apparent wavelength-dependent values of Φ_Δ are not related to different states initially populated.

Also this explains why the most fluorescent dye, **3.1c**, is seemingly the best singlet oxygen generator. These considerations are relevant if it could be taken advantage of the inner filter effect to boost the $O_2(^1\Delta_g)$ production of otherwise inefficient sensitizers for specific applications (photodynamic therapy, photochemical synthesis, …). Also, the Φ_Δ values were systematically lower in acetonitrile which is a more polar solvent, and this is consistent with a CT mechanism.

3.2.3 Singlet oxygen quenching rates, k_q

Kinetic analysis showed an appreciable shortening of the singlet oxygen lifetime compared with the value in the neat solvent (30 μs in toluene and ~ 80 μs in acetonitrile).[32] This reduction in the observed lifetime could be explained by quenching phenomena related to physical deactivation of $O_2(a^1\Delta_g)$.[33-35] (the photostability observed for these dyes, except **3.1c**, denies the occurrence of chemical deactivation processes). It is well known that molecules with triplet energies higher than 94 kJ mol^{-1} and oxidation

potentials lower than 1.9 V vs SCE quench singlet oxygen very efficiently.[36] These processes involve the photosensitization of singlet oxygen followed by the formation of a singlet encounter complex, usually referred to as an oxyplex ($^1M_0\ldots O_2(^1\Delta_g)$), between the ground state quencher ($^1M_0$) – in our case the squaraine - and singlet oxygen. Transfer of electron density from the quencher to singlet oxygen stabilizes a charge-transfer (CT) singlet complex, $^1(M^{\bullet+}\ldots O_2^{\bullet-})$, that decays, mainly by intersystem crossing, to a triplet complex which dissociates to the ground state quencher and $O_2(X^3\Sigma^-_g)$ (Scheme 3.12).[37]

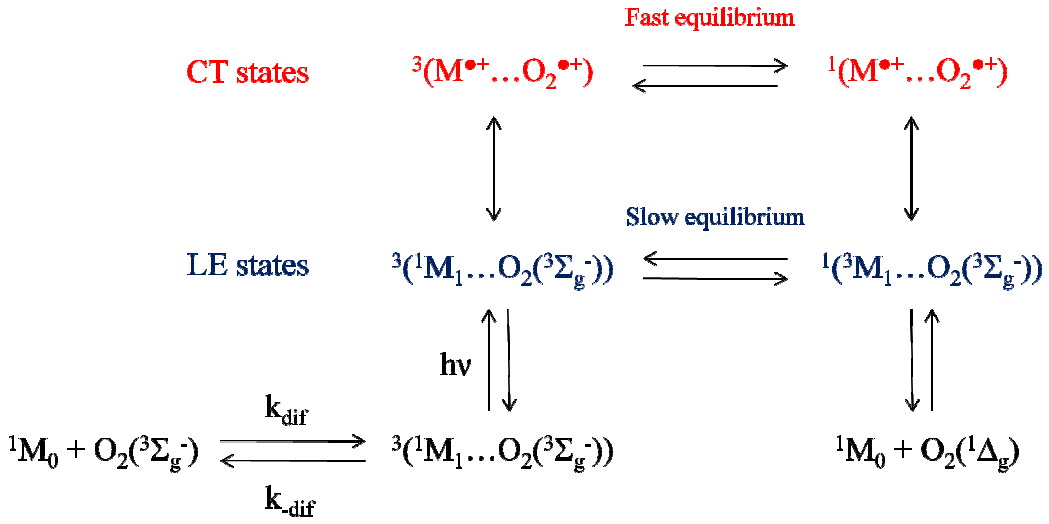

Scheme 3.12: Energy diagram showing pertinent states involved in oxyplex formation and decay.

To estimate k_q values for squaraine dyes, we measured the lifetimes of $O_2(a^1\Delta_g)$ produced by irradiating perinaphthenone at 355 nm in air-equilibrated acetonitrile and toluene, at different concentration of the squaraine (Figure 3.4).

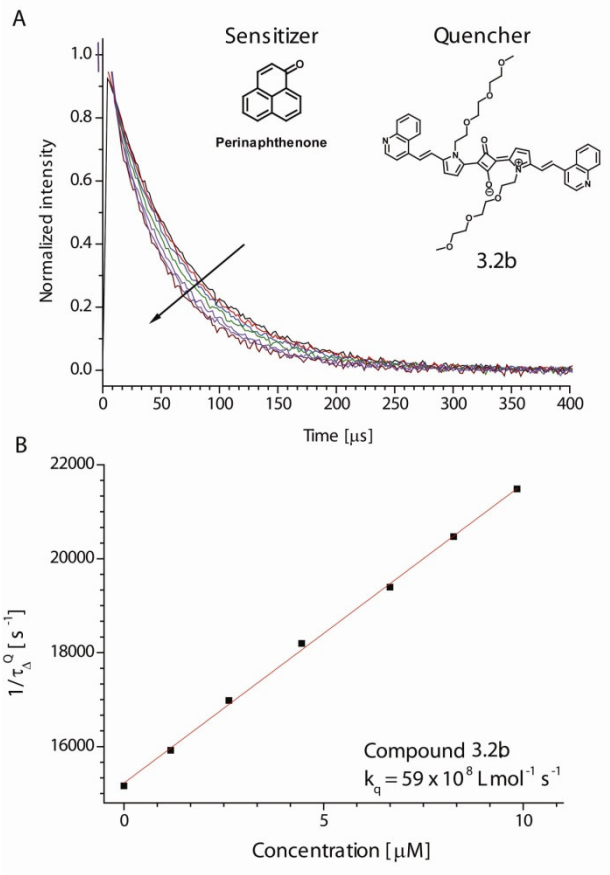

Figure 3.4: (A) Representative time-resolved decays of the signal observed at 1270 nm upon irradiation of an air-equilibrated solution of perinaphthenone at 355 nm in acetonitrile for different concentration of 3.2b. (B) Plot of $\tau_\Delta^0/\tau_\Delta^Q$ against 3.2b absorbance.

The high k_q values here reported (Table 3.6) are consistent with similar values reported for aromatic amines and enamines[38] (*N,N,N,N*'-tetramethyl-*p*-phenylenediamine (TMPD) 5.2×10^9 L mol^{-1} s^{-1} in acetonitrile and 2.6×10^9 L mol^{-1} s^{-1} in benzene, *p*-phenylendiamine 2.8×10^{10} L mol^{-1} s^{-1} in acetonitrile and 2.9×10^9 L mol^{-1} s^{-1} in benzene, *p*-aminodiphenylamine 1.2×10^9 L mol^{-1} s^{-1} in acetonitrile and 1.1×10^8 L mol^{-1} s^{-1} in benzene), for aromatic heterocycles (pyrrole 5×10^8 L mol^{-1} s^{-1},[39] quinoline 1×10^8 L mol^{-1} s^{-1} [40]), and for polymethine dyes (3,3'-diethyl-2,2'-thiatricarbocyanine iodide 2.7×10^9 L mol^{-1} s^{-1} [41]). The higher quenching rates we reported for the pyrrole derivatives are in accordance with a decrease in singlet oxygen production for these dyes. The solvent dependence is in agreement with a charge-transfer oxyplex in acetonitrile that is more stabilized than in toluene, leading to an increase in k_q and a contextual decrease in singlet oxygen production due to a better coupling with the ground state oxyplex.

Table 3.6: Singlet oxygen quenching rates (k_q [10^8 L mol^{-1} s^{-1}] ±10%) for various squaraine dyes in

air-saturated toluene and acetonitrile[a]

Solvent	*Compound*					
	3.1a	**3.1b**	**3.1c**	**3.1d**	**3.2a**	**3.2b**
Toluene	5.0	4.0	3.0	5.9	35	37
Acetonitrile	8.1	n.a.[a]	n.a.[b]	21	52	59

[a] Strong ground-state aggregation. [b] Not stable under irradiation.

3.2.4 Triplet yields

To further assess the role of CT, we used a method developed by Wilkinson and co-workers[42, 43] by which the triplet yield (Φ_T) can be quantified. This utilizes that many singlet excited state ($^1M_1$) quenchers will specifically induce intersystem crossing to yield triplet excited state ($^3M_1$). Importantly, ground state oxygen will also behave as a quencher and, under oxygen-saturated conditions one can observe a reduction in the fluorescence lifetime (as opposed to air-saturated conditions). This will in turn translate into a related difference in the magnitude of the triplet absorption spectrum, and from this it is possible to evaluate the triplet yield (Φ_T). The values obtained are affected by large errors due to weak signals, however the values are compatible with the singlet oxygen yields in Table 3.7.

From the triplet state lifetimes extracted from these experiments, we confirmed that for all molecules the triplet state is quantitatively quenched by ground state oxygen. In this case the efficiency of energy transfer from the squaraine triplet to molecular oxygen to produce singlet oxygen, S_Δ, is easily obtained using the expression $S_\Delta = \Phi_\Delta/\Phi_T$. In the framework of the model presented by Wilkinson, CT oxyplex excited states, $^1(M^{\bullet+}\ldots O_2^{\bullet-})$ and $^3(M^{\bullet+}\ldots O_2^{\bullet-})$, rapidly equilibrate. If CT is in play, then S_Δ will be significantly less than unity. Our measurements are in agreement with the formation of an oxyplex where the interaction is governed by the electronrich moieties of the squaraine and the oxidative character of molecular oxygen. This strong interaction affects the singlet oxygen generation limiting the efficiency of energy transfer between the squaraine triplet excited state and molecular oxygen. In this case it will not be possible to achieve high singlet oxygen yield from squaraine dyes despite their triplet yield contribution.

Table 3.7: Sensitized singlet oxygen yield, Φ_Δ(air), squaraine triplet state yield in the absence,

$\Phi_T(N_2)$, and presence of air, Φ_T(air), and the fraction of triplet states quenched by oxygen that yield singlet oxygen, S_Δ, in solutions of toluene.

Compound	Φ_Δ(air)	$\Phi_T(N_2)$	Φ_T(air)	S_Δ
3.1a	0.018 ± 0.004 (UV) [a] 0.010 ± 0.004 (Vis) [b]	0.022 ± 0.008	0.045 ± 0.016	0.40 ± 0.23
3.1b	0.021 ± 0.008 (UV) [a] 0.006 ± 0.001 (Vis) [b]	0.024 ± 0.009	0.06 ± 0.03	0.35 ± 0.30
3.1c	0.05 ± 0.02 (UV) [a] 0.012 ± 0.004 (Vis) [b]	0.020 ± 0.004	0.13 ± 0.03	0.38 ± 0.24
3.1d	< 0.005 [c]			
3.2a	< 0.005 [b]			
3.2b	< 0.005 [b]			

[a] Φ_Δ data obtained upon irradiation at 395 nm, whereas Φ_T data obtained upon 355 nm irradiation. [b] Irradiated at 655 nm. [c] Irradiated at 592 nm.

3.2.5 Electrochemical characterization

We investigated the electrochemistry of class **3.1** squaraines with cyclic voltammetry to evaluate the redox character of these dyes and their ability to form a CT oxyplex. We have previously characterized the redox processes for class **3.2** squaraines.[44] The two one-electron processes we observed refer to the coupling of the two redox-active centers in all of the symmetric derivatives.

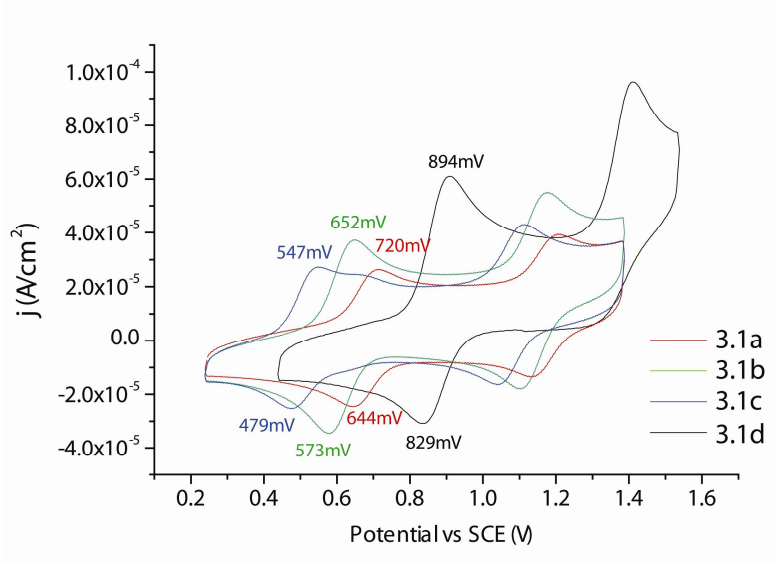

Figure 3.5: Cyclic voltammetry of class 3.1 squaraines in CH_2Cl_2 using tetrabutylammonium esafluorophosphate as the supporting electrolyte at a scan rate of 50 mV/s.

Table 3.8 shows the half-wave potentials ($E_{1/2}$ vs Fc/Fc^+), peak separation between the first and the second redox process (ΔE), and half-wave potentials for irreversible reduction ($E_{1/2}^{red}$) of class **3.1** squaraines in CH_2Cl_2 using tetrabutylammonium esafluorophoshpate as the supporting electrolyte at a scan rate of 50 mV/s. We reported the value for class **3.2** squaraine in acetonitrile with tetrabutylammonium *p*-toluenesulphonate as the supporting electrolyte. All of the class **3.1** squaraine CV plots display two redox waves at positive potentials, corresponding to the reversible oxidation of the enaminic moieties for **3.1a-c** and to the reversible oxidation of the enaminic moiety and the irreversible one of pyrrole moiety for **3.1d**. Squaraine **3.2a** CV plot shows two positive potential waves related to the oxidations of the two hydrazonic moieties, while compound **3.2b** CV plot show an irreversible behavior in oxidation matching with the oxidation of the pyrrole moieties. The low oxidation potentials verified by CV are plausibly the cause for the high affinity of squaraine dyes to the formation of CT oxyplex. Moreover, the reported oxidation potentials are similar to those of efficient singlet oxygen quenchers (TMPD 0.16 V vs. SCE, *p*-phenylendiamine 0.18 V vs. SCE, *p*-aminodiphenylamine 0.27 V vs. SCE).[49]

Table 3.8: Half-Wave potentials ($E_{1/2}$ vs Fc/Fc^+), peak separation values for each process for which an $E_{1/2}$ value is reported (ΔEp), peak separation between the first and the second redox processes (ΔE), of class 3.1 in CH_2Cl_2 with Tetrabutylammonium esafluorophosphate as the supporting electrolyte and of class 3.2 squaraines in CH_3CN with Tetrabutylammonium *p*-toluenesulphonate as the supporting electrolyte.[a]

Compound	$E_{1/2}(1)$	$\Delta Ep(1)$	$E_{1/2}(2)$	$\Delta Ep(2)$	ΔE
3.1a	0.682	0.076	1.17	0.071	0.49
3.1b	0.612	0.079	1.14	0.070	0.53
3.1c	0.513	0.068	1.08	0.069	0.57
3.1d	0.861	0.065	1.410		0.55
3.2a	0.18	0.065	0.46	0.060	0.28
3.2b	0.55				

[a] values are in V ± 0.010.

3.3 Photobleaching and photooxidation capabilities of squaraine dyes

We found an interesting photochemical behavior for **3.1c** while dealing with its photophysical characterization. In particular, this squaraine is susceptible to extensive photobleaching in acetonitrile and in the presence of oxygen. Moreover, this phenomena is completely hindered when nitrogen replaces oxygen in the solution and the photobleaching rate is slower in a less polar solvent (i.e., air-equilibrated toluene). As suggested by the photophysical study, we attribute this behavior to a charge-transfer encounter complex between the squaraine and molecular oxygen that evolves to give a new chemical species. To unveil the photochemical mechanism involved, we analyzed a completely sun-bleached solution of **3.1c** in air-equilibrated acetonitrile by GC-MS. We observed the formation of two compounds: 3-hexylbenzo[*d*]thiazol-2(3*H*)-one and a not yet identified species characterized by a molecular ion with a mass of 279 and a fragmentation compatible with an alkyl chain and a 1,2-disubstituted benzene ring.

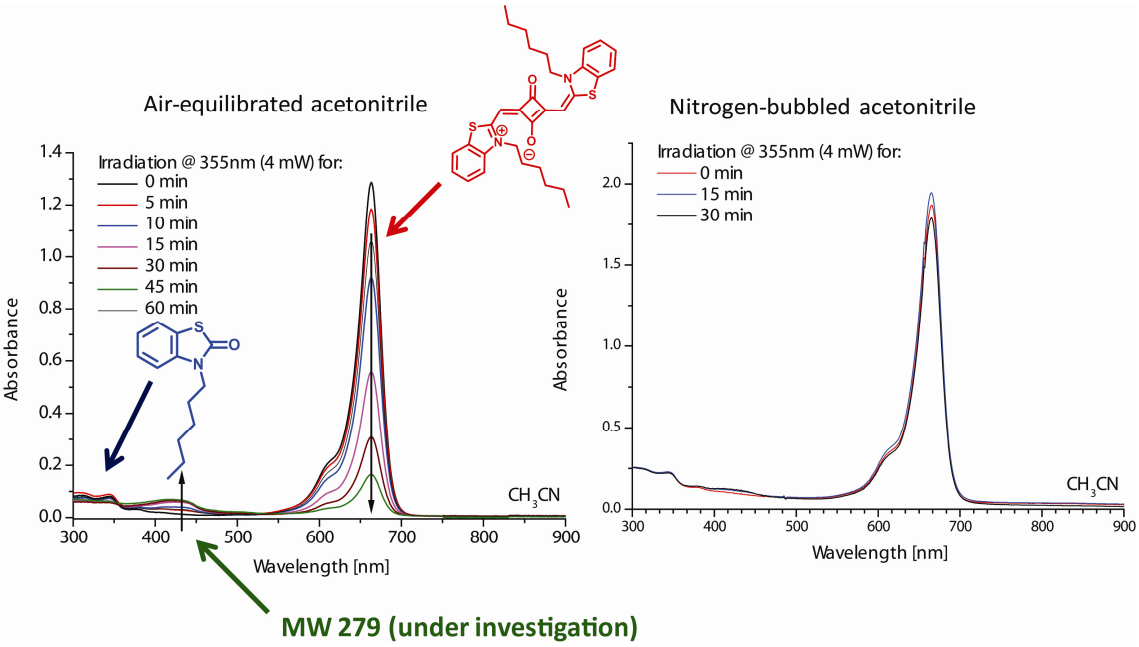

Figure 3.6: Change in the absorption spectra of 3.1c in air-equilibrated and nitrogen-bubbled acetonitrile upon irradiation with a laser source at 355 nm.

We ascribed this photochemical behavior to the photooxygenation of electron-rich double bond (i.e., enamine) without allylic hydrogens as demonstrated by Foote [45, 46] among the others. The probable mechanism is a nonconcerted 1,2-cycloaddition to give a dioxetane intermediate which cleaves to two carbonyl derivatives, one of the two in its triplet state (Scheme 3.13). The formed excited carbonyl compound can then react according to both Norrish Type I and Type II reactions: α-Cleavage of the excited carbonyl compound leading to an acyl-alkyl radical pair (from an acyclic carbonyl compound) or an acyl-alkyl diradical (from a cyclic carbonyl compound) as the primary photoproduct and intramolecular abstraction of a γ-hydrogen to produce a 1,4-diradical as the primary photoproduct, respectively. The radicals formed can establish a radical reaction chain that could be responsible for the phototoxicity behavior observed in benzothiaziolium based squaraines **3.1c** and **3.30**. (See Section 3.4).

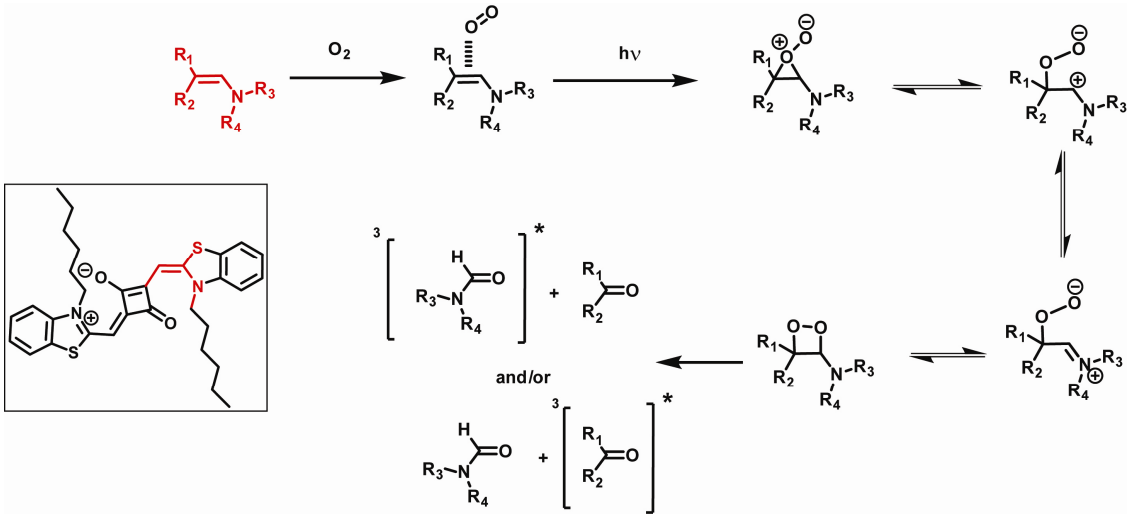

Scheme 3.13

We studied the product distribution of the reaction between light, squaraines and oxidable substrates (i.e., limonene, cholesterol, and methyl linoleate) to look for the other possible mechanisms leading to photooxidative damage but photogeneration of singlet oxygen. We carried out photosensitized oxygenations by irradiating a solution of squaraine dye filtered below 500 nm (white halogen lamp, 300 W) for half an hour and we analyzed the product peroxides reduced with $NaBH_4$ by GC-MS analysis. The oxygenation of (*R*)-(+)-limonene provides a particularly sensitive fingerprint for the reactive intermediate. This substrate contains two double bonds, one disubstituted and one trisubstituted. Photooxygenation yields all six possible products of singlet oxygen attack at the trisubstituted double bond; no products with unshifted double bond are formed, and the disubstituted double bond is inert. The predominant products have the double bond exocyclic, and formation of endocyclic products is unfavorable. Byproducts which involve shift of the tertiary hydrogen atom from an isopropyl group to oxygen are formed only in minor amounts, probably because the most favorable conformation for the isopropyl hydrogen is in the plane of the double bond. As can be seen when we compared our results with the study by Foote, the photoreaction promoted by the squaraine is not compatible with singlet oxygen mediated oxygenation, but with Type I radical processes (Figure 3.7). Furthermore, the attempt to photooxygenate cholesterol gave no products, in accordance to the radical scavenger role played by the hydroxyl group of cholesterol (Figure 3.8).

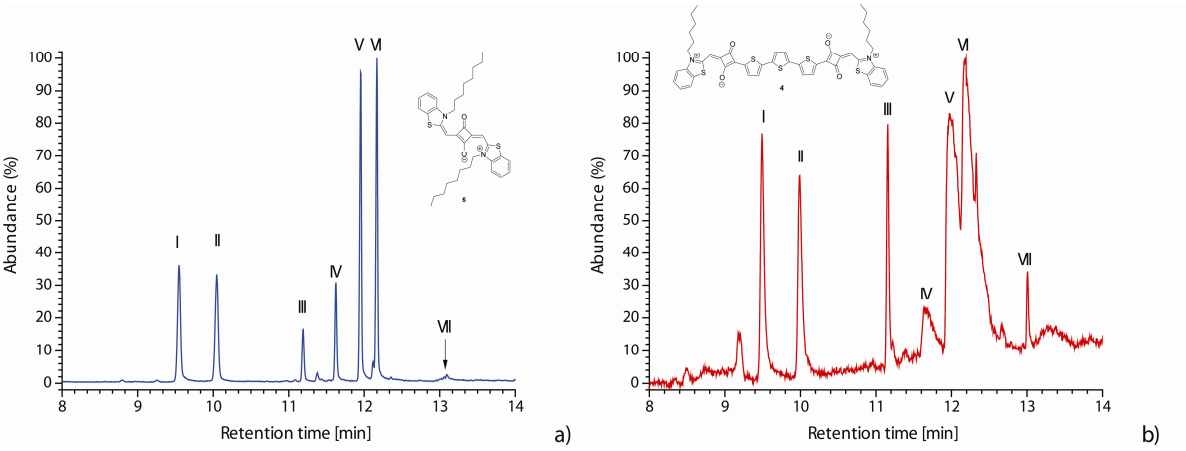

Figure 3.7: GC-MS GC-MS chromatograms showing resolution of a solution of (*R*)-(+)-limonene in acetonitrile photosensitized by a) 3.1c and b) 3.30. Peak identification: (I) and (II): either (1*S*,4*R*)- or (1*R*,4*R*)-1-methyl-4-(prop-1-en-2-yl)cyclohex-2-enol, (III) and (IV): either (1*R*,5*S*)- or (1*S*,5*S*)-2-methylene-5-(prop-1-en-2-yl)cyclohexanol, (V) (1*R*,5*S*)-2-methyl-5-(prop-1-en-2-yl)cyclohex-2-enol, (VI) (1*S*,5*S*)-2-methyl-5-(prop-1-en-2-yl)cyclohex-2-enol, (VII) (*R*)-(4-(prop-1-en-2-yl)cyclohex-1-enyl)methanol.

Table 3.9: Product distributions in photosensitized oxygenation of (*R*)-(+)-limonene

Product	I	II	III	IV	V	VI	VII
Singlet oxygen sensitization[5]	10	34	19	23	9	4	0
Photo sensitization by 5	17 + 16		5 + 9		25	26	1
Photo sensitization by 4	11 + 11		6 + 6		29	33	2

Table 3.10: name, characteristic ions and GC retention times of the photosensitized oxygenated products of (*R*)-(+)-limonene.

Peak	Product	Characteristic ions (*m/z*)	Retention times (min)
I	(1*S*,4*R*)- or (1*R*,4*R*)-1-methyl-4-(prop-1-en-2-yl)cyclohex-2-enol	91 119 79 134	9.55
II	(1*S*,4*R*)- or (1*R*,4*R*)-1-methyl-4-(prop-1-en-2-yl)cyclohex-2-enol	91 119 134 79	10.05
III	(1*R*,5*S*)- or (1*S*,5*S*)-2-methylene-5-(prop-1-en-2-yl)cyclohexanol	91 109 134 119	11.19
IV	(1*R*,5*S*)- or (1*S*,5*S*)-2-methylene-5-(prop-1-en-2-yl)cyclohexanol	91 119 134 109	11.63
V	(1*R*,5*S*)-2-methyl-5-(prop-1-en-2-yl)cyclohex-2-enol	109 91 84 119	11.95

VI	(1*S*,5*S*)-2-methyl-5-(prop-1-en-2-yl)cyclohex-2-enol	84 91 134 119	12.17
VII	(*R*)-(4-(prop-1-en-2-yl)cyclohex-1-enyl)methanol	79 91 67 55	13.09

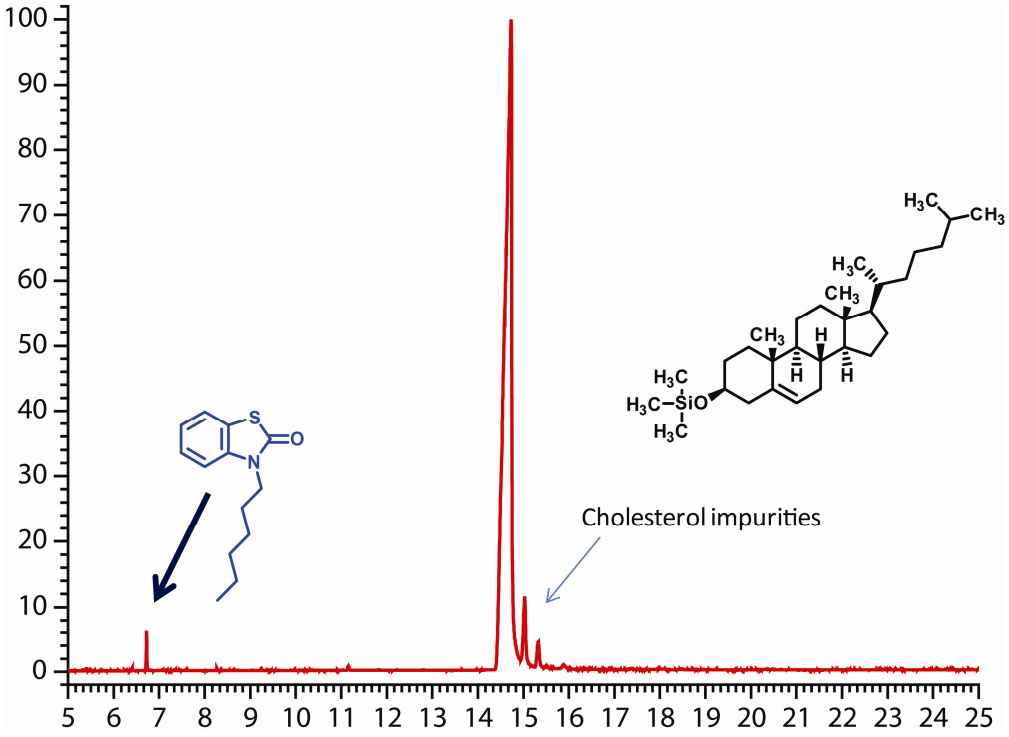

Figure 3.8: GC-MS chromatogram of solution of cholesterol (toluene:CH_3CN 3:2) photosensitized by 3.1c and then reduced with $NaBH_4$.

Moreover, the photooxygenation of methyl linoleate, a constituent of cellular and subcellular membranes, gives eight photoproducts mainly. Despite the attribution of their chemical identities is complicated by a very similar fragmentation for each of them, their number is consistent with a radical mediated oxygenation as reported by Frankel.[47]

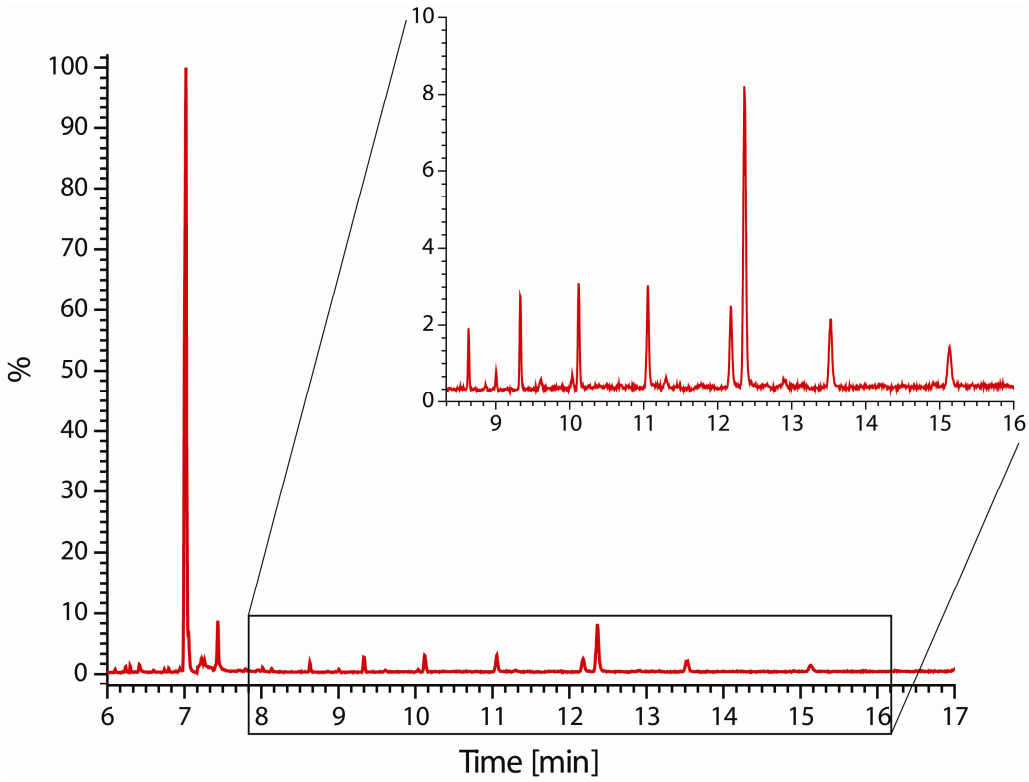

Figure 3.9: GC-MS chromatogram of a solution of methyl linoleate (CH_3CN) photosensitized by 3.1c and then reduced with NaBH4.

The photochemical data collected are in agreement with the photophysical one. Indeed, the view that emerged is that the encounter complex between squaraine and molecular oxygen could evolve either by photooxygenation of the enaminic bond in the squaraine backbone or by ROS production (Scheme 3.14). In both cases, the photogenerated products can then establish radical chain events (i.e., lipid peroxidation) that lead to Type I citotoxicity in cells. Interestingly, some of the literature points out to an analogous behavior in the class of cyanine-based photosensitizers (e.g., merocyanine 540, indocyanine green, and MKT-077).[48-50]

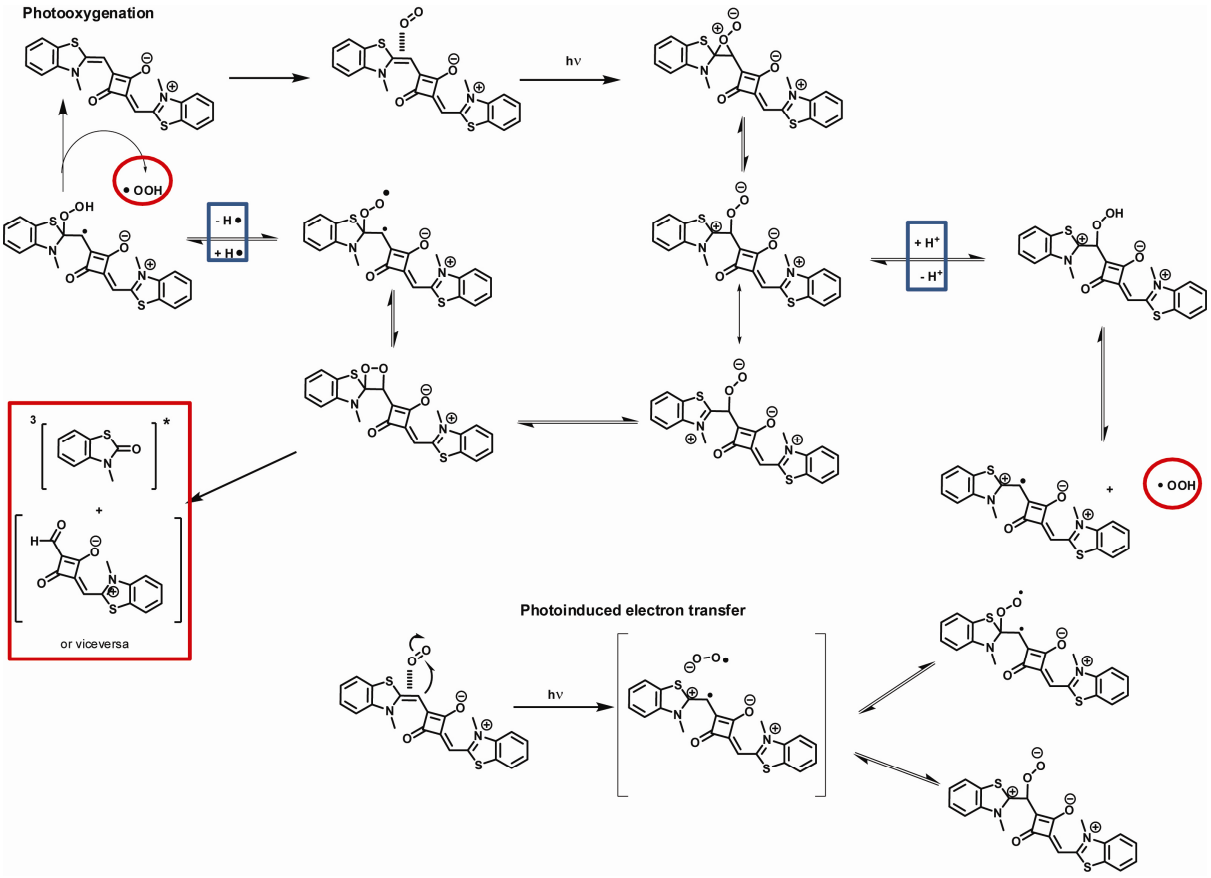

Scheme 3.14

3.4 Photosensitizing activity of π-extended squaraines in cancer cells

We report here the synthesis and photodynamic properties of two squarainic compounds, namely **3.1c** and **3.30,** with one or two squaric rings.

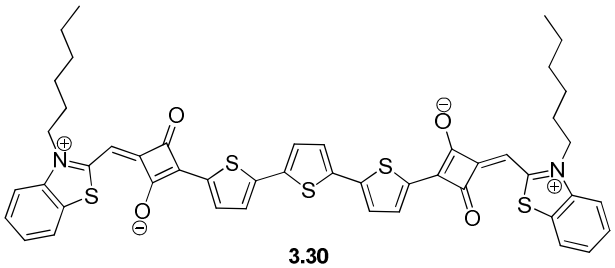

3.30

Scheme 3.15

Both mono- and bis-squaraines contain two C-8 hydrocarbon chains that should favor their association to the cell membranes. Little is known about the photosensitizing properties of squaraines in cell cultures. Ramaiah et al.[51] reported that halogenated mono-squaraines significantly reduce the clonogenicity of AS52 Chinese hamster ovary

cells after photoactivation and Devi et al.[52] showed that a tetraiodo-squaraine caused a reduction of tumor volume and reversal of biochemical markes to near normal level in mice bearing a skin tumor, treated with tetra-iodo squaraine and exposed to a 1000 W halogen lamp. In our study we tested the photosensitizing properties of mono and bis-squaraines in four different cancer cells and provide for the first time some clues about the mechanism of cell death promoted by these new and promising class of photosensitizers.

The bis-squaraine **3.30** was prepared according to Scheme 3.16.

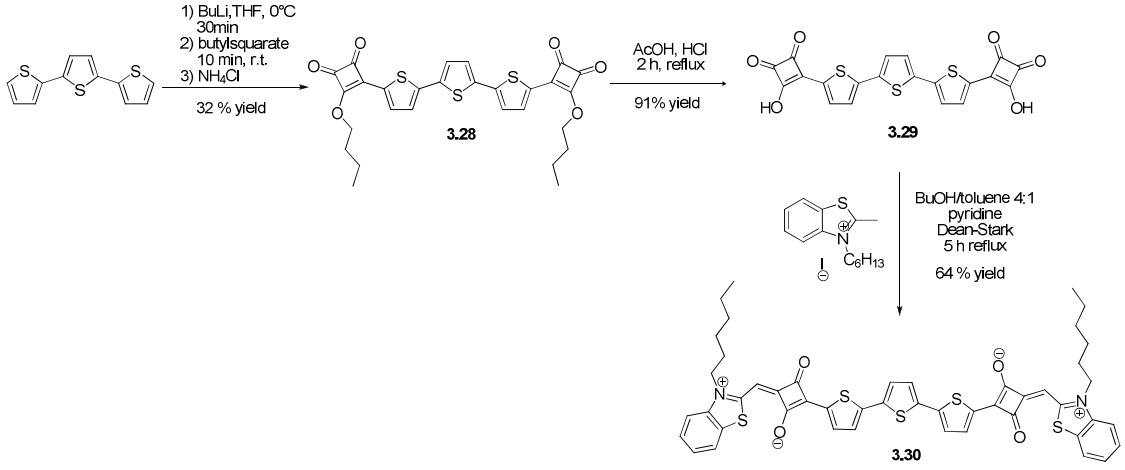

Scheme 3.16

Briefly, commercially available 2,2':5',2''-terthiophene was treated with two equivalents of BuLi at 0°C in THF. The lithiated terthiophene was subsequently treated with two equivalents of commercially available butylsquarate to give, after acidic work-up, bis-emisquarate (**3.28**). Acidic hydrolysis in refluxing AcOH and in the presence of aqueous HCl gave the bis-emisquaraine (**3.29**), which was finally converted in the bis-squaraine (**3.30**) as recently reported.[52] The compound was 100% pure obtained as a golden brown precipitate. The UV-Vis spectra of squaraine **3.30** in water (containing x% v/v DMSO) show a strong absorption band between 550 and 750 nm.

To evaluate whether **3.1c** and **3.30** activate type I or type II photoreactions,[53-56] we carried out a qualitative photo-oxidation assay following the degradation of 1,3-diphenylisobenzofuran (DPBF) by photoactivated squaraines in the presence of oxygen dissolved in ethanol. It is accepted that DPBF is able to react rapidly and efficiently with singlet oxygen, $O_2(^1\Delta_g)$, to yield an endoperoxide that does not absorb light at 415 nm (Figure 3.10b). We exposed for 30 min an ethanol solution containing 50 μM DPBF

and 5 µM **4** or **5** to a filtered light source of wavelength $\lambda > 550$ nm. For comparison we analysed the photo-oxidation of DBPF by HpD (haematophorphyrin), a well known singlet oxygen sensitizer. Figure 3.10b shows a typical DBPF quenching obtained with squaraine **4**. The time-dependent absorbance decrease at 415 nm of DBPF for **4** , **5** and HpD is shown in Figure 3.10c.

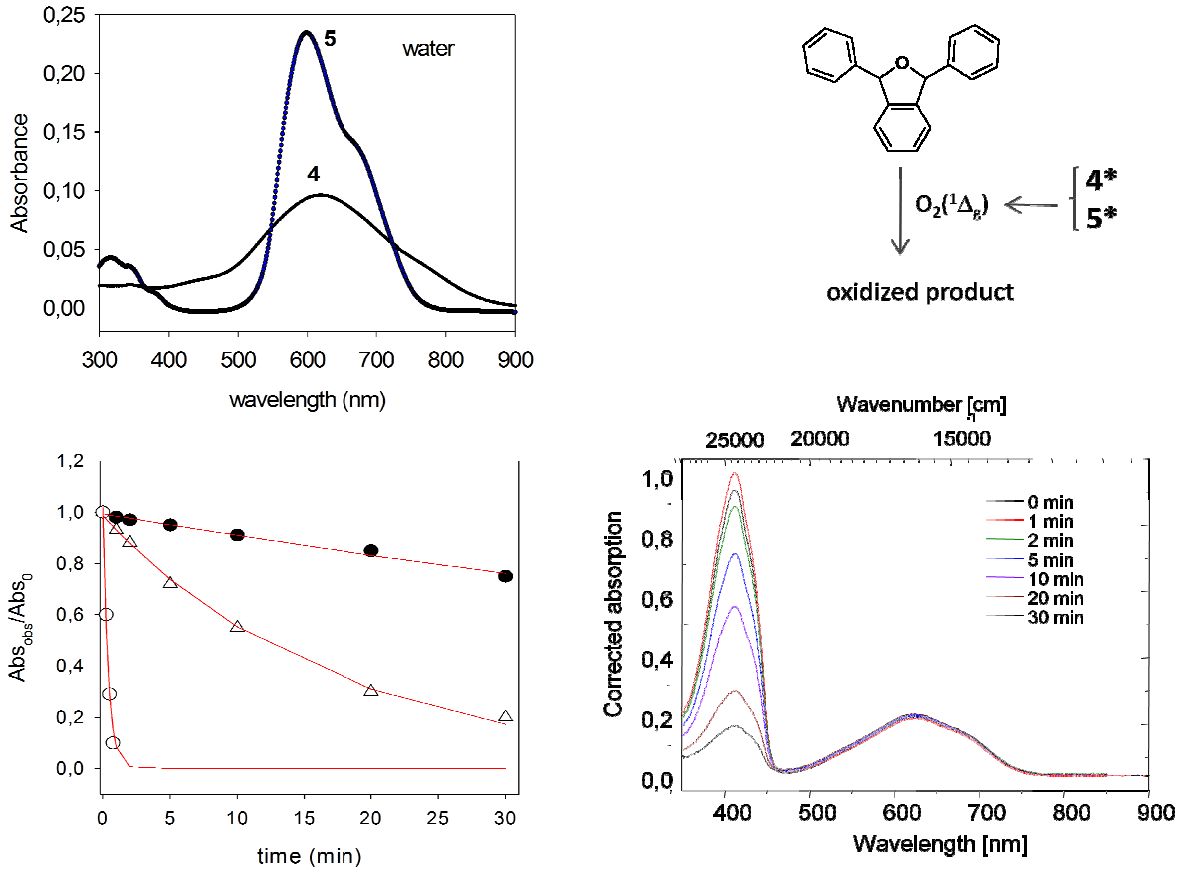

Figure 3.10: Spectral properties of squaraines 3.1c and 3.30. (a) Absorption and fluorescence spectra of squaraines 3.1c and 3.30 in water containing 1% (v/v) DMSO.; (b) time evolution of the UV-vis spectrum of a DPBF (50 µM) and 3.30 (5 µM) air-equilibrated ethanolic solution exposed to a filtered light source of wavelength λ > 550 nm; (c) DPBF absorbance at 415 nm as a function of time for 3.30, 3.1c and HpD in ethanol solutions irradiated as in (b).

The data were best-fitted to a first-kinetic decay curve which gave the following values for the kinetic constant k_{obs} (s^{-1}): $5.8\times10^{-3}\pm2\times10^{-4}$ for **3.30**, $8.8\times10^{-2}\pm4\times10^{-4}$ for **3.1c**, 2.3±0.2 for HpD. This experiment, showing that squaraines **3.30** and **3.1c** are much weaker phtooxidizing agents than HpD, suggests that HpD activates a type II photo-oxidizing process leading to singlet oxygen whereas squaraines **3.30** and **3.1c** activate primarily a type I process involving the generation of ROS other than $O_2(^1\Delta_g)$.

The different DBPF quenching efficiency between mono and bis-squaraines may correlate with the higher propensity to aggregate of the latter compared to the former. As squaraines emit fluorescence when excited at 580 nm, we used confocal microscopy to investigate whether they are taken up by HeLa cells. The images shown in Figure 3.11 have been obtained after the cells were treated for 3 h with **3.30** or **3.1c**.

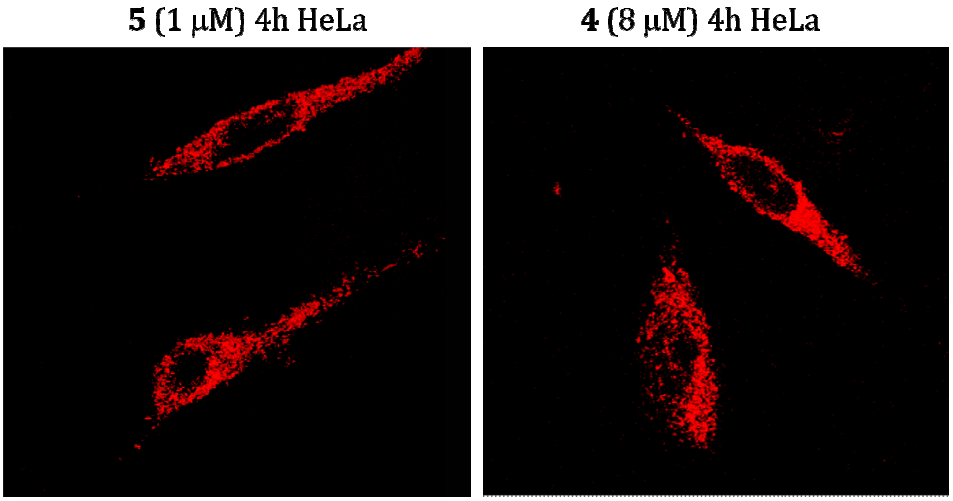

Figure 3.11: Squaraines cell internalization. Confocal laser microscopy images of Hela cells treated for 4 h with squaraines 3.30 (8 μM) and 3.1c (1 μM).

It can be seen that both squaraines locate mainly in the cytoplasm: the punctuate distribution of the fluorescence may suggest that these compounds reside in endocytotic vescicles and/or associate to the organelle membranes, through their double hydrocarbon chains. The fact that squaraines do not accumulate in the nucleus suggest that their potential to cause DNA damage, mutations and carcinogenesis should be low. The photodynamic effects promoted by the squaraines was tested in four cell lines: cervix adenocarcinoma HeLa, hepatic carcinoma HepG2, B78-H1 amelanotic clone and MCF-7 human breast cancer cell lines. An important property that a photosensitizer must possess is non-cytotoxicity in the dark. We evaluated the cytotoxycity in the dark and after irradiation of **3.1c** and **3.30** and the results obtained have been plotted together for comparison. Figure 3.12 shows that while in the dark mono-squaraine **3.1c** promotes a fairly small cytotoxic effect (~20 %), when is photoactivated it raises a dramatic cytototoxic effect (~80%).

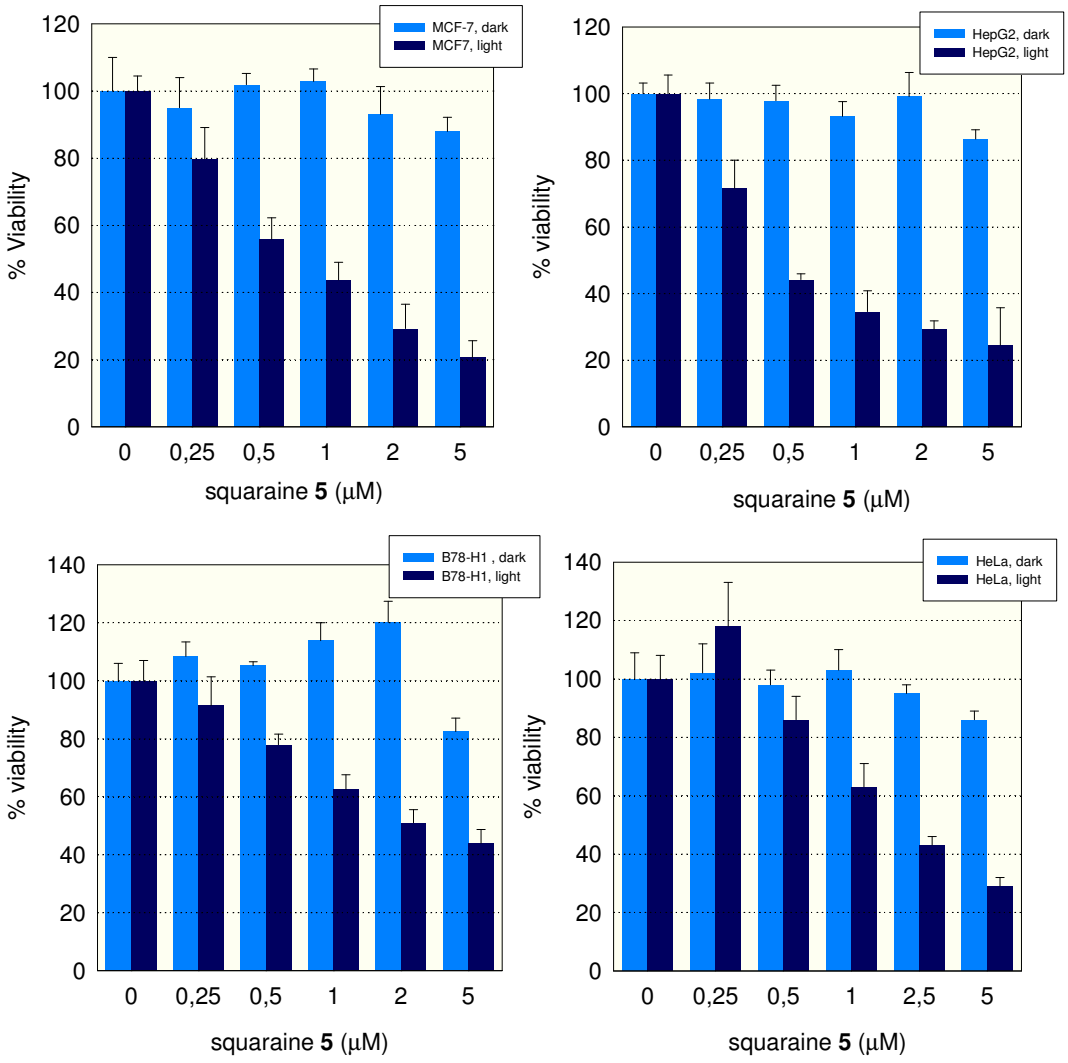

Figure 3.12: Phototoxicity of squaraines 3.1c. Cytotoxicity of increasing amounts of squaraine 3.1c in the dark and after light treatment (fluence rate 14 J/cm^2) Viable cells were measured with resazurin. Histograms report in ordinate the percent of viable cells , i.e the ratio RFUT/RFUC x 100, where RFUT is the fluorescence of treated cells , while RFU$_C$ is the fluorescence of untreated cells. The data are the means ±sd of three experiments. A standard t-test versus control was performed (: P<0.01; *: P<=.05).**

The experiment was carried treating the cells for 3 h with increasing amounts of **3.1c**, followed by irradiation with a metal halogen white lamp at an irradiance of 8 mW/cm^2 and resazurin proliferation assay carried out 24 h after light treatment. As a control we treated the cells with the same amount of DMSO present in the squaraine treatment (squaraines were dissolved in DMSO and diluted with PBS). From these plots we estimated the IC$_{50}$ values reported in the Table 3.11.

Table 3.11: IC$_{50}$ values relative to squaraines 4 and 5 delivered to cancer cells&

Cells	Squaraine **3.30** IC_{50} (μM)	Squaraine **3.1c** IC_{50} (μM)
HepG2	10	0.7
B78-H1	15	2.0
MCF-7	7.5	0.65
HeLa	6.7	1.8

[&] IC_{50} obtained by treating the cells for 3h with squaraines, irradiation for 30 min (8 mW/cm^2), resazurine assay performed after 24h.

Similar dose-response plots were obtained also with the bis-squaraine **3.30**. The data obtained clearly indicate that **3.1c** is a stronger photokilling agent than **3.30**: IC_{50} values of **3.30** (7-15 μM) are about 5-folds higher than those of **3.1c** (0.6-2 μM) (Table 3.11). Little is known about the photosensitizing properties of squaraines. Ramaiah et al (2002) reported that halogenated mono-squaraines, irradiated at 33.8 J/cm^2 strongly inhibited the cloning efficiency of AS52 chinese hamster ovary cells, with an estimated IC_{50} between 1-2 μM, rather similar to that observed with **3.1c**. We also tested the antiproliferative effect in HeLa and MCF cells of **3.30** and **3.1c**, up to 72 h following irradiation (Figure 3.13).

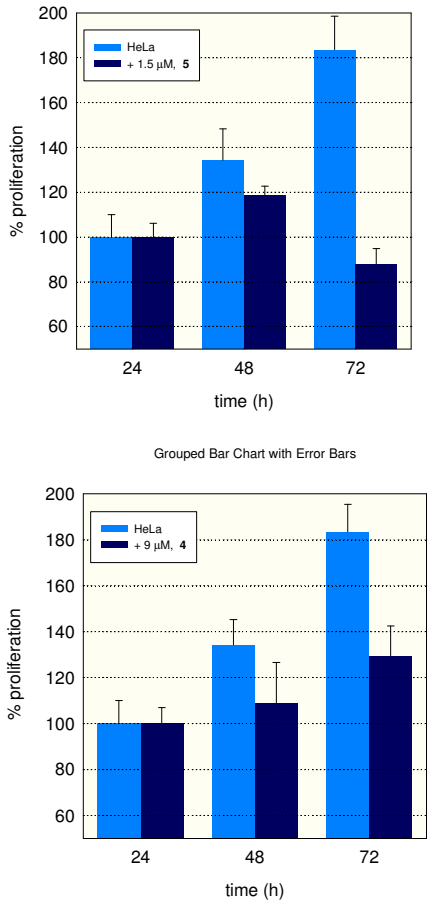

Figure 3.13: Phototoxicity of squaraines 3.30 (9 µM) and 3.1c (1.5 µM) in HeLa cells up to 72 h after light treatment (15 J/cm2).

When **3.30** and **3.1c** are used at concentrations close to IC_{50}, they completely arrest the growth over the entire range of time considered (72h); whereas lower doses reduce the rate of growing, but do not arrest proliferation (not shown). Since **3.30** and **3.1c** possess two hydrocarbon chains they are expected to associate to the cell membranes and cause lipid peroxidation. To test this hypothesis we measured in squaraine-treated and -untreated HeLa cells, the level of TBARS, malonyldialdheide bound to thiobarbituric acid, as this adduct is indicative of lipid peroxidation (Figure 3.14).

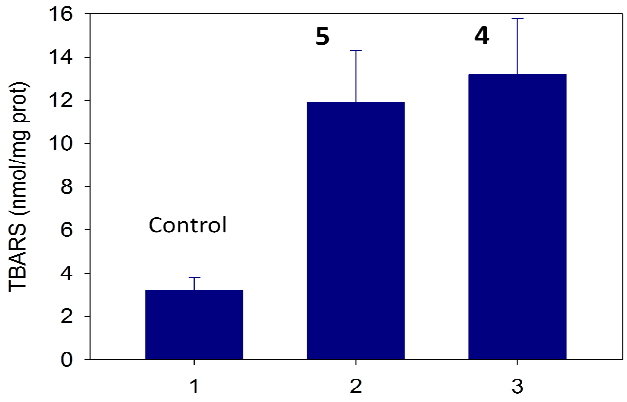

Figure 3.14: Squarines 3.1c and 3.30 cause lipid peroxidation. Level of malonildyaldheide bound to thiobarbitiric acid (TBARS) in HeLa and MCF-7 cells treated photodynamically with squaraines 3.1c and 3.30.

Compared to untreated cells, showing a TBARS level of 3, treated cells (with squaraine doses < IC_{50}) show and 4-fold increase of TBAS, which clearly indicate the occurrence of lipid peroxidation. To investigate whether the antiproliferative effect observed at concentration sclose to IC_{50} is due to apoptosis and/or necrosis, we analysed by FACS the cells stained with annexin and propidium iodide (PI). In early apoptosis cell membranes loose their phospholipid asymmetry and phosphatidyl serine (PS), normally located in the inner leaflet, jumps into the outer leaflet. As annexin shows a high affinity for PS, annexin-FITC can mark the cells in early apoptosis. In contrast, necrotic cells being permeable to annexin and PI, are stained by both dyes. Figure 3.15 shows the FACS analysis performed after irradiation (8 mW/cm^2) of HeLa cells treated with **3.1c** and **3.30**, at concentrations above and below IC_{50}. Below IC_{50} (weak cell insult), there are roughly an equal distribution between apoptotic and necrotic cells, though in a very low amount (not shown). But, at a concentrations > IC_{50}, the fraction of cells in necrosis is roughly 3-4-fold higher, indicating that necrosis becomes the primary photokilling mechanism triggered by the squaraines. The percent of necrotic cells is not very high because, to observe apoptosis. the FACS experiment was performed 30 min after light treatment. However, a time-lapse experiment up to 72 h with living HeLa cells treated with **3.1c** and **3.30** near IC_{50} and grown in the presence of Hoechst (it stains living cells in blue) and PI (it stains necrotic cells in red) show that most cells die by necrosis (Figure 3.15b).

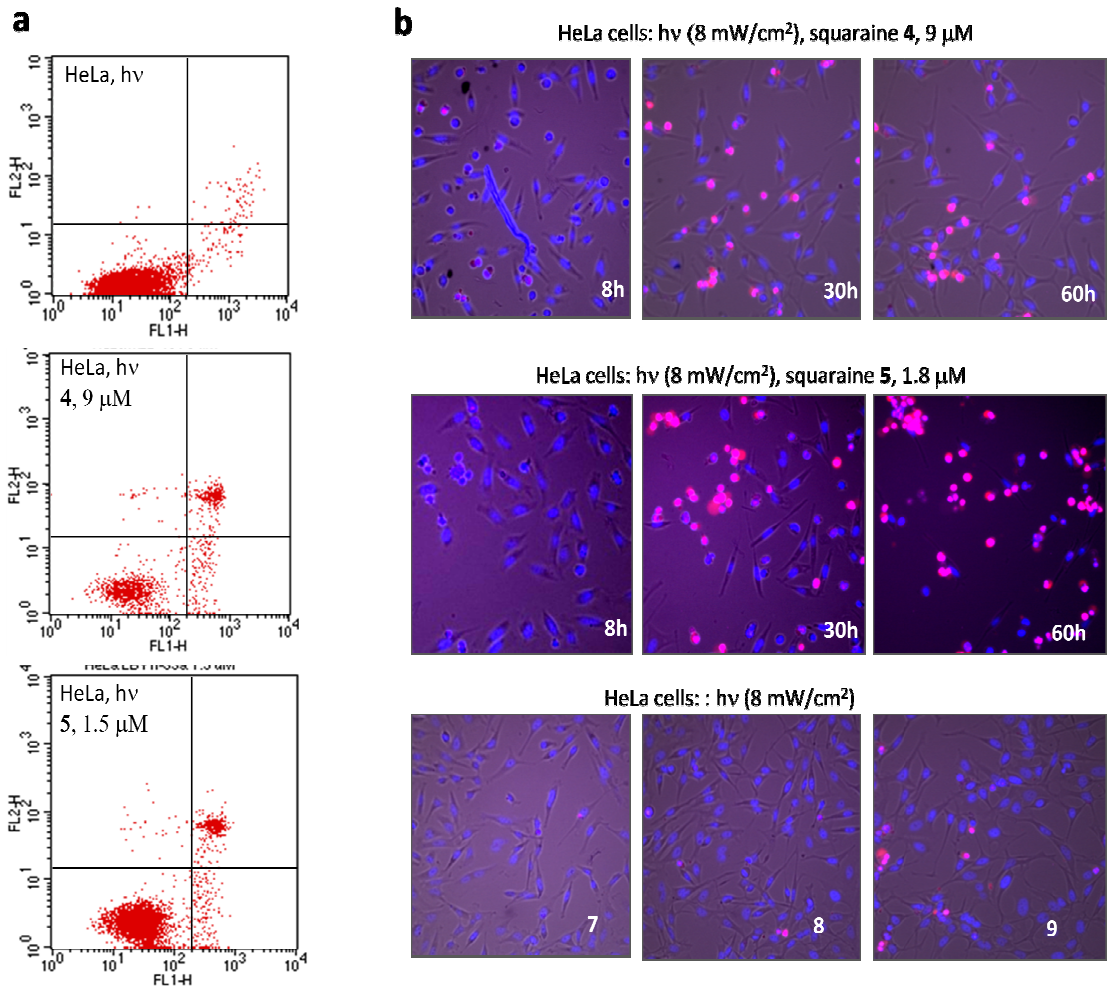

Figure 3.15: (a) FACS analysis of squaraine-treated HeLa cells stained with annexin-FITC and PI; (b) time-lapse experiment performed on living HeLa cells treated with Hoerchst and PI, after 6, 30 and 60 h of incubation. Red cells are necrotic, blue cells are viable.

Note that the cells photodynamically treated with squaraine **3.1c** appear, after 60h of growth, necrotic in a proportion larger than that observed with **3.30**. The fact that **3.30** induces a lower extent of cell death by necrosis compared to **3.1c**, suggest than the photokilling process induced by **3.30** may involve necrosis as well as apoptosis. In fact, this is in keeping with caspase-3/7 assay carried out on HeLa and MCF-7 cells photo-treated with squaraines **3.30** and **3.1c** (Figure 3.16). It can be seen that the executioner caspase 3/7 is found activated in the cells treated with **3.30** but not with **3.1c**.

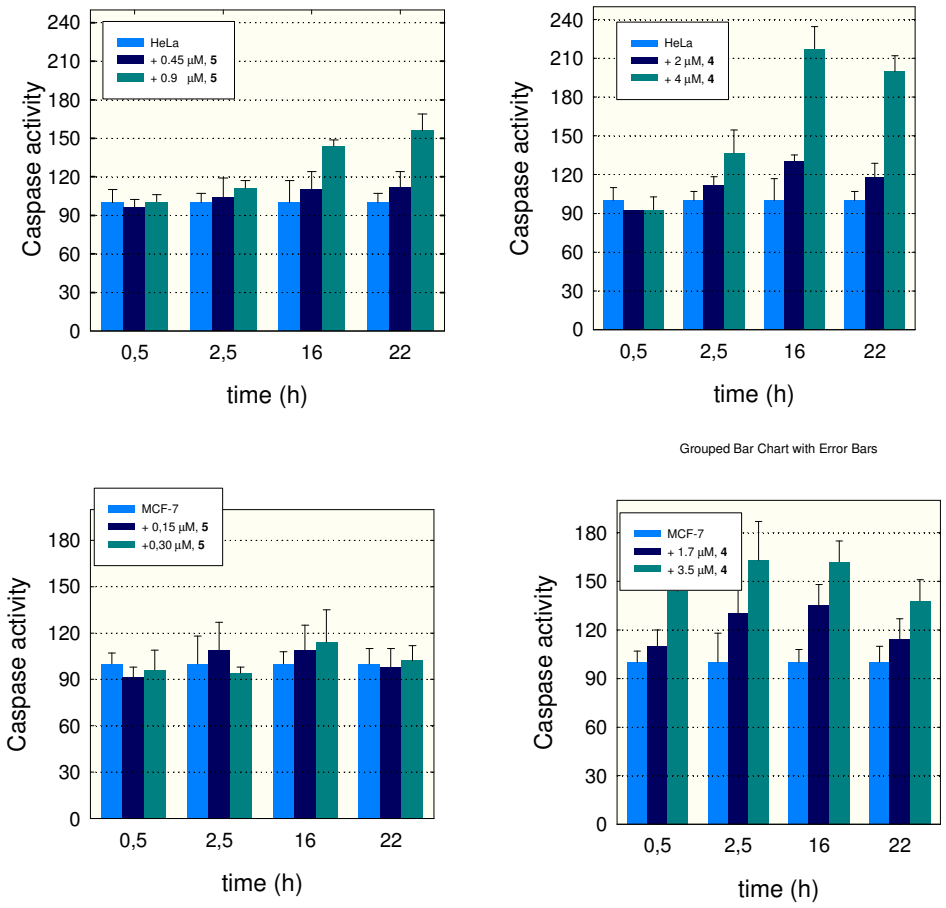

Figure 3.16: Apoptosis assay showing the activity of caspases 3/7 in untreated or squaraine –tretaed HeLa cells. The cells were incubated with the squaraine 3.1c and 3.30 for 3h; after irradiation at 14 J/cm2 , Apo-ONE TM caspase-3/7 assay was performed. The data are the means ±SD of three experiments.

In conclusion, in this paper we describe the synthesis squaraines which in cancer cells show a strong photodynamic activity, which mediated by a type I photo-process, leading to cell death by necrosis. Confocal miscrocopy shows that these molecules efficiently internalize in HeLa cells where they accumulate in the cytoplasm. The squaraines induce a 4-fold increase of malonyldialdehyde, which is indicative of lipid injury by peroxidation. In the dark the squaraines are largely nontoxic, but when irradiated with light at a fluence of 14 J/cm^2, they promoted a dramatic photodynamic effect that causes cell death in all tested cell lines. The mono-squaraine **3.1c** is found to be a stronger photosensitizer than bis-squaraine **3.30**. In conclusion the results of this paper show that the synthesised squaraines in particular **3.1c**, having alower tendency to aggregate, represent a new class of therapeutic agent for PDT.

3.5 Molecular engineering of the photodamaging activity

The indications arising from both the photophysical and photochemical studies indicate that the electronrich benzothiazole moiety interact with molecular oxygen and light to form a charge-transfer (CT) encounter complex. This intermediate species can evolve to generate cytotoxic species, as discussed in Section 3.3, in an amount proportional to the CT character between the electronrich moiety of the dye and the electronacceptor counterpart, molecular oxygen. To further validate this observation, we designed an experiment aim to activate the production of ROS in a family of cyanine dyes. We chose to engineer the progenitor Cy5 at the molecular level and increase its photooxidation capabilities by exploiting the effect plays by heteroaryl meso-substituents on the cyanine oxidation potential. We take advantage of the procedure reported by Kimura et al.[57] and our expertise as heteroaryl chemists to synthesize the Cy5-inspired compounds **3.31-3.33**. In details, we performed a condensation in Knoevenagel conditions between 3-ethyl-2-((1Z,3E)-3-(3-ethylbenzo[*d*]thiazol-2(3*H*)-ylidene)-2-methylprop-1-enyl)benzo[*d*]thiazol-3-ium iodide (**3.31**) and two pyrrole-2-carboxyaldehyde derivatives, namely **4.9** and **4.16**, with piperidine as catalyst in order to obtain **3.32** and **3.33**, respectively (see Section 4.1). In this way the pyrroles pull electron density toward the delocalized positive charge along the cyaninic backbone, afflicting its redox behavior. The amount of electron density pushed by the pyrroles is regulated by another heterocycle: in the first case, a pyridinium salt acts as electron withdrawing group on the pyrrole reducing its pull effect. On the other end, dimethylaniline exerts its electrondonor effect by enhancing the amount of charge the pyrrole pushes. From the comparison of the absorption spectra in Figure 3.17, we observed that the energy of the electronic transition associated with the cyanine backbone is only marginally affected by the kind of substituent since the conjugation length is not increased. Nevertheless, the broadening of this transition indicates the involvement of a CT process. Moreover, a new broad absorption band compatible with a CT transition between the two molecular branches appears for both **3.32** and **3.33**. The bands at 380 nm for **3.32** and 450 nm for **3.33** are associated to the pyrrole-aniline and to the pyrrole-pyridinium chromophoric side groups, respectively, that behave as independent oscillators.

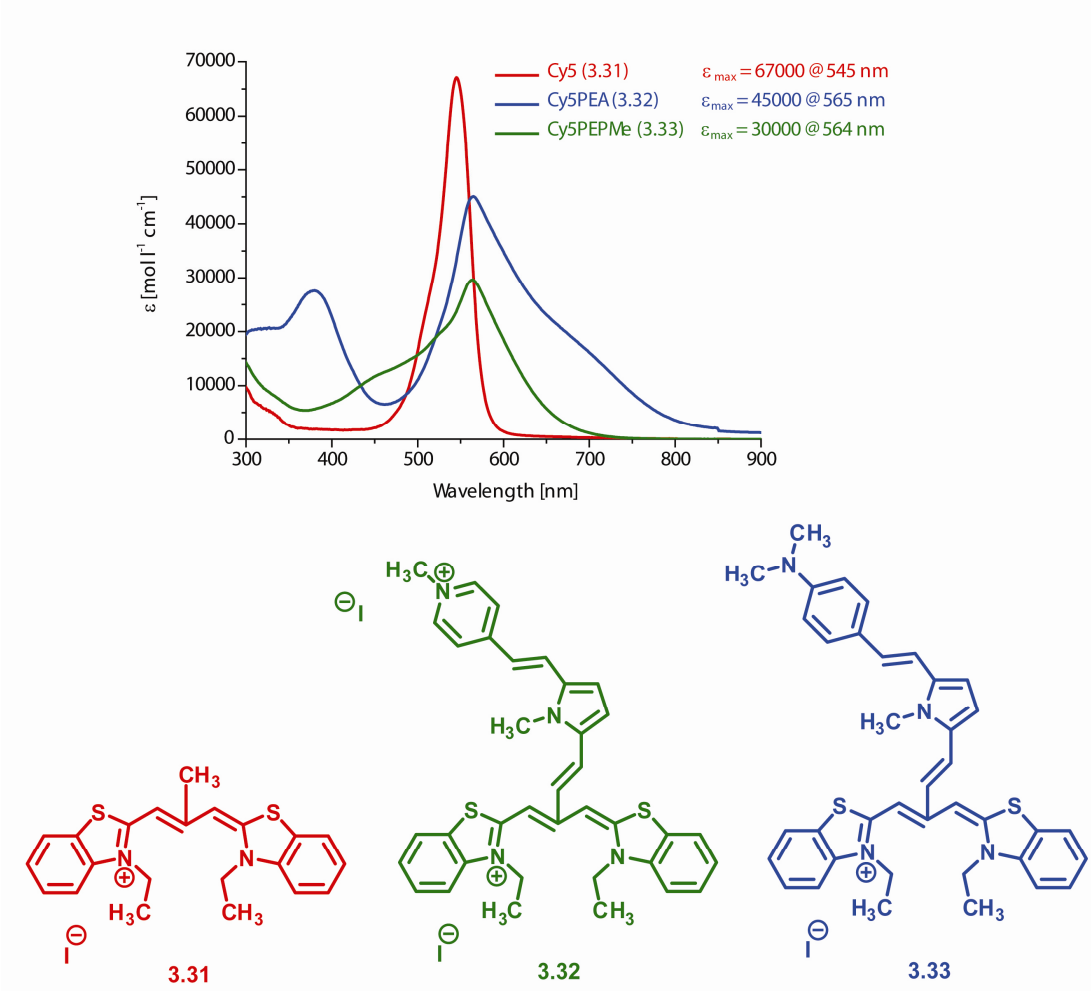

Figure 3.17: Molecular structures and absorption spectra of the cyanine derivatives 3.31-3.33.

To evaluate the photooxidative capabilities for each of these dyes, we carried out a qualitative comparative study by monitoring the degradation of 1,3-diphenylisobenzofuran (DPBF) after irradiation of a sensitizer in the presence of oxygen in solution. It is accepted that DPBF is able to react efficiently with both singlet oxygen and reactive oxygen species yielding byproducts that no longer absorbs at 415 nm. We tried to reproduce the biological environment exposing a solution of DPBF (50 μM) and each dyes (5 μM) in ethanol to a filtered light source of wavelength $\lambda > 550$ nm over a period of half an hour. The use of filtered light enabled us to prevent DPBF from selfbleaching and to take into account the role of the tissue transparency window. We used the cell-killer squaraine **3.1c** as benchmark.

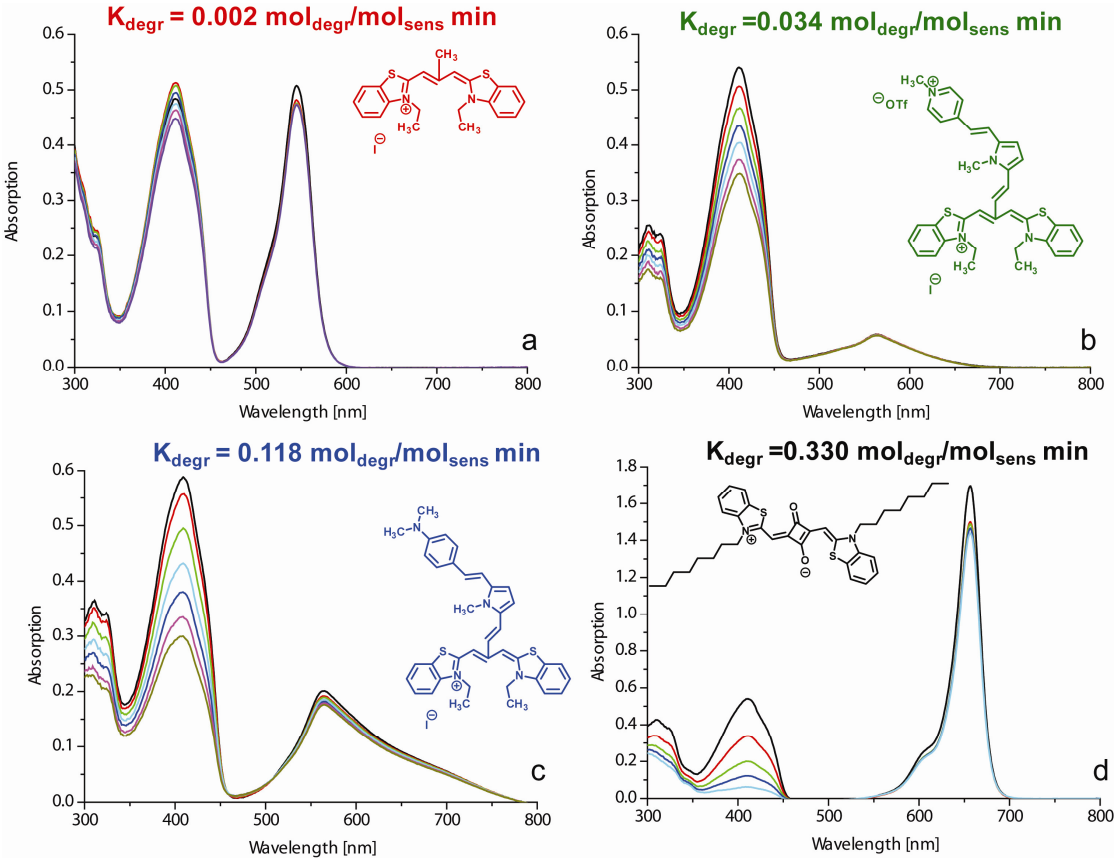

Figure 3.18: time evolution of the UV-vis spectra of a DPBF (50 µM) and each dye (5 µM) air-equilibrated ethanolic solution exposed to a filtered light source of wavelength λ > 550 nm.

The data reported in Figure 3.18 clearly show that we succeed in boosting the photooxidative capability in the series of cyanine derivatives investigated. Indeed, while the prototype **3.31** is scarsely able to induced the degradation of DPBF after light exposure, we control the redox behavior, hence the ROS production, by modulating the extent of electron density pulled by the chromophoric side-group in the meso position.

3.3 Molecular Engineered Fluorescent Quadrupolar Bioprobes

Visible linear fluorescent probes are today widely used in many fields including cell biology, [58, 59] biochemistry, [60-62] biophysics, [63] genomics, [64, 65] neuronal activity, [66-68] and cancer diagnosis. [69-71] We previously communicated the design, synthesis, and two-photon absorption (TPA) characterization of some all-heterocycle quadrupolar and branched TPA dyes, [72-76] along with the biological characterization of 2,5-Bis[1-(4-*N*-methylpyridinium)ethen-2-yl)]-*N*-methylpyrrole ditriflate (**3.34a**), a representative chromophore of a large family of heterocyclic fluorescent dyes.

The state of the art in the imaging field is represented by green fluorescent proteins (GFPs).[77] GFPs are peptides which peculiar amino acid sequence is able to fold in the presence of oxygen to give a fluorophoric unit. The main applications of GFPs has been their use as a genetic fusion partner in the monitoring of proteins localization and fate. The gene encoding a GFP is fused in frame with the gene encoding the endogenous protein and the resulting chimera expressed in the cell or organism of interest. The ideal result is a fusion protein that maintains the normal functions and localizations of the host protein but is now fluorescent. While these systems show advanced specific performances, new synthetic fluorophores with absorptions close to suitable operational wavelength, large signal-to-noise ratio in the fluorescence detection, and ease of availability are still in great demand. [78-80] The present research was prompted by carefully considering the state of the art of the subcellular localization of fluorescent bioprobes: a) the renewed interest in the selective accumulation of cationic dyes in tumor cells, [81] b) the physicochemical features of probes in favoring different localization according to Horobin.[82-85] Mitochondrial localization is favored by cationic character of the probes ($Z > 0$), their planar aromatic system (below a certain conjugated bond number, i.e. $CBN < 40$) and their lipophilic character ($5 > \log P > 0$), while either hydrophilicity or specific protein binding followed by pinocytosis ($CBN > 40$) increase accumulation of cationic dyes in lysosomes. We decided to performed the chemical engineering of the parent compound **3.34a** either by varying the residues on the pyridinium nitrogen atoms or substituting the pyrrole core moiety with different units. We report herein the desing, synthesis, subcellular localization imaging, citotoxicity, logP values, and photophysical study including measurements of fluorescence quantum yields for the five dicationic dyes **3.34a-c**, **3.35**, **3.36** in Scheme 3.17.

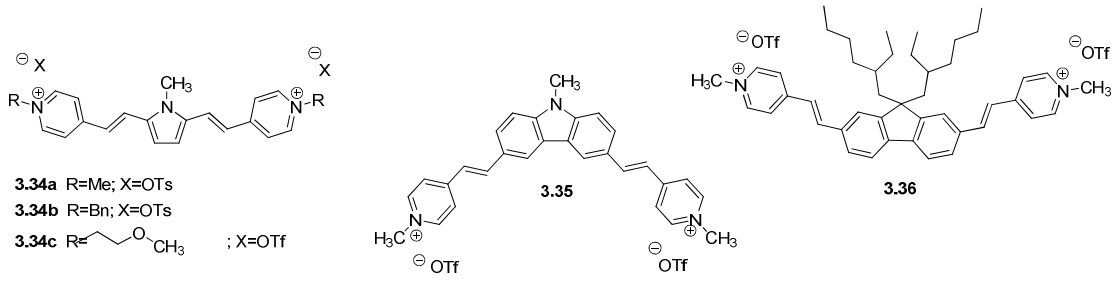

Scheme 3.17

3.3.1 Design and synthesis

To elucidate the structure-subcellular localization relationships that lead the parent

compound **3.34a** to localize in mitochondria, we differentiated the nitrogen terminals with two polar metoxyethyl groups for **3.34c** and two lipophylic benzyl groups for **3.34b**. We then explored the synthesis of core-modified derivatives replacing the pyrrole moiety with a more bulky carbazole one (**3.35**) and a less electronrich fluorene one (**3.36**). The preparation of the terminal modified derivatives **3.34a-c** required the quaternarization of the known dipyridyl compound 4,4'-(1*E*,1'*E*)-2,2'-(1-methyl-1*H*-pyrrole-2,5-diyl)bis(ethene-2,1-diyl)dipyridine (**3.37**) with methyl *p*-toluensulfonate, benzyl bromide and 2-methoxyethyl trifluoromethanesulfonate in acetonitrile as alkylation reagents, respectively (Scheme 3.18). We replaced the bromide anions in **3.34b** with *p*-toluensulfonate ones using silver *p*-toluensulfonate in CH_3CN for analytical purpose. The unsophisticated synthetic chemistry involved is particularly suitable for bioconjugability, bearing each dye two terminal distinguishable functionalization sites. The synthesis of the core-modified derivatives **3.35** and **3.36** is illustrated in Scheme 3.19 and Scheme 3.20. In both cases, the commercially available fluorene and carbazole dibromo derivatives were treated with two equivalents of BuLi at 0°C in THF. The lithiated intermediates were subsequently treated with two equivalents of anhydrous DMF and poured into aqueous $AcONH_4$ to give, after work-up, the bis-aldehydes derivatives **3.39** and **3.40**. Condensation of the aldehydes with 1-methylpicolinium triflate under Knoevenagel conditions gave the dicationic derivatives **3.35** and **3.36** in good yield.

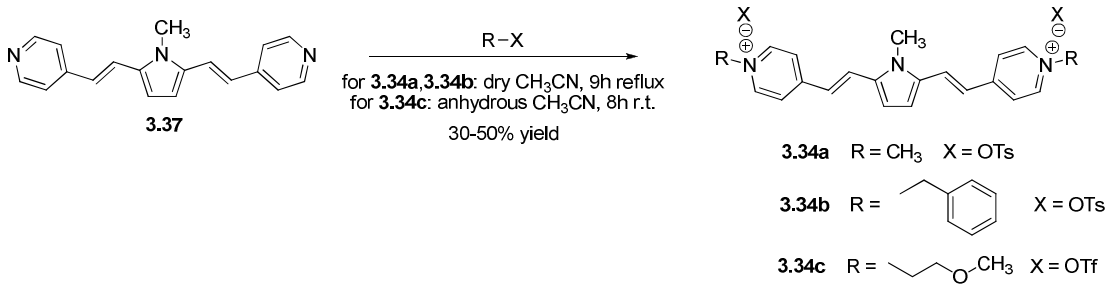

Scheme 3.18

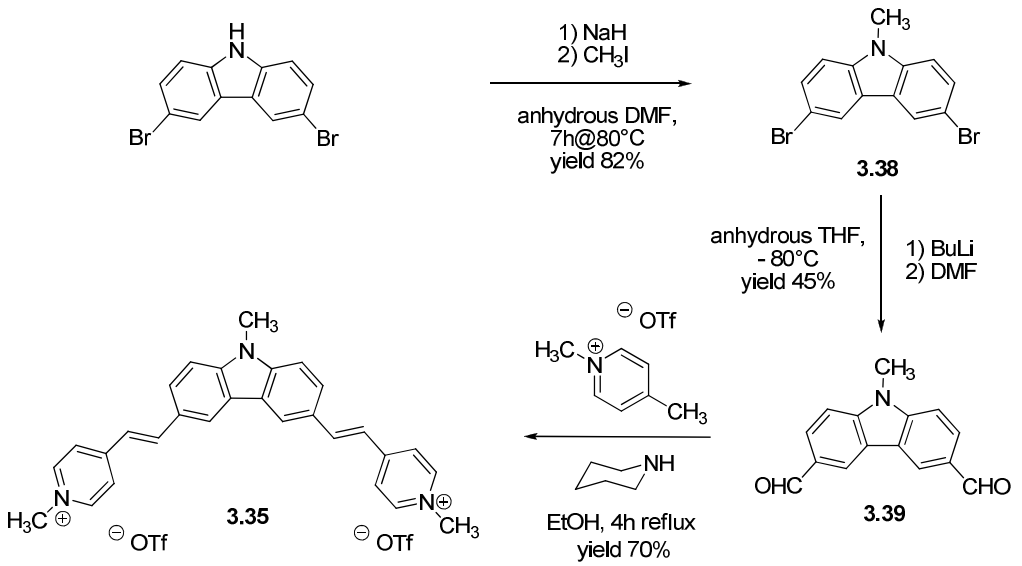

Scheme 3.19

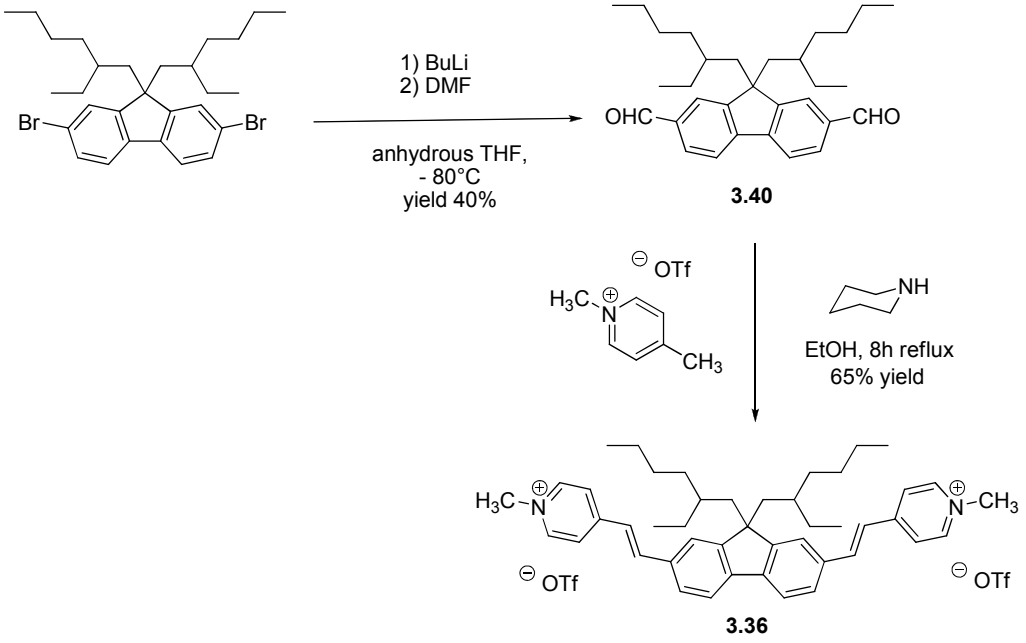

Scheme 3.20

3.3.2 Spectroscopic characterization.

Fluorescence quantum yields, Φ_f, were determined by comparing the integrated intensity of the emission recorded upon irradiation of each sensitizer at a given wavelength to the integrated intensity obtained after irradiation of a standard, with a known quantum yield of fluorescence, at the same wavelength (Rhodamine 6G at 488 nm in water, for which $\Phi_f = 0.95$ and Rhodamine B at 514 nm in water, for which $\Phi_f =$

0.31) [86]. The integrated intensities were recorded at different absorbances and the slopes obtained were then used to obtained Φ_f according to equation (**2**):

$$\Phi_f = \Phi_f^{std}\left(\frac{slope_{sens}}{slope_{std}}\right)\left(\frac{n_{sens}}{n_{std}}\right)^2 \qquad (\mathbf{2})$$

Table 3.12: Spectroscopic properties of compounds 3.34a-c, 3.35 and 3.36 in air-equilibrated PBS

Compound	$\lambda_{abs,max}$ [a]	$\lambda_{em,max}$ [b]	Stokes shift[c]	ε [d]	Φ_f [e]
3.34a	500	594	3160	40000	0.10
3.34b	514	604	2900	37900	0.06
3.34c	510	607	3133	42000	0.13
3.35	446	617	6214	39500	0.15
3.36	458	540	3315	23700	0.37

[a]Absorption maximum wavelength, in nm ± 0.5. [b]Emission maximum wavelength, in nm ± 0.5. [c]Stokes shift, in cm^{-1} ±30. [d]Extinction molar coefficient, in l mol^{-1} cm^{-1}, estimated error 10%. [e]Fluorescence quantum yield.

Derivatives **3.34a-c, 3.35** and **3.36** show a broad absorption band in the visible region associated with a strong intramolecular charge-transfer between the donor (pyrrole, carbazole or fluorene) and acceptor (pyridinium) moieties. Such a broad absorption enables the chromophores to be excited over a large range of wavelength (400 – 600 nm) with many different commercial light sources, both lasers and lamps. The comparison between the absorption in PBS of the class **3.34** derivatives shows that the optical properties are only marginally affected by the kind of substituent present on the pyridine nitrogen (Table 3.12). Coherently, the emission band shapes of class **3.34** compounds are also very similar.

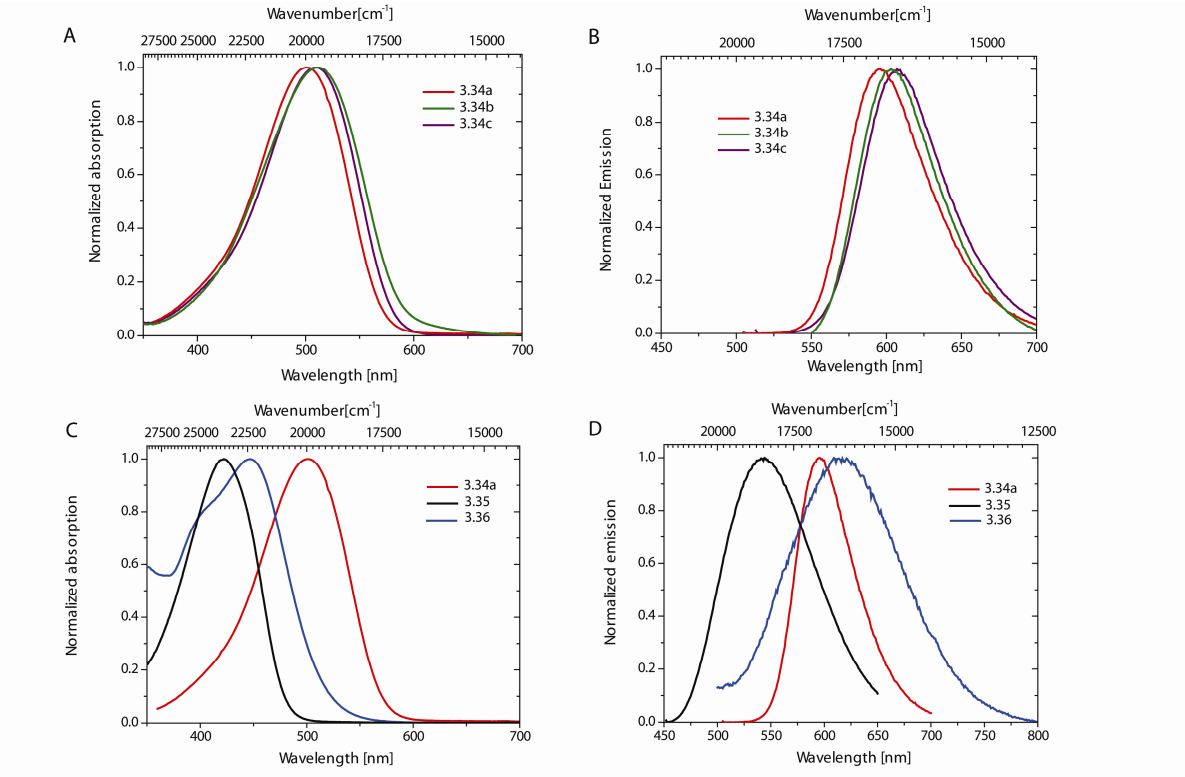

Figure 3.19: (A) Absorption spectra for compound 3.34a (red line), 3.34b (green line) and 3.34c (blue line) in PBS. (B) Emission spectra for compound 3.34a (red line), 3.34b (green line) and 3.34c (blue line) in PBS. (C) Absorption spectra for compound 3.34a (red line), 3.35 (black line) and 3.36 (blue line) in PBS. (D) Emission spectra for compound 3.34a (red line), 3.35 (black line) and 3.36 (blue line) in PBS.

The absorption bands of **3.35** and **3.36** are hypsochromically shifted by substituting the pyrrole ring with less electronrich carbazole and fluorene groups. The large Stokes shift that characterized all these dyes, up to 6000 cm^{-1} for **3.35**, might also be attributed to an excited-state intramolecular charge transfer (ICT). This is a strong advantage with respect to commercial mitochondrial probes, i.e. the MitoTracker probes, which have the known disadvantage that their Stokes shifts are less than 1684 cm^{-1} for MitoTracker Red 580.[87] A small Stokes shift can cause self-quenching and measurement error by excitation light and scattered light.[22] Both of these can decrease the detection sensitivity to a great extent. Therefore, suitable chromophores with a larger Stokes shift are very promising for fluorescence bioassays.

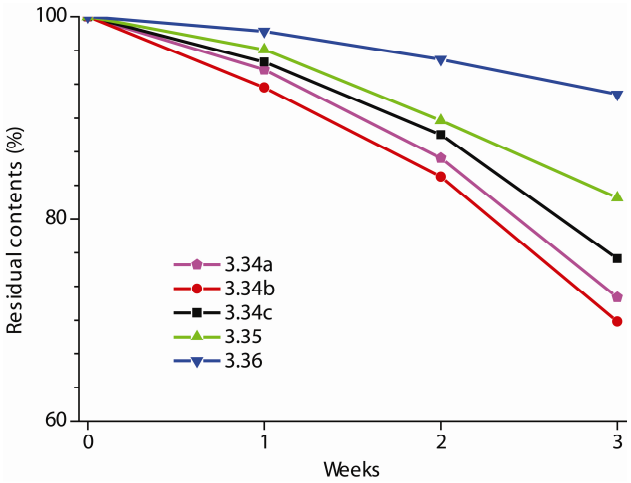

Figure 3.20: Photostability for each of the investigated dyes.

Moreover, the quadrupolar structures presented in this work bear two electrondrawing groups that stabilize all the compounds investigated with respect to photooxidation, ensuring low photobleaching rates. In Figure 3.20 we report the residual contents of solution of each of the studied compounds in PBS up to three weeks of sunlight illumination.

3.3.3 Biological characterization.

Selectivity of mitochondrial probes is controlled by competitive accumulation in cellular organelles. Since slight modifications of the terminals may cause changes in the hydrophilicity, hence in staining capability, we calculated the logP value for all of the derivatives in order to establish a hydrophilicity series. At the same time we studied the subcellular localization in the series **3.34a-c** in HUVEC cells by means of confocal microscopy. Firstly we confirmed the reported mitochondrial localization of **3.34a** and we found a similar behavior for the more lipophilic benzyl-terminated derivative **3.34b**. In the case of the more hydrophilic metoxyethyl-terminated derivative **3.34c** we observed the appearance of a scattered vesicular pattern concurrently with the almost disappearance of the mitochondrial network as proved by the double staining with Mitotracker Deep Red 633. We attributed the observed structure to lysosome staining consistently with the work by Ihida and Predescu on HUVEC cells,[88] and with the overall quantitative structure–activity relationships (QSAR) for cationic probes reported by Horobin and Rashid.[83, 89]

We then modified the size of the planar conjugated system by substituting the pyrrole ring with the carbazole moiety in order to change the number of conjugated bonds (CBN). In this way we altered dramatically the staining capability, changing the

localization from mitochondria to lysosomes (Figure 3.23). This behavior may reflects a different cellular uptake: cationic lipophilic ($Z > 0$; $0 < \log P < 8$) dyes with no strong protein-binding (CBN < 40) enter cells by free diffusion, they diffuse in the cytosol and accumulate in mitochondria. Nevertheless, if the cationic probe has a high protein affinity (CBN > 40), it is trapped in the plasmalemma and could accumulate in lysosome membranes after plasmalemmal internalization.[83] This could be the case of derivative **3.35**, which more extended conjugated system (CBN = 33) respect to **3.34a-c** may increase protein affinity. Another possibility implies that the dye enters the cell by pinocytosis, a biological process actives in HUVEC cells that leads to lysosomal accumulation.[90] Compound **3.36** displays a borderline behavior with both mitochondrial and lysosomal accumulation (Figure 3.25). We suppose that the enhanced mitochondrial accumulation respect to **3.35** is mainly due to the insertion of two aliphatic chains in the fluorene structure leading to an increase in lipophilicity (Table 3.13). The residual lysosomal staining may be due to the larger fluorene conjugated fragment respect the pyrrole one in the **3.34a-c** series, as discussed for the carbazole derivative.

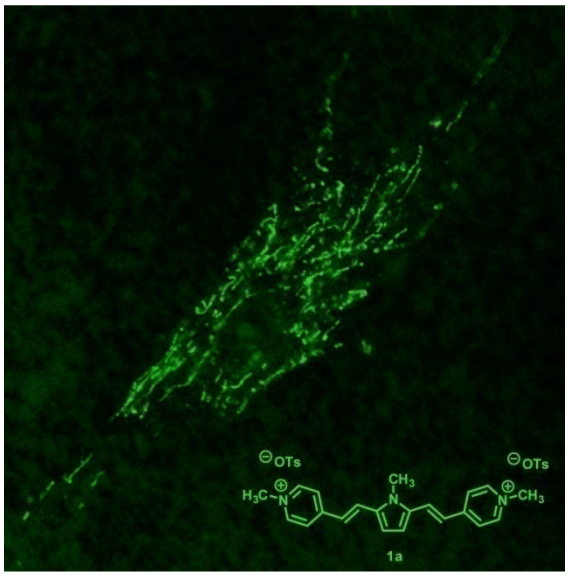

Figure 3.21: Confocal images of the HUVEC cells labeled with 3.34a at 10 μM for 1 h incubation.

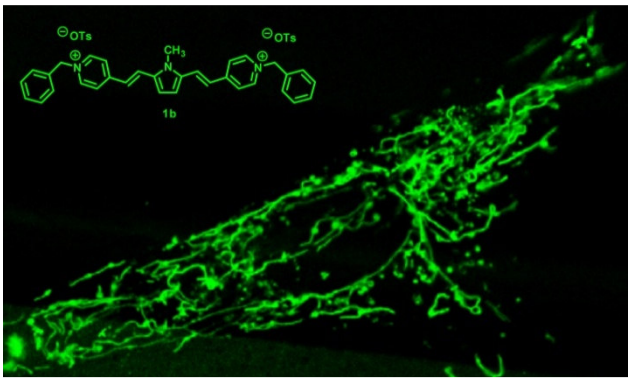

Figure 3.22: Confocal images of the HUVEC cells labeled with 3.34b at 5 µM for 30 min incubation.

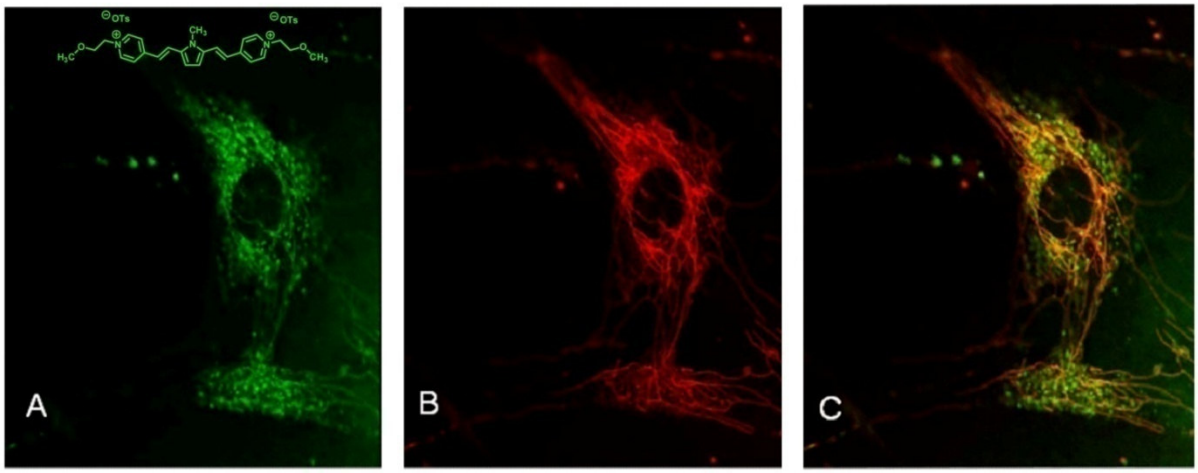

Figure 3.23: Confocal images of the HUVEC cells labeled with MitoTracker Deep Red 633 and 3.34c at 5 µM for 30 min incubation.incubation. To determine a possible mitochondrial localization a double staining (C) with 3.34c (A) and Mitotracker Deep Red 633 (B) has been performed.

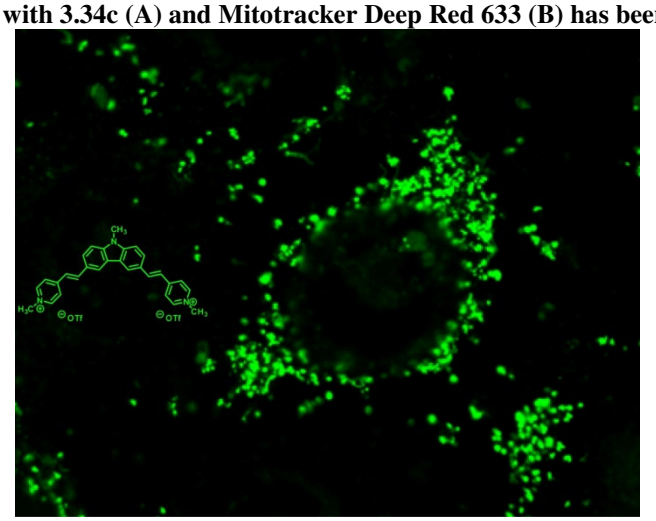

Figure 3.24: Confocal images of the HUVEC cells labeled with 3.35 at 10 µM for 30 min incubation.

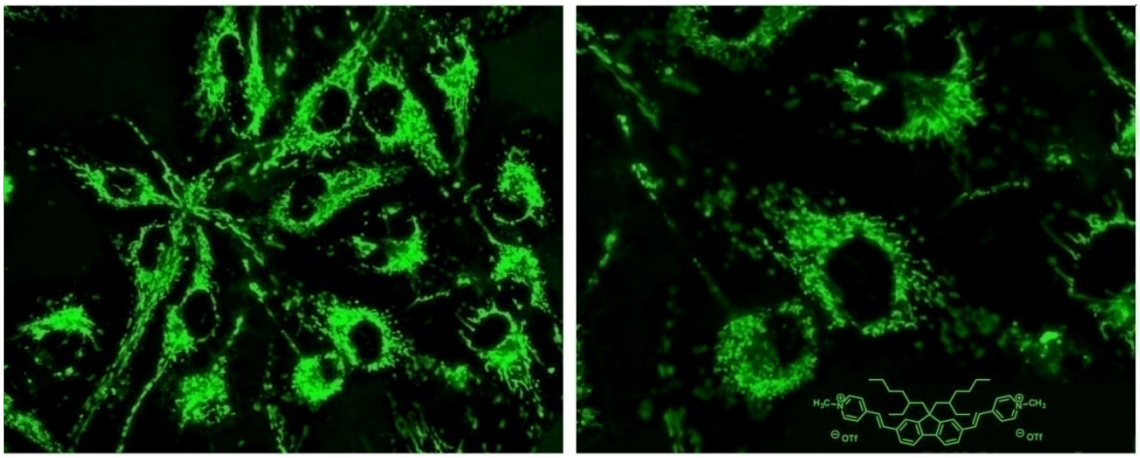

Figure 3.25: Confocal images of the HUVEC cells labeled with 3.36 at 10 μM for 15 min incubation.

Table 3.13: Staining behavior and selected structure parameters of dicationic (Z = +2) compounds 3.34a-c, 3.35 and 3.36.

Compound	Cellular staining[a]	logP[b]	LCF[c]	CBN[d]
3.34a	M	-0.5	23	23
3.34b	M	-0.4	23	35
3.34c	L/M	-0.6	23	23
3.35	L	+0.1	33	33
3.36	L/M	+0.80	31	31

[a]M or L indicates mitochondrial and lysosomal localizations, respectively. [b]Logarithm of the octanol-water partition coefficient, ± 0.1. [c]Largest conjugated fragment. [d]Conjugated bond number.

All the derivative studied are basically non toxic also at such higher concentration as 10 μM, but **3.36**. The absence of citotoxicity is surely a desirable property in the development of cellular fluorescent probes. The high citotoxicity of compound **3.36** prevents its utilization as biological marker, but it could be used as a favorable chemotherapeutic agent with theranostical applications in cancer treatment. Indeed cationic lipophilic dyes can accumulate in mitochondria of tumor cells because plasma and mitochondrial membrane potentials of tumor cells were typically higher than those of normal cells. [81] The dicationic lipophilic character and the fluorescence of **3.36** could provide the basis for selective diagnosis and therapy of tumors.

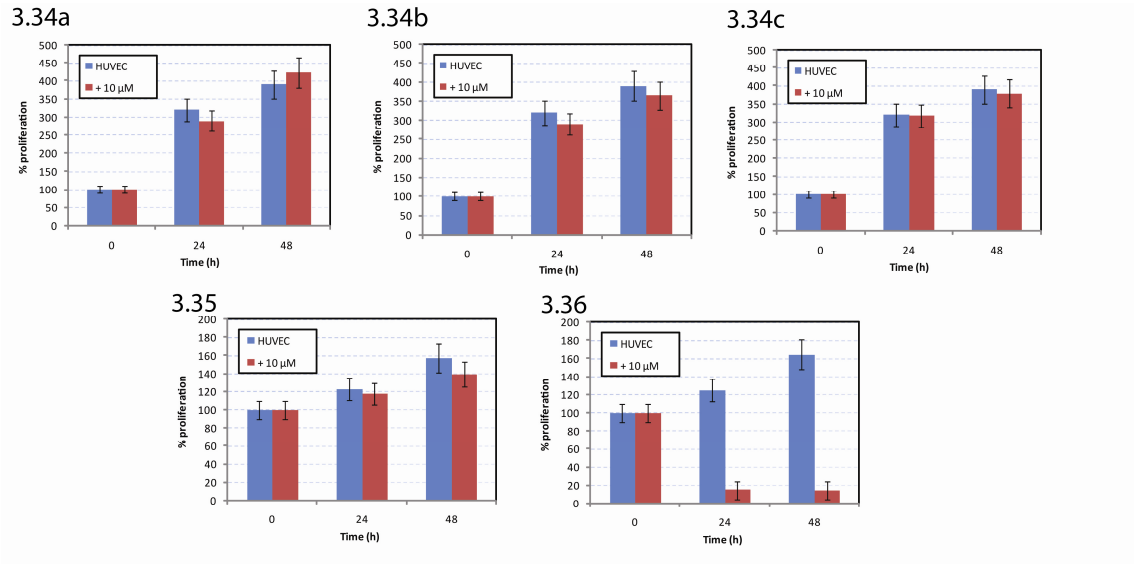

Figure 3.26: Cytotoxicity of compounds 3.34a-c, 3.35 and 3.36 (10 µM) in HUVEC cells up to 48 h.

3.3.4 Ex vivo micro-fluorescence.

From what reported, it has emerged that compound **3.34a** is the optimal mitochondrial tracker in the series under investigations. It is an heteroaromatic dye with a broad absorption in the visible spectrum, a high Stokes shift, elevated photostability, selectivity for mitochondria and almost absent cytotoxicity. Because of the relevant application as mitochondrial tracker this compound could have, we designed a further experiment aimed at collecting the fluorescence emission of **3.34a** in HUVEC ex vivo. An exemplificative micro-fluorescence spectrum is reported in Figure 3.27. Despite we have not observed a drastic shift of the emission energy, the structure of its emission band is changed with respect to that in free solvent. This feature may be ascribed to an increased stiffness of the molecular backbone in the biological environment, leading to the loss of some conformational degrees of freedom and hence to a more structured emission. Indeed, changes in fluorescence properties due to biological interactions are suitable in modern fluorescent bioassays. [91]

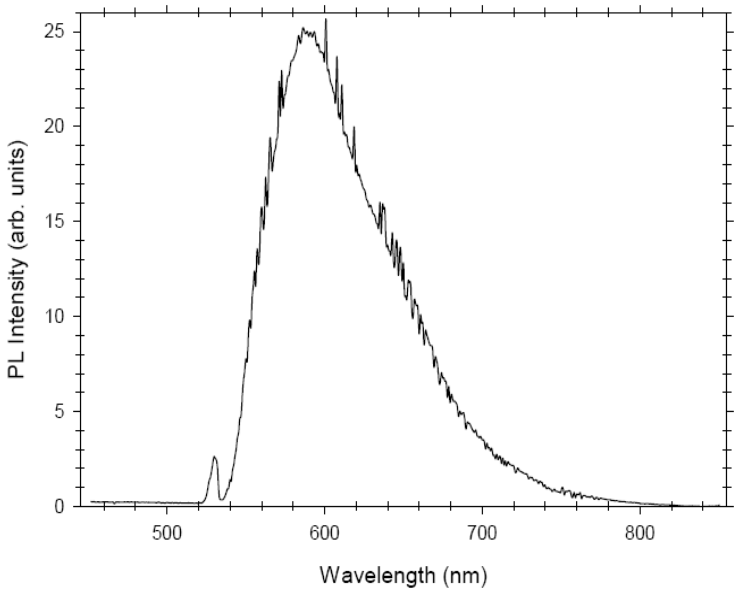

Figure 3.27: Ex vivo micro-fluorescence spectrum of compound 3.34a collected from HUVEC cells.

3.3.5 Further development

These heteroaryl derivatives provide a suitable substrate for molecular engineering. Beside the class of symmetric quadrupolar compounds here presented, we implemented some non symmetrical derivatives of the azine and azole series in order to exploit novel molecular functionalities. Among these, we present here the anthracene derivative **3.37** and the fluorescent tricationic organic salt **3.38**. The first one was synthesized according to Scheme 3.21 starting from commercial 9-(chloromethyl)anthracene by substitution with triphenylposphine, followed by a Wittig condensation with 1-methyl-1*H*-pyrrole-2-carbaldehyde. The *E*-isomer **4.12** was formylated according to the Vilsmaier-Haak procedure and the resulting product was reacted with 1,4-dimethylpyridinium triflate in Knoevenagel condition to yield **3.37**.

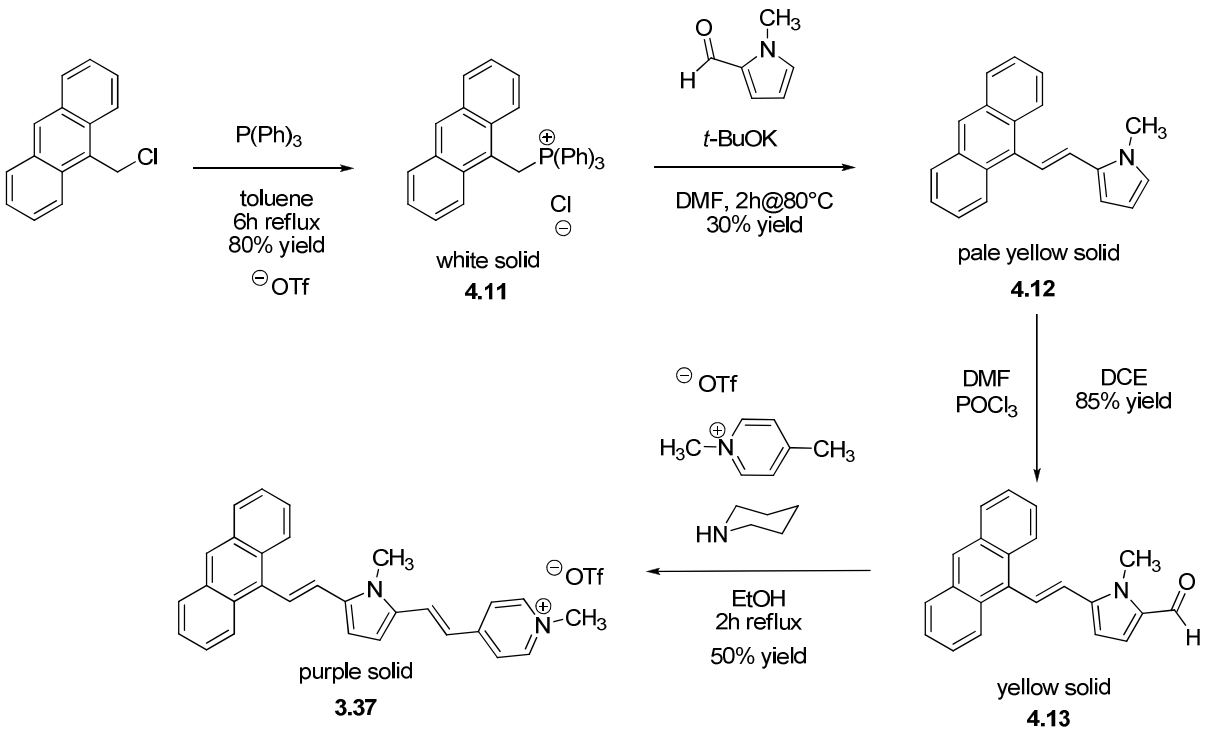

Scheme 3.21

From the photophysical point of view, it is characterized by a broad absorption band centered at 511 nm and a structured broad emission at 653 nm in ethanol (Figure 3.28). The position of these transitions and the relatively large Stokes shift make **3.37** interesting in biological applications. Moreover, its chemical structure has been designed to maximize cell permeability, higher for lipophilic cation, and the anthracene moiety is suitable as sensor of singlet oxygen. Indeed, the anthracene central ring could react with singlet oxygen to yield an endoperoxide resulting in a change in the effective conjugation length and consequently in the absorption and emission properties. Despite further photophysical, photochemical and biological evaluation are needed, we could conclude that this cationic derivative is a promising candidate as oxidative stress sensor in cells.

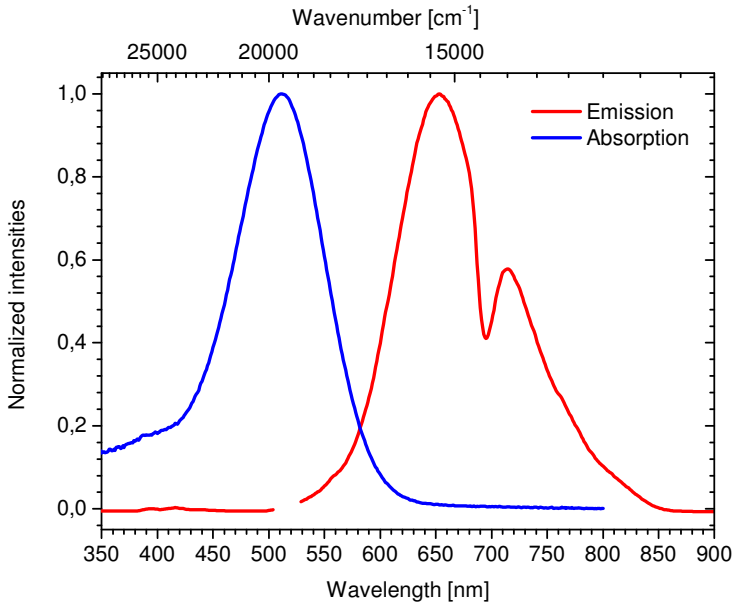

Figure 3.28: absorption (blue) and emission (red) spectra for 3.37 in ethanol.

We synthesized the non symmetrical derivative **3.38** according to Scheme 3.22. Briefly, 4-picoline was alkylated with 1,3-dibromopropane and the resulting salt was reacted with dimethilaminoethanol to yield the choline derivative **4.18**. The latter one was condensate with the aldehyde **4.9** under Knoevenagel condition and alkylated with methyl iodide to yield the desired trisaline compound **3.38**.

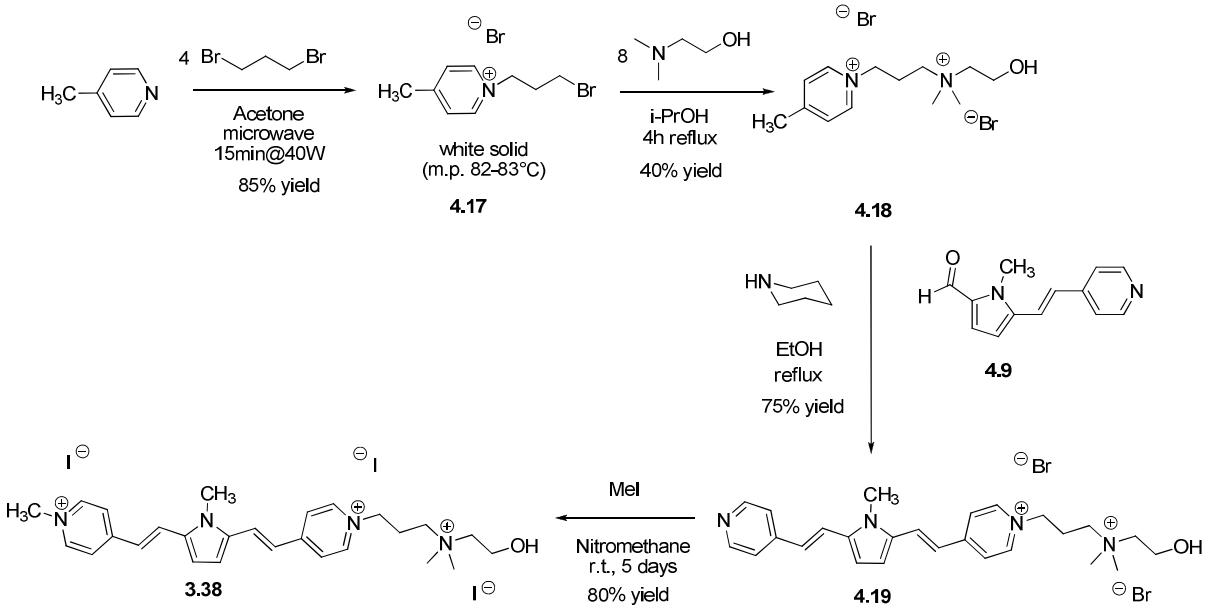

Scheme 3.22

This derivative has electronic transitions similar to its disaline progenitor **3.34a** with a broad absorption band at 508 nm in water and 527 nm in DMSO and a broad emission

band at 601 nm in water and 609 nm in DMSO, but it is more fluorescent than **3.34a** having a fluorescence quantum yield of $(16 \pm 1)\%$ in water and $(39 \pm 2)\%$ in DMSO.

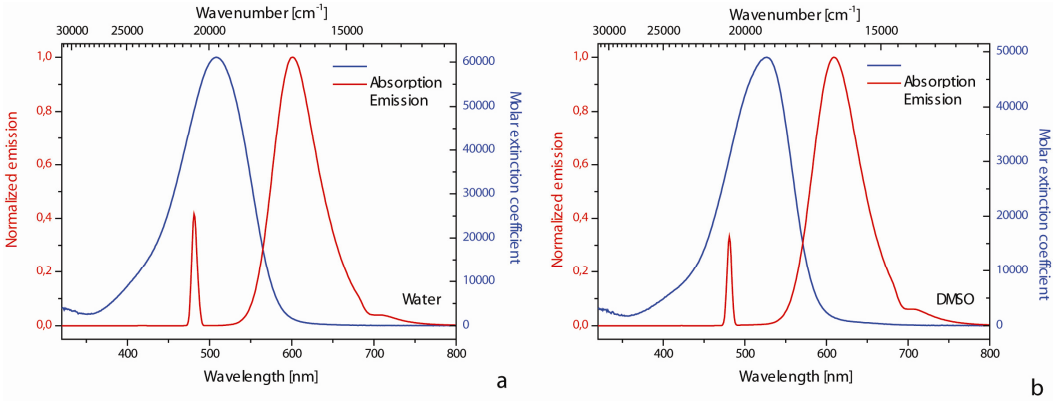

Figure 3.29: One-photon absorption (blue line) and emission (red line) spectra of PS-IV-8 in a) water and b) dimethylsulfoxide (DMSO). The fluorescence spectra were recorded after excitation at 480 nm

Considering the fact that pluricationic dyes show a preferential accumulation in tumor cells and tissues, we have indeed presented a potential water soluble fluorescent probes for cancer diagnosis.

Bibliography

1. Maahs, G.; Hegenberg, P., Synthesen und Derivate der Quadratsäure. *Angewandte Chemie* **1966,** *78* (20), 927-931.

2. Schmidt, A. H., Reaktionen von Quadrature und Quadrature-Derivaten. *Synthesis* **1980,** *1980* (12), 961-994.

3. Schmidt, A. H.; Ried, W., Die präparative Chemie der Cyclobutendione; III. Synthese von Quadratsäure, Benzocyclobutendion und deren Derivaten. *Synthesis* **1978,** *1978* (12), 869-880.

4. Schmidt, A. H.; Ried, W., Die präparative Chemie der Cyclobutendione; I. Synthese von Cyclobutendion und dessen Alkyl-, Alkenyl-und Aryl-Derivaten. *Synthesis* **1978,** *1978* (01), 1-22.

5. Seitz, G.; Imming, P., Oxocarbons and pseudooxocarbons. *Chemical Reviews* **2002,** *92* (6), 1227-1260.

6. Treibs, A.; Jacob, K., Cyclotrimethine Dyes Derived from Squaric Acid. *Angewandte Chemie International Edition in English* **1965,** *4* (8), 694.

7. Treibs, A.; Jacob, K., Cyclobutenderivate der Pyrrolreihe, II Über Vierring-trimethin-Farbstoffe. *Justus Liebigs Annalen der Chemie* **1968,** *712* (1), 123-137.

8. Law, K.; Bailey, F., Squaraine chemistry. Synthesis, characterization, and optical properties of a class of novel unsymmetrical squaraines[4-(dimehylamino) phenyl](4'-methoxyphenyl) squaraine and its derivatives. *Journal of organic chemistry* **1992,** *57* (12), 3278-3286.

9. Law, K., Squaraine chemistry. Design, synthesis and xerographic properties of a highly sensitive unsymmetrical fluorinated squaraine. *Chemistry of Materials* **1992,** *4* (3), 605-611.

10. Chen, C.; Marder, S.; Cheng, L., Syntheses and linear and nonlinear optical properties of unsymmetrical squaraines with extended conjugation. *Journal of the American Chemical Society* **1994,** *116* (7), 3117-3118.

11. Dirk, C.; Herndon, W.; Cervantes-Lee, F.; Selnau, H.; Martinez, S.; Kalamegham, P.; Tan, A.; Campos, G.; Velez, M., Squarylium dyes: structural factors pertaining to the negative third-order nonlinear optical response. *Journal of the American Chemical Society* **1995,** *117* (8), 2214-2225.

12. Meyers, F.; Chen, C.; Marder, S.; Brédas, J., Electronic Structure and Linear and Nonlinear Optical Properties of Symmetrical and Unsymmetrical Squaraine Dyes. *Chemistry-A European Journal* **1997,** *3* (4).

13. Cohen, S.; Cohen, S., Preparation and Reactions of Derivatives of Squaric Acid. Alkoxy-, Hydroxy-, and Aminocyclobutenediones1. *Journal of the American Chemical Society* **1966,** *88* (7), 1533-1536.

14. Law, K.; Bailey, F., Squaraine chemistry. Synthesis of bis (4-dimethylaminophenyl) squaraine from dialkyl squarates. Mechanism and scope of the synthesis. *Canadian Journal of Chemistry* **1986,** *64* (12), 2267-2273.

15. De Selma, R.; Fox, C.; Riordan, R., Reactions of squaric acid and some derivatives with thionyl chloride/N, N-dimethylformamide. *Tetrahedron Lett* **1970,** *11*, 781-782.

16. Santos, P. F.; Reis, L. V.; Almeida, P.; Oliveira, A. S.; Ferreira, L. F. V., Singlet Oxygen Generation Ability of Squarylium Cyanine Dyes. *J. Photochem. Photobiol, A: Chem.* **2003,** *160*, 159-161.

17. Treibs, A.; Jacob, K., Squaraines. *Justus Liebigs Annalen der Chemie* **1968,** *712*, 123.

18. Beverina, L.; Crippa, M.; Landenna, M.; Ruffo, R.; Salice, P.; Silvestri, F.; Versari, S.; Villa, A.; Ciaffoni, L.; Collini, E.; Ferrante, C.; Bradamante, S.; Mari, C. M.; Bozio, R.; Pagani, G. A., Squaraines. *J. Am. Chem. Soc.* **2008,** *130*, 1894-1902.

19. Reichardt, C., *Solvents and solvent effects in organic chemistry*. WILEY-VCH Verlag GmbH & Co. KGaA: Weinheim, 2003.

20. Law, K.-Y., Squaraine Chemistry. Absorption, Fluorescence Emission, and Photophysics of Unsymmetrical Squaraines. *The Journal of Physical Chemistry* **1995,** *99* (24), 9818-9824.

21. Horobin, R.; James, N., The staining of elastic fibres with direct blue 152. A general hypothesis for the staining of elastic fibres. *Histochemistry and cell biology* **1970,** *22* (4), 324-336.

22. Lakowicz, J., R, *Principles of fluorescence spectroscopy*. 2nd ed.; 1983.

23. Seybold, P.; Gouterman, M., Porphyrins XIII: fluorescence spectra and quantum yields. *J. Mol. Spectrosc* **1969,** *31* (1).

24. Ros-Lis, J.; Martinez-Manez, R.; Sancenon, F.; Soto, J.; Spieles, M.; Rurack, K., Squaraines as Reporter Units: Insights into their Photophysics, Protonation, and Metal-Ion Coordination Behaviour. *Chemistry-A European Journal* **2008,** *14* (32).

25. Santos, P. F.; Reis, L. V.; Almeida, P.; Oliveira, A. S.; Vieira Ferreira, L. F., Singlet oxygen generation ability of squarylium cyanine dyes. *Journal of Photochemistry and Photobiology A: Chemistry* **2003,** *160* (3), 159-161.

26. Santos, P. F.; Reis, L. V.; Almeida, P.; Serrano, J. P.; Oliveira, A. S.; Vieira Ferreira, L. F., Efficiency of singlet oxygen generation of aminosquarylium cyanines. *Journal of Photochemistry and Photobiology A: Chemistry* **2004,** *163* (1-2), 267-269.

27. Santos, P. F.; Reis, L. V.; Duarte, I.; Serrano, J. P.; Almeida, P.; Oliveira, A. S.; Vieira Ferreira, L. F., Synthesis and Photochemical Evaluation of Iodinated Squarylium Cyanine Dyes. *Helvetica Chimica Acta* **2005,** *88* (5), 1135-1143.

28. Ramaiah, D.; Joy, A.; Chandrasekhar, N.; Eldho, N. V.; Das, S.; George, M. V., Halogenated Squaraine Dyes as Potential Photochemotherapeutic Agents. Synthesis and Study of Photophysical Properties and Quantum Efficiencies of Singlet Oxygen Generation*. *Photochemistry and Photobiology* **1997,** *65* (5), 783-790.

29. Krieg, M.; Redmond, R. W., PHOTOPHYSICAL PROPERTIES OF 3,3'-DIALKYLTHIACARBOCYANINE DYES IN HOMOGENEOUS SOLUTION. *Photochemistry and Photobiology* **1993,** *57* (3), 472-479.

30. Krieg, M.; Bilitz, J.; Srichai, M.; Redmond, R., Effects of structural modifications on the photosensitizing properties of dialkylcarbocyanine dyes in homogeneous and heterogeneous solutions. *Biochim. Biophys. Acta* **1994,** *1199*, 149–156.

31. Schmidt, R.; Tanielian, C.; Dunsbach, R.; Wolff, C., Perinaphthenone, a universal reference compound for the determination of quantum yields of singlet oxygen O 2 (1 ? g) sensitization. *J. Photochem. Photobiol. A: Chem* **1994,** *79*, 11-17.

32. Wilkinson, F.; Helman, W.; Ross, A., Rate constants for the decay and reactions of the lowest electronically excited singlet state of molecular oxygen in solution. An expanded and revised compilation. *Journal of Physical and Chemical Reference Data* **1995,** *24* (2), 663-1022.

33. Ogilby, P. R.; Foote, C. S., Chemistry of singlet oxygen. 42. Effect of solvent, solvent isotopic substitution, and temperature on the lifetime of singlet molecular oxygen (1.DELTA.g). *Journal of the American Chemical Society* **1983,** *105* (11), 3423-3430.

34. Scurlock, R. D.; Ogilby, P. R., Effect of solvent on the rate constant for the radiative deactivation of singlet molecular oxygen ($^1\Delta_g$). *The Journal of Physical Chemistry* **1987,** *91* (17), 4599-4602.

35. Scurlock, R. D.; Nonell, S.; Braslavsky, S. E.; Ogilby, P. R., Effect of Solvent on the Radiative Decay of Singlet Molecular Oxygen ($^1\Delta_g$). *The Journal of Physical Chemistry* **1995,** *99* (11), 3521-3526.

36. Schweitzer, C.; Schmidt, R., Physical Mechanisms of Generation and Deactivation of Singlet Oxygen. *Chemical Reviews* **2003,** *103* (5), 1685-1758.

37. Kristiansen, M.; Scurlock, R. D.; Iu, K. K.; Ogilby, P. R., Charge-transfer state and singlet oxygen ($^1\Delta_g$ O_2) production in photoexcited organic molecule-molecular oxygen complexes. *The Journal of Physical Chemistry* **1991,** *95* (13), 5190-5197.

38. Darmanyan, A. P.; Jenks, W. S.; Jardon, P., Charge-Transfer Quenching of Singlet Oxygen $O_2(^1\Delta_g)$ by Amines and Aromatic Hydrocarbons. *The Journal of Physical Chemistry A* **1998,** *102* (38), 7420-7426.

39. Venediktov, Y.; Perfilev, V.; Titova, Y.; Karavayev, B.; Berezin, B., QUENCHING OF THE LUMINESCENCE OF SINGLET MOLECULAR OXYGEN BY SUBSTITUTED PYRROLE DERIVATIVES IN CC14 SOLUTION. *Biophysics* **1957**, 217.

40. Dalle, J. P.; Magous, R.; Mousseron-Canet, M., INHIBITION DE L'OXYGENE SINGULET. *Photochemistry and Photobiology* **1972,** *15* (4), 411-419.

41. Carre, C.; Reichardt, C.; Lougnot, D., Etude physicochimique d'une série de cyanines. VII: Rendement en état triplet et photosensibilisation de l'oxygène singulet.

Journal de chimie physique **1987,** *84* (4), 577-585.

42. Horrocks, A.; Kearvell, A.; Tickle, K.; Wilkinson, F., Mechanism of fluorescence quenching in solution. Part 2.—Quenching by xenon and intersystem crossing efficiencies. *Transactions of the Faraday Society* **1966,** *62*, 3393-3399.

43. Wilkinson, F.; McGarvey, D. J.; Olea, A. F., Factors governing the efficiency of singlet oxygen production during oxygen quenching of singlet and triplet states of anthracene derivatives in cyclohexane solution. *Journal of the American Chemical Society* **1993,** *115* (25), 12144-12151.

44. Beverina, L.; Crippa, M.; Landenna, M.; Ruffo, R.; Salice, P.; Silvestri, F.; Versari, S.; Villa, A.; Ciaffoni, L.; Collini, E.; Ferrante, C.; Bradamante, S.; Mari, C. M.; Bozio, R.; Pagani, G. A., Assessment of Water-Soluble π-Extended Squaraines as One- and Two-Photon Singlet Oxygen Photosensitizers: Design, Synthesis, and Characterization. *Journal of the American Chemical Society* **2008,** *130* (6), 1894-1902.

45. Foote, C. S.; Lin, J. W.-P., Chemistry of singlet oxygen. VI. Photooxygenation of enamines: evidence for an intermediate. *Tetrahedron Letters* **1968,** *9* (29), 3267-3270.

46. Mazur, S.; Foote, C. S., Chemistry of singlet oxygen. IX. Stable dioxetane from photooxygenation of tetramethoxyethylene. *Journal of the American Chemical Society* **1970,** *92* (10), 3225-3226.

47. Frankel, E., Chemistry of free radical and singlet oxidation of lipids program. *Lipid Res* **1985,** *23*, 197.

48. Kawakami, M.; Suzuki, M.; Kawai, H.; Ogawa, K.; Shishido, T., A self-sensitized photoreaction of rhodacyanine dye, MKT 077. *Tetrahedron Letters* **1998,** *39* (13), 1763-1766.

49. Urbanska, K.; Romanowska-Dixon, B.; Matuszak, Z.; Oszajca, J.; Nowak-Sliwinsk, P.; Stochel, G., Indocyanine green as a prospective sensitizer for photodynamic therapy of melanomas. *Acta Biochimica Polonica* **2002,** *49* (2), 387.

50. Hoebeke, M.; Piette, J.; van de Vorst, A., Photosensitized production of singlet oxygen by merocyanine 540 bound to liposomes. *Journal of Photochemistry and Photobiology B: Biology* **1991,** *9* (3-4), 281-294.

51. Ramaiah, D.; Eckert, I.; Arun, K.; Weidenfeller, L.; Epe, B., Squaraine dyes for photodynamic therapy: study of their cytotoxicity and genotoxicity in bacteria and mammalian cells. *Photochemistry and Photobiology* **2002,** *76* (6), 672-677.

52. Gayathri Devi, D.; Cibin, T. R.; Ramaiah, D.; Abraham, A., Bis(3,5-diiodo-

2,4,6-trihydroxyphenyl)squaraine: A novel candidate in photodynamic therapy for skin cancer models in vivo. *Journal of Photochemistry and Photobiology B: Biology* **2008,** *92* (3), 153-159.

53. Dolmans, D.; Dai Fukumura, R., Photodynamic therapy for cancer. *Nature Reviews Cancer* **2003,** *3* (5), 380-387.

54. Castano, A.; Mroz, P.; Hamblin, M., Photodynamic therapy and anti-tumour immunity. *Nature Reviews Cancer* **2006,** *6* (7), 535-545.

55. Dougherty, T.; Gomer, C.; Henderson, B.; Jori, G.; Kessel, D.; Korbelik, M.; Moan, J.; Peng, Q., Photodynamic therapy. *J. Natl. Cancer Inst.* **1998,** *90* (12), 889-905.

56. Miller, J., Photodynamic therapy: the sensitization of cancer cells to light. *Journal of Chemical Education* **1999,** *76*, 592.

57. Mitekura, H.; No, T.; Suzuki, K.; Satake, K.; Kimura, M., Spectroscopic properties of meso-substituted cyanine dyes: evidences for intramolecular charge transfer from a julolidine moiety as a meso-substituent to the cyanine chromophore. *Dyes and Pigments* **2002,** *54* (2), 113-120.

58. Zhang, J.; Campbell, R. E.; Ting, A. Y.; Tsien, R. Y., Creating new fluorescent probes for cell biology. *Nat Rev Mol Cell Biol* **2002,** *3* (12), 906-918.

59. Kim, H. M.; Cho, B. R., Two-Photon Probes for Intracellular Free Metal Ions, Acidic Vesicles, And Lipid Rafts in Live Tissues. *Accounts of Chemical Research* **2009,** *42* (7), 863-872.

60. Royall, J.; Ischiropoulos, H., Evaluation of 2',7'-dichlorofluorescin and dihydrorhodamine 123 as fluorescent probes for intracellular H_2O_2 in cultured endothelial cells. *Archives of biochemistry and biophysics* **1993,** *302* (2), 348-355.

61. Lakowicz, J.; Gryczynski, I.; Laczko, G., Distribution of distances between the tryptophan and the N-terminal residue of melittin in its complex with calmodulin, troponin C, and phospholipids. *Protein Science* **1994,** *3* (4), 628-637.

62. Miller, E. W.; Bian, S. X.; Chang, C. J., A Fluorescent Sensor for Imaging Reversible Redox Cycles in Living Cells. *Journal of the American Chemical Society* **2007,** *129* (12), 3458-3459.

63. Demchenko, A. P.; Mély, Y.; Duportail, G.; Klymchenko, A. S., Monitoring Biophysical Properties of Lipid Membranes by Environment-Sensitive Fluorescent Probes. *Biophysical Journal* **2009,** *96* (9), 3461-3470.

64. Morrison, L. E.; Stols, L. M., Sensitive fluorescence-based thermodynamic and kinetic measurements of DNA hybridization in solution. *Biochemistry* **2002,** *32* (12),

3095-3104.

65. Santangelo, P. J.; Nix, B.; Tsourkas, A.; Bao, G., Dual FRET molecular beacons for mRNA detection in living cells. *Nucl. Acids Res.* **2004,** *32* (6), e57-.

66. Tsien, R. Y., Fluorescent Probes of Cell Signaling. *Annual Review of Neuroscience* **1989,** *12* (1), 227-253.

67. Nagayama, S.; Zeng, S.; Xiong, W.; Fletcher, M. L.; Masurkar, A. V.; Davis, D. J.; Pieribone, V. A.; Chen, W. R., In Vivo Simultaneous Tracing and Ca^{2+} Imaging of Local Neuronal Circuits. *Neuron* **2007,** *53* (6), 789-803.

68. Fisher, J. A. N.; Barchi, J. R.; Welle, C. G.; Kim, G.-H.; Kosterin, P.; Obaid, A. L.; Yodh, A. G.; Contreras, D.; Salzberg, B. M., Two-Photon Excitation of Potentiometric Probes Enables Optical Recording of Action Potentials From Mammalian Nerve Terminals In Situ. *J Neurophysiol* **2008,** *99* (3), 1545-1553.

69. Weissleder, R.; Tung, C.-H.; Mahmood, U.; Bogdanov, A., In vivo imaging of tumors with protease-activated near-infrared fluorescent probes. *Nat Biotech* **1999,** *17* (4), 375-378.

70. He, W.; Wang, H.; Hartmann, L. C.; Cheng, J.-X.; Low, P. S., In vivo quantitation of rare circulating tumor cells by multiphoton intravital flow cytometry. *Proceedings of the National Academy of Sciences* **2007,** *104* (28), 11760-11765.

71. Achilefu, S.; Dorshow, R. B.; Bugaj, J. E.; Rajagopalan, R., Novel Receptor-Targeted Fluorescent Contrast Agents for In Vivo Tumor Imaging. *Investigative Radiology* **2000,** *35* (8), 479-485.

72. Abbotto, A.; Beverina, L.; Bozio, R.; Facchetti, A.; Ferrante, C.; Pagani, G.; Pedron, D.; Signorini, R., Novel heterocycle-based two-photon absorbing dyes. *Org. Lett* **2002,** *4* (9), 1495-1498.

73. Abbotto, A.; Baldini, G.; Beverina, L.; Chirico, G.; Collini, M.; D'Alfonso, L.; Diaspro, A.; Magrassi, R.; Nardo, L.; Pagani, G., Dimethyl-pepep: a DNA probe in two-photon excitation cellular imaging. *Biophysical chemistry* **2005,** *114* (1), 35-41.

74. Abbotto, A.; Beverina, L.; Pagani, G. A.; Collini, M.; Chirico, G.; D'Alfonso, L.; Baldini, G. In *Novel efficient and stable heteroaromatic two-photon absorbing dyes*, Confocal, Multiphoton, and Nonlinear Microscopic Imaging, Munich, Germany, SPIE: Munich, Germany, 2003; pp 223-230.

75. Abbotto, A.; Baldini, G.; Beverina, L.; Chirico, G.; Collini, M.; D'Alfonso, L.; Diaspro, A.; Magrassi, R.; Nardo, L.; Pagani, G. A., Dimethyl-pepep: a DNA probe in two-photon excitation cellular imaging. *Biophysical chemistry* **2005,** *114* (1), 35-41.

76. Versari, S.; Villa, A. M.; Villa, A.; Doglia, S. M.; Pagani, G. A.; Bradamante, S., Novel nontoxic mitochondrial probe for confocal fluorescence microscopy. *Journal of Biomedical Optics* **2006,** *11* (3), 034014-4.

77. Tsien, R., The green fluorescent protein. *Annual review of biochemistry* **1998,** *67* (1), 509-544.

78. Heilemann, M.; van de Linde, S.; Schüttpelz, M.; Kasper, R.; Seefeldt, B.; Mukherjee, A.; Tinnefeld, P.; Sauer, M., Subdiffraction-Resolution Fluorescence Imaging with Conventional Fluorescent Probes*. *Angew. Chem. Int. Ed* **2008,** *47*, 6172–6176.

79. Fernandez-Suarez, M.; Ting, A. Y., Fluorescent probes for super-resolution imaging in living cells. *Nat Rev Mol Cell Biol* **2008,** *9* (12), 929-943.

80. Luker, G. D.; Luker, K. E., Optical Imaging: Current Applications and Future Directions. *J Nucl Med* **2008,** *49* (1), 1-4.

81. Trapp, S.; Horobin, R., A predictive model for the selective accumulation of chemicals in tumor cells. *European Biophysics Journal* **2005,** *34* (7), 959-966.

82. Horobin, R., Biological staining: mechanisms and theory. *Biotechnic and Histochemistry* **2002,** *77* (1), 3-13.

83. Horobin, R.; Stockert, J.; Rashid-Doubell, F., Fluorescent cationic probes for nuclei of living cells: why are they selective? A quantitative structure–activity relations analysis. *Histochemistry and cell biology* **2006,** *126* (2), 165-175.

84. Horobin, R.; Trapp, S.; Weissig, V., Mitochondriotropics: A review of their mode of action, and their applications for drug and DNA delivery to mammalian mitochondria. *Journal of Controlled Release* **2007,** *121* (3), 125-136.

85. Rashid, F.; Horobin, R., Interaction of molecular probes with living cells and tissues. Part 2. *Histochemistry and cell biology* **1990,** *94* (3), 303-308.

86. Magde, D.; Rojas, G.; Seybold, P., Solvent dependence of the fluorescence lifetimes of xanthene dyes. *Photochemistry and Photobiology* **1999,** *70* (5), 737-744.

87. Haugland, R.; Larison, K., *Handbook of Fluorescent Probes and Research Chemicals: Euro Version*. Molecular Probes: 1999.

88. Ihida, K.; Predescu, D.; Czekay, R.; Palade, G., Platelet activating factor receptor (PAF-R) is found in a large endosomal compartment in human umbilical vein endothelial cells. **1999,** *112* (3), 285-295.

89. Rashid, F.; Horobin, R.; Williams, M., Predicting the behaviour and selectivity of fluorescent probes for lysosomes and related structures by means of structure-activity

models. *The Histochemical Journal* **1991,** *23* (10), 450-459.

90. Kluger, M.; Johnson, D.; Pober, J., Mechanism of sustained E-selectin expression in cultured human dermal microvascular endothelial cells. *J Immunol* **1997,** *158* (2), 887-896.

91. Lakowicz, J., *Principles of fluorescence spectroscopy*. 2008; p 029901.

4. Experimental part

4.1 Synthesis of the investigated compounds

Squaraine 3.1a.

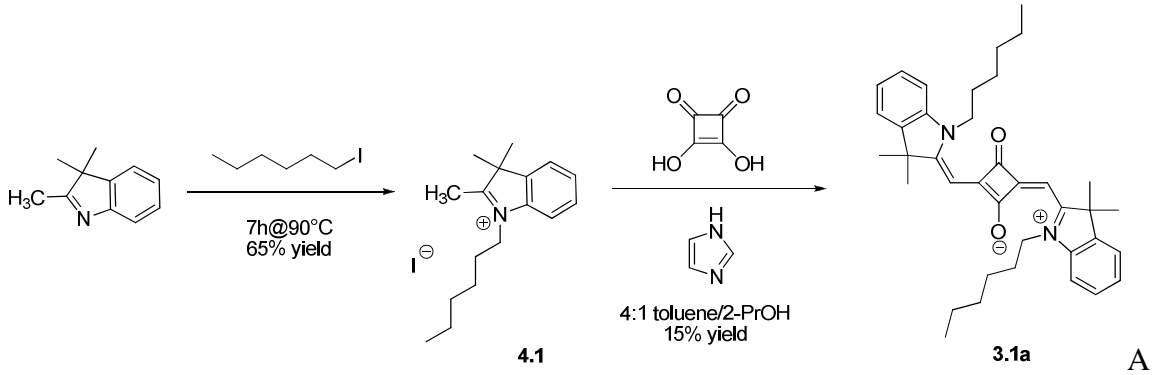

A mixture of 2,3,3-trimethyl-3*H*-indole (1.0 g, 6.3 mmol) in 1-iodohexane (3.2 g, 15.0 mmol) was heated at 90 °C for 7 h under a nitrogen atmosphere. Toluene (15 mL) was then added and the mixture refluxed for 30 min. The white precipitate was isolated by suction filtration and washed directly on the filter with 10 ml of toluene to give 1-hexyl-2,3,3-trimethyl-3*H*-indolium iodide (**4.1**) (1.5 g, 4.0 mmol, 65% yield). A mixture of **4.1** (0.40 g, 1.1 mmol), imidazole (73 mg, 1.1 mmol) and squaric acid (61 mg, 0.54 mmol) in a solution of 48 mL of 2-propanol and 12 mL of toluene was refluxed for 6 h by microwave-assisted heating under a Dean-Stark trap to azeotropically remove the water formed. The dark residue obtained after removing the solvent at reduced pressure was purified by column chromatography (silica gel, dichloromethane:methanol 20:1) to afford a green solid that was crystallized from ethanol to give pure **3.1a** as green metallic solid (75 mg, 0.13 mmol) in 15% yield. Mp > 250 °C (dec). ^{1}H NMR (500 MHz, $CDCl_3$, δ): 7.35 (d, *J* = 7.26 Hz, 2H), 7.29 (t, *J* = 7.26 Hz, 2H), 7.13 (t, *J* = 7.38 Hz, 2H), 6.97 (d, *J* = 7.87 Hz, 2H), 5.95 (s, 2H), 3.97 (t, *J* = 6.26 Hz, 4H), 1.79 (s, 12H), 1.47-1.38 (m, 4H), 1.37-1.27 (m, 12H), 0.93-0.84 (m, 6H). ^{13}C NMR (125.7 MHz, $CDCl_3$, δ): 182.5 (2C), 179.6 (2C), 170.1 (2C), 142.6 (2C), 127.8 (2C), 123.7 (2C), 122.4 (2C), 109.4 (2C), 86.6 (2C), 49.4 (2C), 43.8 (2C), 31.6 (2C), 30.1 (2C), 27.2 (2C), 27.1 (2C), 26.8 (2C), 22.6 (4C), 14.1 (2C). Anal. Calcd for $C_{38}H_{48}N_2O_2\bullet 7/2H_2O$: C, 72.69; H, 8.83; N, 4.46. Found: C, 72.36; H, 8.68; N, 4.16.

Squaraine 3.1b.

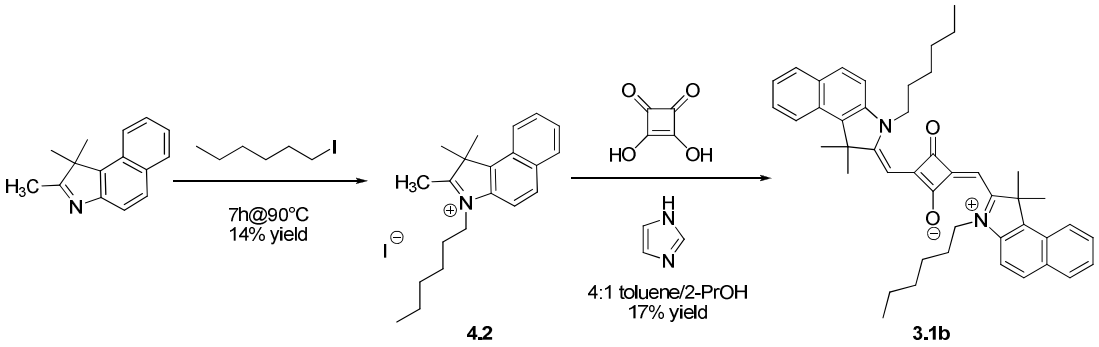

A mixture of 1,1,2-trimethyl-1*H*-benzo[*e*]indole (1.0 g, 5.0 mmol) in 1-iodohexane (3.2 g, 15.0 mmol) was heated at 90 °C for 6 h under a nitrogen atmosphere. 2-Butanone (5 mL) was then added and the mixture refluxed for 10 min. The white precipitate was isolated by suction filtration and washed directly on the filter with 5 mL of 2-butanone to give 3-hexyl-1,1,2-trimethyl-1*H*-benzo[*e*]indolium iodide (**4.2**) (0.30 g, 0.71 mmol, 14% yield). A mixture of **4.2** (0.30 g, 0.71 mmol), imidazole (48 mg, 0.71 mmol) and squaric acid (46 mg, 0.35 mmol) in a solution of 48 mL of 2-propanol and 12 mL of toluene was refluxed for 6 h by microwave-assisted heating under a Dean-Stark trap to azeotropically remove the water formed. The dark residue obtained after removing the solvent at reduced pressure was purified by column chromatography (silica gel, ethyl acetate) to afford a blue solid that was crystallized from ethanol to give pure **3.1b** as green metallic solid (40 mg, 0.060 mmol) in 17% yield. Mp > 250 °C (dec). ^{1}H NMR (500 MHz, $CDCl_3$, δ): 8.20 (d, J = 8.51 Hz, 2H), 7.89 (d, J = 8.06 Hz, 2H), 7.88 (d, J = 8.75 Hz, 2H), 7.57 (td, J_1 = 6.84 Hz, J_2 = 1.11 Hz, 2H), 7.41 (td, J_1 = 7.48 Hz, J_2 = 0.67 Hz, 2H), 7.28 (d, J = 8.77 Hz, 2H), 6.02 (s, 2H), 4.11 (t, J = 7.10 Hz, 4H), 2.08 (s, 6H), 1.92-1.83 (m, 4H), 1.71-1.63 (m, 4H), 1.23-1.41 (m, 8H), 0.89 (t, J = 7.02 Hz, 6H). ^{13}C NMR (125.7 MHz, $CDCl_3$, δ): 177.9 (2C), 171.3 (2C), 139.6 (2C), 133.9 (2C), 131.2 (2C), 129.6 (4C), 128.7 (2C), 127.2 (2C), 124.2 (2C), 122.6 (2C), 86.2 (2C), 51.1 (2C), 43.8 (2C), 31.5 (2C), 26.8 (2C), 26.7 (4C), 22.5 (4C), 46.4 (2C), 31.4 (2C), 27.4 (4C), 22.5 (4C), 14.0 (2C). Anal. Calcd for $C_{46}H_{52}N_2O_2 \bullet 1.5\ H_2O$: C, 79.85; H, 8.01; N, 4.05. Found: C, 79.93; H, 8.08; N, 3.84.

Squaraine 3.1c.

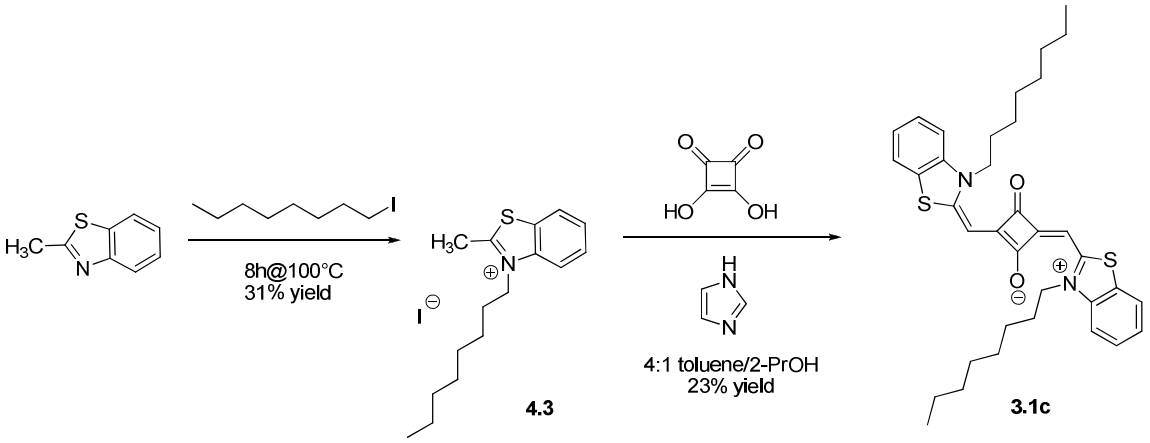

A mixture of 2-methylbenzo[*d*]thiazole (1.0 g, 6.7 mmol) in 1-iodooctane (4.1 g, 17.0 mmol) was heated at 100 °C for 8 h under a nitrogen atmosphere. Toluene (10 mL) was then added and the mixture refluxed for 30 min. The white precipitate was isolated by suction filtration and washed directly on the filter with 5 mL of toluene to give 2-methyl-3-octylbenzo[*d*]thiazol-3-ium iodide (**4.3**) (0.81 g, 2.1 mmol, 31% yield). A mixture of **4.3** (0.30 g, 0.77 mmol), imidazole (52 mg, 0.77 mmol) and squaric acid (44 mg, 0.38 mmol) in a solution of 48 ml of 2-propanol and 12 mL of toluene was refluxed for 12 h under a Dean-Stark trap to azeotropically remove the water formed. The dark residue obtained after removing the solvent at reduced pressure was purified by column chromatography (silica gel, dichloromethane:methanol 15:1) to afford a blue solid that was crystallized from ethanol to give pure **3.1c** as green metallic solid (108 mg, 0.18 mmol) in 23% yield. Mp > 250 °C (dec). ^{1}H NMR (500 MHz, $CDCl_3$, δ): 7.54 (d, *J* = 7.77 Hz, 2H), 7.37 (t, *J* = 7.38 Hz, 2H), 7.20 (t, *J* = 7.49 Hz, 2H), 7.14 (d, *J* = 8.16 Hz, 2H), 6.00 (s, 2H), 4.08 (t, *J* = 7.43 Hz, 4H), 1.81 (q, *J* = 7.62 Hz, 4H), 1.49-1.41 (m, 4H), 1.37-19.29 (m, 20H), 0.89 (t, *J* = 7.14 Hz, 6H). ^{13}C NMR (125.7 MHz, $CDCl_3$, δ): 181.3 (2C), 159.9 (2C), 141.1 (2C), 128.6 (2C), 127.1 (2C), 124.0 (2C), 122.1 (2C), 111.5 (2C), 85.7 (2C), 46.4 (2C), 31.4 (2C), 27.4 (4C), 26.5 (4C), 22.5 (2C), 14.0 (2C). Anal. Calcd for $C_{36}H_{44}N_2O_2S_2 \bullet H_2O$: C, 69.86; H, 7.49; N, 4.53. Found: C, 69.58; H, 7.55; N, 4.19.

2,3,3-trimethyl-5-nitro-3*H*-indole (3.8).

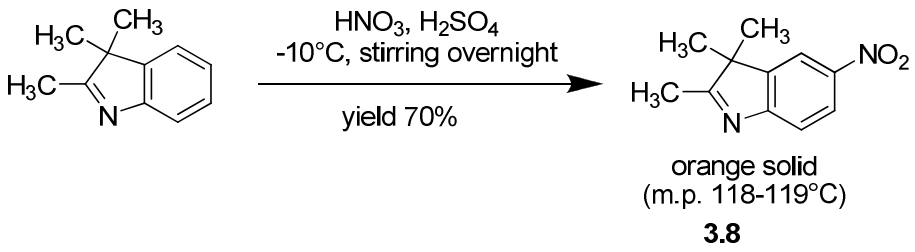

To an iced-cooled solution of 2,3,3-trimethylindolenine (3,0 g, 18,8 mmol) in H_2SO_4 (15 ml) was slowly added a mixture of HNO_3 (3,5 ml) e H_2SO_4 (3 ml). The mixture was stirred overnight, poured into ice (200 ml), and neutralized with NaOH (aq) till basic pH. The resulting orange precipitate was collected by filtration, washed several times cold water and hot methanol to afford the desired product as white solid (2,69 g, m.p. 118-119°C). Yield 70%. ^{1}H NMR (DMSO) δ 8.42 (d, J = 2.3 Hz, 1H), 8.24 (dd, J^1 = 8.6 Hz, J^2 = 2.4 Hz, 1H), 7.65 (d, J = 8.5 Hz, 1H), 2.31 (s, 3H), 1.33 (s, 6H).

2,3,3-trimethyl-3*H*-indol-5-amine (3.9).

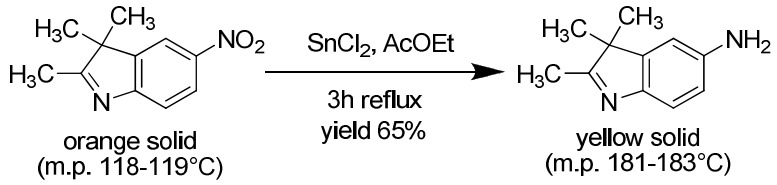

3.8 **3.9**

A solution of 1.2 g of 5-nitro-2,3,3,-trimethylindolenine (5.9 mmol) and 5.7 g of stannous chloride (30 mmol) in 100 ml of ethyl acetate was refluxed for 3 hours (initially the hot mixture turned clear, then a fine precipitated was formed). After 3 hours the mixture was poured into an aqueous solution of NaOH (300 ml, pH = 10). The resulting precipitate was filtered on buchner and the water was extractred with ethyl acetate (3x30 ml). The organic phase was dried over Na_2SO_4 and solvent was distilled off under reduced pressure to yield the desired product as a yellow solid. Recrystallized from toluene. (0.67 g, m.p. 181-183°C). 65% yield. ^{1}H NMR (DMSO) δ 7.05 (d, J = 8.1 Hz, 1H), 6.56 (d, J = 2.1 Hz, 1H), 6.42 (dd, J^1 = 8.1 Hz, J^2 = 2.2 Hz, 1H), 2.09 (s, 3H), 1.15 (s, 6H).

Cholesteryl(2,3,3-trimethyl-3*H*-indol-5-yl)carbamate (3.10).

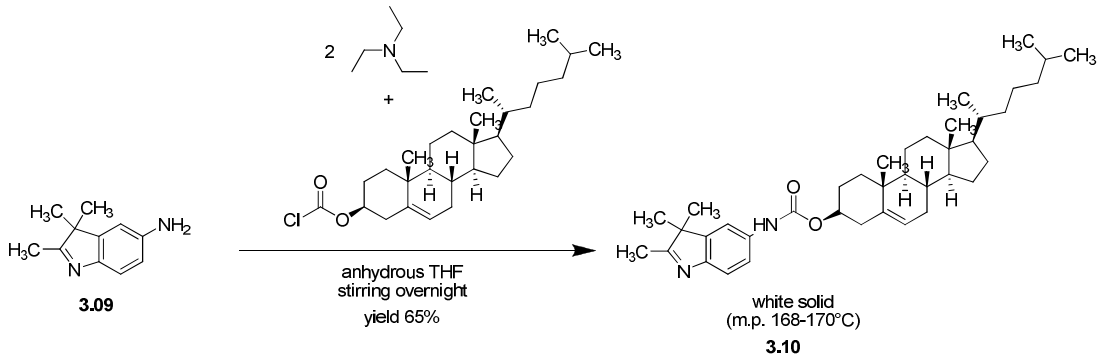

3.09 **3.10**

To a solution of 5-nitro-2,3,3,trimethylindolenine (0.70 g, 4,0 mmol) in 20 ml of

anhydrous THF, a solution of cholesteryl chloroformiate (1.8 g, 4.0 mmol) in 10 ml of anhydrous THF and triethylamine (1.4 ml, 10 mmol) in 10 ml of anhydrous THF were added dropwise simultaneously under stirring. After 1 hour there was evidence of product formation (TLC with AcOET:exane 1:1 as eluent; $Rf_{reagent}$ = 0.25; $Rf_{product}$ = 0.50). After stirring overnight the mixture was washed with distilled water (3x100 mL). The organic phase was dried over Na_2SO_4. Removal of the solvent gave a residue, which was subjected to column chromatography over silica gel. Elution of the column with a mixture AcOET:hexane 1:2 gave the cholesterol-conjugated benzothiazole derivative (0.94 g, 40% yield) as a white solid (m.p. 168-170 °C). ^{1}H NMR ($CDCl_3$) δ 7.65 (bs, 1H), 7.45 (d, J = 8.3 Hz, 1H), 7.04 (dd, J^1 = 8.2 Hz, J^2 = 2.0 Hz, 1H), 6.63 (bs, 1H), 5.42-5.40 (m, 1H), 4.66-4.55 (m, 1H), 2.47-2.36 (m, H), 2.35 (s, 3H), 2.05-1.86 (m, H), 1.64-1.32 (m, H), 1.31 (s, 6H), 1.24-1.06 (m, H), 1.03 (s, 3H), 0.92 (d, J = 6.4 Hz, 1H), 0.87 (d, J = 6.6 Hz, 6H), 0.68 (s, 3H).

5-(cholesterolcarbonylamino)-1,2,3,3-tetramethyl-3*H*-indolium trifluoromethanesulfonate (3.11).

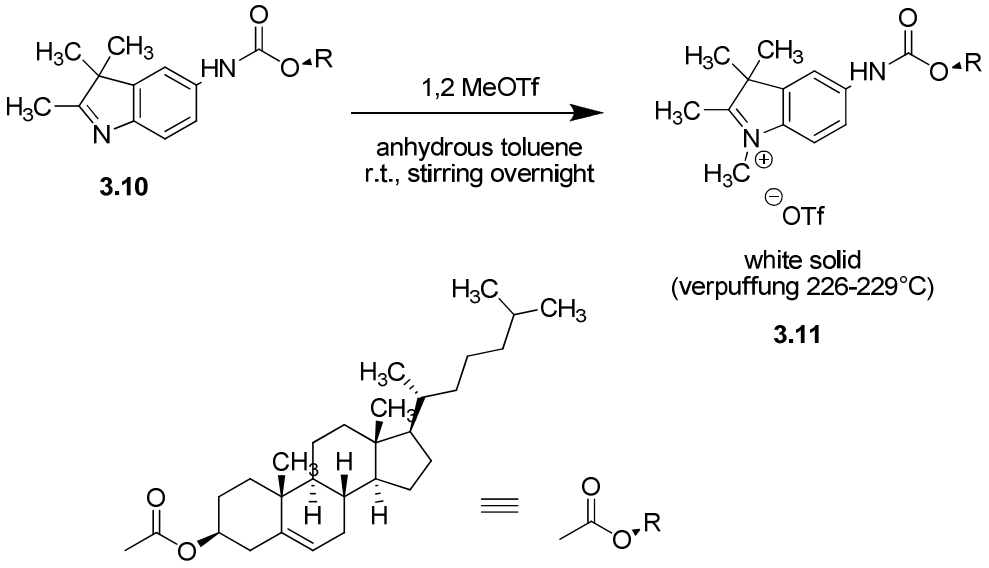

To a solution of the indolenine derivative **3.10** (0.30 g, 0.51 mmol) in 15 ml of anhydrous toluene was added 0.1 ml of methyl triflate with formation of a precipitate. After 4 hours, the resulting precipitate was collected by filtration, washed several times with toluene afford the desired product as white solid (0.30 g, verpufflung 250°C). 80% yield. ^{1}H NMR (DMSO) δ 10.08 (bs, 1H), 7.93 (d, J = 1.6 Hz, 1H), 7.81 (d, J = 8.7 Hz), 7.51 (dd, J^1 = 8.7 Hz, J^2 = 1.6 Hz, 1H), 5.42-5.40 (m, 1H), 4.51-4.43 (m, 1H), 3.91 (s, 3H), 2.70 (s, 3H), 2.47-2.36 (m, H), 2.05-1.86 (m, H), 1.64-1.32 (m, H), 1.48 (s, 6H), 1.24-1.06 (m, H), 1.03 (s, 3H), 0.92 (d, J =

6.4 Hz, 1H), 0.87 (d, *J* = 6.6 Hz, 6H), 0.68 (s, 3H).

2-methyl-6-nitrobenzo[*d*]thiazole (3.12).

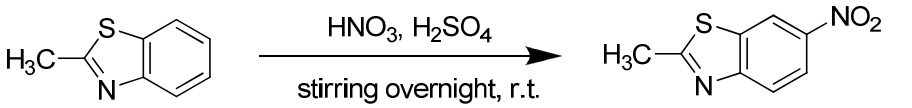

white solid (m.p. 163-164°C)

3.12

To an iced-cooled solution of 2-methyl-1,3-benzothiazole (6.0 g, 40 mmol) in H_2SO_4 (25 cc) was slowly added a mixture of HNO_3 (5.0 ml) e H_2SO_4 (3.5 ml). The mixture was stirred overnight, then poured into ice (250 cc), The resulting precipitate was collected by filtration, washed several times cold water and hot methanol to afford the desired product as white solid (4.1 g, 21 mmol) 52% yield. m.p. 163-164°C.

2-methylbenzo[*d*]thiazol-6-amine (3.13).

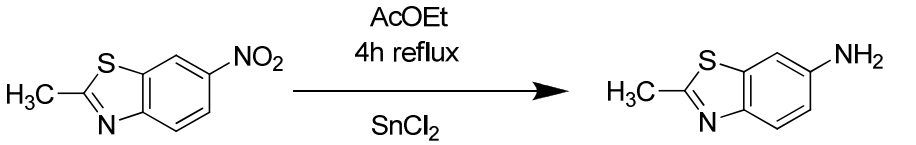

white solid (m.p. 118-119°C)

3.13

A solution of 1.28 g of 2-methyl-6-nitrobenzothiazole and 8.6 g of stannous chloride in 200 ml of ethyl acetate was refluxed for 4 hours (initially the hot mixture turned clear, then a fine precipitated was formed). After 4 hours the mixture was poured into an acqueous solution of NaOH (300 ml, pH = 10). The resulting precipitate was filtered on seesand and the water was extractred with ethyl acetate (3x50 ml). The organic phase was dryed over Na_2SO_4 and solvent was distilled off under reduced pressure to yield the desired product as a white solid. (4 g, m.p. 118-119°C). 60% yield.

Cholesteryl(2-methylbenzo[*d*]thiazol-6-yl)carbamate (3.14).

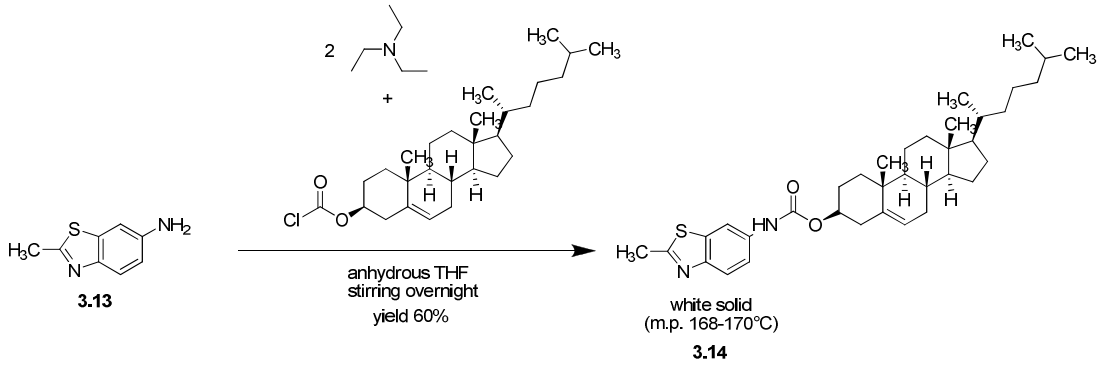

3.13 3.14

To a solution of 2-methylbenzothiazol-6-amine (0.180 g, 1.1 mmol) in 10 mL of anhydrous THF, a solution of cholesteryl chloroformiate (0.50 g, 1.1 mmol) in 5 mL of anhydrous THF and triethylamine (0.7 mL, 2.2 mmol) in 5 mL of anhydrous THF were added dropwise simultaneously under stirring. After 1 hour there was evidence of product formation (TLC with AcOET:exane 1:1 as eluent; $Rf_{reagent}$ = 0.15; $Rf_{product}$ = 0.55). After stirring overnight the mixture was washed with acidic water (3x50 mL, pH = 6). The organic phase was dried over Na_2SO_4. Removal of the solvent gave a residue, which was subjected to column chromatography over silica gel. Elution of the column with a mixture AcOET:hexane 1:2 gave the cholesterol-conjugated benzothiazole derivative (0.280 g, yield 44%) as a white solid (m.p. 168-170 °C).

6-(cholesterolcarbonylamino)-2,3-dimethylbenzo[*d*]thiazolium trifluoromethanesulfonate (3.15).

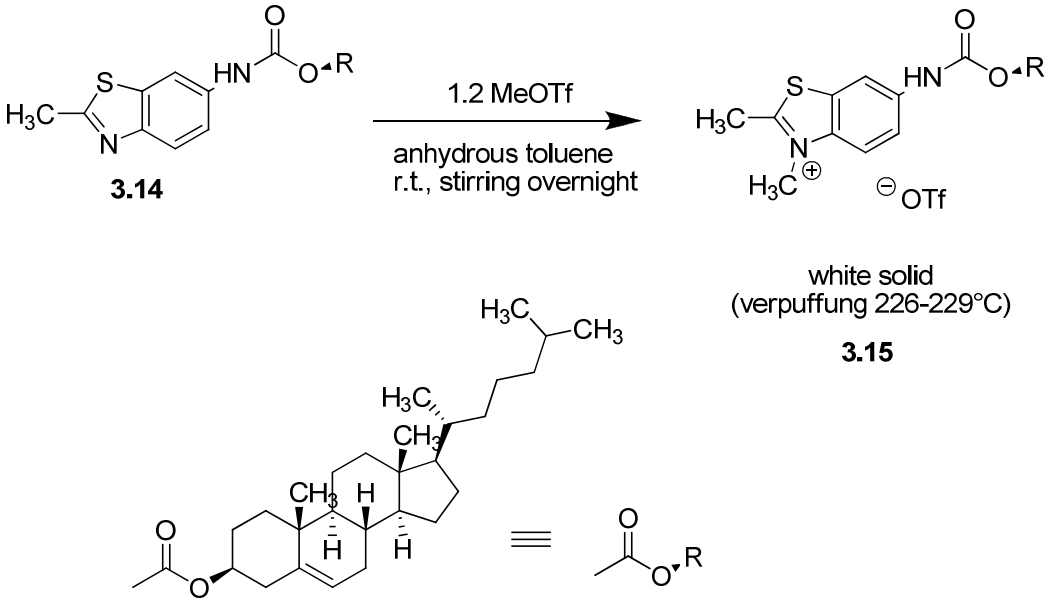

3.14 3.15

To a solution of the benzothiazole derivative (100 mg, 0.17 mmol) in 10 mL of anhydrous

toluene was added 20 μL of methyl triflate with formation of a precipitate. After stirring overnight, the resulting precipitate was collected by filtration, washed several times with toluene afford the desired product as white solid (0.160 g, 0.16 mmol). 85% yield. Verpufflung 226-229°C.

Squaraine 3.1d.

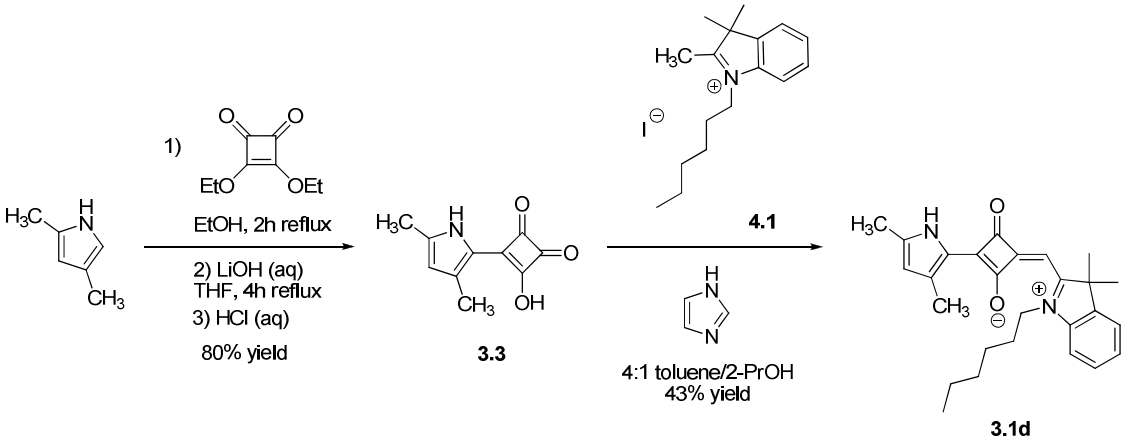

A solution of 2,4-dimethyl-1*H*-pyrrole (1.0 g, 10.5 mmol) and 3,4-diethoxycyclobut-3-ene-1,2-dione (1.8 g, 11 mmol) in ethanol (15 mL) was refluxed for 2 h. The pale yellow precipitate formed after cooling the reaction mixture at 0 °C was collected by filtration, washed with ethanol (5 mL) and added to a mixture of THF (10 mL), water (10 mL) and lithium hydroxide (0.30 g). The resulting suspension was refluxed for 4 h. An aqueous solution of 1M HCl was then added to reach pH 5. The yellow precipitate formed was collected by filtration to afford 3-(3,5-dimethyl-1*H*-pyrrol-2-yl)-4-hydroxycyclobut-3-ene-1,2-dione (**3.3**) (1.6 g, 8.4 mmol, 80% yield). A suspension of **3.3** (100 mg, 0.52 mmol), imidazole (35 mg, 0.52 mmol) and **4.1** (200 mg, 0.52 mmol) in a solution of 40 mL of 2-propanol and 10 mL of toluene was refluxed for 14 h under a Dean-Stark trap to azeotropically remove the water formed. The dark residue obtained after removing the solvent at reduced pressure was purified by column chromatography (silica gel, ethyl acetate) to afford a blue solid that was crystallized from ethanol to give pure **3.1d** as blue solid (75 mg, 0.13 mmol) in 45% yield. m.p. > 250 °C (dec). ^{1}H NMR (500 MHz, $CDCl_3$, δ): 9.95 (bs, 1H), 7.39 (d, *J* = 7.31 Hz, 1H), 7.35 (t, *J* = 6.76 Hz, 1H), 7.22 (t, *J* = 7.32 Hz, 1H), 7.06 (d, *J* = 7.94 Hz, 1H), 6.04 (bs, 2H), 4.05 (t, *J* = 7.58 Hz, 2H), 2.62 (s, 3H), 2.34 (s, 3H), 1.86-1.76 (m, 2H), 1.78 (s, 6H), 1.48-1.39 (m, 2H), 1.38-1.28 (m, 2H), 0.88 (t, *J* = 7.04 Hz, 1H). ^{13}C NMR (125.7 MHz, $CDCl_3$, δ): 172.8 (1C), 142.6 (1C), 142.0 (1C), 141.0 (1C), 134.8 (1C),

128.1 (1C), 124.9 (1C), 124.1 (1C), 122.5 (1C), 115.1 (1C), 110.3 (1C), 88.5 (1C), 50.0 (1C), 44.2 (1C), 31.5 (1C), 27.3 (1C), 26.8 (2C), 26.7 (1C), 22.6 (1C), 14.1 (1C), 14.0 (1C), 13.2 (1C). Anal. Calcd for $C_{27}H_{32}N_2O_2$: C, 77.85; H, 7.74; N, 6.73. Found: C, 77.39; H, 8.01; N, 6.34.

(Z)-3-butoxy-4-((1,3,3-trimethylindolin-2-ylidene)methyl)cyclobut-3-ene-1,2-dione (4.4).

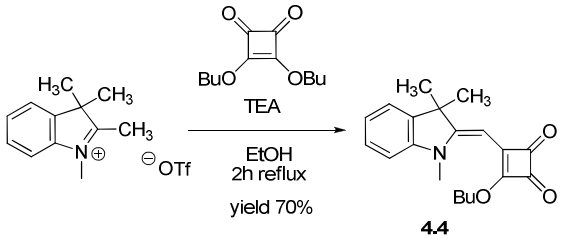

4.4

To a solution of 1,2,3,3-tetramethylindoleninium triflate (570 mg, 1,76 mmol) in 15 ml of ethanol was added 0,4 g of butyl squarate (1,76 mmol) and 0,25 ml of triethylamine (1,76 mmol). Reaction mixture was refluxed for 2h, then solvent was evaporated under reduced pressure and the resulting residue was washed with hot cyclohexane giving the desired product as yellow solid (400 mg, 1,23 mmol). Yield 70%. ^{1}H NMR ($CDCl_3$) δ 7.32-7.25 (m, 2H), 7.11-7.03 (m, 1H), 6.89 (d, *J* = 8.3 Hz, 1H), 5.36 (bs, 1H), 4.85 (t, *J* = 6.6, 2H), 3.37 (bs, 3H), 1.88 (q, *J* = 6.8, 2H), 1.62 (s, 6H), 1.00 (t, *J* = 7.4, 3H).

(Z)-3-hydroxy-4-((1,3,3-trimethylindolin-2-ylidene)methyl)cyclobut-3-ene-1,2-dione (3.22).

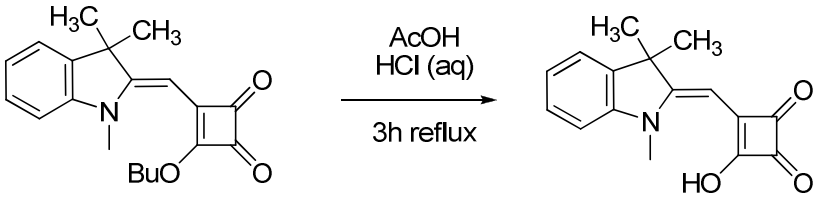

4.4 **3.22**

380 mg of emisquarate were refluxed in 5 ml of AcOH, 5 ml of deionized water and 1 ml of HCl 37%. The desired product was isolated by filtration of the yellow precipitate formed after cooling. (285 mg, 1,06 mmol). 90% yield. ^{1}H-NMR ($CDCl_3$) δ 7.39 (d, *J* = 7.2 Hz, 1H), 7.27 (t, *J* = 7.4, 1H), 7.12 (d, *J* = 7.9 Hz, 1H), 7.02 (t, *J* = 7.3 Hz, 1H), 5.45 (s, 1H), 3.35 (s, 3H), 1.56 (s, 6H).

Squaraine 3.16.

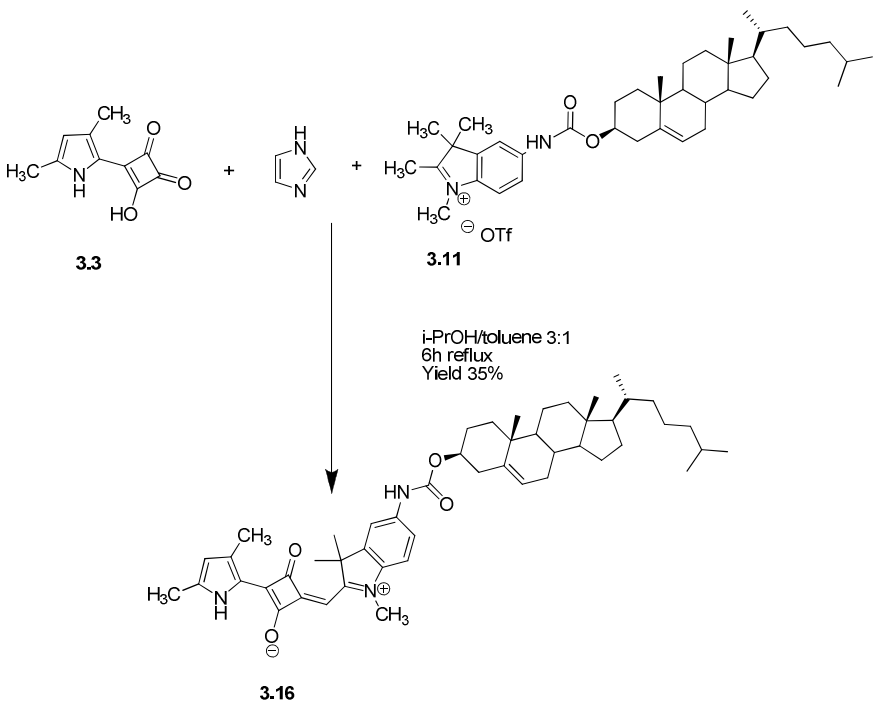

A solution of the indolenine derivative (200 mg, 0.36 mmol), emisquaraine (50 mg, 0.36 mmol) and imidazole (25 mg, 0.36 mmol) in 25 mL of 2-PrOH/toluene 3:1 was refluxed for 6 hours under azeotropic conditions. The mixture turned blue in half an hour. After 6 hours the solvent was distilled off under reduced pressure and the residue was purified by chromatography on silica gel. Elution of the column with a mixture CH_2Cl_2:MeOH 9:1 gave the cholesterol-conjugated squaraine derivative (70 mg, 0.093 mmol) as a purple solid (dec. 270 °C). 35% yield. ^{1}H NMR ($CDCl_3$) δ 9.36 (bs, 1H), 7.60 (d, J = 1.6 Hz, 1H), 7.34 (dd, J^1 = 8.8 Hz, J^2 = 1.5 Hz, 1H), 7.04 (d, J = 8.9 Hz), 6.74 (s, 1H), 6.06 (bs, 1H), 5.45-5.41 (m, 1H), 4.66-4.60 (m, 1H), 3.66 (s, 3H), 2.63 (s, 3H), 2.47-2.36 (m, H), 2.05-1.86 (m, H), 1,78 (s, 6H), 1.64-1.32 (m, H), 1.48 (s, 6H), 1.24-1.06 (m, H), 1.03 (s, 3H), 0.92 (d, J = 6.4 Hz, 1H), 0.87 (d, J = 6.6 Hz, 6H), 0.68 (s, 3H). Anal. Calcd for $C_{50}H_{67}N_3O_4 \bullet H_2O$: C, 75.82; H, 8.78; N, 5.30. Found: C, 75.93; H, 9.19; N, 5.94.

Synthesis of squaraine 3.23.

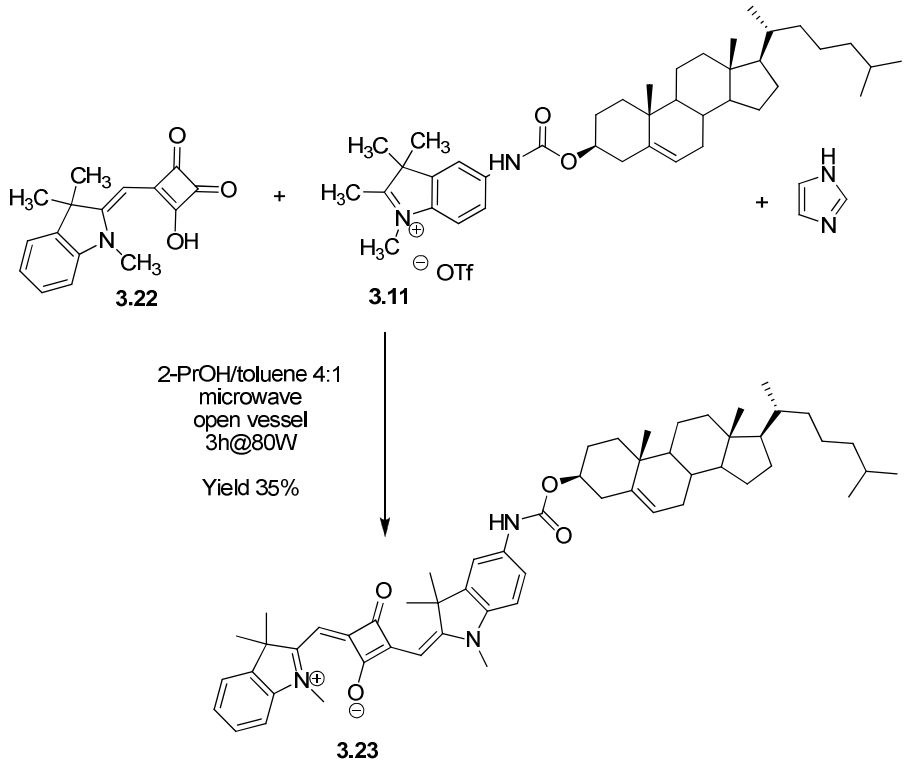

The reaction was carried out in a microwave oven, in nitrogen atmosphere and under azeotropic conditions. A solution of the indoleninium derivative (200 mg, 0.27 mmol) and emisquaraine (72 mg, 0.27 mmol) in 15 ml of *i*-PrOH/toluene 4:1 was refluxed in open vessel mode at 80 W. A solution of imidazole (20 mg, 0.27 mmol) in 1 ml of 2-PrOH was added dropwise to the hot reaction mixture. After 3 hours the solvent was distilled off under reduced pressure and the residue was purified by chromatography on silica gel. Elution of the column with a mixture CH_2Cl_2:MeOH 9:1 gave the cholesterol-conjugated squaraine derivative (80 mg, 0.094 mmol) as a purple solid (dec. 282 °C). Yield 35% ^{1}H NMR ($CDCl_3$) δ 9.32 (bs, 1H), 7.60 (d, *J* = 1.7 Hz, 1H), 7.38-7.32 (m, 2H), 7.29 (t, *J* = 7.29 Hz, 1H), 7.15-7.05 (m, 2H), 6.97 (d, *J* = 7.87 Hz, 1H), 6.01 (bs, 2H), 5.43-5.39 (m, 1H), 4.64-4.58 (m, 1H), 3.89 (bs, 6H), 2.60 (s, 3H), 2.47-2.37 (m, H), 2.05-1.84 (m, H), 1,78 (s, 12H), 1.65-1.32 (m, H), 1.48 (s, 6H), 1.25-1.06 (m, H), 1.02 (s, 3H), 0.92 (d, *J* = 6.4 Hz, 1H), 0.89 (d, *J* = 6.6 Hz, 6H), 0.69 (s, 3H). Anal. Calcd for $C_{56}H_{73}N_3O_4 \bullet 2H_2O$: C, 75.72; H, 8.74; N, 4.73. Found: C, 75.72; H, 8.86; N, 4.45.

3-Chloro-4-(dithieno[3,2-*b*:2′,3′-*d*]thiophene-2-yl)cyclobut-3-ene-1,2-dione (4.5)

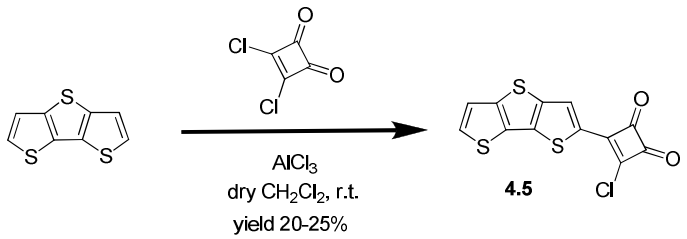

$AlCl_3$ (200 mg, 1,53 mmol) was added portionwise to a solution of ditienothiophene (300 mg, 1.53 mmol) and acid squaric chloride (230 mg, 1.53 mmol) in 10 ml of dry CH_2Cl_2. Immediately the solution turn red. After 2h the reaction was assumed completed by TLC (AcOEt/hexane 1:1). The reaction mixture was poured into acid water (100 cc, pH 3) and the organic phase was separated, dried over Na_2SO_4, filtered over silica and evaporated under reduced pressure to afford the desired product as a red solid (120 mg, 25% yield).

3-Hydroxy-4-(dithieno[3,2-*b*:2′,3′-*d*]thiophene-2-yl)cyclobut-3-ene-1,2-dione (3.17)

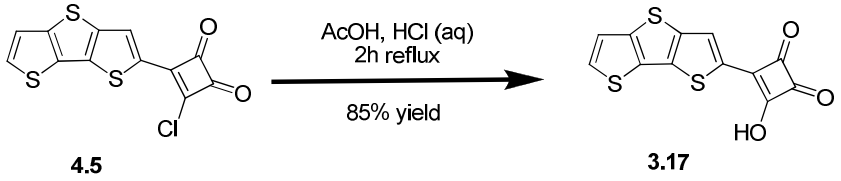

4.5 **3.17**

The reactant (200 mg, 0.64 mmol) was refluxed for 4h in a mixture of water (7 cc), acetic acid (7 cc) and acqueous HCl (1 cc). The desired product was collected by filtration after cooling the mixture at room temperature (160 mg, 85% yield).

Synthesis of squaraine 3.18.

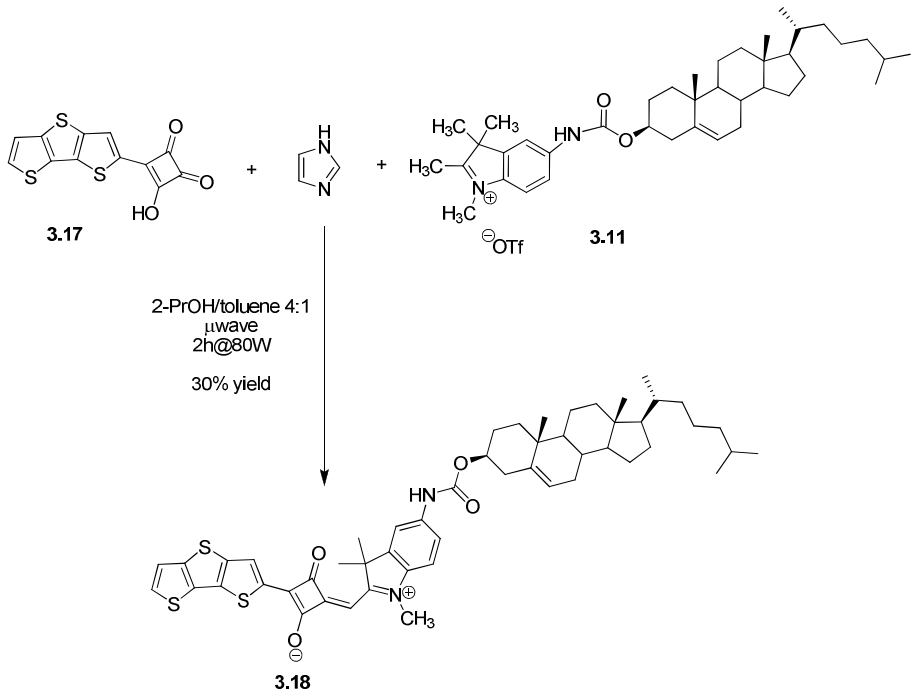

The reaction was carried out in a microwave oven, in nitrogen atmosphere and under azeotropic conditions. A solution of the indolenine derivative (130 mg, 0,17 mmol) and emisquaraine (50 mg, 0,17 mmol) in 15 ml of 2-PrOH/toluene 4:1 was refluxed in open vessel modality at 80 W. A solution of imidazole (12 mg, 0,17 mmol) in 1 ml of 2-PrOH was added dropwise to the hot reaction mixture. After 2 hours the solvent was distilled off under reduced pressure and the residue was purified by chromatography on silica gel. Elution of the column with a mixture CH_2Cl_2:MeOH 9:1 gave the cholesterol-conjugated squaraine derivative (42 mg, 30% yield) as a purple solid. Anal. Calcd for $C_{52}H_{62}N_2O_4S_3 \bullet ½H_2O$: C, 70.63; H, 7.18; N, 3.17. Found: C, 70.35; H, 7.32; N, 3.19.

3-Butoxy-4-(3,4,5-tribromothiophen-2-yl)cyclobut-3-ene-1,2-dione (3.19).

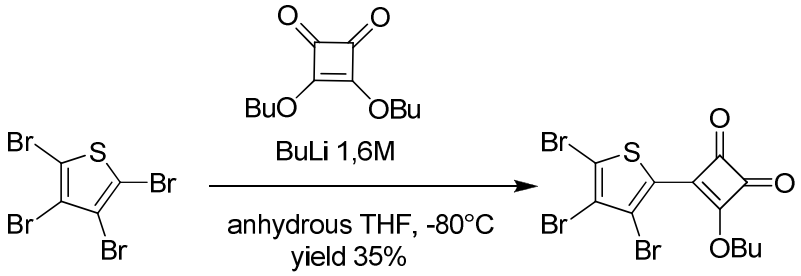

(m.p. 108.109°C)

3.19

A solution 1.6 M of butyl lithium (1,8 ml, 1.1 mmol) was added dropwise to a solution of tetrabromothiophene (400 mg, 1.0 mmol) in 15 cc of anhydrous THF cooled at -80°C. The

solution turn slightly yellow. After 30 minutes at -80°C, butyl squarate (226 mg, 1.0 mmol) was added to the mixture. After 30 minutes at -80°C, the reaction mixture was allowed to warm up at room temperature slowly. The reaction mixture was pured into 200 cc of a acidic water and extracted with 3x20cc of ethyl acetate; the organic phase was washed with brine (3x100 cc) and dried over Na_2SO_4. Removal of solvent gave a residue that was crystallized from cyclohexane to obtain the desired product as yellow solid (165 mg, 35 %). m.p. 108-109°C.

3-Hydroxy-4-(3,4,5-tribromothiophen-2-yl)cyclobut-3-ene-1,2-dione (3.20).

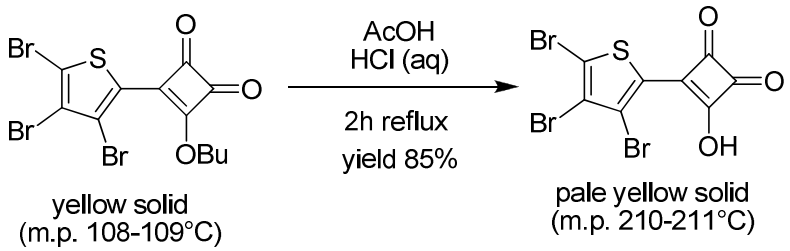

yellow solid
(m.p. 108-109°C)
3.19

pale yellow solid
(m.p. 210-211°C)
3.20

The reactant (150 mg, 0.31 mmol) was refluxed for 2h in a mixture of water (3 cc), acetic acid (7 cc) and aqueous HCl (1 cc). The desired product was obtained by filtration of the mixture cooled at room temperature (110 mg). Yield 85%. m.p. 210-211°C. ^{1}H NMR (DMSO) δ 5.32 (bs, 1H). ^{13}C NMR (DMSO) δ 213.1, 192.6, 167.4, 131.7, 119.1, 115.0, 112.4, 109.3.

Synthesis of squaraine 3.21.

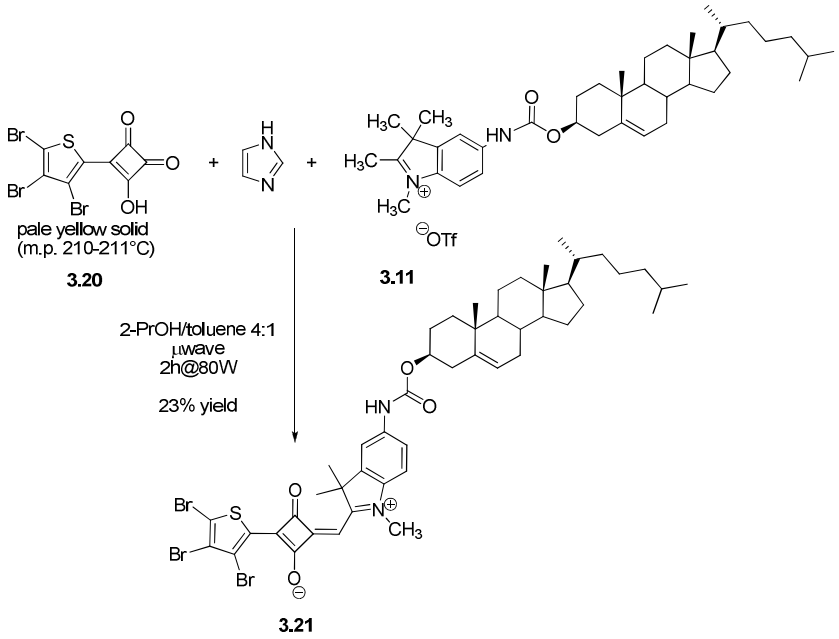

The reaction was carried out in a microwave oven, in nitrogen atmosphere and under azeotropic conditions. A solution of the indolenine derivative (70 mg, 0.093 mmol) and emisquaraine (40 mg, 0.093 mmol) in 15 ml of 2-PrOH/toluene 4:1 was refluxed in open vessel mode at 80 W. A solution of imidazole (6 mg, 0.093 mmol) in 1 ml of 2-PrOH was added dropwise to the hot reaction mixture. After 2 hours the solvent was distilled off under reduced pressure and the residue was purified by chromatography on silica gel. Elution of the column with a mixture CH_2Cl_2:MeOH 9:1 gave the cholesterol-conjugated squaraine derivative (20 mg, 23% yield) as a dark solid. ^{1}H NMR ($CHCl_3$) δ 9.39 (bs, 1H), 7.62 (d, J = 1.5 Hz, 1H), 7.38 (dd, J^1 = 8.86 Hz, J^2 = 1.4 Hz, 1H), 7.06 (d, J = 8.6 Hz, 1H), 6.03 (bs, 1H), 5.44-5.40 (m, 1H), 4.67-4.62 (m, 1H), 3.70 (s, 3H), 2.49-2.35 (m, H), 2.08-1.84 (m, H), 1.77 (s, 6H), 1.65-1.32 (m, H), 1.47 (s, 6H), 1.24-1.05 (m, H), 1.05 (s, 3H), 0.92 (d, J = 6.4 Hz, 1H), 0.88 (d, J = 6.6 Hz, 6H), 0.69 (s, 3H). Anal. Calcd for $C_{48}H_{59}N_2O_4SBr_3 \bullet H_2O$: C, 56.64; H, 6.04; N, 2.75. Found: C, 56.42; H, 5.69; N, 2.70.

1-(2-carboxyethyl)-2,3,3-trimethyl-3*H*-indolium bromide (4.6).

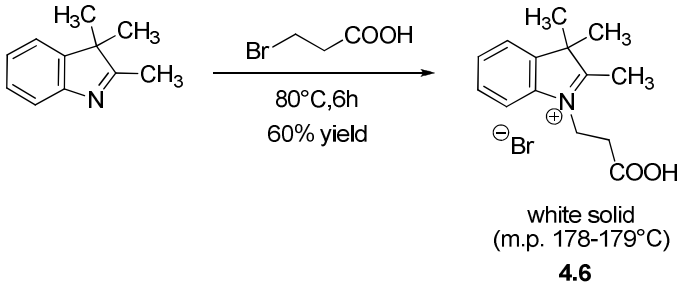

3-bromopropanoic acid (0.9 g, 5.9 mmol) was added to 2,3,3-trimethylindolenine (0.5 g, 3.1 mmol) under nitrogen atmosphere and the resulting mixture was heated at 80°C for 6h. The desired product was obtain by washing the reaction mixture with boiling ethylmethylketone and filtering the resulting white solid (600 mg, 0.93 mmol). 60% yield. m.p. 178-179°C. ^{1}H NMR (DMSO) δ 8.04-7.97 (m, 1H), 7.87-7.81 (m, 1H), 7.66-7.57 (m, 2H), 4.65 (t, *J* = 7.0 Hz, 2H), 2.98 (t, *J* = 6.9 Hz, 2H), 2.86 (s, 3H), 1.53 (s, 6H).

Synthesis of squaraine 3.5.

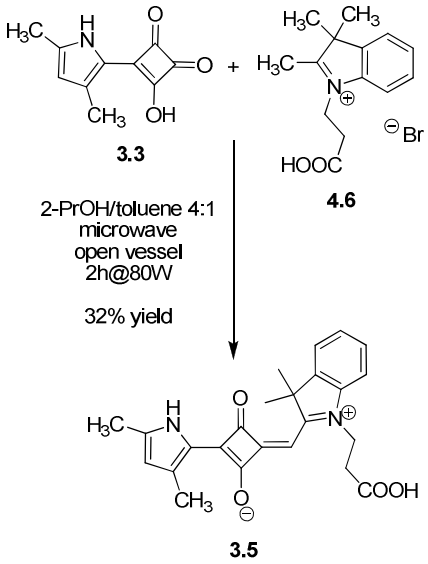

The reaction was carried out in a microwave oven, in nitrogen atmosphere and under azeotropic conditions. A solution of the indolenine derivative (300 mg, 1.0 mmol) and emisquaraine (190 mg, 1.0 mmol) in 15 ml of 2-PrOH/toluene 4:1 was refluxed in open vessel mode at 80 W. After 2 hours the solvent was distilled off under reduced pressure to give a dark residue which was recrystallized from 2-PrOH to afford a purple solid (130 mg, 0.32 mmol). 32% yield. ^{1}H NMR (500 MHz, DMSO, δ): 10.12 (s, 1H), 7.41 (d, *J* = 7.36 Hz, 1H), 7.36 (t, *J* = 6.75 Hz, 1H), 7.25 (t, *J* = 7.29 Hz, 1H), 7.09 (d, *J* = 7.97 Hz, 1H), 6.07 (bs, 1H), 5.98 (s, 1H), 4.59 (t, *J* = 7.05 Hz, 2H), 2.98 (t, *J* = 6.9 Hz, 2H), 2.62 (s, 3H), 2.34 (s, 3H), 1.78 (s, 6H), 1.53 (s, 6H). Anal. Calcd for $C_{24}H_{24}N_2O_4 \bullet 1.5H_2O$: C, 66.81; H, 6.31; N, 6.44. Found: C, 66.56; H, 6.58; N, 6.34.

3-(3-(1,3-dioxoisoindolin-2-yl)propyl)-2-methylbenzo[d]thiazol-3-ium bromide (4.7).

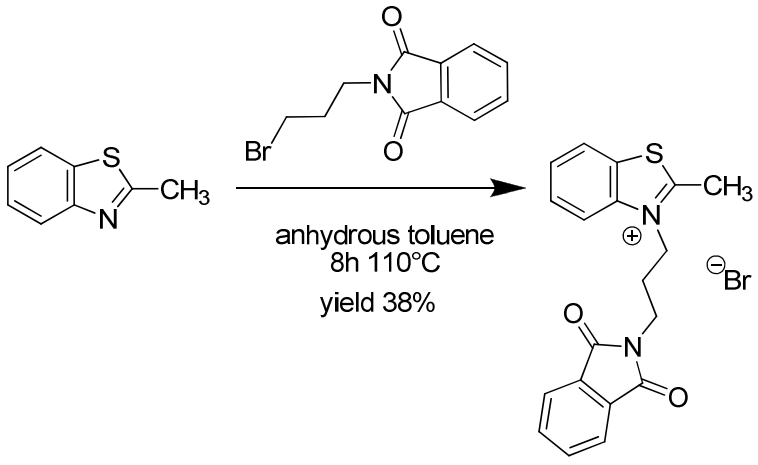

white solid
(m.p. 235-236°C)

4.7

A solution of 2-methylbenzothiazole (2 g, 13.4 mmol) and (3-bromopropyl)-phthalimide (3.6 g, 13.4 mmol) in 5 mL of anhydrous toluene was heated at 110°C for 8 hours. Initially the mixture turned clear and then a white precipitated was formed. The precipitated was filtered and washed with toluene giving the desired product as white solid (2.1 g, 5.1 mmol) 38% yield.

Squaraine 3.6.

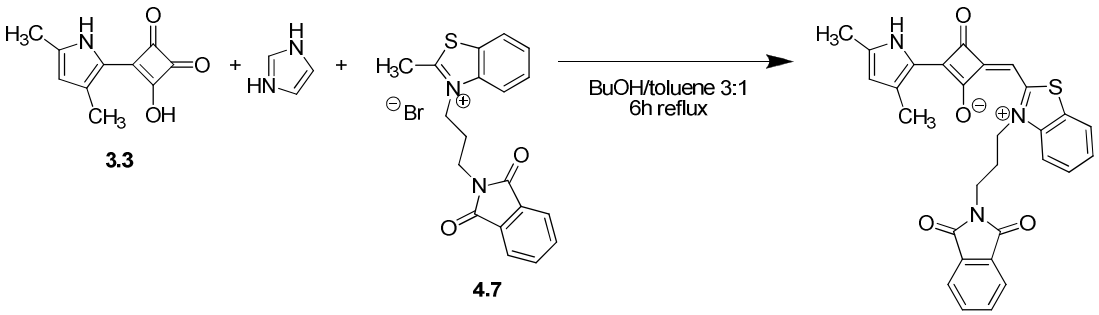

3.3 **4.7** **3.6**

A solution of the benzothiazole derivative (150 mg, 0.36 mmol), emisquaraine (65 mg, 0.36 mmol) and imidazole (25 mg, 0.36 mmol) in 25 mL of BuOH/toluene 3:1 was refluxed for 6 hours under azeotropic conditions. The mixture turned blue in half an hour. After 6 hours the solvent was distilled off under reduced pressure and the residue obtained was washed several times in distilled, acidic water. The black powder obtained was crystallized from 2-PrOH to afford the desired product as purple solid (51 mg, 0.10 mmol) 28% yield. ^{1}H NMR (500 MHz, DMSO, δ): 7.89-7.83 (m, 4H), 7.38 (d, *J* = 7.37 Hz, 1H), 7.33 (t, *J* = 6.64 Hz, 1H), 7.23 (t, *J* = 7.35 Hz, 1H), 7.12 (d, *J* = 7.85 Hz, 1H), 6.02 (bs, 1H), 5.97 (s, 1H), 4.42

(t, *J* = 7.12 Hz, 2H), 3.57 (t, *J* = 6.7 Hz, 2H), 2.62 (s, 3H), 2.34 (s, 3H), 1.78 (s, 6H), 1.53 (s, 6H). Anal. Calcd for $C_{29}H_{23}N_3O_4S\bullet H_2O$: C, 70.29; H, 5.09; N, 8.48. Found: C, 69.89; H, 5.51; N, 8.12.

Squaraine 3.4.

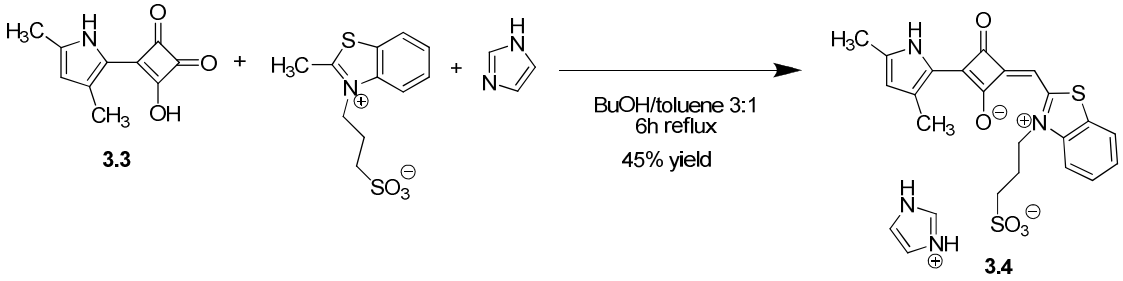

3.3 3.4

A solution of the benzothiazole derivative (340 mg, 1.21 mmol), emisquaraine (230 mg, 1.21 mmol) and imidazole (82 mg, 1.21 mmol) in 20 mL of BuOH/toluene 3:1 was refluxed for 6 hours under azeotropic conditions. The resulting precipitate was filtered giving the desired product as purple solid (280 mg, 0.55 mmol). 45% yield. m.p. > 300°C ^{1}H NMR (500 MHz, DMSO, δ):9.89 (s, 1H), 7.41 (d, *J* = 7.36 Hz, 1H), 7.36 (t, *J* = 6.75 Hz, 1H), 7.25 (t, *J* = 7.29 Hz, 1H), 7.09 (d, *J* = 7.97 Hz, 1H), 6.07 (bs, 1H), 5.98 (s, 1H), 4.59 (t, *J* = 7.05 Hz, 2H), 2.98 (t, *J* = 6.9 Hz, 2H), 2.62 (s, 3H), 2.34 (s, 3H), 1.78 (s, 6H), 1.53 (s, 6H). Anal. Calcd for $C_{24}H_{24}N_2O_4\bullet 1.5H_2O$: C, 66.81; H, 6.31; N, 6.44. Found: C, 66.56; H, 6.58; N, 6.34.

3-ethyl-2-methylbenzo[*d*]thiazol-3-ium iodide (4.8).

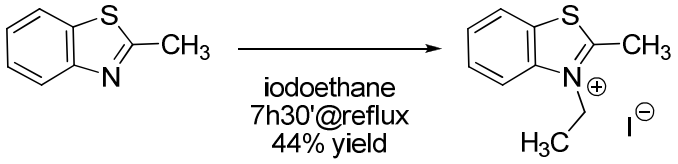

white solid

4.8

The reaction was carried out under nitrogen atmosphere. A solution of 2-methylbenzothiazole (1.0 g, 6.7 mmol) in 4 ml of iodoethane was refluxed for 8h. The reaction mixture was poured into 15 ml of diethyl ether and filtered on an Hirsh funnel to give **2** as white solid (900 mg, 2.9 mmol) 44% yield. ^{1}H NMR (200 MHz, DMSO-d_6, δ): 8.47 (d, *J* = 8.43 ,1H), 8.35 (d, *J* = 8.06,1H), 7.91 (td, J_1 = 7.20, J_2 = 1.16, 1H), 7.81 (t, *J* = 6.95 ,1H), 4.78 (q, *J* = 7.30, 2H), 1.46 (t, *J* = 7.23, 3H).

Cyanine 3.31.[1]

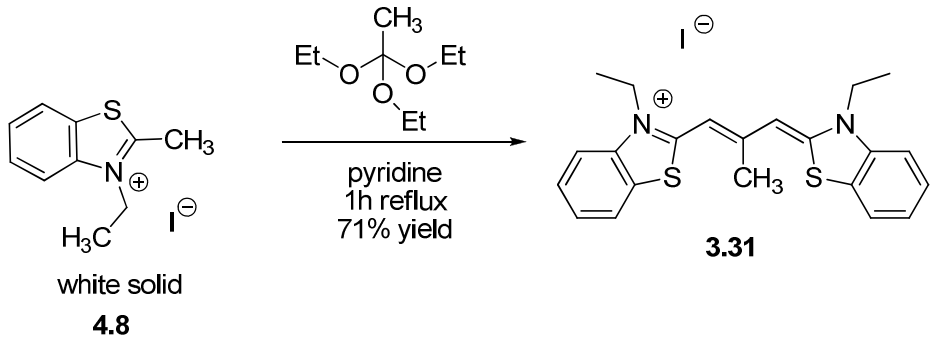

A mixture of **4.8** (400 mg, 0.79 mmol) and triethyl orthoacetate (260 mg, 1.58 mol) in pyridine (10 ml) was refluxed for 2 hours in the dark. Ethyl acetate (100 ml) was added and the precipitate was filtered and dried under vacuum at 100°C for 8 h affording **3.31** as metallic like solid (500 mg, 0.56 mmol) 71% yield. ^{1}H NMR (200 MHz, DMSO-d_6, δ): 9.11 (d, J = 5.70, 2H), 8.17 (t, J = 6.60, 2H), 8.10 (d, J = 7.94, 2H), 7.64 (t, J = 7.36, 2H), 6.63 (s, 2H), 4.64 (q, J = 7.31, 4H), 2.51 (s, 3H), 1.54 (t, J = 7.31, 6H).

Cyanine 4.10.

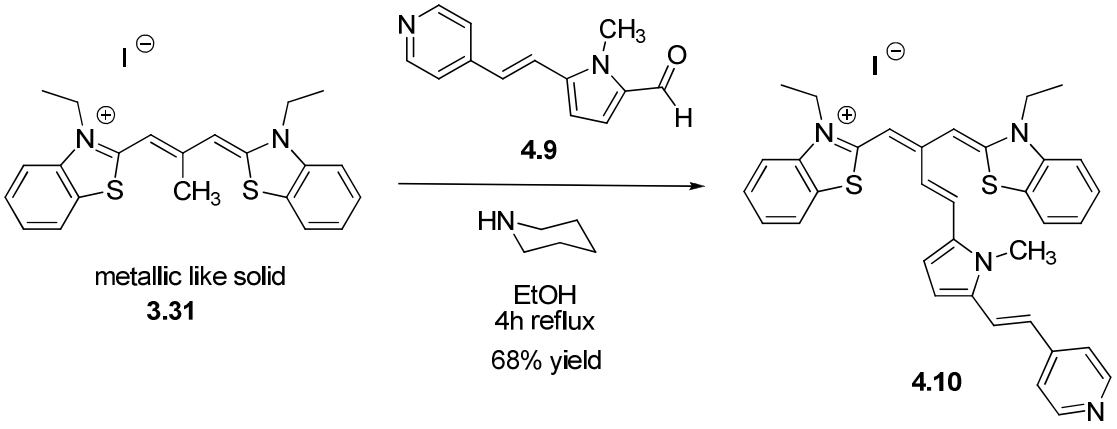

A mixture of *meso* methyl trimethine cyanine **3.31** (100 mg, 0.2 mmol), PEPAL (50 mg, 0.24 mmol, **4.9**) and piperidine (one droplet) in ethanol was refluxed for 4 h in the dark. After cooling at room temperature, the solvent was removed under reduced pressure and the dark residue was washed with 2-propanol (8 ml). The precipitate was collected by filtration to give **4.10** as dark red solid (95 mg, 0.14 mmol) 68% yield. ^{1}H NMR (500 MHz, DMSO-d_6, δ): 8.53 (d, J = 5.94, 2H), 7.99 (d, J = 7.94, 2H), 7.79 (d, J = 8.37, 2H), 7.63 (d, J = 17.14, 1H), 7.51 (t, J = 6.19, 2H), 7.49 (d, J = 15.31, 1H), 7.39 (d, J = 7.66, 2H), 7.16 (d, J = 15.10, 1H), 7.13 (d, J = 16.04, 1H), 7.09 (d, J = 4.16, 1H), 6.96 (d, J = 4.25, 1H), 6.65 (s, 2H), 4.54

(q, *J* = 6.73, 4H), 3.85 (s, 3H), 1.45 (t, *J* = 7.07, 6H).

Cyanine 3.32.

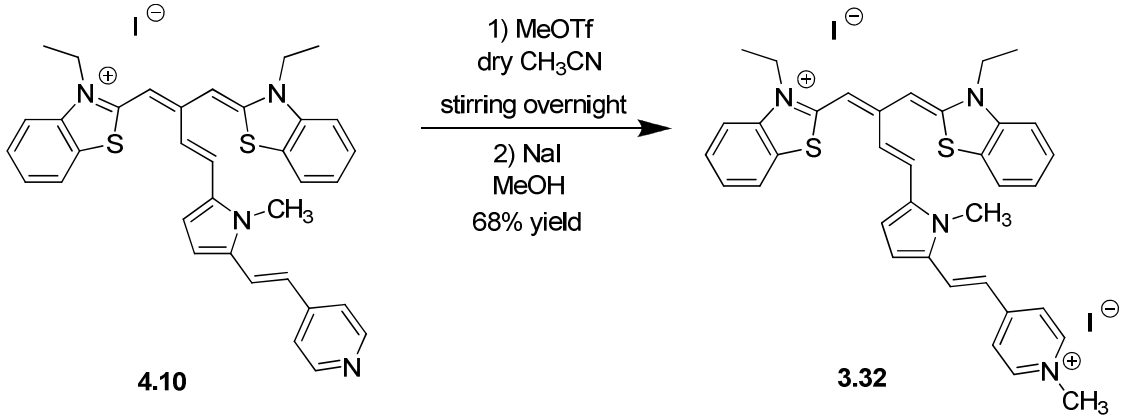

Methyl triflate (22 mg, 0.13 mmol) was added to a solution of **3** (80 mg, 0.11 mmol) in 6 ml of dry acetonitrile. The solution turned purple. The reaction mixture was evaporated after stirring overnight and the dark residue obtained was crystallized from 2-propanol (5 ml). The hygroscopic solid collected by filtration was dissolved in 8 ml of MeOH. A saturated solution of sodium iodide in methanol (4 ml) was then added and the mixture was heated at 60 °C for 2h. The dark precipitate formed after cooling the mixture at room temperature was collected by filtration to give the desired product (0.075 mmol, 63 mg) 68% yield. ^{1}H-NMR (500 MHz, DMSO-d_6) δ 8.74 (2H, d, *J* = 6.77 Hz), 8.17 (2H, d, *J* = 6.72 Hz), 8.03 (1H, d, *J* = 15.82), 7.99 (2H, d, *J* = 7.90 Hz), 7.81 (2H, d, *J* = 8.39), 7.61 (2H, t, *J* = 7.80), 7.49 (1H, d, *J* = 15.69 Hz), 7.41 (2H, t, *J* = 7.62 Hz), 7.35-7.28 (3H, m), 7.17 (2H, s), 6.68 (2H, s), 4.55 (4H, q, *t* = 7.12), 4.21 (3H, s), 3.90 (3H, s), 1.45 (6H, t, J = 7.03). ^{13}C NMR (DMSO-d_6, δ): 161.3, 153.2, 151.1, 145.1, 140.5, 136.9, 135.3, 129.0, 128.9, 126.6, 125.4, 123.6, 123.1, 122.5, 121.6, 121.1, 121.0, 114.1, 113.9, 113.6, 47.1, 31.3, 23.7, 13.5. Anal Calcd. For $C_{36}H_{36}N_4S_2I_2 \bullet 4H_2O$: C, 47.42; H, 3.32; N, 4.30. Found: C, 47.27; H, 4.85; N, 6.13.

(Anthracen-9-ylmethyl)triphenylphosphonium chloride (4.11)

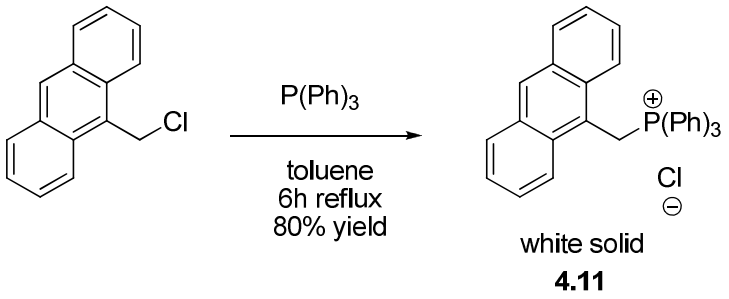

A mixture of 9-chloromethylanthracene (2.0 g, 8.8 mmol) and triphenylposphine (2.6 g, 10 mmol) in dry toluene (15 ml) was refluxed for 6 h in the dark. The white precipitate formed was collected by filtration to give **4.11** (3.4 g, 7.0 mmol) 80% yield.

(*E*)-2-(2-(anthracen-9-yl)vinyl)-1-methyl-1H-pyrrole (4.12).

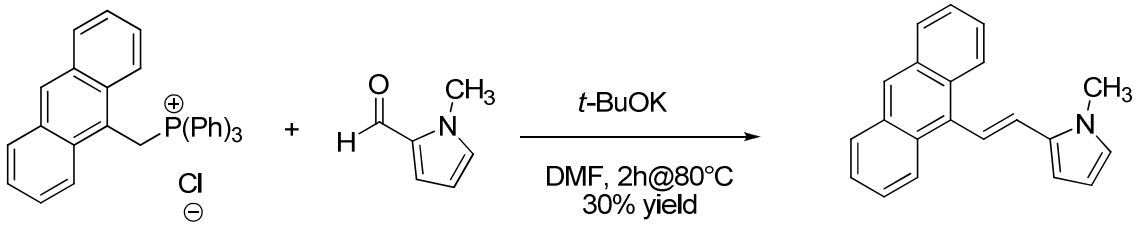

white solid
4.11

pale yellow solid
4.12

The reaction was carried out under nitrogen and in the dark. *t*-BuOK (135 mg, 1.20 mmol) was added dropwise to a suspension of **4.11** (500 mg, 1.02 mmol) and *N*-methylpyrrole-2-carboxyaldehyde (130 mg, 1.20 mmol) in 10 ml of anhydrous DMF cooled at 0 °C. The mixture turned red initially and then yellow. The reaction mixture was poured into water (150 ml) after heating at 80 °C for 2h and stirring overnight. A yellow precipitate was formed. The organic phase was extracted with ethyl acetate (2x80 ml) and the organic phase was washed with water (150 ml) and dried over sodium sulfate. The dark yellow residue obtained after removing the solvent at reduced pressure was purified by column chromatography (eluent: AcOEt:cyclohexane 1:1) on silica gel to afford **4.12** as yellow solid (86 mg, 0.31 mmol) 30% yield.

Note: also the *cis* derivative was isolated but it bleached rapidly after light exposure to give an aldehyde.

(E)-5-(2-(anthracen-9-yl)vinyl)-1-methyl-1H-pyrrole-2-carbaldehyde (4.13)

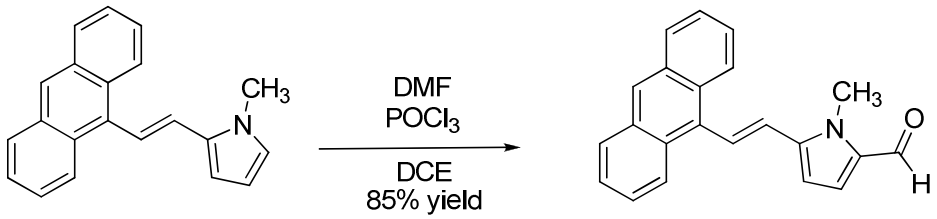

pale yellow solid
4.12

yellow solid
4.13

The reaction was carried out in the dark. $POCl_3$ (90 mg, 0.60 mmol) was slowly added to

DMF (44 mg, 0.60 mmol) cooled at -5 °C. The white Vilsemeier's intermediate formed was diluted in 5 ml of dry DCE. A solution of **4.12** (86 mg, 0.31 mmol) in dry DCE (5 ml) was added in the flask. The reaction mixture turned dark yellow immediately. The solution was poured into an aqueous solution of $NaHCO_3$ (1g of $NaHCO_3$ in 100 ml of water). The yellow precipitate formed was collected by filtration to give **4.13** (80 mg, 0.26 mmol) 85% yield

Synthesis of 3.37.

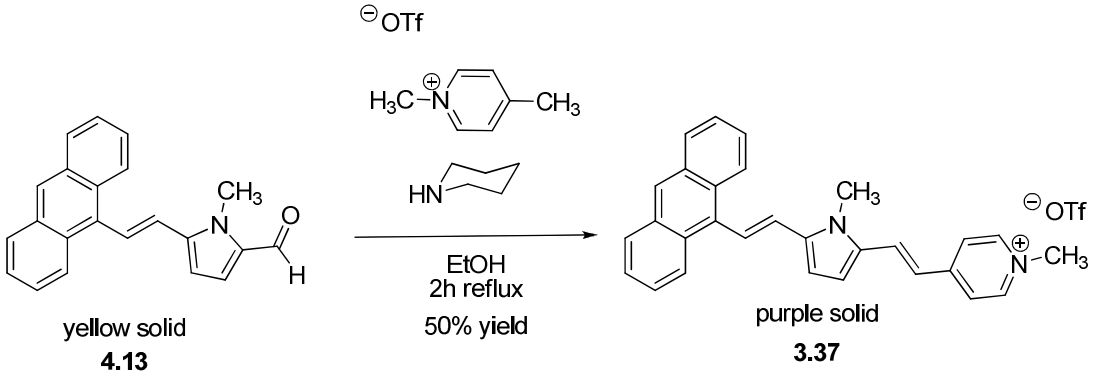

The reaction was carried out in the dark. A solution of **4.13** (80 mg, 0.26 mmol), *N*-methylpicolinium triflate (75 mg, 0.29 mmol) and piperidine (one droplet in ethanol (8 ml) was refluxed for 2 h. The solvent was then removed under reduced pressure and the dark residue was washed with hot 2-propanol (6 ml) to afford the desire product as purple solid (70 mg, 0.26 mmol) 50% yield. ^{1}H-NMR (500 MHz, DMSO-d_6, δ) 8.67 (2H, d, J = 6.79 Hz), 8.58 (1H, s), 8.42-8.38 (2H, m), 8.16-8.11 (4H, m), 8.08 (1H, d, J = 16.42 Hz), 8.03 (1H, d, J = 15.69), 7.58-7.56 (4H, m), 7.19-7.14 (3H, m), 7.08 (1H, d, J = 16.28 Hz), 4.17 (3H, s), 3.84 (3H, s). ^{13}C NMR (DMSO-d_6, δ): 153.5, 144.6, 138.2, 132.9, 132.6, 132.0, 131.6, 129.5, 129.2, 126.9, 126.5, 126.1, 125.9, 125.8, 125.4, 122.4, 118.3, 113.7, 110.5, 46.7, 31.1.

Synthesis of (4-(dimethylamino)benzyl)triphenylphosphonium iodide (4.14).

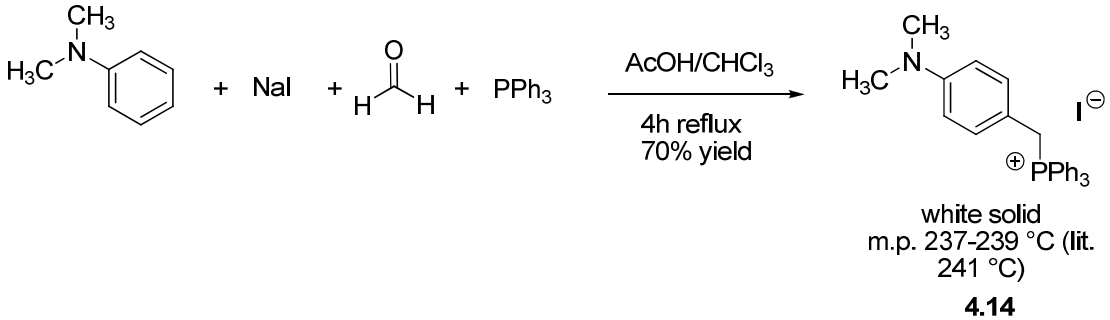

A suspension of *N,N*-dimethylaniline (5 g, 41 mmol), 37% aqueous formaldehyde solution

(4.1 g, 41 mmol), PPh_3 (10.2 g, 41 mmol), and NaI (6.2 g, 41 mmol), in a mixture of acetic acid (8 mL) and chloroform (30mL) was vigorously stirred and heated to reflux for 6 h and subsequently left to stand at rt overnight. The chloroform was evaporated, 100mL of water was added, the insoluble residue collected by filtration, washed several times with water and diethyl ether and dried in vacuum. The reaction yielded 15 g of white solid (29 mmol, 70%). m.p. 237–239 °C (lit. 240 C).

Synthesis of 4.15

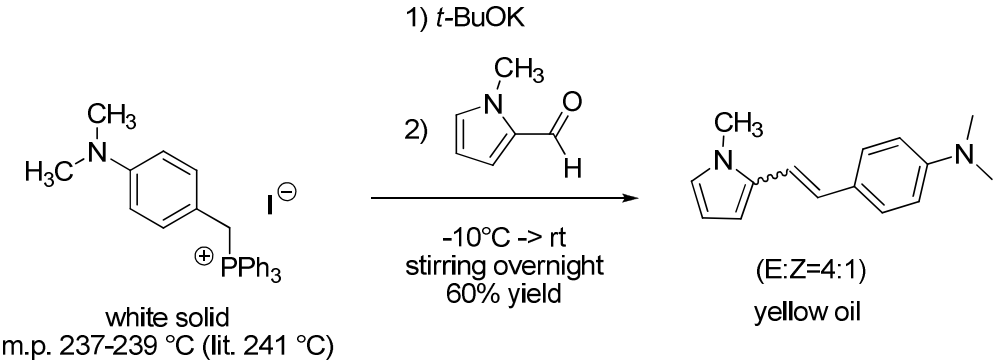

t-BuOK (0.45 g, 4.0 mmol) was added portionwise to a solution of the phosphonium salt **4.14** (2.0 g, 3.8 mmol) in anhydrous DMF (20 ml) cooled at -10°C. The raction mixture turned red. A solution of pyrrole-2-carboxyaldehyde (0.44 g, 4.0 mmol) in 10 ml of anhydrous DMF was added dropwise after 30 minutes. The reaction mixture faded. The mixture was allowed to warm up to room temperature and stirred overnight. The solvent was evaporated, the residue was mixed with water and extracted with ethyl acetate (3x100 ml), combined organic layers were dried over Na_2SO_4, evaporated and the residue was purified by column chromatography (SiO_2, *n*-hexane/AcOEt 5:1) to give a yellow oil (540 mg, 2.4 mmol, E:Z=4:1, overall yield 60%).

Synthesis of (*E*)-5-(4-(dimethylamino)styryl)-1-methyl-1*H*-pyrrole-2-carbaldehyde (4.16)

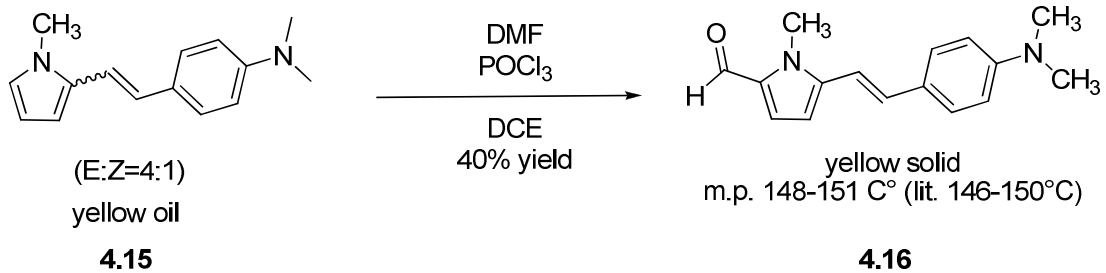

$POCl_3$ (0.2 ml, 0.32 g, 2.0 mmol) was added dropwise to anhydrous DMF (0.15 ml, 0.15 g, 2 mmol) cooled at -10 °C. The white Vilsemeier intermediate formed was dissolved in dry 1,2-dichloroethane (15 ml). A solution of **4.15** (410 mg, 1.8 mmol) in dry DCE (5 ml) was added dropwise with cooling. The mixture was allowed to warm up to room temperature and was stirred overnight. Afterwards the mixture was washed with saturated aqueous solution sodium acetate (2x100 ml), was extracted with $CHCl_3$ (3x70 ml), combined organic layers were washed with brine, dried over sodium sulphate and evaporated. The crude product was purified by column chromatography (SiO_2, *n*-hexane/EtOAc 4:1) to yield a yellow solid (200 mg, 0.8 mmol, 40%, E isomer).

Cyanine 3.33.

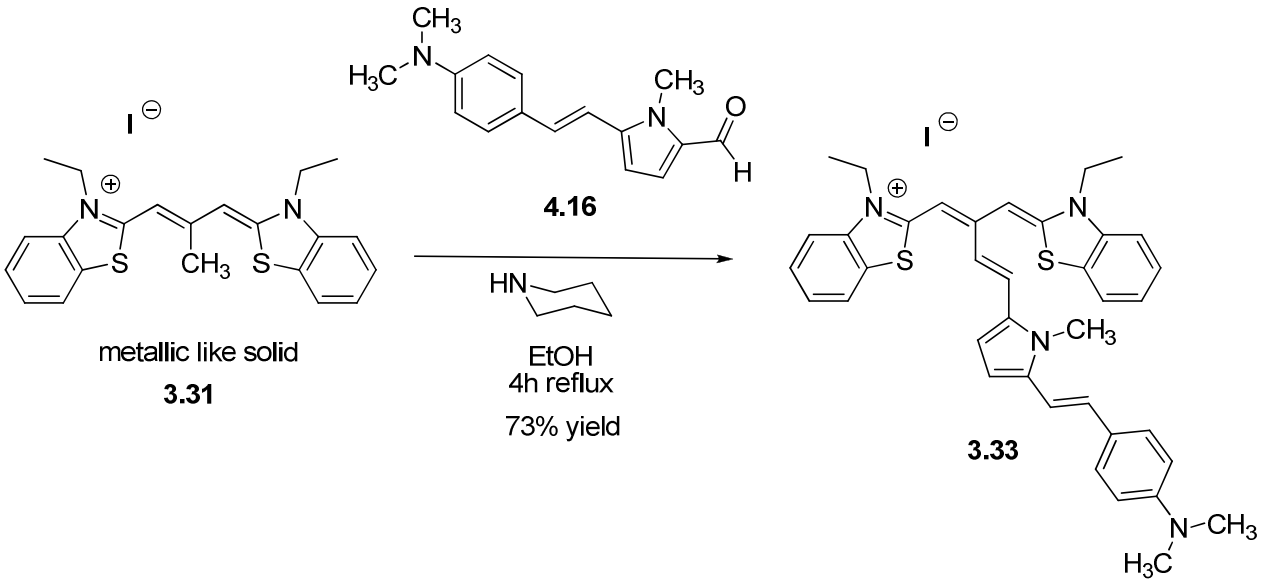

A mixture of *meso* methyl trimethine cyanine **3.31** (100 mg, 0.2 mmol), (*E*)-5-(4-(dimethylamino)styryl)-1-methyl-1*H*-pyrrole-2-carbaldehyde (60 mg, 0.24 mmol) and piperidine (one droplet) in ethanol was refluxed for 4 h in the dark. After cooling at room temperature, the solvent was removed under reduced pressure and the dark residue was washed with 2-propanol (8 ml). The precipitate was collected by filtration to give **3.33** as dark purple solid (110 mg, 0.15 mmol) 73% yield. ^{1}H-NMR (DMSO-d_6) δ 7.96 (2H, d, *J* = 7.98 Hz), 7.76 (2H, d, *J* = 8.38 Hz), 7.58 (2H, t, *J* = 7.35), 7.54-7.48 (3H, m), 7.37 (2H, t, *J* = 7.64), 7.08-7.03 (4H, m), 6.77 (1H, d, *J* = 4.25 Hz), 6.73 (2H, d, *J* = 8.92 Hz), 6.59 (2H, s), 4.52 (4H, q, *J* = 7.14), 3.80 (3H, s), 2.96 (6H, s), 1.45 (6H, t, J = 7.16). Anal Calcd. For $C_{38}H_{39}N_4S_2I$: C, 61.45; H, 5.29; N, 7.54. Found: C, 61.10; H, 5.53; N, 7.40.

5-methoxy-2,3,3-trimethyl-3*H*-indole (3.24).

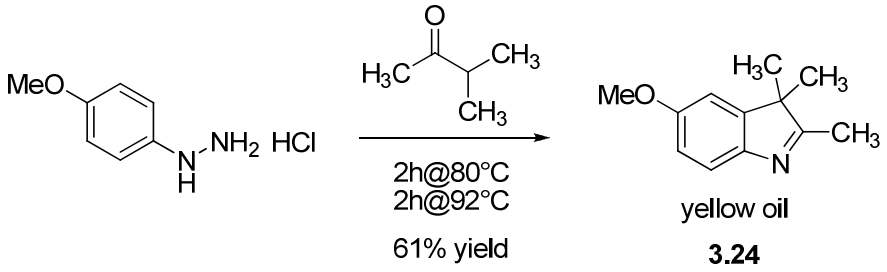

3-methylbutan-2-one (13 mL) was heated at 80°C. Solid 4-methoxyphenylhydrazine hydrochloride (0.727 g, 4.2 mmol) was added portionwise to the reaction mixture in 2 hours time. The reaction mixture turned yellow. The mixture was then refluxed for 2 hours and poured in sodium bicarbonate solution (0.5 g of $NaHCO_3$ in 100 mL of deionized water). The aqueous phase was extracted with 4x20mL of diethyl ether. The residue obtained by removing the solvent at reduced pressure was filtered on silica gel eluted with AcOEt to give a dark yellow oil. **3.24** (480 mg, 2.54 mmol) 61% yield.

2,3,3-trimethyl-3*H*-indol-5-ol (3.25).

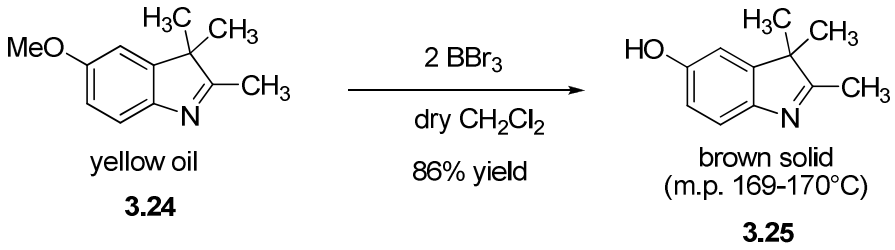

A solution of **3.24** (1.5 g, 7.9 mmol) in 15 mL of dry CH_2Cl_2 was cooled at 0°C. A solution 1M of BBr_3 (18 mL, 18 mmol) was slowly added to the reaction mixture which immediately turned dark purple. The reaction was poured in an aqueous solution of sodium bicarbonate (12 g of $NaHCO_3$ in 300 mL of deionized water) after stirring overnight at room temperature. The dark tarry residue on the glassware was dissolved in 5 mL of MeOH. The organic phase was separated and the aqueous phase was extracted with 3x40mL of diethyl ether. The organic phases were washed with 150 mL of brine. The product was extracted with 3x70 mL of aqueous NaOH 5% wt. The aqueous phase was brought to pH 9 with ammonium chloride solution (8 g of NH_4Cl in 30 mL of deionized water). The product was extracted with 3x30 mL of a solution of CH_2Cl_2/THF 20:1. The product was obtained as brown solid after removing the solvent at reduced pressure. **3.25** (1.2 g, 6.84 mmol) 86% yield.

5-hydroxy-1,2,3,3-tetramethyl-3*H*-indolium iodide (3.26).

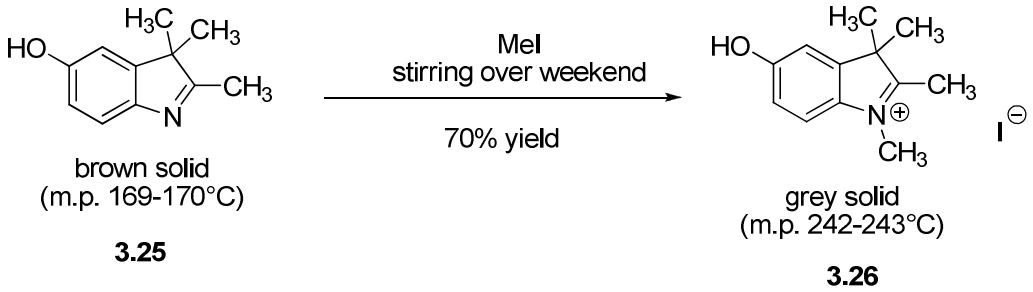

brown solid
(m.p. 169-170°C)

3.25

grey solid
(m.p. 242-243°C)

3.26

The reaction was carried out in anhydrous conditions under nitrogen atmosphere. **3.25** (0.8 g, mmol) was added portionwise with caution to MeI (8 mL) cooled at 0°C. After stirring over weekend at room temperature the solvent was removed at reduced pressure and the residue was washed with boiling methylethylketone (10 mL). A grey solid was obtained which was collected by filtration on a Hirsh funnel. **3.26** (480 mg, 2.54 mmol) 61% yield.

Squaraine 3.27.

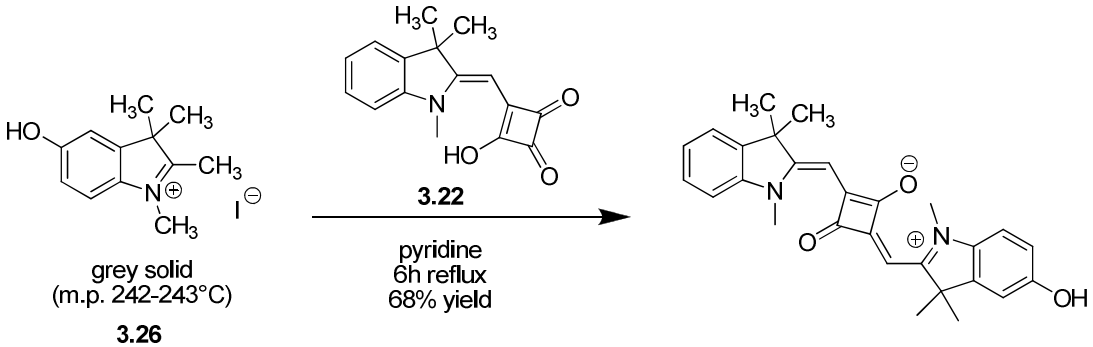

grey solid
(m.p. 242-243°C)

3.26

metallic green solid

3.27

A suspension of the emisquaraine **3.22** (0.27 g, 1.0 mmol) and of the indoleninium salt **3.26** (0.32 g, 1 mmol) was refluxed for 6h in pyridine (10 ml) and subsequently left to stand at room temperature overnight. Water (150 ml) was added and the pH was adjusted to 3 by HCl aqueous solution 37%. The blue precipitate obtained was collected by filtration and washed with Et_2O (3x50 ml) to afford **3.27** (300 mg, 0.68 mmol, 68% yield).

Synthesis of 4,4'-(2,2':5',2''-terthiophene-5,5''-diyl)bis(3-butoxycyclobut-3-ene-1,2-dione) 2.

Under nitrogen atmosphere to a 0°C solution of 2,2':5',2''-terthiophene (0.65 g, 2.60 mmol)

in anhydrous THF (100 ml) was added dropwise a 1.6 M solution (2.6 ml) of butyllithium in n-hexane. Suddenly a green-yellow precipitate was formed. After 30 minutes at room temperature a second solution of 3,4-dibutoxycyclobut-3-ene-1,2-dione (0.81 g, 5.20 mmol) in anhydrous THF (5 ml) was added to the reaction mixture. The resulting red solution was stirred for 10 minutes and then poured into a saturated NH4Cl solution (100 ml). After 30 minutes stirring, the mixture was extracted with AcOEt (2x50 ml). The organic layer was dried over anhydrous Na2SO4, then the solvent was removed under reduced pressure. The residual red oil was taken up with cyclohexane to afford the pure product as a red precipitate that was collected by filtration (0.53 g, 0.96 mmol, 37%). ^{1}H NMR ($CDCl_3$) δ 7.78 (2H, d, *J* = 3.98 Hz), 7.32 (2H, d, *J* = 4.00 Hz), 7.26 (2H, s), 4.94 (4H, m), 1.92 (4H, m), 1.54 (4H, m), 1.03 (6H, m).

Synthesis of 4,4'-(2,2':5',2''-terthiophene-5,5''-diyl)bis(3-hydroxycyclobut-3-ene-1,2-dione) 3.

A solution of compound 2 (0.73 g, 1.32 mmol) in AcOH (30 ml) and water (15 ml) was refluxed for 2h in a mixture of 20 ml of AcOH and 1 ml of 10 % HCl. After this period the reaction mixture was cooled at ambient temperature. The red precipitate thus obtained was filtered off and washed directly on the filter with Et_2O to give the desired product as brown solid (0.53 g, 1.20 mmol, 91%). 1H NMR (DMSO-d6) δ 7.47 (2H, d, J = 3.77 Hz), 7.41 (2H, d, J = 4.03 Hz), 7.38 (2H, s).

Synthesis of squaraine 3.30.

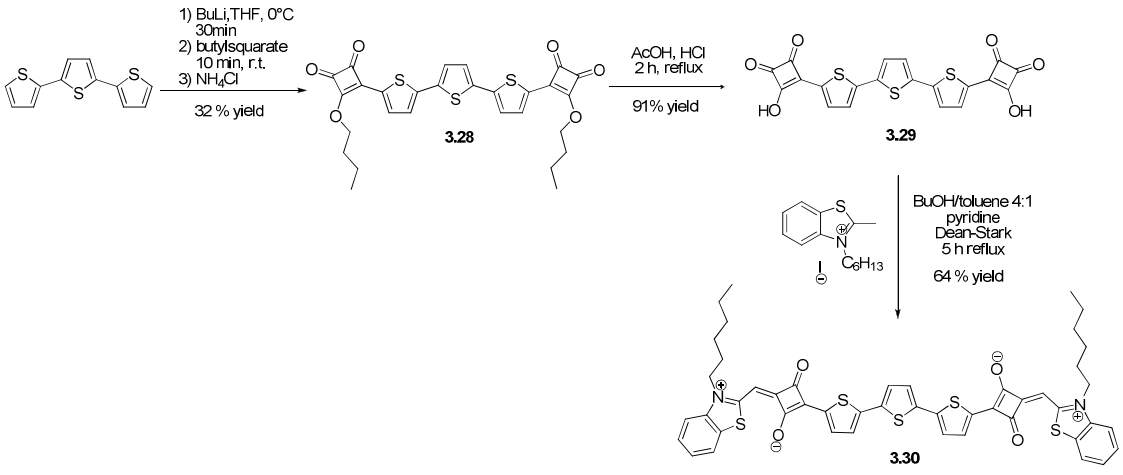

A suspension of N-hexyl-2-methylbenzothiazolium iodide (0.195 g, 0.54 mmol) and the bis-emisquaraine 3 (0.119 g, 0.27 mmol) was suspended in a solution of 25 ml of BuOH, 5

ml of toluene and 0.1 ml of pyridine. The red suspension was refuxed for 5 h under a Dean-Stark trap to azeotropycally remove the water formed. The reaction mixture was then cooled at 0° and a golden brown precipitate was formed. The precipitate was isolated by suction filtration and washed directly on the filter with 20 ml of MeOH to give the pure title compound and a dark powder. (0.160 g, 0.17 mmol, 64 %). Mp. > 250 °C (dec). ^{1}H NMR (DMSO-d_6) δ 8.31 (2H, d, *J* = 7.91 Hz), 8.08 (2H, d, *J* = 8.47 Hz), 7.74 (2H, t, *J* = 7.87 Hz), 7.63 (2H, t, *J* = 7.64 Hz), 7.49 (2H, d, *J* = 3.84 Hz), 7.47 (2H, d, *J* = 3.75 Hz), 7.44 (2H, s), 6.64 (2H, s), 4.72 (4H, t, *J* = 6.26 Hz), 1.79 (4H, quint, *J* = 7.51 Hz), 1.47-1.36 (4H, m), 1.36-1.20 (8H, m), 0.90-0.80 (6H, m). Anal Calcd. For C48H42N2O4S5*7/2 H2O: C, 61.71; H, 5.29; N, 3.00. Found: C, 61.78; H, 4.69; N, 2.83.

4,4'-(1*E*,1'*E*)-2,2'-(1-methyl-1*H*-pyrrole-2,5-diyl)bis(ethene-2,1-diyl)bis(1-benzylpyridinium) triflate (3.34b).

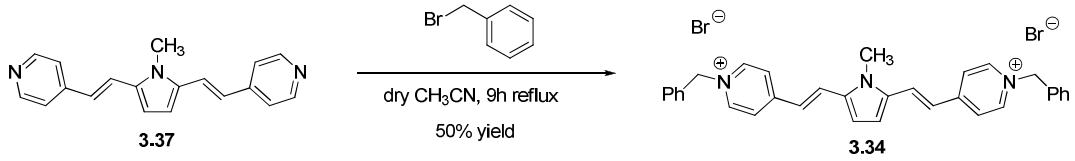

A solution of benzyl bromide (0.500 g, 7.15 mmol) and compound **3.37** (0.223 g, 0.78 mmol) in 35 mL of acetonitrile was refluxed for 5 hours. The resulting precipitate was collected by filtration and crystallized from 2-propanol (0.320 g, 0.51 mmol, 65%): 314-315°C; ^{1}H-NMR (DMSO-d_6) δ 8.97 (d, 4H, J = 6.67), 8.23 (d, 4H, J = 6.44), 8.04 (d, 2H, J = 15.86), 7.47 (b, 10H), 7.33 (d, 2H, J = 15.85), 7.13 (s, 2H), 5.71 (s, 4H), 3.96 (s, 3H). The precipitate (0.314 g, 0.50 mmol) and silver *p*-toluenesulfonate (0.280 g, 1.0 mmol) were dissolved in 30 mL of acetonitrile and refluxed for 7 hours. The hot solution was then filtered. The residue obtained after removal of the solvent was crystallized by 2-propanol affording compound **3.34b** as a purple solid (0.233 g, 0.29 mmol, 50%): m.p. 304-306°C; ^{1}H-NMR (DMSO-d_6, δ): 8.96 (d, *J* = 6.07 Hz, 4H), 8.22 (d, *J* = 6.05 Hz, 4H), 8.03 (d, *J* = 15.8 Hz, 2H), 7.53-7.47(m, 14H), 7.32 (d, *J* = 15.7 Hz, 2H), 7.13 (s, 2H), 7.11 (d, *J* = 8.14 Hz, 2H), 5.70 (s, 4H), 3.96 (s, 3H), 2.28 (s, 6H); ^{13}C NMR (DMSO-d_6, δ): 153.7, 146.3, 144.2, 138.0, 136.3, 135.3, 129.7, 129.6, 129.1, 128.9, 128.5, 125.9, 123.8, 121.8, 114.3, 62.4, 31.4, 21.2. Anal. Calcd for $C_{47}H_{45}N_3O_6S_2$: C, 68.01; H, 5.71; N, 5.06. Found: C, 67.85; H, 5.68; N, 4.99.

4,4'-(1*E*,1'*E*)-2,2'-(1-methyl-1*H*-pyrrole-2,5-diyl)bis(ethene-2,1-diyl)bis(1-(2-methoxyethyl)pyridinium) triflate (3.34c).

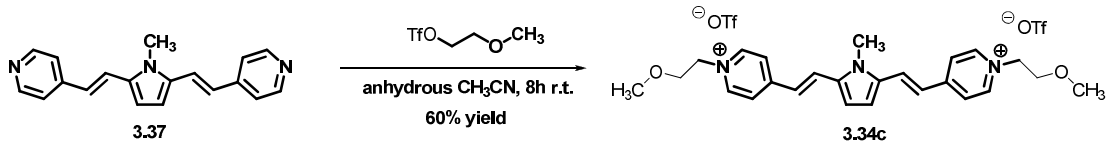

3.37 3.34c

A solution of trifluoromethansulfonic anhydride (2.045 g, 7.25 mmol) in 3 mL of dry dichloromethane was added to a solution of 2-metoxyethanol (0.443 g, 5.82 mmol) in 15 mL of dry dichloromethane cooled at 0°C. After 4 hours the organic phase is washed with 5x40 mL of distilled water and dried over sodium sulfate. Removing of the solvent at reduced pressure give an incolor oil (0.150 g, 0.72 mmol, 15%); ^{1}H-NMR ($CDCl_3$) δ 4.62 (t, 2H, J = 4.24), 3.70 (t, 2H, J = 4.46), 3.41 (s, 3H). 2-metoxyethan-1-triflate was diluted with 5 mL of anhydrous acetonitrile and added to a solution of compound 7 (50 mg, 0.17 mmol). After stirring overnight the solvent was removed under reduced pressure and the residue obtained was crystallized by 2-propanol affording a purple solid (73 mg, 10.4 mmol, 60%): m.p. 298-300°C; ^{1}H-NMR (DMSO-d_6, δ): 8.82 (d, *J* = 6.87 Hz, 4H), 8.20 (d, *J* = 6.93 Hz, 4H), 8.03 (d, *J* = 15.8 Hz, 2H), 7.32 (d, *J* = 15.8 Hz, 2H), 7.14 (s, 2H), 4.65 (t, *J* =4.79 Hz, 4H), 3.97 (s, 3H), 3.81 (t, *J* = 5.15 Hz, 4H), 3,28 (s, 6H); ^{13}C NMR (DMSO-d_6, δ): 153.6, 144.6, 136.1, 128.9, 123.2, 121.8, 114.1, 70.6, 59.3, 58.7, 31.7. Anal. Calcd for $C_{27}H_{31}N_3O_8S_2$: C, 46.09; H, 4.60; N, 5.84. Found: C, 45.87; H, 4.44; N, 5.97.

4,4'-(1*E*,1'*E*)-2,2'-(9-methyl-9*H*-carbazole-3,6-diyl)bis(ethene-2,1-diyl)bis(1-methylpyridinium) triflate (3.35).

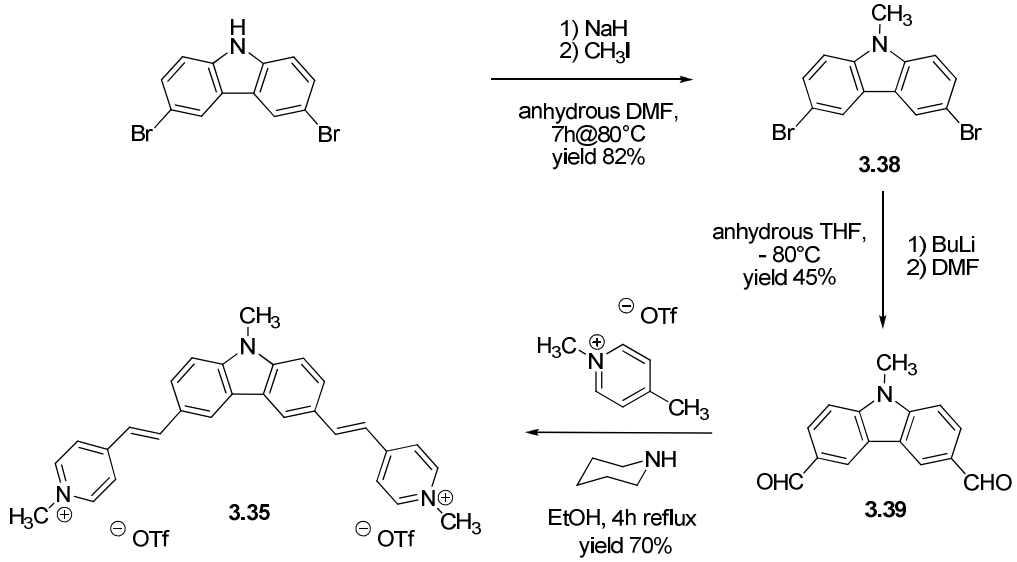

The reaction was carried out under nitrogen. A suspension of NaH 60% dispersion in mineral oil (0.15 g, 3.7 mmol) was washed with 10 ml of dry 1-hexane and then diluted with 10 ml of anhydrous DMF. A solution of 3,6-dibromo-9*H*-carbazole (**5**; 1.0 g, 3.1 mmol) in 10 ml of anhydrous DMF was added to the reaction mixture. Iodomethane (0.23 ml, 3.7 mmol) was added dropwise after 30 minutes and the reaction mixture was heated at 80 °C for 7 h. The intermediate **3.38** was collected by filtration after cooling the solution to room temperature (0.85 g, 2.51 mmol, 82%): m.p. 151-153 °C. The carbazole derivative **3.38** (0.50 g, 1.47 mmol) was dissolved in 20 ml of anhydrous THF and the solution was cooled at -80 °C. A solution of butyllithium 1.6 M (1.8 ml, 2.9 mmol) in hexanes was added dropwise and the reaction mixture was stirred for 30 minutes. Anhydrous DMF (0.24 ml, 3.1 mmol) was added and the reaction mixture was allowed to warm up to room temperature. The mixture was poured into an aqueous solution of 2 g of ammonium acetate in 200 ml of water and extracted with 3x30 ml of CH_2Cl_2. The organic phase was washed with 2x100 ml of water and was dried over sodium sulphate. The residue obtained by evaporating the solvent at reduced pressure was crystallized by CH_2Cl_2/*n*-hexane 1:1 to afford **3.39** (0.16 g, 0.68 mmol, 45%): m.p. 211-213 °C. A solution of 9-methyl-9*H*-carbazole-3,6-dicarbaldehyde (**3.39**) (0.15 g, 0.63 mmol), 1,4-dimethylpiridinium triflate (0.32 g, 1.2 mmol) and picoline (0.11 g, 1.2 mmol) in 15 ml of ethanol was refluxed for 4 hours. The resulting precipitate was collected by filtration and washed with hot 2-butanone giving the desired product as a yellow solid. (0.31 g, 0.44 mmol, 70%): m.p. 345-346 °C; ^{1}H-NMR (DMSO-d_6, δ): 8.83 (d, J = 6.74 Hz, 4H), 8.60 (s, 2H), 8.23 (d, J = 15.5 Hz, 2H), 8.21 (d, J = 6.43 Hz, 4H), 7.99 (dd, J_1 = 8.71 Hz, J_2 = 1.38 Hz, 2H), 7.56 (d, J = 16.21 Hz, 4H), 4.26 (s, 6H), 3.99 (s, 4H); ^{13}C NMR (DMSO-d_6, δ): 153.5, 145.5, 143.1, 142.6, 127.7, 127.3, 123.5, 123.1, 121.8, 121.2, 111.3, 47.3, 30.2. Anal. Calcd for $C_{31}H_{27}N_3O_6F_6S_2$*1/2 H_2O: C, 51.38; H, 3.89; N, 5.80. Found: C, 51.18; H, 4.15; N, 5.65.

4,4'-(1*E*,1'*E*)-2,2'-(9,9-bis(2-ethylhexyl)-9*H*-fluorene-2,7-diyl)bis(ethene-2,1-diyl)bis(1-methylpyridinium) trifluoromethanesulfonate (3.36).

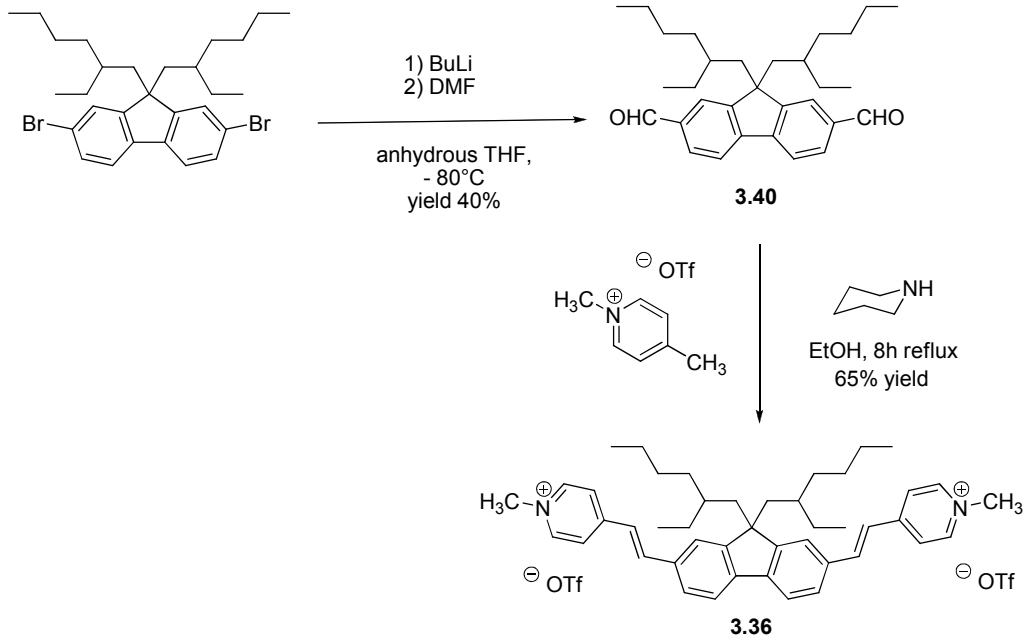

The commercial carbazole derivative (1.7 g, 3.1 mmol) was dissolved in 30 ml of anhydrous THF and the solution was cooled at -80 °C. A solution of butyllithium 1.6 M (12 ml, 7.4 mmol) in hexanes was added dropwise and the reaction mixture was stirred for 30 minutes. Anhydrous DMF (0.60 ml, 8.0 mmol) was added and the reaction mixture was allowed to warm up to room temperature. The mixture was poured into an aqueous solution of 2.5 g of ammonium acetate in 250 ml of water and extracted with 4x40 ml of CH_2Cl_2. The organic phase was washed with 2x200 ml of water and was dried over sodium sulphate. The residue obtained by evaporating the solvent at reduced pressure was purified by column chromatography over silica gel (eluent AcOEt:MeOH 20:1) to afford **3.40** (0.55 g, 1.23 mmol, 45%): m.p. 211-213 °C. A solution of **3.40** (0.50 g, 1.1 mmol), picoline (0.20 g, 2.7 mmol) and 1,4-dimethylpiridinium triflate (0.70 g, 2.7 mmol) in 10 ml of ethanol was refluxed for 8 hours. The solvent was removed under reduced pressure giving an oil which was washed with ETP. The resulting solid was washed with hot 2-butanone giving the desired product as a yellow solid. (0.67 g, 0.73 mmol, 65%): m.p. 250-252 °C. Anal. Calcd for $C_{47}H_{58}N_2O_6F_6S_2$: C, 61.02; H, 6.32; N, 3.03. Found: C, 60.79; H, 6.03; N, 3.02.

1-(3-bromopropyl)-4-methylpyridinium bromide (4.17).

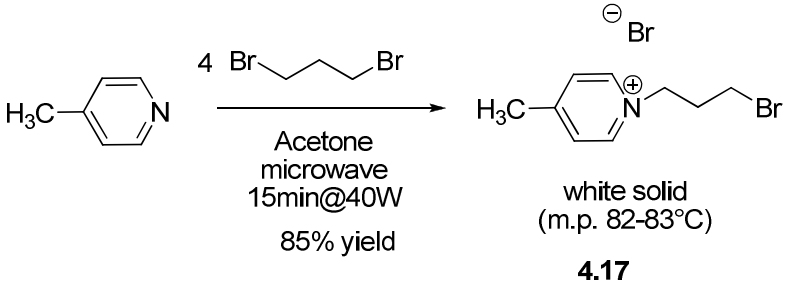

A solution of 4-picoline (0.5 g, 5.4 mmol) and 1,3-dibromopropane (4.3 g, 21 mmol) in 2 mL of acetone was brought to 120°C and 4.5 bar for 15 min by microwave-assisted heating (40W, cooling on). 4 mL of diethyl ether were added to the reaction mixture after cooling. The white precipitate formed was collected by filtration and washed with 2 mL of diethyl ether. Quantitative yield. (m.p. 82-83°C)

Synthesis of 4.18.

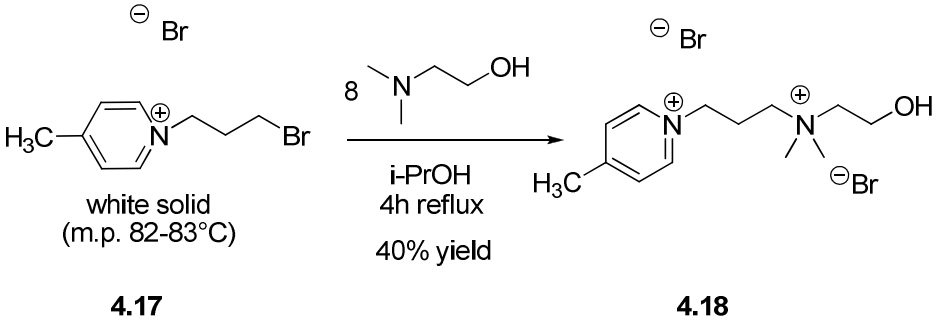

A solution of **4.17** (0.3 g, 1.0 mmol) and dimethylaminoethanol (0.71 g, 8.0 mmol) in 15 mL of 2-propanol was refluxed for 4 hours. 20 mL of diethyl ether were added to this solution risulting in the formation of a white precipitate. The white hygroscopic solid was collected by filtration, washed with 5 mL of diethyl ether and characterized by ^{1}H-NMR: **4.18** (150 mg, 0.4 mmol) 40% yield.

Synthesis of 4.19.

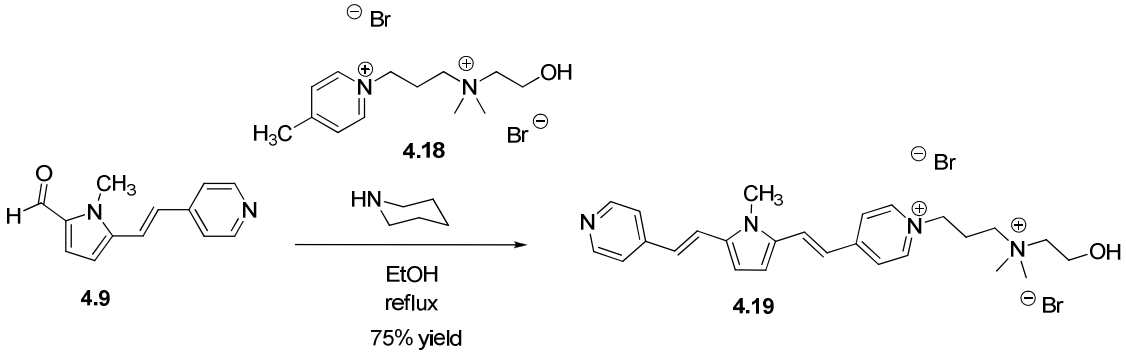

A mixture of **4.9** (53 mg, 0.25 mmol), the picolinium salt **4.18** (80 mg, 0.2 mmol) and one drop of piperidine was refluxed in ethanol (6 mL) for 3 hours. The reaction mixture progressively turned reddish. The ethanolic solution was cooled to room temperature. A reddish precipitate was formed which was collected by filtration on a Hirsch funnel and washed with 2-propanol (6 ml) (90 mg, 0.15 mmol) 75% yield.

Synthesis of 3.38.

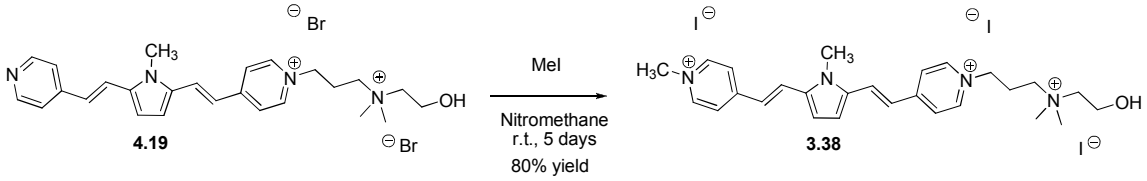

Iodomethane (0.2 ml, 3.2 mmol) was added to a solution of **4.19** (90 mg, 0.15 mmol) in 6 mL of freshly distilled nitromethane cooled to 0°C. A purple precipitate was gradually formed. The suspension was warmed up to room temperature and stirred in the dark for five days. The precipitate was then collected by filtration and washed with 5 mL of boiling 2-propanol. (100 mg, 0.12 mmol) 80% yield. ^{1}H NMR (500 MHz, DMSO) δ 8.86 (d, *J* = 6.8 Hz, 2H), 8.78 (d, *J* = 6.8 Hz, 2H), 8.26 (d, *J* = 6.8 Hz, 2H), 8.20 (d, *J* = 6.9 Hz, 2H), 8.05 (dd, *J* = 18.9, 15.9 Hz, 2H), 7.35 (dd, *J* = 15.7, 9.6 Hz, 2H), 7.15 (d, *J* = 3.5 Hz, 2H), 5.27 (t, *J* = 4.8 Hz, 1H), 4.52 (t, *J* = 7.1 Hz, 2H), 4.22 (s, 3H), 3.99 (s, 3H), 3.84 (s, 2H), 3.48 – 3.40 (m, 4H), 3.11 (s, 6H). ^{13}C NMR (500 MHz, DMSO) δ 153.70 (s, 1H), 152.86 (s, 1H), 145.07 (s, 2H), 144.30 (s, 2H), 136.32 (s, 1H), 136.01 (s, 1H), 129.08 (s, 1H), 128.50 (s, 1H), 123.47 (s, 1H), 123.21 (s, 1H), 121.95 (d, *J* = 6.8 Hz, 1H), 121.56 (d, *J* = 7.4 Hz, 1H), 114.23 (s, 1H), 114.06 (s, 1H), 65.36 (s, 1H), 60.90 (s, 1H), 56.73 (s, 1H), 55.40 (s, 2H), 51.69 (s, 1H), 47.09 (s, 1H), 31.55 (s, 1H), 24.34 (s, 1H). Anal. Calcd for $C_{27}H_{37}I_3N_4O$: C, 39.82; H, 4.58; N, 6.88. Found: C, 39.53; H, 5.10; N, 6.64.

4.2 Photophysical experimental setup

All steady-state UV/VIS absorption spectra were recorded using either a Hewlett-Packard/Agilent diode array HP8453 spectrometer or a Shimadzu UV3600 UV-VIS NIR spectrophotometer. All the steady state emission spectra were recorded using a Horiba Jobin Yvon fluorimeter (Fluoromax P). For fluorescence lifetime experiments, the output at 790 nm of a femtosecond Ti:sapphire laser (Spectra Physics, Tsunami 3941) was amplified by a

regenerative amplifier (Spectra Physics Spitfire pumped by a Spectra Physics Evolution Nd:YLF laser) and doubled to 395 nm by a BBO crystal prior to sample irradiation. The luminescence from the sample, collected at 90°, was passed through a suitable interference filter positioned in front of a fast photodiode (Newport model 818-BB-21, 300 ps rise time) connected to a digital oscilloscope (Tektronix TDS754A). The collection efficiency was enhanced by a parabolic mirror placed on the backside of the cuvette. Singlet oxygen quantum yields, (Φ_Δ), were determined using instruments and an approach that has been previously described.[2, 3] Briefly, air-equilibrated solutions containing the sensitizers were irradiated using a femtosecond laser, the output wavelength of which is tuned to match the low-energetic absorption band. 2,3,7,8,12,13,17,18-octaethyl-porphyrin in toluene (Φ_Δ = 0.75),[4] 5,10,15,20-tetraphenyl-21*H*,23*H*-porphine in toluene (Φ_Δ = 0.69)[5, 6] and zinc-phthalocyanine in pyridine (Φ_Δ = 0.5),[5] were used as standards. The singlet oxygen phosphorescence emitted from the sample was detected by a liquid nitrogen cooled photomultiplier tube (Hamamatsu model R5509-42) coupled to a single-photon counting setup. For the determination of singlet oxygen quenching rates (k_q), solutions containing the sensitizer and the quenchers were irradiated using the third harmonic at 355 nm of a ns Nd:YAG laser (Quanta-Ray GCR 230). The singlet oxygen phosphorescence emitted was detected by a liquid nitrogen cooled germanium detector (North Coast EO-817P) positioned at a 90° angle to the laser beam. To enhance the signal collection efficiency, a parabolic mirror was positioned at the backside of the cuvette. In order to collect the desired signal a Si-filter (CVI optics) and a 1270 nm bandpass filter (50 nm FWHM) were inserted after the detector window. The kinetics of the sensitizer triplet state was studied in a pump-probe experiment using instruments and approaches that have likewise been previously described.[7] Briefly, a $5x10^{-5}$ M solution of the sensitizer was irradiated at 355 nm and, following intersystem crossing from the initially produced excited singlet state, an excited triplet state population was created. The absorption of the triplet state was then probed by a steady-state 200W xenon lamp. The light from the xenon lamp passed through a water filter to remove the IR-components. The light from the xenon lamp transmitted through the sample was focused down and dispersed by a grating onto a PMT (Hamamatsu R928). A filter was inserted in front of the entrance to the detector with the purpose of removing any scattered laser light. The resulting time-resolved signal was digitized and monitored with an oscilloscope (Tektronix TDS5032B). Because the PMT is combined with a monochromator, we could selectively observe the amount of light absorbed at 530 nm, ΔA_{530}, where the triplet

absorbance is strong. Toluene and acetonitrile (Sigma-Aldrich, spectroscopic grade) were used as received. Samples for measurements performed in the absence of oxygen were prepared by gently bubbling nitrogen through the solution for approximately 30 min.

4.2.1 Absorption and fluorescence spectra of the squaraines.

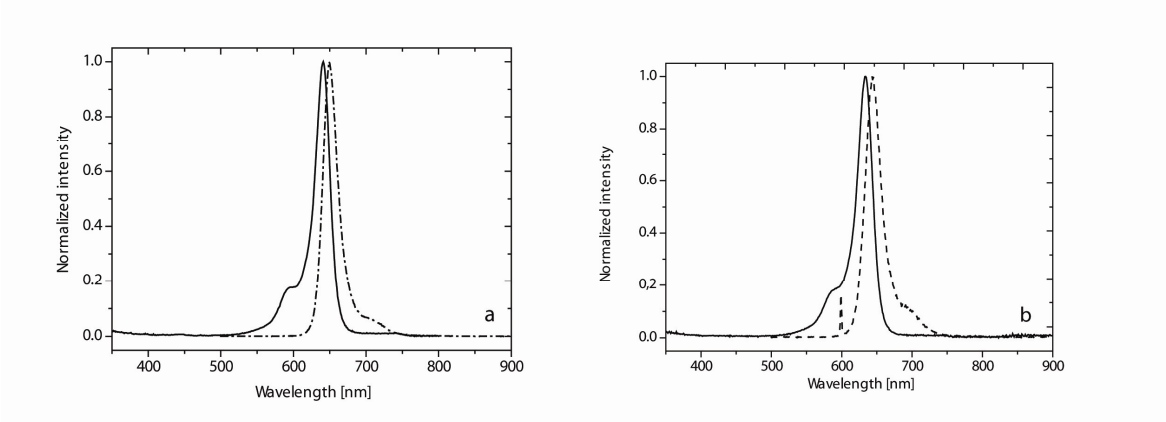

Figure 4.1: a) One-photon absorption (solid line) and fluorescence (dashed line) spectra of 3.1a in toluene and b) one-photon absorption (solid line) and fluorescence (dashed line) spectra of 3.1a in acetonitrile. In the latter spectrum, residual scattered excitation light is seen as a sharp peak.

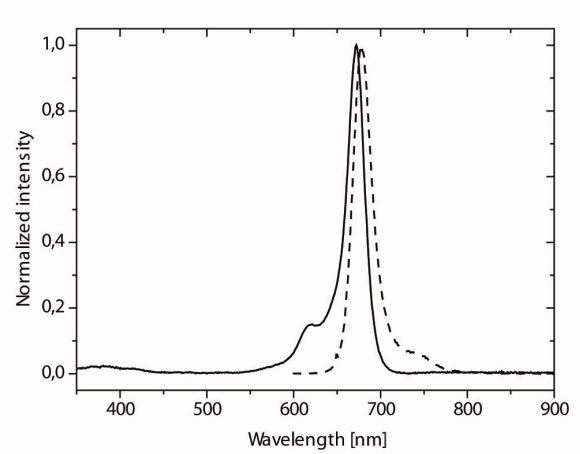

Figure 4.2: a) One-photon absorption (solid line) and fluorescence (dashed line) spectra of 3.1b in toluene.

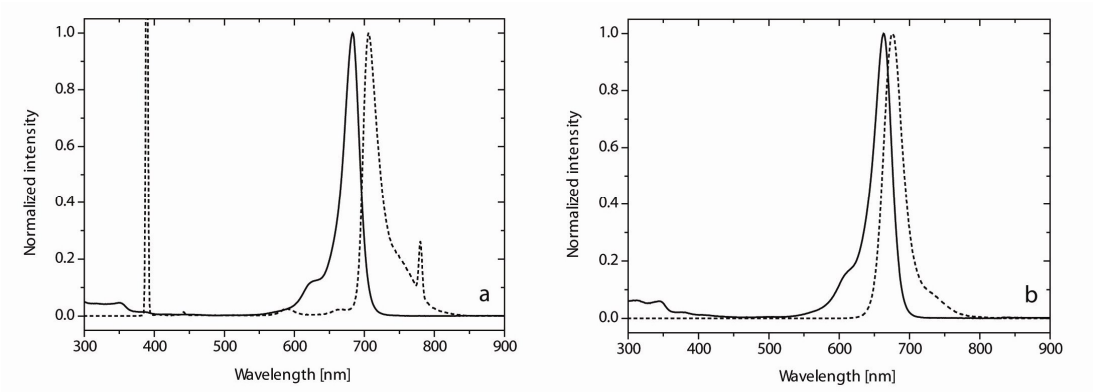

Figure 4.3: a) One-photon absorption (solid line) and fluorescence (dashed line) spectra of 3.1c in toluene. Residual scattered excitation light, and its first-order component from the grating, is seen as sharp peaks. b) One-photon absorption (solid line) and fluorescence (dashed line) spectra of 3.1c in acetonitrile.

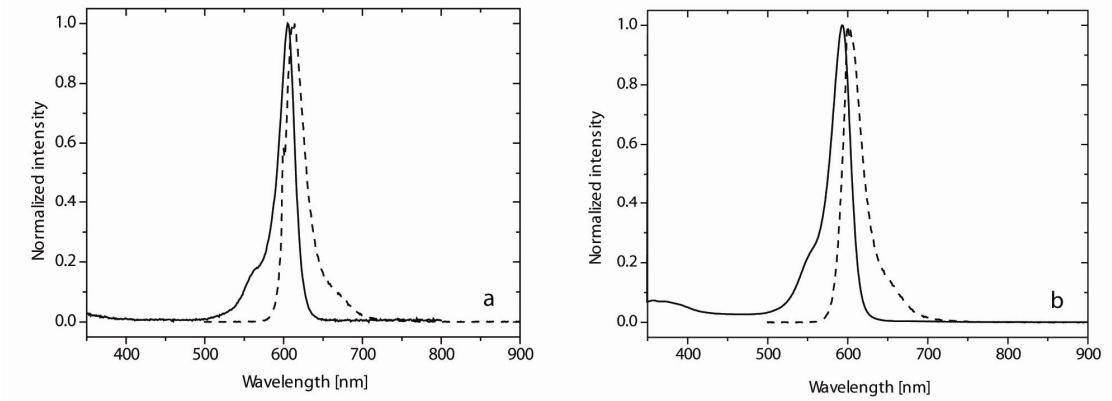

Figure 4.4: a) One-photon absorption (solid line) and fluorescence (dashed line) spectra of 3.1d in toluene and b) one-photon absorption (solid line) and fluorescence (dashed line) spectra of 3.1d in acetonitrile.

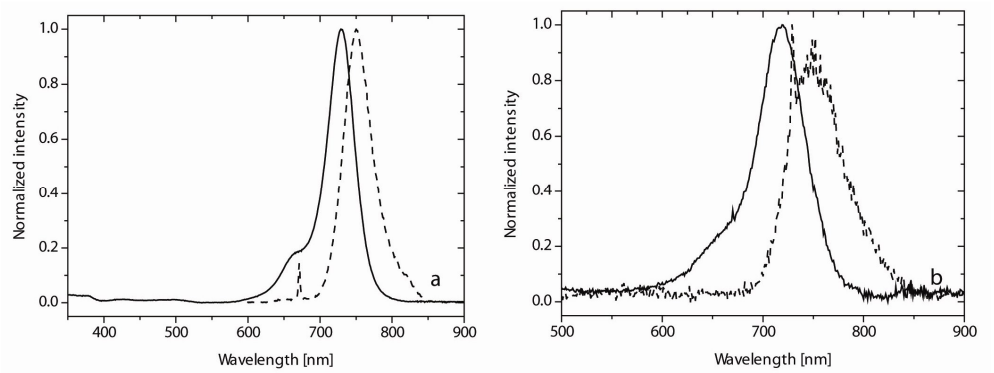

Figure 4.5: a) One-photon absorption (solid line) and fluorescence (dashed line) spectra of 3.2a in toluene and b) one-photon absorption (solid line) and fluorescence (dashed line) spectra of 3.2a in acetonitrile. Residual scattered excitation light is seen as sharp peaks in the emission spectra.

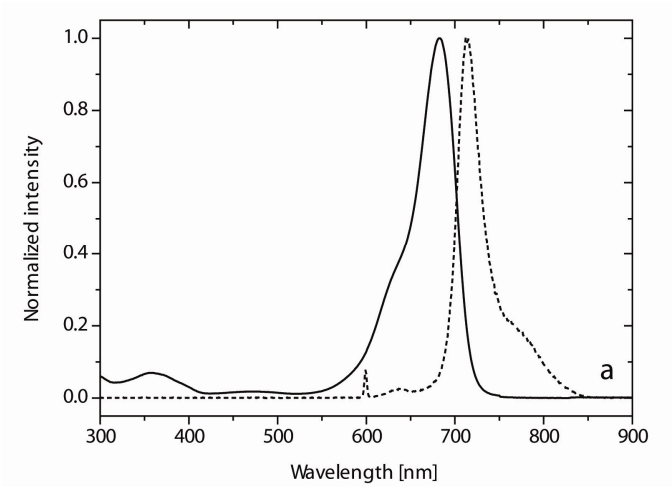

Figure 4.6: One-photon absorption (solid line) and fluorescence (dashed line) spectra of 2b in acetonitrile.

4. 2.2 Time-resolved fluorescence data.

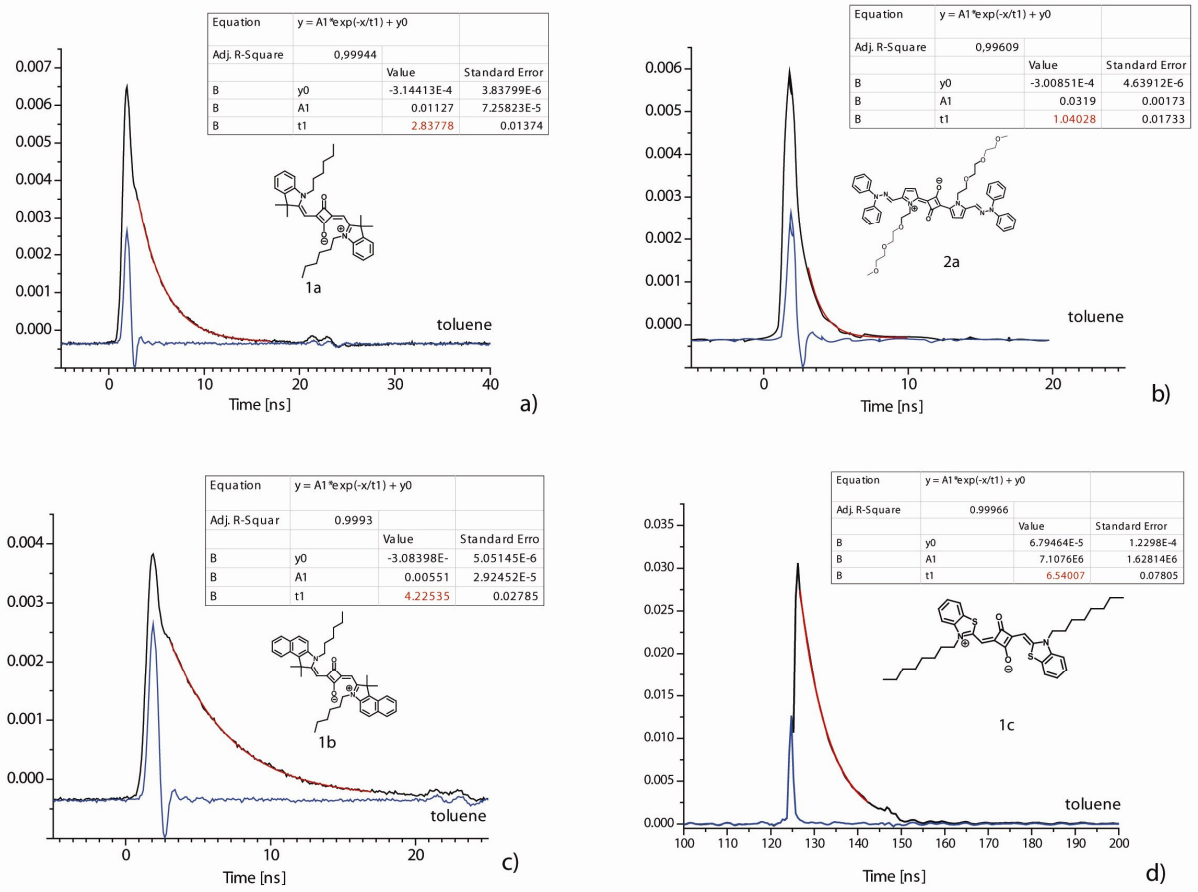

Figure 4.7: Representative fluorescence response traces (in black) recorded for solutions of 3.1a (a), 3.2a (b), 3.1b (c) and 3.1c (d) in air-saturated toluene upon pulsed irradiation at 395 nm. The blue line, obtained from scattered laser light, represents the response time of our system. Lifetimes obtained by simple monoexponential fits (in red) were equivalent to those obtained via deconvolution (not shown).

4.2.3 Representative data used to quantify triplet state yields

As outlined in the text of the manuscript, experiments were performed according to the approach established by Wilkinson and colleagues.[8, 9]

For the experiments performed here, 20 mL of a fresh solution of each dye (5×10^{-4} M) was divided into two aliquots. The first one was gently bubbled with nitrogen gas for 30 min, while the second was left air-equilibrated. Each aliquot was then distributed into 4 cuvettes (2.5 mL each). The solutions in the cuvettes were irradiated at 355 nm (35 mW of the third harmonic of a Nd:YAG laser operated at 10 Hz) and the transient absorption signal at 530 nm processed by an oscilloscope was averaged using data from over 1000 independent laser pulses. Each measurement was repeated three times for each sample. The decay curves obtained were fit with a single exponential function which was then extrapolated to time "zero" to obtain the signal intensity proportional to the concentration of the triplet states initially populated; A_T(air) and $A_T(N_2)$, respectively. The mean values for A_T(air) and $A_T(N_2)$ were used in the Wilkinson expression shown below.

$$\frac{I(N_2) - I(air)}{I(air)} = \phi_T(nitrogen)\left(\frac{A_T(air)}{A_T(N_2)}\frac{I(N_2)}{I(air)} - 1\right)$$

Using these same solutions, values for the intensity of sample fluorescence, I(air) and $I(N_2)$, were obtained analogously. The value for $\Phi_T(N_2)$ was then obtained using the expression shown above. Thereafter, the value for Φ_T(air) for a given squaraine was obtained using the expression shown below. Data are summarized in Table 4.1.

$$\phi_T(air) = \frac{A_T(air)}{A_T(N_2)}\phi_T(nitrogen)$$

Table 4.1: Squaraine fluorescence intensities in the absence, I(N_2), and presence of air, I(air), triplet absorbance intensities in the absence, $A_T(N_2)$, and presence of air, A_T(air), and triplet state yields in the absence, $\Phi_T(N_2)$, and presence of air, Φ_T(air), in solutions of toluene.

Compound	I(N_2)	I(air)	$A_T(N_2)$	A_T(air)	$\Phi_T(N_2)$	Φ_T(air)
3.1a	1.898 ± 0.008	1.854 ± 0.012	6.18 ± 0.38	12.53 ± 0.74	0.022 ± 0.008	0.045 ± 0.016
3.1b	1.524 ± 0.024	1.465 ± 0.014	4.91 ± 0.69	12.68 ± 0.34	0.024 ± 0.009	0.06 ± 0.03
3.1c	1.409 ± 0.006	1.253 ± 0.014	20.8 ± 1.7	3.23 ± 0.30	0.020 ± 0.004	0.13 ± 0.03

4.3 Characterization of Fluorescent Quadrupolar Bioprobes

Partition coefficients. The lipophilic and hydrophilic properties of the new dyes were characterized by determining the log P, the logarithm of their partition coefficients, between 1-octanol and water. Chromophores were added to 1-octanol. The test tubes containing octanol and water were inverted and shaken at least 50 times in order to establish equilibrium of the two phases. The subsequent separation of the phases was obtained by centrifugation and the concentration for each dye in both PBS and octanol was determined.[10] The log P values were calculated using the relationship:

$$\log\left[\frac{|solute|_{o,f}}{|solute|_{w,f}}\right] = \log\left[\frac{\left(|solute|_{w,i} - |solute|_{w,f}\right)(V_w/V_o)}{|solute|_{w,f}}\right]$$

$$= \log\left[\left(\frac{|solute|_{w,i}}{|solute|_{w,f}} - 1\right)(V_w/V_o)\right]$$

where the subscripts *w* and *o* refer to water and ethanol respectively and *i* and *f* refer to the the concentrations before and after partitioning, respectively. The concentrations were determined spectroscopically by measuring the maximum absorption in water in experimental conditions that hold Beer-Lambert law. Determinations were repeated three times.

Cytotoxicity study. We analyzed the dark cytotoxicity of compounds **3.34a-c**, **3.35** and **3.36** on HUVEC (Human Umbilical Vein Endothelial Cells). Cytotoxicity had been assessed using MTT kit, designed for the spectrophotometric measurement of cell growth as a function of mitochondrial activity in living cells. The MTT system is a simple, accurate, reproducible mean of measuring the activity of living cells via mitochondrial dehydrogenase activity. Mitochondrial dehydrogenases of viable cells cleave the tetrazolium ring, yielding purple MTT formazan crystals which are insoluble in aqueous solutions. The crystals can be dissolved in acidified isopropanol. The resulting purple solution is spectrophotometrically measured. An increase in cell number results in an increase in the amount of MTT formazan formed and an increase in absorbance at 570 nm. The experiment had been performed on HUVEC using 24-wells plates. HUVEC have been cultured in M199 medium containing 10% calf serum (Sigma). Cells have been incubated with a 10 μM cromophore solution for 24, 48 (and 72 h) at 37°C, and then incubated in dark with MTT for 4 h at 37°C.

Intracellular localization study. We determined the intracellular localization of our

compounds with a laser scanning confocal microscope, BioRad MRC1024 mounted on an upright fluorescence microscope (Nikon E600) equipped for the observation and acquisition of images in the interferential contrast mode (DIC). Cells were seeded in flasks and allowed to grow at 37°C and 5% CO_2 up to 50–70% confluence. The medium was then removed and the cells were washed twice with phosphate buffered saline (PBS) and incubated at 37°C and 5% CO_2 in PBS containing the appropriate dye. For each compound we optimized the proper working concentration (2 to 10 μM) and the suitable incubation time (15 min to 1h).

Ex vivo micro-fluorescence. Photoluminescence spectra of **3.34a** in HUVEC cells have been collected with an home-made setup based on a Nikon Eclipse 80i confocal microscope, equipped with a fiber-coupled 532 nm DPSS Green Laser Module (LaserWorld) as light source. Reference confocal images of the cells were firstly collected in order to localize the dye within the biological environment. The light emitted from a 5 μm x 5 μm area was accordingly collected through a fiber-coupled 190 mm polychromator and an N_2-cooled CCD camera. The obtained fluorescence spectra were then corrected for instrumental spectral responses.

Bibliography

1. Mitekura, H.; No, T.; Suzuki, K.; Satake, K.; Kimura, M., Spectroscopic properties of meso-substituted cyanine dyes: evidences for intramolecular charge transfer from a julolidine moiety as a meso-substituent to the cyanine chromophore. *Dyes and Pigments* **2002,** *54* (2), 113-120.

2. Skovsen, E.; Snyder, J. W.; Lambert, J. D. C.; Ogilby, P. R., Lifetime and Diffusion of Singlet Oxygen in a Cell. *The Journal of Physical Chemistry B* **2005,** *109* (18), 8570-8573.

3. Snyder, J.; Skovsen, E.; Lambert, J.; Ogilby, P., Subcellular, time-resolved studies of singlet oxygen in single cells. *J. Am. Chem. SOC* **2005,** *127* (42), 14558-14559.

4. Ganzha, V.; Gurinovich, G.; Dzhagarov, B.; Egorova, G.; Sagun, E.; Shul'Ga, A., Influence of the molecular structure on the quenching of triplet states of porphyrins by molecular oxygen. *Journal of Applied Spectroscopy* **1989,** *50* (4), 402-406.

5. Schmidt, R.; Afshari, E., Effect of solvent on the phosphorescence rate constant of singlet oxygen. *J. Phys. Chem* **1990,** *94*, 4377-4378.

6. Redmond, R.; Valduga, G.; Nonel, S.; Braslavsky, S.; Schaffner, K.; Vogel, E.;

Pramod, K.; Köcher, M., The photophysical properties of porphycene incorporated in small unilamellar lipid vesicles. *Journal of photochemistry and photobiology. B, Biology* **1989,** *3* (2), 193-207.

7. Arnbjerg, J.; Johnsen, M.; Frederiksen, P.; Braslavsky, S.; Ogilby, P., Two-photon photosensitized production of singlet oxygen: Optical and optoacoustic characterization of absolute two-photon absorption cross sections for standard sensitizers in different solvents. *J. Phys. Chem. A* **2006,** *110* (23), 7375-7385.

8. Horrocks, A. R.; Kearvell, A.; Tickle, K.; Wilkinson, F., Mechanism of Fluorescence quenching in solution. Part 2. Quenching by xenon and intersystem crossing efficiencies. *Trans. Faraday Soc.* **1966,** *62*, 3393-3399.

9. Wilkinson, F.; McGarvey, D. J.; Olea, A. F., Factors Governing the Efficiency of Singlet Oxygen Production during Oxygen Quenching of Singlet and Triplet States of Anthracene Derivatives in Cyclohexane Solution. *J. Am. Chem. Soc.* **1993,** *115*, 12144-12151.

10. Leo, A.; Hansch, C.; Elkins, D., Partition coefficients and their uses. *Chemical Reviews* **1971,** *71* (6), 525-616.

Conclusions

I described the synthesis, the photophysical, photochemical and biological characterization of some organic aromatic heterocycle derivatives and their theranostical applications to cancer treatment.

I explored the synthetic accessibility of squaraine dyes and I reported on two strategies aimed at the improvement of the reaction yield, of byproducts removal and of time sparing. In order to demonstrate the readiness of squaraine tailoring, I surveyed the synthetic possibilities arising from the condensation of the emisquaraine 3-(3,5-dimethyl-1*H*-pyrrol-2-yl)-4-hydroxycyclobut-3-ene-1,2-dione (**3.3**) with different anhydrobases derivatives. Specifically, I inserted in the squaraine backbone: a) an alkyl chains (**3.1d**); b) a sulphonate group (**3.4**); c) a carboxylic acid (**3.5**); c) cholesterol (**3.7**); and d) a phthalimide group (**3.6**). Moreover, I chose to take advantage of cholesterol to improve squaraine bioavailability. To this aim I synthesized six novel squarylium dyes functionalized with either one or two cholesteryl moieties to be incorporated in liposomes, a suitable choice to improve the drug pharmacokinetics and increase the accumulation in the tumor tissues. Finally, I developed a readily post-functionalizable squaraine that could be bioconjugated with biological agents.

I also investigated the photophysical behavior of heterocycle-based π-extended polymethine dyes to get further insight into the possible oxygen-mediated mechanism leading to cellular phototoxicity. To this aim, I have evaluated the interaction between molecular oxygen and several pyrrole-containing and anhydrobase derived squaraine candidates as second-generation photosensitizers for photodynamic therapy. I measured low singlet oxygen yields in toluene and acetonitrile and I designed a series of experiment in the direction of explaining this peculiar behavior. All of the collected data point out that these electronrich polymethine compounds have a strong affinity with molecular oxygen leading to the formation of a charge transfer oxyplex. The squaraines we presented, thank to this interaction, are simultaneously valuable singlet oxygen quenchers and poor singlet oxygen generators. This issue could be overcome due to squaraine noteworthy spectral features: I demonstrated that it is possible to irradiate squaraines dyes in the near UV resulting in a boost of singlet oxygen as a result of the inner filter effect.

To elucidate the photodamaging mechanism I designed simple photochemical

experiments: firstly, I analyzed the photobleaching behavior of a benzothiazole-based squaraine by GC-MS and I observed the formation of two carbonyl compounds in accordance with a photooxygenation of the enaminic bond; secondly, I studied the product distribution of the reaction between light, squaraines and biologically relevant targets (i.e., limonene, cholesterol, and methyl linoleate) pointing out the presence of a radical chain of oxidative events. Consistently with the photophysical characterization, I established that the encounter complex between squaraine and molecular oxygen could evolve either by photooxygenation of the enaminic bond in the squaraine backbone or by ROS production leading to lipid peroxidation that culminate in cell death by a Type I mechanism.

Indeed, the in-depth biological evaluation of two benzothiazole-based squaraine dyes showed that these dyes internalized in lipid vesicles in the cytoplasm and, although they are non-significantly cytotoxic in the dark, they promote a strong dose-dependent phototoxic effect in four different cancer cells after irradiation. In HeLa and MCF-7 cells **3.1c** and **3.30,** through their hydrocarbon chain substitutions, associate to the membranes and induce lipid peroxidation, as expected from the photophysical and photochemical study, causing cell death primarily by necrosis

To further validate the previous observations, I designed an experiment aim to activate the production of ROS in a family of cyanine dyes. I chose to engineer the progenitor Cy5 (**3.31**) at the molecular level and increase its photooxidation capabilities by exploiting the effect plays by heteroaryl meso-substituents on the cyanine oxidation potential. By monitoring the degradation of 1,3-diphenylisobenzofuran (DPBF) after irradiation of a sensitizer in the presence of oxygen in solution I showed that it is possible to control the redox behavior, hence the ROS production, by modulating the extent of electron density pulled by the chromophoric side-group in the meso position and boost the photooxidative capability in the series of cyanine derivatives investigated.

Moreover, I report on the synthesis, characterization and spectroscopic study both in solution and ex vivo of seven quadrupolar eteroaryl compounds which have been designed to be promising candidates as tumor-specific fluorescent molecular probes. Basic photophysical characteristics of these dyes, their subcellular localization in human umbilical vein endothelial cells (HUVEC), and their hydrophilicity based on logP values have provided in-depth insight into the processes that lead to accumulation in either mitochondria or lysosomes. I have also succeeded in recording its fluorescence

spectrum ex vivo, obtaining further information about the interaction between this heteroaromatic dicationic dye and the biological environment.

In conclusions I demonstrated how it is possible to molecular engineered classes of heteroaryl derivatives in order to exploit desired properties, among these reactive oxygen species induced phototoxicity and specific subcellular localization. It is noteworthy to mention that what we have found for the class of squaraine dyes could be extended to a wider family of anhydrobases derivatives (e.g., MKT-077, indocyanine green, and merocyanine 540) and bring fresh insight in the debate about the role of singlet oxygen and reactive oxygen species induced phototoxicity. Further studies will investigate PDT efficiencies in vivo for the library of squaraine dyes here presented. From the mechanistic point of view, we will attempt to clarify which reactive oxygen species triggers the response in the biological chain of events leading to cell death.

Publications

This thesis work has led to the following publications:

[1] Beverina, L.; Crippa, M.; Landenna, M.; Ruffo, R.; Salice, P.; Silvestri, F.; Versari, S.; Villa, A.; Ciaffoni, L.; Collini, E.; Ferrante, C.; Bradamante, S.; Mari, C. M.; Bozio, R.; Pagani, G. A., *Assessment of Water-Soluble π-Extended Squaraines as One- and Two-Photon Singlet Oxygen Photosensitizers: Design, Synthesis, and Characterization.* Journal of the American Chemical Society **2008**, *130* (6), 1894-1902.

[2] Beverina, L.; Crippa, M.; Salice, P.; Ruffo, R.; Ferrante, C.; Fortunati, I.; Signorini, R.; Mari, C. M.; Bozio, R.; Facchetti, A.; Pagani, G. A., *Indolic squaraines as two-photon absorbing dyes in the visible region: X-ray structure, electrochemical, and nonlinear optical characterization.* Chemistry of Materials **2008**, *20* (10), 3242-3244.

[3] Rapozzi, V.; Beverina, L.; Salice, P.; Pagani, G.A.; Xodo, L.E., *Photosensitizing activity of π-extended squaraines in cancer cells*, submitted to the Journal of Medicinal Chemistry

[4] Salice,P.; Arnbjerg, J.; Wett Pedersen, B.; Toftegaard, R.; Beverina, L.; Pagani, G.A.; Ogilby, P.R., *Photophysics of Squaraine Dyes: Role of Charge-transfer in Singlet Oxygen Production and Removal*, to be submitted to the Journal of Physical Chemistry

[5] Salice, P.; Bradamante, S.; Versari, S.; Villa, A.; Meinardi, F.; Macchi, G.; Beverina, L.; Pagani, G.A., *Molecular Engineered Fluorescent Quadrupolar Bioprobes: Synthesis, Spectroscopic, and Imaging Characterization*, to be submitted to the Journal of Organic Chemistry

[6] Beverina, L.; Salice, P., *Squaraine compounds. Tailored design and synthesis towards a variety of material science applications,* Microreview to be submitted to the European Journal of Organic Chemistry.

[7] Salice, P.; Beverina, L.; Pagani, G.A., *Photochemistry of Squaraine Dyes: Photooxidation Capabilities Towards Biological Substrates*, in preparation.